

Characterisation and Engineering of  
Plastic-Degrading Enzymes

**Inauguraldissertation**

zur

Erlangung des akademischen Grades eines

Doktors der Naturwissenschaften

(Dr. rer. nat.)

der

Mathematisch-Naturwissenschaftlichen Fakultät

der

Universität Greifswald

vorgelegt von

Lara Pfaff

Greifswald, Oktober 2022

**Dekan:** Prof. Dr. Gerald Kerth

**1. Gutachter:** Prof. Dr. Uwe T. Bornscheuer

**2. Gutachter:** Dr. Gregg T. Beckham

**Tag der Promotion:** 19.12.2022

---

## Table of Contents

Table of Contents.....	i
Abbreviations.....	iii
Scope and Outline.....	v
1 Background.....	1
1.1 Plastics.....	1
1.2 Polyethylene Terephthalate (PET).....	2
1.2.1 Discovery, Synthesis and Properties of PET.....	2
1.2.2 Recycling of PET.....	4
1.3 PET-Hydrolysing Enzymes.....	7
1.3.1 Evolution of Thermophilic PET Hydrolases.....	8
1.3.2 Proposed Mechanism of the Interfacial Enzymatic PET Hydrolysis.....	10
1.3.3 High-Throughput Screening Methods.....	12
1.4 Protein Engineering.....	17
2 Results and Discussion.....	19
2.1 Characterisation and Engineering of PET Hydrolases.....	19
2.1.1 Multiple Substrate Binding Mode-Guided Engineering of a Thermophilic PET Hydrolase (Article I).....	19
2.1.2 Engineering of mesophilic <i>IsPETase</i> for higher thermostability (Article II).....	23
2.2 High-Throughput Screening of PET Hydrolase Activity.....	25
2.2.1 Fluorimetric High-Throughput Screening in Crude Cell Lysate using PET-NP (Article III).....	26
2.2.2 Biosensor-based High-Throughput Screening in Living Cells and Efforts towards a Circular Economy (Article IV).....	29
3 Conclusions.....	33
4 References.....	35
5 Author Contributions.....	43
Articles.....	45

## Table of Contents

---

Article I .....	47
Article II .....	101
Article III .....	123
Article IV .....	143
Eigenständigkeitserklärung .....	169
List of Publications .....	171
Acknowledgments .....	173

## Abbreviations

1,4-BDM	1,4-Benzenedimethanol
4-CBAL	4-Carboxybenzaldehyde
4-HMBAL	4-(Hydroxymethyl) benzaldehyde
2-HOTP	2-Hydroxyterephthalate
2-PAA	2-Phenylacetaldehyde
BAM	Benzylamine
BHET	Bis(2-hydroxyethyl) terephthalate
BHETA	Bis(2-hydroxyethyl) terephthalamide
CAR <sub>Mm</sub>	Carboxylic acid reductase from the marine bacterium <i>Mycobacterium marinum</i>
CO <sub>2</sub>	Carbon dioxide
DLS	Dynamic light scattering
DMSO	Dimethyl sulfoxide
DMT	Dimethyl terephthalate
<i>E. coli</i>	<i>Escherichia coli</i>
EG	Ethylene glycol
ePCR	Error-prone PCR
FACS	Fluorescence-activated cell sorting
GC/FID	Gas chromatography equipped with a flame ionization detector
Gf	Goodfellow
hcPET	High-crystallinity PET
HEMT	1-(2-Hydroxyethyl) 4-methyl terephthalate
HFIP	Hexa-fluoro-2-propanol
HPLC	High performance liquid chromatography
HT	High-throughput
<i>IsPETase</i>	PETase from <i>Ideonella sakaiensis</i>
IBM	Intermediate ligand binding mode
LCC ICCG	LCC F243I/D238C/S283C/Y127G variant
lcPET	Low-crystallinity PET
LuxAB	Luciferase from <i>Photobacterium luminescens</i>
MD	Molecular dynamics
MHET	Mono-(2-hydroxyethyl) terephthalate
MHETA	4-(2-Hydroxyethylcarbamoyl) benzoic acid

## Abbreviations

---

$M_n$	Number-average molecular mass
NADP <sup>+</sup> /NAPH	Nicotinamide adenine dinucleotide phosphate
OD <sub>600</sub>	Optical density at 600 nm
PES-H	Polyester hydrolase
PET	Polyethylene terephthalate
PET-NP	Polyethylene terephthalate nanoparticle
PPT <sub>Ni</sub>	Phosphopantetheinyl transferase from <i>Nocardia iowensis</i>
QM/MM	Quantum mechanics/molecular mechanic
PUR	Polyurethane
RCs	Resting cells
RCM	Resting cell medium
RFU	Relative fluorescence units
RP-HPLC	Reverse phase HPLC
SEM	Scanning electron microscopy
sfGFP	Superfolder green fluorescent protein
TAL	Terephthalaldehyde
TF	Transcription factor
$T_m$	Melting points
$T_{opt}$	Optimal operating temperature
TPA	Terephthalic acid

Units of measurements and of physical and chemical quantities are abbreviated as commonly used or based on the International System of Units (SI). Amino acids and nucleotides are abbreviated as designated by the International Union of Pure and Applied Chemistry (IUPAC).

## Scope and Outline

This thesis deals with the characterisation and engineering (**Articles I and II**) of new thermophilic PET hydrolases as potential candidates for an eco-friendly biocatalytic recycling approach for the upcycling or downcycling of polyethylene terephthalate (PET) on industrial scale. Furthermore, high-throughput screening methods are described that detect the products of PET hydrolysis (**Articles II and IV**). The high demand of PET in the packaging and textile industries with a global production of 82 million metric tons per year has significantly contributed to the global solid waste stream and environmental plastic pollution after its end-of-life. Although PET hydrolases have been identified in various microorganisms, only a handful of benchmark enzymes have been engineered for industrial applications. Therefore, the identification of new PET hydrolases from metagenomes or via protein engineering approaches, especially thermophilic PET hydrolases with optimal operating temperatures (i.e., increased thermostability and activity) near the glass transition temperature of the polymer PET, is a crucial step towards a bio-based circular plastic economy. **Article I** demonstrates that metagenome-derived thermophilic PET hydrolases can be significantly improved using different engineering approaches to achieve a similar activity level as the well-established leaf-branch-compost cutinase (LCC) F243I/D238C/S283C/Y127G variant (LCC ICCG). In **Article II**, thermostable variants of a mesophilic enzyme (PETase from *Ideonella sakaiensis*) were identified from a mutant library and characterised against PET substrates in various forms. **Articles III and IV** describe the application of high-throughput methods for the identification of novel PET hydrolases by directly assaying terephthalic acid (TPA), one of the monomeric building blocks of PET. Furthermore, **Article IV** describes the possibility of a one-pot conversion of the TPA-based aldehydes produced to their diamines as example for an open-loop upcycling method.

### **Article I      Multiple Substrate Binding Mode-Guided Engineering of a Thermophilic PET Hydrolase**

L. Pfaff, J. Gao, Z. Li, A. Jäckering, G. Weber, J. Mican, Y. Chen, W. Dong, X. Hu, C. G. Feiler, Y. Ao, C. P. S. Badenhorst, D. Bednar, G. J. Palm, M. Lammers, J. Damborsky, B. Strodel, W. Liu, U. T. Bornscheuer, R. Wei, *ACS Catal.* **2022**, *12*, 9790-9800.

By determining the crystal structures of two metagenome-derived thermophilic polyester hydrolases (PES-H1 and -H2) in their apo-form and in complexes with PET monomer

analogues, multiple substrate binding modes were observed, and key substrate-binding residues were identified. Molecular dynamic (MD) simulations supported the involvement of these residues in the PET binding. The structural and mechanistic understanding of the enzymatic hydrolysis at the solid-liquid interface is crucial for the design of efficient PET depolymerising biocatalysts. The rational engineering of PES-H1 led to several variants with significantly improved thermostability and PET hydrolysis activity which hold promise for future applications in the biocatalytic plastic recycling.

### **Article II      Engineering and evaluation of thermostable *IsPETase* variants for PET degradation**

S. Brott, L. Pfaff, J. Schuricht, J. Schwarz, D. Böttcher,  
C. P. S. Badenhorst, R. Wei, U. T. Bornscheuer, *Eng. Life Sci.* **2021**, *22*,  
192-203.

Screening of a mutant library based on a thermostable triple mutant of *IsPETase* against a commercially available polyester-polyurethane led to the identification of several variants with higher melting points. The most promising thermostabilising mutations were incorporated in previously published *IsPETase* variants and compared with respect to increased thermostability and activity on different PET materials.

### **Article III      Fluorimetric High-Throughput Screening Method for Polyester Hydrolase Activity Using Polyethylene Terephthalate Nanoparticles**

L. Pfaff, D. Breite, C. P. S. Badenhorst, U. T. Bornscheuer, R. Wei, in  
*Methods in Enzymology*, Elsevier, **2021**, Vol. 648, 253-270.

High-throughput screening assays for PET-hydrolysing activity still remain challenging due to technical limitation of individual approaches and thus have rarely been applied. Assaying terephthalate as a major product of the enzymatic PET hydrolysis in a 96-well microtiter plate format enables the rapid identification of outstanding PET hydrolase variants from large metagenome or mutant libraries. As a proof of concept, crude cell lysates of TfCut2 and an inactive variant of TfCut2 were directly used for the hydrolysis of PET nanoparticles (PET-NP) and the subsequent Fenton chemistry-mediated fluorimetric detection of terephthalate.



**Article IV      Biosensor and chemo-enzymatic one-pot cascade applications to detect and transform PET-derived terephthalic acid in living cells**

T. Bayer, L. Pfaff, Y. Branson, A. Becker, S. Wu, U. T. Bornscheuer, R. Wei, *iScience* **2022**, 25, 104326.

In this study, a LuxAB-based biosensor system semi-quantitatively monitoring the TPA production in living *Escherichia coli* (*E. coli*) cells by converting TPA into the corresponding aldehydes was established. Furthermore, the produced aldehydes were transformed in a chemo-enzymatic one-pot cascade reaction into their primary amines supporting efforts towards a circular plastic economy.



# 1 Background

## 1.1 Plastics

Plastics are the most advanced materials in terms of application and property range, with a global demand of over 400 million tonnes per year,<sup>[1]</sup> but they have recently faced strong public opposition due to the environmental plastic pollution. Bio-based and especially biodegradable plastics have gained attention as potential solutions to the problems of sustainable plastics, plastic waste, and plastic littering. The growing awareness of these issues among governments and policymakers, industries producing or relying on plastics, and end-users of plastic products has recently accelerated research and development of novel plastic replacement materials and waste plastic valorisation strategies to enable the transition from a linear to a circular plastic economy.<sup>[2-5]</sup>

By definition, plastic is a material that contains a polymer (molecular weight >10 kDa) which is usually composed of repeating units of low-molecular weight, e.g. ethylene or propylene and can be shaped by flow at some stage in its processing into the finished product.<sup>[6]</sup> To make the polymer softer, more flexible and/or workable chemical modifications or the addition of plasticiser is sometimes necessary. Furthermore, the plastic can be modified in terms of durability, strength or working properties by adding a filler, a relatively inert solid material. Plastics can be categorised into fossil-based and bio-based plastics (Figure 1) and find applications in various segments such as the packaging, textile, building and construction, automotive, agriculture and other industries.<sup>[7]</sup> With 90%, fossil-based plastics account for the majority of the worldwide plastic production, followed by recycled plastics and bio-based plastics with 9%, and 1% production share, respectively.<sup>[1]</sup> The most conventional plastics, such as PET, polyethylene (PE), polypropylene (PP), polystyrene (PS), poly(vinyl chloride) (PVC) and polyurethanes (PUR), are not biodegradable. On the contrary, polycaprolactone (PCL) and poly(butylene adipate-co-terephthalate) (PBAT) are fossil-based, but biodegradable plastics. Bio-based plastics are either partly or fully derived from biomass (plants), e.g. cellulose, starch, or corn. Bio-based and biodegradable plastics are polybutylene succinate (PBS), polyhydroxyalkanoate (PHA) and polylactic acid (PLA). Due to the increased use of bioplastics, there has been a surge of interest in biodegradation technologies such as oxo-degradation and enzymatic-based to convert conventional plastics, e.g. polyamide (PA), PE, PP, and PET into biodegradable plastics.<sup>[7]</sup> The incorporation of CO<sub>2</sub> into polymers is by far the most established and production-volume-related advanced technology. CO<sub>2</sub> can be used directly to produce polycarbonates (PC) such as polyethylene carbonate and

polypropylene carbonate, as well as polyol precursors, which are then used to produce CO<sub>2</sub>-based PUR.<sup>[6]</sup> Several technologies which indirectly apply CO<sub>2</sub> for polymer synthesis, for e.g. PHA, PLA, ethylene, are developing.<sup>[8-10]</sup> This thesis solely focuses on the degradation of PET as one of the most abundant and widespread polyesters.

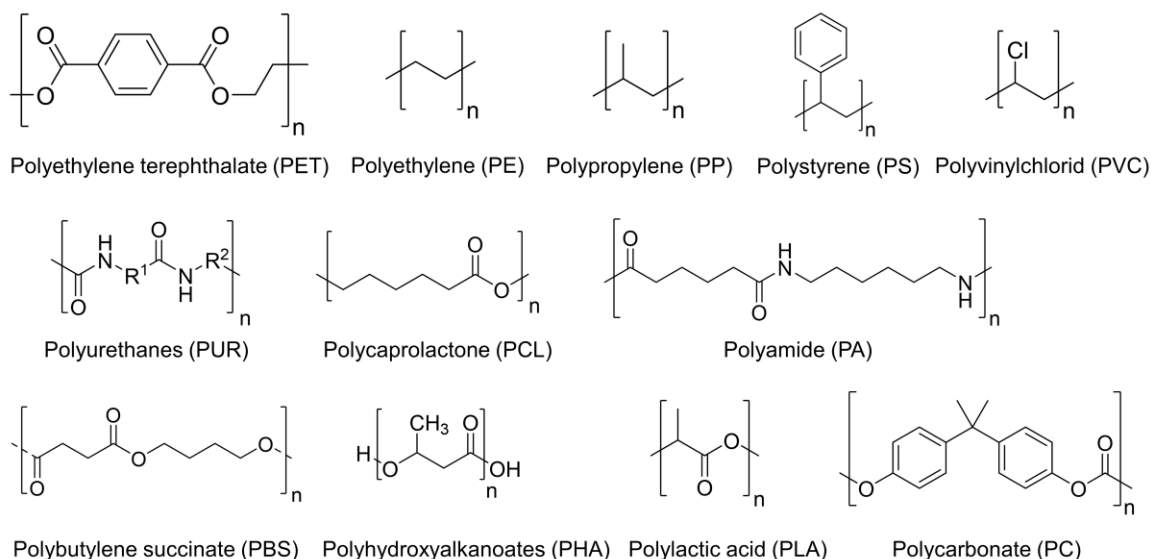


**Figure 1.** Overview of different types of plastics including the conventional plastics (PET, PE, PP, PS, PVC and PUR), fossil-based and biodegradable plastics (PCL), bio-based and non-biodegradable plastics (bioPE and PA) and bio-based and biodegradable plastics (PHA, PLA and PBS). For PA and PC only one representative example is shown.

## 1.2 Polyethylene Terephthalate (PET)

### 1.2.1 Discovery, Synthesis and Properties of PET

PET is a thermoplastic polyester resin composed of polymerised units of the monomers TPA and ethylene glycol (EG) (Figure 1). The PET monomer units consist of a rigid benzene ring and a flexible alkyl group which are connected by an ester bond resulting in an increased rigidity of the entire molecular chain. Due to relatively large steric hindrance, only motion by segments is allowed when the macromolecular chain rotates around this rigid group, limiting the flexibility of alkyl groups. As a result, PET materials typically have high rigidity but poor toughness, as well as relatively high glass transition temperatures ( $T_g$ ) and melting points ( $T_m$ ).<sup>[11]</sup>

The first patent application on the synthesis of PET from EG and TPA was already filed in 1941 by the British chemists J. R. Whinfield and J. T. Dickson.<sup>[12]</sup> In the following years PET was known under different trade names depending on its purpose including

Terylene<sup>®</sup>[13,14] (PET fabrics) from the British Imperial Chemical Company (London, UK), Dacron<sup>®</sup>[15] (PET fibres) and Mylar<sup>®</sup>[15,16] (PET films) owned by DuPont (Wilmington, USA).

The synthesis of PET includes two reaction steps.<sup>[17]</sup> The first step is the direct esterification of TPA and EG which produces a prepolymer primarily composed of bis(2-hydroxyethyl) terephthalate (BHET) and short-chain oligomers. Water is a major by-product of the esterification and is continuously removed using a column system. Alternatively, the prepolymer can be formed by the transesterification of dimethyl terephthalate (DMT) with EG. Methanol is then released as a by-product. Until high-purity TPA was produced for the first time in the late 1960s the transesterification process played a significant role in the production of industrial PET.<sup>[18]</sup> The second step in the PET synthesis is a stepwise polycondensation of BHET in the melt-phase via a transesterification reaction. The main by-product EG is removed from the melt under high-vacuum conditions. Additionally, high-viscosity graded PET used for bottles or technical yarn can be produced via solid-state polycondensation of PET oligomers which is usually carried out under inert gas atmosphere or vacuum.<sup>[17,19]</sup>

PET exists both as an amorphous and a semi-crystalline (highly transparent and colourless) thermoplastic with a crystallinity of less than 60% based on its processing and thermal history. Semi-crystalline PET has good strength, heat resistance, dimensional stability, ductility, stiffness, and hardness whereas the amorphous PET has a higher ductility. At room temperature it is generally resistant to mineral oils, non-polar organic solvents, most of the polar organic solvents and acids, but not to bases, phenols or esters.<sup>[20,21]</sup> At higher temperatures, PET is soluble in several polar organic solvents including nitrobenzene and trifluoroacetic acid, and in hexafluoro-2-propanol (HFIP) at room temperature.<sup>[22]</sup>

PET, the most abundant synthetic polyester, is widely used in the packaging and textile industry. The global production of PET recently reached 82 million metric tons per year<sup>[23]</sup> which significantly contributes to the global solid waste stream and environmental plastic pollution after its end-of-life. PET fibres have several remarkable properties for the textile industry, including resistance to many chemicals and mechanical effects such as abrasion, stretching, shrinking, and wrinkling.<sup>[24]</sup> On the other hand PET is difficult to dye and has poor wearing comfort due to its low water absorption capacity. Alkali<sup>[25]</sup> and enzyme treatments<sup>[24,26–30]</sup> have the potential to increase the water absorbing ability of PET and thus improve its applicability in the textile industry. PET is distinguished by its high strength, low weight, chemical resistance, and low permeability to gases such as oxygen and CO<sub>2</sub>.<sup>[31]</sup> Based on these properties, PET is an excellent packaging material for a wide

range of food products and other consumer goods such as soft drinks, alcoholic beverages, detergents, cosmetics, pharmaceutical products, and edible oils.

### 1.2.2 Recycling of PET

Despite of the many useful applications of PET contributing to our daily lives, its mismanaged disposal in the environment caused a worldwide pollution of the terrestrial and marine habitats as plastics, e.g. PET bottles, take approximately 450 years to decompose naturally.<sup>[32]</sup> Recalcitrant micro- and nanoplastics are dispersed in the air and can thus reach even the most remote parts of the planet, such as glaciers and arctic regions.<sup>[33,34]</sup> Recycling technologies for PET were developed already 30 years ago.<sup>[5]</sup> The recycling of PET can be categorized into primary, secondary, tertiary, and quaternary recycling.<sup>[35]</sup> Each method has its own set of benefits and drawbacks in terms of cost, quality, and environmental impact.

Both, the primary and secondary recycling are mechanical recycling methods, e.g. extrusion and melting, in which PET waste is processed into a recyclate maintaining the chemical polymer properties. Whereas primary recycling is used for production or pre-consumer waste with a known homogeneous composition,<sup>[36]</sup> secondary recycling is applied on contaminated post-consumer waste. Therefore, post-consumer waste is pre-processed through collection, sorting, cleaning, drying, and chipping, before being extruded or pelletised.<sup>[37]</sup> Although the chemical nature of the polymeric material is not altered by physical recycling, it impacts the molecular weight of the recycled PET.<sup>[35]</sup> Under high-temperature conditions, e.g. melt extrusion, PET is hydrolysed, resulting in the decrease of the average molecular weight which consequently affects the mechanical properties, melt viscosity and resistance.<sup>[38]</sup> To address this issue, the molecular weight of the PET is typically increased by solid-state polymerisation.<sup>[35]</sup> Although critical factors such as heterogeneity, cleanliness and degradation levels must be considered with every recycling loop, mechanical recycling is distinguished by low costs and consistent results depending on the feedstock and pre-processing. Nevertheless, in the context of a circular economy, reuse of post-consumer sorted PET is impacted by the deterioration of materials performance.<sup>[39]</sup>

The tertiary recycling, also known as chemical recycling, either describes the complete depolymerisation of the polymer structure into its building blocks and the repolymerisation to a new oligomer or the solvation (solvolysis) to dissolve the polymer for subsequent purification.<sup>[35]</sup> In comparison to mechanical recycling, chemical recycling can be applied

for a broad range of plastics, such as PUR, polyamines and PE<sup>[40]</sup> and requires minimum pretreatment of the plastic waste. In general, PET can be chemically recycled in five different ways via methanolysis, glycolysis, hydrolysis, ammonolysis or aminolysis (Figure 2). However, only glycolysis and methanolysis are widely used on a commercial scale.<sup>[31,35]</sup>

Methanolysis describes the depolymerisation of PET by methanol under high-temperature (180-280 °C) and high-pressure conditions (2-4 MPa) to DMT and EG. DMT and EG are both raw materials for the PET synthesis. The reaction may be catalysed by typical transesterification catalysts including zinc acetate, magnesium acetate, cobalt acetate, and lead dioxide. The reaction products are a combination of alcohols, glycols, and phthalate derivatives.<sup>[31,35]</sup> Following the reaction, the catalyst must be removed to avoid further polymer degradation and potential DMT loss. DMT is recovered from the post-reaction mixture by centrifugation, vacuum distillation, and re-crystallisation.<sup>[31]</sup> Nowadays, methanolysis is only rarely used in industrial applications due to the reduced importance of polyester production based on DMT.

Glycolysis is the most cost-effective and economically viable chemical PET recycling method and is typically used for the recycling of high-quality PET bottles. During glycolysis PET is decomposed under pressure and at high temperatures (180-240 °C) by EG and other glycols such as diethylene glycol, propylene glycol and di-propylene glycol, to predominantly BHET. BHET can be reused for manufacturing virgin PET. Oligomers with lower molecular masses can be obtained by partial PET glycolysis under specific preselected conditions as the ratio of PET to EG and the process control factors and are important raw materials for the synthesis of unsaturated polyesters and other polymers.<sup>[41]</sup>

PET can be hydrolysed into EG and TPA. Depending on the pH requirements the hydrolysis can be further categorised into acid hydrolysis, alkaline hydrolysis, and neutral hydrolysis. Acid hydrolysis is most commonly performed using concentrated sulphuric acid at atmospheric pressure and temperatures less than 90 °C. In contrast, alkaline hydrolysis is typically carried out at temperatures ranging from 210 to 250 °C and higher pressures of 1.4-2 MPa in concentrated sodium hydroxide or potassium hydroxide (<20%).<sup>[31,35]</sup> Neutral hydrolysis using hot water or steam has gained popularity in recent decades as a much less aggressive process for both the apparatus and the environment.<sup>[42]</sup> The neutral hydrolysis requires pressures ranging from 1 to 4 MPa and temperatures ranging from 200 °C to 300 °C. One of the drawbacks of the neutral hydrolysis is the low purity of TPA compared to acid and alkaline hydrolysed TPA which results in impurities in the repolymerised PET if TPA is not previously purified. Recently, a biocatalytic recycling

technology has been developed which describes the hydrolysis of thermomechanical processed PET waste into TPA and EG and the readily synthesis of the recovered monomers into virgin polymers.<sup>[43]</sup> This enzyme-based approach has several advantages compared to thermal or chemical depolymerisation, e.g. relatively mild reaction conditions. Possible enzyme candidates that show a high potential for the application in PET recycling on an industrial scale are presented in chapter 1.3.1.

PET can be depolymerised through the reaction of anhydrous ammonia (NH<sub>3</sub>) with PET in the presence of EG to generate terephthalamide (ammonolysis). Terephthalamide can further be processed into terephthalonitrile or *para*-xylylene diamine which can be used to produce polyamides or epoxide resins.<sup>[35]</sup>

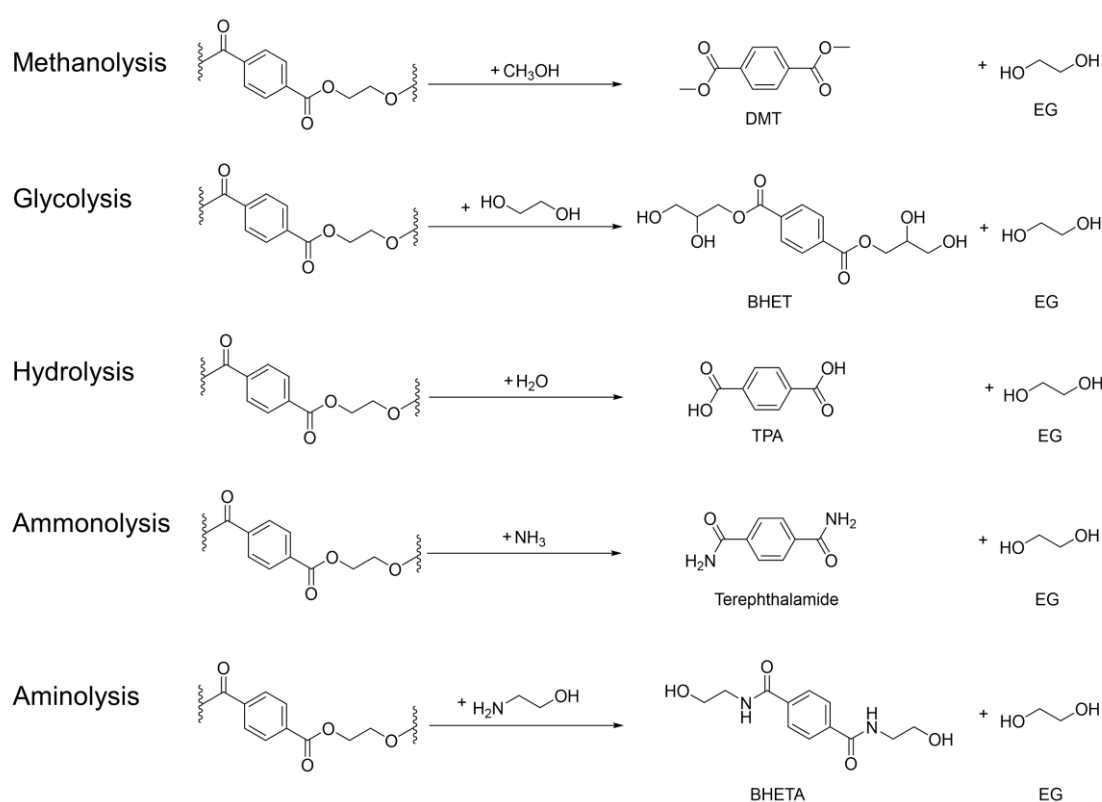


**Figure 2.** Chemical recycling techniques for PET. PET is depolymerized either by methanol (methanolysis)<sup>[31,35]</sup>, EG and glycols, e.g. propylene glycol (glycolysis),<sup>[41]</sup> anhydrous ammonia (ammonolysis)<sup>[35]</sup> or ethanolamine (aminolysis)<sup>[44]</sup> to DMT, BHET, terephthalamide and bis(2-hydroxyethyl) terephthalamide (BHETA). Furthermore, PET can be hydrolysed into the building blocks EG and TPA.<sup>[31,35]</sup>

The aminolysis of PET produces diamides of TPA and EG, e.g. BHETA. Commercially, this method of PET recycling has received less attention. At temperatures ranging from 20 °C to 100 °C, aqueous amine solutions including methylamine, ethylamine, ethanolamine, morpholine and hydrazine are used in the aminolysis process. Additionally,



catalysts such as glacial acetic acid, sodium acetate and potassium sulphate are needed.<sup>[44]</sup>

Quaternary recycling describes the process of energy recovery from plastic waste by incineration. Plastic waste has a high caloric value and can therefore be converted into heat energy during the process. The heat energy can further be transformed into electricity. The produced CO<sub>2</sub> can be captured and recycled as a secondary valuable material, along with the remaining non-burning components such as minerals and metals. In comparison to other methods, quaternary recycling is suitable for a wide range of feedstocks including municipal solid waste without requiring excessive pre-processing.<sup>[6,35]</sup>

### 1.3 PET-Hydrolysing Enzymes

The biocatalytic recycling of PET has emerged as a promising technology to face the global plastic pollution as an eco-friendly method compared to chemical recycling as mentioned in chapter 1.2.2. The biological degradation of plastic waste was already studied in the early 1970s. However, enzymes have to be able to cleave the ester bond in the amorphous domain to break down PET in its entirety into the building blocks TPA and EG (Figure 3).<sup>[5]</sup> Various enzymes have been identified for this purpose belonging to the enzyme classes of carboxylesterases<sup>[45]</sup>, lipases<sup>[46]</sup> and cutinases.<sup>[47–50]</sup> Cutinases, which can hydrolyse cutin, an insoluble aliphatic polyester excreted from the plant cuticle, represent the majority of this type of enzyme. Notably, cutinases have a broad substrate specificity; these enzymes have hydrolytic activities for both water soluble esters (substrates for esterases) and insoluble triglycerides (typical substrates for lipases).<sup>[51]</sup> Although several lipases have been reported to be able to hydrolyse PET, their activity is extremely low.<sup>[46,52,53]</sup> Only a few esterases such as *p*-nitrobenzylesterase from *Bacillus subtilis* (BsEstB) are classified as polyester-degrading enzymes.<sup>[54]</sup>

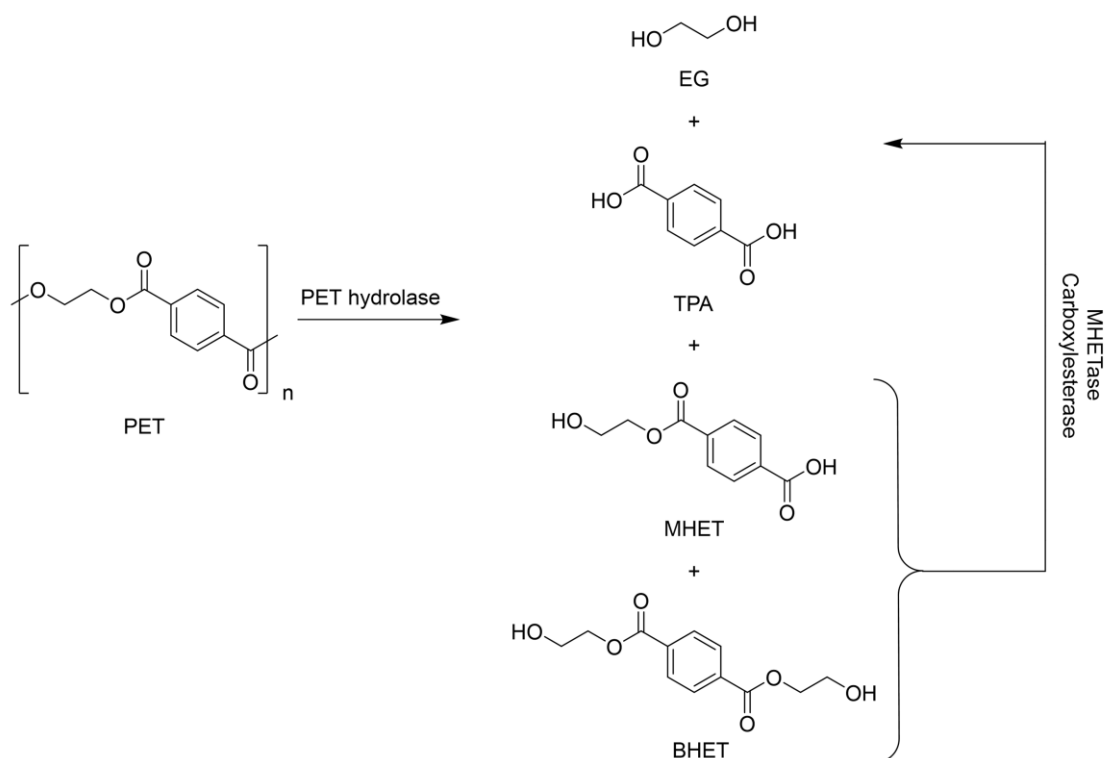


**Figure 3.** Enzymatic degradation of PET into its building blocks TPA and EG as well as its oligomers mono-(2-hydroxyethyl) terephthalate (MHET) and BHET. MHET and BHET are known to inhibit the activity of various PET hydrolases thus applying MHETase or carboxylesterases to the reaction converts MHET and BHET to solely TPA and EG.<sup>[55,56]</sup>

### 1.3.1 Evolution of Thermophilic PET Hydrolases

Earlier studies on the enzymatic degradation of aliphatic and aromatic copolyesters indicated that raising the proportion of aromatic moieties increases their  $T_m$ , thereby lowering the polymer chain mobility and biodegradability at the optimal reaction temperatures ( $T_{opt}$ ) of the used hydrolases.<sup>[57,58]</sup> For a long time, enzymatic depolymerization of PET with a  $T_m$  greater than 260 °C was thought to be impossible, until Müller et al. demonstrated a significant weight loss of amorphized PET waste (>50%) within 3 weeks of incubation using the cutinase *TfH* from *Thermobifida fusca*.<sup>[59]</sup> At temperatures approaching the glass transition temperature of PET ( $T_g$ , 65-71 °C), amorphous PET polymer chains become more accessible to enzymatic hydrolysis.<sup>[60]</sup> Water acts as a plasticizer in aqueous environments, lowering the  $T_g$  of PET by up to 16 °C.<sup>[60-62]</sup> This effect increases the flexibility of the polymer chains at the PET surface layer, allowing mesophilic PET hydrolases with  $T_{opt}$  of around 40 °C, such as *IsPETase*, to degrade PET at ambient temperatures.<sup>[63]</sup> Despite this, the advantage of using thermophilic and thermostable PET hydrolases over their mesophilic counterparts is obvious and evident.<sup>[64-67]</sup> Searching for new thermophilic enzymes, such as those found

in metagenomic libraries<sup>[68,69]</sup> as well as the engineering of known thermostabilised enzymes, offers viable options for improving degradation performance.<sup>[66]</sup>

Many homologous PET hydrolases have been found to be stabilized in the presence of calcium or magnesium ions,<sup>[69–72]</sup> as evidenced by higher  $T_m$  by 10–16 °C and  $T_{opt}$  by up to 10 °C, increased PET-hydrolyzing activity, or both including Cut190 from *Saccharomonospora viridis*,<sup>[73,74]</sup> TfCut2<sup>[70,71]</sup> and PET2.<sup>[75]</sup> Metagenomic approaches have enabled the identification of a more active leaf-branch-compost cutinase (LCC),<sup>[47]</sup> which has emerged as the most promising benchmark thermophilic PET hydrolase. Structure-based engineering of LCC has resulted in the variant LCC ICCG. LCC ICCG efficiently depolymerises amorphized postconsumer PET bottles within 10 h at 72 °C which enables the biocatalytic recycling of PET waste at industrially relevant scales.<sup>[43]</sup> In a recent study, LCC ICCG was further engineered resulting in a A59K/V63I/N248P variant which exhibited a  $T_m$  of 98.9 °C. Despite the increased  $T_m$ , the  $T_{opt}$  of this variant for degrading low-crystallinity PET (IcPET) was only 2 °C higher than for LCC ICCG.<sup>[76]</sup>

The recombinant expression of PET hydrolases in alternative hosts other than *E. coli* such as *Bacillus subtilis*<sup>[77,78]</sup> or *Pichia pastoris*<sup>[79]</sup> has shown to be successful for enhancing the thermostability.

In 2016, Yoshida et al. identified two key enzymes, the *IsPETase* and the related monoester-hydrolysing MHETase, both discovered in the mesophilic bacterium *I. sakaiensis*, which was isolated from plastic-contaminated sediment samples.<sup>[63,80]</sup> *I. sakaiensis* was described as the first natural bacterium that completely degrades and metabolises highly amorphous PET as its major carbon source at 30 °C under laboratory conditions. In a tandem mechanism, *IsPETase* catalyses the hydrolysis of PET to MHET as the main product which is then depolymerised by the MHETase to the building blocks TPA and EG<sup>[63,80,81]</sup> thereby solving the issue of product inhibition which often occurs for various PET hydrolases.<sup>[55,56]</sup> Even though the mesophilic *IsPETase* shows its highest PET hydrolysing activity at ambient temperatures it has been widely subjected to protein engineering to improve its thermostability. A structure-based engineering strategy discovered a ThermoPETase mutant (*IsPETase* S121E/D186H/R280A) with an 8.8 °C higher  $T_m$  and up to 14-fold higher PET-hydrolyzing activity at 40 °C than the wild-type *IsPETase*.<sup>[82]</sup> Cui et al. used a novel GRAPE (greedy accumulated strategy for protein engineering) computational method to design DuraPETase, a variant with a 31 °C higher  $T_m$  and 300-fold improved PET hydrolysis activity than the wild-type enzyme.<sup>[83]</sup> More recently, a machine-learning-aided approach was used to engineer *IsPETase* to produce Fast-PETase, a variant with a  $T_m$  of 67.1 °C and improved depolymerization efficiency

against low-crystallinity PET waste at 50 °C.<sup>[84]</sup> At least one of their computationally targeted stability-related hotspots was discovered while screening a randomised *IsPETase* library based on an error-prone polymerase chain reaction (ePCR) (**Article II**).<sup>[65]</sup> Other protein engineering strategies have found additional substitutions related to thermostabilizing *IsPETase* that are distributed across the entire sequence. Another recent study evaluated over 13,000 *IsPETase* variants using catalytic activity at elevated temperatures as a primary selection pressure. This procedure resulted in a HotPETase variant with 21 mutations compared to wild-type *IsPETase* and a  $T_m$  of 82.5 °C.<sup>[85]</sup> Accordingly, the thermostability of *IsPETase* and other homologous enzymes is dependent on the interaction of numerous effects, e.g. the flexibility of the protein, necessitating additional comprehensive research.

Besides these bacterial PET hydrolases, HiC from *Thermomyces insolens*, a prominent member of the fungal PET hydrolase family, drew attention since its commercialisation, but with the focus on process engineering rather than protein engineering.<sup>[64,86–88]</sup>

### 1.3.2 Proposed Mechanism of the Interfacial Enzymatic PET Hydrolysis

Enzymatic PET hydrolysis is a surface erosion process that exposes the inside of the material by primarily degrading the exterior polymer.<sup>[59,64,89]</sup> The number of accessible ester bonds is limited since neither the biocatalyst nor water (as a solvent and a reactant) can penetrate the inner core of the polymer, implying that the reaction takes place primarily in the presence of an excess of enzyme.<sup>[90]</sup> As a result, research on PET hydrolysis kinetics has frequently used an inverse Michaelis-Menten equation<sup>[91–93]</sup> or its mathematically equivalent expression based on the derivation of the Langmuir adsorption isotherm.<sup>[94–97]</sup> The accessible enzyme attack sites on the PET surface can be calculated based on the ratio of parameters derived from the conventional and inverse Michaelis-Menten kinetics.<sup>[91,93]</sup>

Various biophysical approaches, such as fluorescence,<sup>[98]</sup> chemiluminescence,<sup>[99]</sup> and quartz crystal microbalance<sup>[99–101]</sup> were used to investigate the degradation-relevant binding of these PET hydrolases and variants. Based on the concentrations of free enzymes in the supernatant after incubation with PET binding isotherms could be directly assessed.<sup>[100–102]</sup> Selected PET hydrolases were found to have a high affinity for the PET surface, as evidenced by the rapid formation of a monolayer, though this was thought to

be primarily due to nonspecific adsorption.<sup>[104]</sup> A related kinetic study stated that PET polymers were hydrolysed at a much slower rate than PET oligomers, with no regard to their water solubility.<sup>[93]</sup> Conversion rates of the oligomers in the same range as small-molecule *p*-nitrophenol esters indicate that the complexation or dissociation with the degradable polyester strands necessitates large activation barriers which determine the overall conversion rate rather than the chemical catalysis itself.<sup>[92]</sup> Quantum mechanics/molecular mechanic (QM/MM) MD simulations or adiabatic mapping mimicking polyester degradation were applied to study the hydrolysis reaction mechanism of several PET hydrolases.<sup>[105–108]</sup>

So far, only four studies including **Article I** have reported crystal structures soaked with PET analogues.<sup>[76,109–111]</sup> Hence, studies on the substrate interaction in the binding groove as well as with the catalytic triad of various PET hydrolases were almost solely done by molecular docking of oligomeric aromatic esters.<sup>[32,43,112–115]</sup> The combination of both facilitates more precise computational simulations to elucidate the mechanism of enzymatic depolymerisation as well as predicting more efficient mutants.

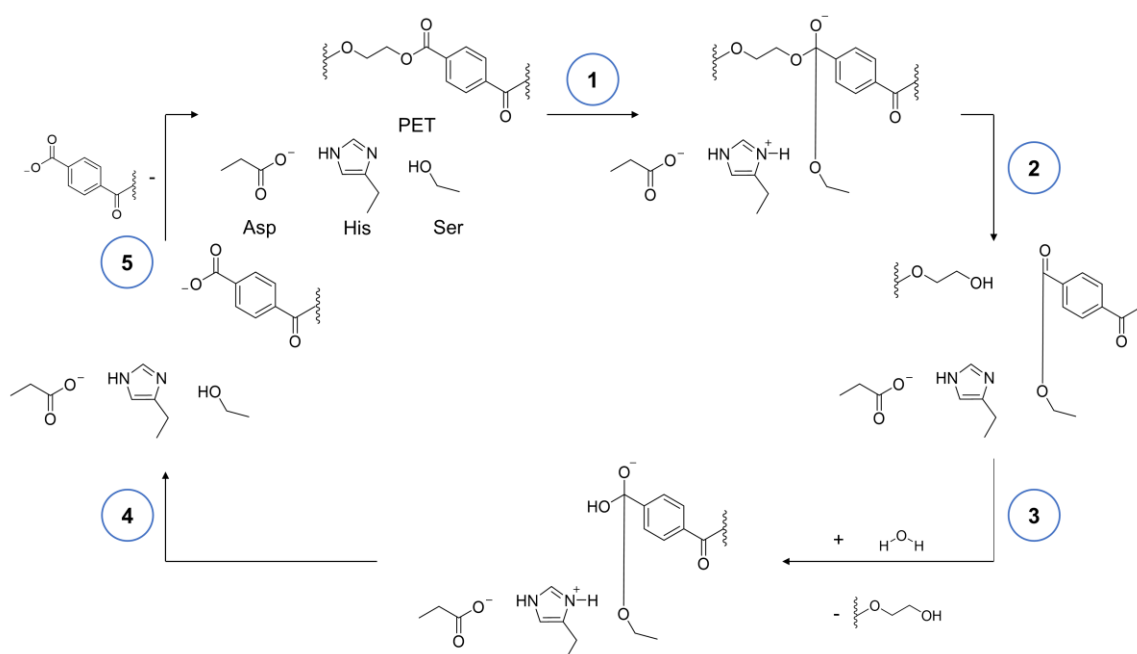


**Figure 4.** Proposed mechanism of the interfacial biocatalytic hydrolysis of PET. A nucleophilic attack by the catalytic serine results in a tetrahedral intermediate (1) stabilized by a catalytic histidine, an aspartic acid, and the oxyanion hole, followed by breakdown of the tetrahedral intermediate (1) into an acyl enzyme intermediate and the release of an alcohol (2). The aspartate histidine pair activates the water for attack on the carbonyl acyl enzyme intermediate, resulting in the formation of the second tetrahedral intermediate (3). The carboxylic acid product is produced by deacylation of this tetrahedral intermediate (4). The hydrolysed PET unit leaves the active site and a new PET molecule can enter (5). The initial nucleophilic attack is regarded as the rate-limiting step. The figure was adapted with permission from Wei et. al.<sup>[60]</sup>

In close proximity to the catalytic triad, the protein surface landscapes of bacterial PET hydrolases are comparable, requiring a high conformational selectivity of accommodated PET repeating units directly around the target ester bond at favoured twisting angles.<sup>[32,51,115]</sup> In contrast, whether distal PET repeating units are involved in a catalysis-related interaction with additional surface residues that requires a long PET strand to adopt a specific conformation is unclear and unlikely.<sup>[77,115]</sup> Nonetheless, to form the productive tetrahedral intermediate via the initial nucleophilic attack by the catalytic serine, the defined polymer segment conformation directly next to the target ester bond will necessitate a steric reconfiguration of the polymer chains with adequate mobility.<sup>[77]</sup> The highest activation free energy barrier determined by QM/MM adiabatic mapping suggests that the nucleophilic attack is a likely rate-limiting step (Figure 4).<sup>[105,107]</sup> According to recent findings in kinetic studies, the PET hydrolysis mechanism's subsequent reaction steps are canonically the same as for other conventional ester hydrolases.<sup>[93]</sup>

However, how the adsorption and desorption of biocatalysts onto the polymer surface influences the overall degradation performance and kinetics is not yet fully understood.

### 1.3.3 High-Throughput Screening Methods

The increasing number of new PET hydrolases discovered from natural resources such as metagenome libraries and via protein engineering efforts necessitates the development of high-throughput (HT) screening tools for their rapid characterisation. Several attempts have been made to adapt traditional analytical methods<sup>[5,116,117]</sup> to HT screening scenarios for characterising PET hydrolysis activity (Figure 5).

An efficient strategy to increase the speed of the enzymatic hydrolysis of PET is to increase the specific surface area of the polymer substrate, for example by using PET-NP with diameters in the nano (<100 nm) to submicron (100-1000 nm) range as substrates.<sup>[65,92,110,118-124]</sup> Due to the Tyndall effect, which causes significant scattering of the incident light through the PET-NP suspension, changes in PET-NP size and concentration caused by the hydrolysis can be measured by tracking the change in turbidity at 600 nm.<sup>[120,125]</sup> As many PET hydrolases require higher concentrations of buffer to maintain their activity, PET-NP may precipitate at high temperatures and cause errors in specific turbidity measurements. This problem can be solved by immobilising the NP as well as the reaction system in polyacrylamide gels, thereby improving the reproducibility of the measurements. By performing the immobilisation technique in 96-well plates, the throughput of the characterisation for the enzyme screening and kinetic analysis can be

enhanced. A similar approach can be used to characterise and screen the enzymatic hydrolysis of small molecule substrates, e.g. BHET, and other polymers such as poly(butylene succinate-co-adipate),<sup>[126]</sup> polycaprolactone (PCL)<sup>[121]</sup> and Impraniil® DLN-SD,<sup>[65,127]</sup> a commercial polyester-based polyurethane dispersion. In contrast to microtiter plate-based assays, agar plate-based assays have a much higher throughput (Figure 5A). By adding 0.4 % to 0.5 % (w/v) polyester NP to agar plates, colonies with high polyester hydrolytic activity can be screened turbidimetrically. The secretion of active hydrolases leads to the formation of clear halos around the colonies.<sup>[118]</sup> This method allows the screening of millions of clones per week. Due to the high price of HFIP used in the PET-NP preparation<sup>[92,120,128–130]</sup> Impraniil® and PCL dispersions are often used as a readily and inexpensive alternative.<sup>[118,131,132]</sup> Notably, enzymes and strains screened with these alternative substrates usually have strong aliphatic polyester hydrolysis activity, but not necessarily show sufficient PET hydrolysis activity. Therefore, further activity validation on PET substrates is required. Recently, Charnock addressed this issue by preparing PET-agar plates by dissolving PET in dimethyl sulfoxide (DMSO) at 180 °C and rapidly adding pre-warmed low concentration top agar,<sup>[133]</sup> which ensures the direct screening of PET hydrolytic activity and effectively controls costs. The trade-off between the  $T_{opt}$  for the enzymatic hydrolysis ( $T_{opt} > 50$  °C) and the optimal growth temperature for the microorganisms ( $\leq 40$  °C) is currently the bottleneck limiting the application of this method.

The most common method for the quantitative analysis of the PET hydrolysis products TPA, MHET and BHET is high performance liquid chromatography (HPLC).<sup>[134,135]</sup> According to the Lambert-Beer law, the measurement of the absorbance values in the wavelength range of 240-244 nm<sup>[136]</sup> can be used to calculate the sum of these products, which can be converted into a total equivalent of TPA production to characterise the hydrolase activity.<sup>[43,65,84,126,137]</sup> High throughput of this approach can be achieved by using UV-transparent microtiter plates.<sup>[103]</sup> The main advantage of this method is that no treatment of the soluble hydrolysis products is needed, only the separation from the PET substrate and other non-water soluble products. However, the accuracy of this method is greatly reduced if other soluble UV absorbing compounds, e.g. a large number of proteins or DMSO, are present.<sup>[136,138]</sup> A possibility to reduce the influence of other non-specific products on the results is to measure at a wavelength of 260 nm as previously shown. As MHET and TPA are hydrolysis products with free carboxyl groups, the pH of the reaction system continuously decreases when PET enzymatic degradation is performed in low concentration buffer solutions.<sup>[134]</sup> The change in pH can be monitored by adding acid-basis indicators, e.g. bromothymol blue or phenol red, and quantified by the numerical changes in the UV/Vis absorption spectra.<sup>[139,140]</sup> Colour changes help to observe the

degradation progress and compare the activity of different PET-hydrolysing enzymes.<sup>[140,141]</sup> The addition of acid-base indicators to agar immobilised with PET or other polyester NPs allows for rapid solid-phase screening of microorganisms expressing hydrolytic enzymes.<sup>[142]</sup> The diffusion of acidic reaction products lowers the pH around the colony and changes the colour of the dye thereby aligning the radius of the coloured halo with the expression level and activity of the enzyme, resulting in an improved sensitivity of the normal clear halo assay.

A more sensitive detection method than absorbance is fluorescence and therefore, is suitable for the detection of lower concentrations of hydrolysis products (Figure 5B). As TPA, MHET and BHET do not directly produce fluorescence, pretreatment methods are required. The reaction of terephthalate with hydroxyl radicals produces 2-hydroxyterephthalate (2-HOTP), which exhibits a stable fluorescence at 421 nm.<sup>[129,143]</sup> Initially, the hydroxylation of TPA was achieved by reacting with a high percentage (35%) of hydrogen peroxide at 90 °C for 30 min.<sup>[138]</sup> Thus, this procedure was unwieldy to be applied in HT screening. This obstacle was later resolved by a Fenton-like chemically mediated TPA fluorescence assay<sup>[123]</sup> which was established as a HT method in **Article III**.<sup>[128]</sup> Advantageously, this fluorescence assay specifically detects TPA because neither MHET nor BHET react with hydroxyl groups to produce fluorescence. Furthermore, proteins present in the reaction supernatant do not interfere with the fluorescence reaction ensuring the direct detection.<sup>[123]</sup> Recently, a coupled ketoreductase-diaphorase fluorimetric assay based on EG for the analysis of PET hydrolysis activity was described.<sup>[144]</sup> A ketoreductase (KRED) oxidises EG, MHET or BHET to the corresponding aldehyde using nicotinamide adenine dinucleotide phosphate (NADP<sup>+</sup>) coenzyme II as cofactor. Subsequently, the diaphorase from *Clostridium kluyveri* re-oxidises NADPH to NADP<sup>+</sup>, simultaneously catalysing the reduction of resazurin to the highly fluorescent resorufin (580 nm) with excitation in the visible light range (550 nm).<sup>[144]</sup> Due to the high sensitivity and poor linearity for MHET and BHET detection in the low concentration range and the complex and relatively long reaction steps this method is less advantageous than the TPA-based fluorescence assay. In addition, the low specificity of KRED for EG limits the specific detection of EG in presence of large amounts of MHET and BHET. Qiao et al. reported a fluorescence-activated microfluidic droplet sorting method for the isolation of PET-degrading microorganisms (Figure 5C).<sup>[145]</sup> Individual cells are encapsulated in droplets and incubated for several days to express enough PET hydrolase. The fluorogenic surrogate fluorescein dibenzoate is then injected into the droplets and cells expressing active hydrolase convert the model substrate into fluorescein, thus enabling fluorescent droplet sorting. Fluorescein dibenzoate has long been synthesised and applied



as a typical lipase substrate.<sup>[146]</sup> Due to the low selectivity of fluorescein dibenzoate to specifically identify PET hydrolases, the use of the substrate may be more likely to isolate false positive strains with only typical lipase activity.

According to recent research, developing biosensors that target the PET hydrolysis product TPA might be a suitable approach to achieve ultra-HT screening.<sup>[60]</sup> Bioengineered biosensor systems, such as transcription factors (TFs), riboswitches, and enzyme-coupled sensor devices, have been widely used to detect small molecules. In the last two years, specific biosensors targeting TPA have been reported in literature.<sup>[147–149]</sup> To assess the translocation of TPA in the genetically modified *Acinetobacter baylyi* ADP1 strain, a biosensor consisting of the TF *Comamonas testosteroni* TphR and a fluorescent reporter system (superfolder green fluorescent protein (sfGFP)) was specifically designed (Figure 5D).<sup>[147]</sup> The binding of TphR to TPA initiates the transcription of a cluster of genes related to the TPA metabolism in the strain, which allows for the conversion of TPA to protocatechuate.<sup>[150]</sup> To screen mutant strains for the efficient uptake of TPA in the environment fluorescence-activated cell sorting (FACS) was performed. Combining the biosensor with an ADP1 mutant optimised for an enhanced TPA uptake may help to establish a fast and HT screening protocol for PETase and MHETase genes in large mutant or macrogenomic libraries.<sup>[147]</sup> Li et al. published another TPA-biosensor, recently.<sup>[148]</sup> They constructed mutants specifically binding phthalate (PA) and TPA, respectively, through directed evolution of a TF with promiscuous binding capacity, XylS from *Pseudomonas putida*, and activating the downstream expression of sfGFP (Figure 5D). Based on these components, whole-cell biosensors were developed that allow for the fluorimetric detection of as little as 10  $\mu$ M PA or TPA. Currently, the only biosensor capable of directly detecting TPA is a LuxAB-based biosensor system (Figure 5E).<sup>[151]</sup> This biosensor combines a carboxylic acid reductase from the marine bacterium *Mycobacterium marinum* (CAR<sub>Mm</sub>) and luciferase from *Photobacterium luminescens* (LuxAB) to provide a tool for the rapid characterisation of PET hydrolases and the detection of TPA. This biosensor system is part of the results and will therefore be explained in detail in **Article IV**. Although all three biosensors hold great promise for the HT screening of TPA-producing enzymes in large mutant libraries, none was directly validated by screening actual real mutant libraries indicating that they all need further optimisation for different experimental purposes in future practical applications. Similar biosensors need to have different sensitivities for different application scenarios. For example, screening environmental macrogenomes necessitates highly sensitive biosensors, whereas screening to build a targeted evolutionary library of known PET

hydrolases, may result in the discovery of highly active enzyme mutant more quickly using less sensitive biosensors.

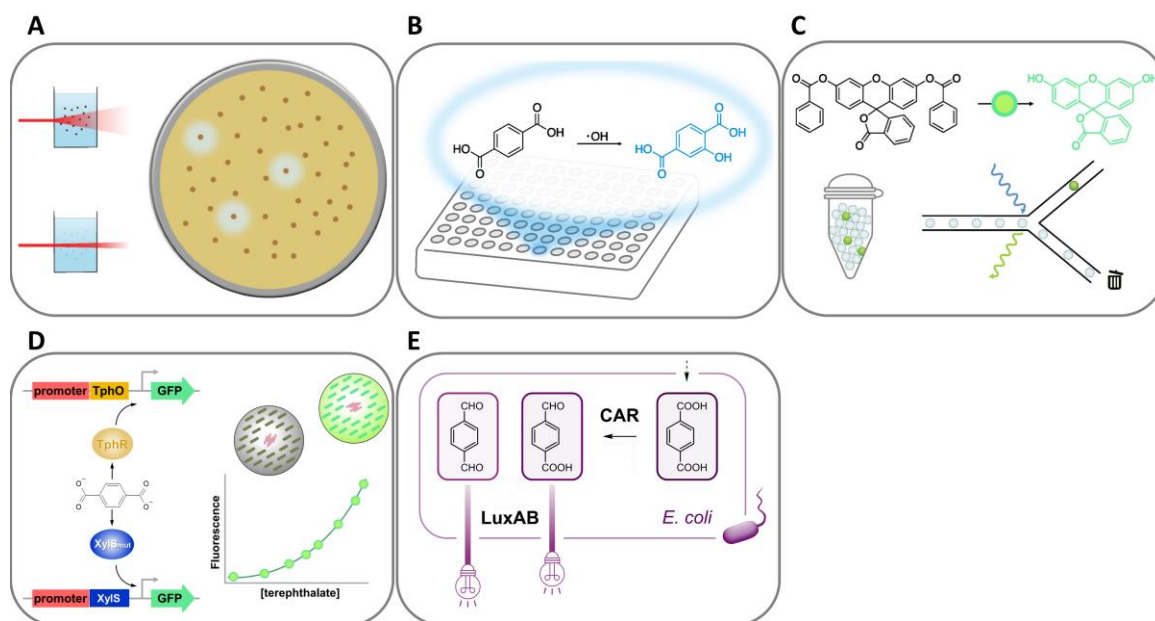


**Figure 5.** HT screening methods to identify potential PET hydrolases. (A) Agar plate assay based on PET-NP hydrolysis. Clear zones (halos) form around clones expressing active polyester-hydrolyzing enzymes, making identification simple. Using this method, millions of clones can be easily screened. (B) Fluorimetric assay based on the radical hydroxylation of TPA to the fluorophore 2-HOTP. Tens of thousands of clones can be screened using microtiter plate-based assays. (C) Fluorescence-activated ultra-HT microfluidic droplet assay. PETase activity was recently measured using an ultra-HT droplet-based assay. The use of the fluorogenic surrogate substrate fluorescein dibenzoate indicates a low selectivity, as this assay would identify many other esterases. (D,E) Ultra-HT assay based on TPA sensors. Cells could be entrapped in hydrogel beads<sup>184</sup> containing reporter cells that express GFP in response to the formation of terephthalic acid by clones expressing reporter active PET-hydrolyzing enzymes. Because the beads can be sorted using FACS, the throughput of this method could be in the hundreds of millions. (D) The XylS- and TphR-based biosensors which are coupled with the fluorescent reporter gene sfGFP allow the indirect analysis of TPA formation. (E) The LuxAB-based biosensor is the only system that is capable of directly monitoring the TPA formation. The figure was adapted and modified with permission from Wei et al.<sup>[60]</sup> and Bayer et al.<sup>[151]</sup>

Most of the reported HT screening protocols for PET hydrolases are based on model substrate deformation, e.g. turbidimetric detection of NP degradation, or hydrolysis product generation, e.g. UV/fluorescence spectrophotometry, and their feasibility has mostly been demonstrated on a small scale. If the benefits of these current methods can be re-integrated, it is expected that effective HT screening methods will be established in a short time. Optimised PET-NP-based agar plate assays, for example, in combination with the use of acid-base indicators, could achieve the goal of screening millions of clones in a short period of time, contributing to the discovery of novel PET hydrolase backbones from environmental macrogenomes. Furthermore, improved biosensors based on the

terephthalate roots that allow cells from engineered strains of *E. coli* or other model organisms to grow with TPA as the sole carbon source could aid in the development of ultra-HT assays based on growth selection,<sup>[147,152]</sup> which would greatly facilitate progress in the development of efficient PET hydrolases. As the most efficient PET hydrolases are derived from thermophilic strains or high temperature environments, adapting thermostable enzymes will be a challenge for the development of future biosensor screening methods.

## 1.4 Protein Engineering

Enzymes isolated from nature are often not suitable for industrial applications due to their low affinity, activity, selectivity, and stability.<sup>[153–156]</sup> Therefore, protein engineering is a central aspect of customising and improving desired enzyme properties, e.g. thermal stability, and adapting the biocatalyst for specific applications.<sup>[154–156]</sup> Besides altering the structure of an existing protein, the design of biocatalysts from scratch via *de novo* design<sup>[157,158]</sup> and random sequence libraries<sup>[159]</sup> is possible. Furthermore, protein engineering largely contributes to the understanding of enzyme functions.<sup>[160–162]</sup> The protein engineering typically consists of three steps. After selecting the engineering strategy, changes are implemented into the target protein by mutagenesis and the protein variants are evaluated for improved properties by selection or screening.<sup>[160]</sup> Depending on the amount of accessible information about the protein, including its class, structure, reaction mechanism, different engineering strategies (directed evolution, rational design or a combination of both methods) can be applied.<sup>[154,160,163]</sup>

When no structural or mechanistic information are available mutations are randomly introduced into the target gene sequence, e.g. by ePCR<sup>[164–166]</sup> or DNA shuffling,<sup>[167]</sup> generating a diverse and large sequence library. If multiple rounds of selection and mutagenesis are involved in the screening process, thereby mimicking natural evolutionary processes, the method is called directed evolution. To screen these large libraries, robust and reliable HT assays, which are described in detail in chapter 1.3.3, as well as screening platforms, such as FACS,<sup>[160,168]</sup> microfluidics<sup>[169]</sup> or a fully automatic robotic system<sup>[170]</sup> are highly required. Machine-learning-guided methods have recently been shown to accelerate the directed evolution of proteins thereby overcoming the limits of this technique.<sup>[171]</sup>

In contrast, rational design necessitates detailed knowledge about the structure-function relationship of the protein. X-ray crystallography, nuclear magnetic resonance

spectroscopy and cryoelectron microscopy enabled the development of the large amount of protein structures currently available.<sup>[172,173]</sup> The combination with databases, such as 3DM<sup>[174]</sup> or BLAST,<sup>[175]</sup> and steadily improving molecular modelling softwares to identify hotspots, tunnels, motifs and reactions, such as FireProt,<sup>[176,177]</sup> Caver,<sup>[178,179]</sup> HotSpot Wizard,<sup>[180,181]</sup> FRESCO,<sup>[182]</sup> Rosetta or QM/MM calculations,<sup>[154,174,183]</sup> enables the generation of smaller and smarter enzyme libraries, significantly reducing screening efforts.<sup>[163]</sup> A recent breakthrough in deep-learning-based prediction of protein structures from their amino acid sequence via artificial intelligence will enable scientist to rationally design proteins, which are extremely difficult to crystallise, in the future.<sup>[184]</sup> Often, a combination of directed evolution and rational design is used which is known as semi-rational design, thus incorporating the benefits of both strategies to generate smart and small enough libraries which can be easily screened.<sup>[185,186]</sup>

## 2 Results and Discussion

### 2.1 Characterisation and Engineering of PET Hydrolases

#### 2.1.1 Multiple Substrate Binding Mode-Guided Engineering of a Thermophilic PET Hydrolase (Article I)

As discussed in chapters 1.3.1 and 1.3.2 identifying and/or engineering thermophilic PET hydrolases as well as understanding the mechanism of PET hydrolysis are crucial steps towards the efficient hydrolysis of PET in its monomeric compounds TPA and EG. Since LCC ICCG<sup>[42]</sup> is currently the only enzyme capable of depolymerising amorphized PET waste on industrial scale the search for alternatives is of great importance.

The highly thermophilic and active metagenome-derived PET hydrolases PES-H1 and PES-H2 were recently disclosed in a patent application.<sup>[187]</sup> As part of this thesis, crystal structures of the metagenome-derived thermophilic enzymes PES-H1 and PES-H2 (PDB codes: 7CUV, 7W69) were solved in collaboration with the groups of Prof. Weidong Liu at the Tianjin Institute of Industrial Biotechnology and the University of Chinese Academy of Sciences in Beijing, Dr. Gert Weber at the Helmholtz-Zentrum Berlin für Materialien und Energie, and Prof. Dr. Lammers at the Institute of Biochemistry, revealing a typical  $\alpha/\beta$ -hydrolase fold with a core consisting of nine  $\beta$ -sheets and ten  $\alpha$ -helices. The catalytic triad is composed of S130, H208 and D176 and a conserved disulfide bridge (C241/C256).

Additionally, crystal structures in complexes with the PET monomer analogous 4-(2-hydroxyethylcarbamoyl) benzoic acid (MHETA) (PDB codes: 7W6C, 7W6O, 7W6Q) and BHET (PDB code: 7W66) were solved to investigate the mechanism of the interfacial PET hydrolysis. These complex structures allowed the identification of six intermediate ligand binding modes (IBMs) as well as several key residues including W155 (Figure 6B-D,F,G), F62 (Figure 6B-D,G), I178 (Figure 6E) and L209 involved in the PET binding (Figure 6). In comparison to the structures of LCC ICCG S165A in complex with MHET<sup>[76]</sup> (PDB code: 7VVE, Figure 6H) and *Is*PETase R103G/S131A in complex with 1-(2-hydroxyethyl) 4-methyl terephthalate (HEMT)<sup>[109]</sup> (PDB code: 5XH3, Figure 6I), which were the only two co-crystallisation structures until now, the PES-H structures revealed multiple noncatalytic IBMs (Figure 6A-G) due to the distance of the ester bonds (or amide bonds in MHETA) and the catalytic S130 restricting the nucleophilic attack. This lends support to the previous hypothesis that PET hydrolysis may involve dynamic reorientation of polymer chains in PET hydrolase active sites.<sup>[77,188]</sup> The presence of multiple IBMs

suggests that the inhibitory degradation intermediates, MHET and BHET,<sup>[55,56]</sup> are more likely to reside in the substrate-binding groove, where they may prevent productive binding of polyester segments. During biocatalysis, the conformational flexibility of predominantly hydrophobic residues surrounding the active site may aid in the recognition and binding of bulky PET substrates. Computational modelling using MD simulations supported the previous observations and identified further hotspots including L92 and Q94.

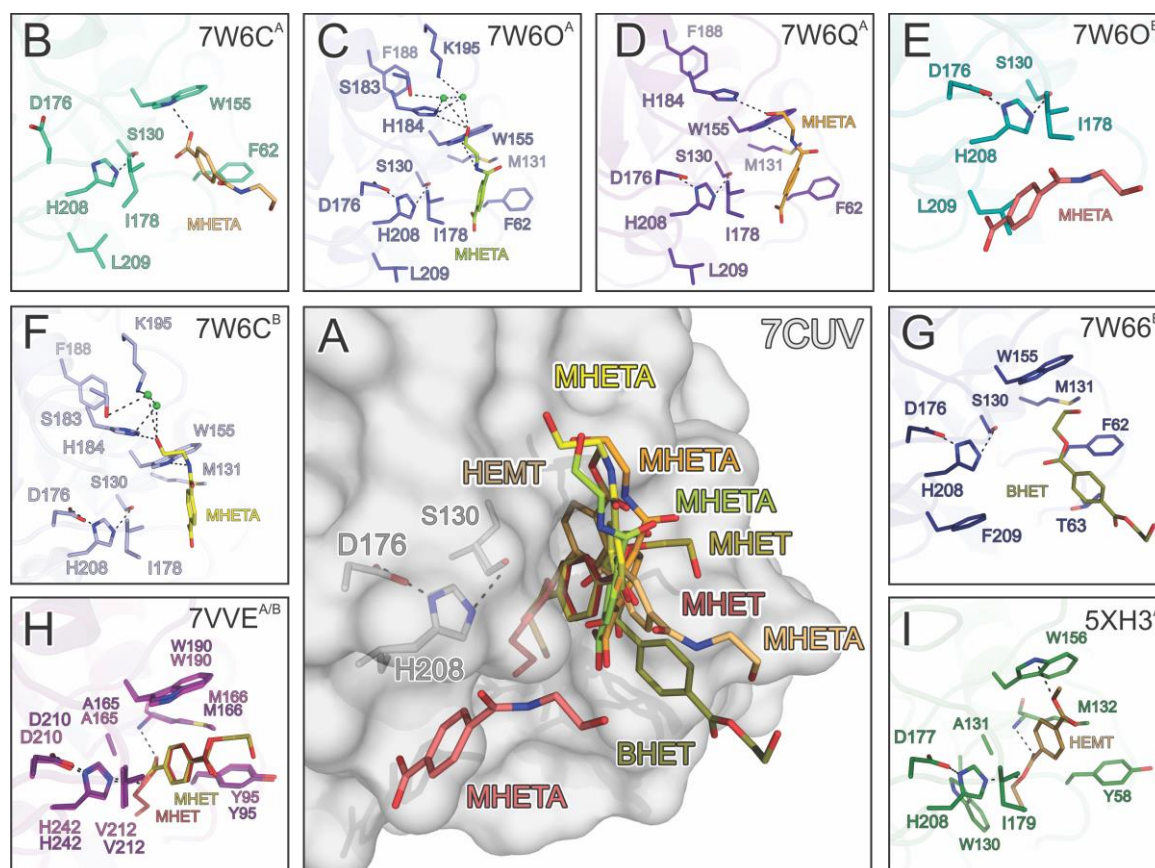


**Figure 6.** Comparison of the PET substrate analogue binding modes in structures of PES-H1, PES-H2, LCC ICCG S165A and *IsPETase* R103G/S131A. Single chains (superscripts for chain A or chain B) were extracted from the deposited structures in the PDB database to identify individual binding modes of the soaked ligands within an asymmetric unit. Dashed lines indicate hydrogen bonds (H-bond cut off of 3.5 Å). Interacting residues are shown as sticks and are colored by element: carbon, as for the respective molecule; nitrogen, blue; oxygen, red; sulphur, yellow. Green spheres represent water oxygens. (A) Superimposed structures show the overlapping binding modes of the substrate analogues with the apo structure of PES-H1 (PDB code: 7CUV). (B–F) PES-H1 in complex with MHETA: (B) 7W6C<sup>A</sup>; (C) 7W6O<sup>A</sup>; (D) 7W6Q<sup>A</sup>; (E) 7W6O<sup>B</sup>; and (F) 7W6C<sup>B</sup>. (G) PES-H2 in complex with BHET (7W66). (H) LCC ICCG S165A in complex with MHET (7VVE<sup>A</sup>, 7VVE<sup>B</sup>). (I) *IsPETase* R103G/S131A in complex with HEMT (5XH3). The figure was copied from Pfaff et al.<sup>[110]</sup>

To improve the thermostability and activity of PES-H1 29 variants were created, based on the above structural analyses and engineering strategies previously discussed in literature<sup>[43,70,75,83,112,136,189]</sup> and in chapter 1.3.1., and analysed for improved thermostability and PET hydrolase activity (Figures 7 and 8). Although several variants showed a higher

$T_m$  than the wild-type, only the variants L92F/Q94Y and R204C/S250C displayed a higher  $T_m$  and could almost completely depolymerise Goodfellow (Gf)-PET film after 24 h at 72 °C,  $T_{opt}$  of the reference enzyme LCC ICCG (Figure 7).

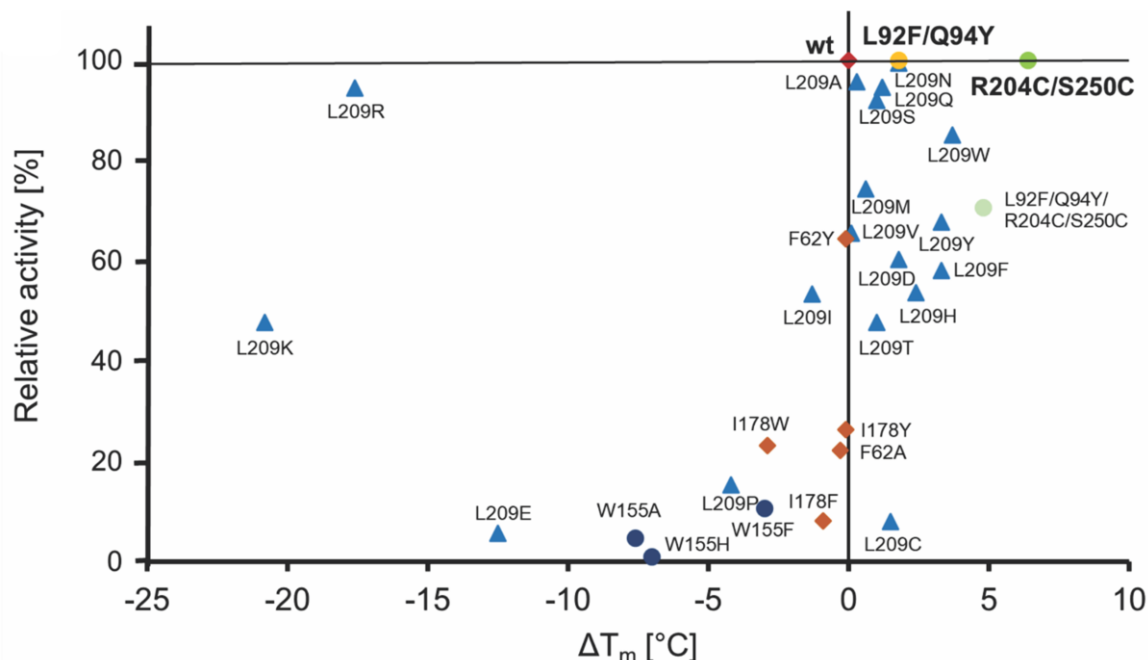


**Figure 7.** Comparison of various PES-H1 variants regarding their thermostability and activity. Changes in  $T_m$  compared to the wild-type enzyme ( $\Delta T_m$  (°C)) are shown. The percentage relative activity compared to the wild-type enzyme was calculated based on the weight loss of Gf-PET film after 24 h at 72 °C. Red square: wild-type PES-H1. Blue triangles: L209 variants. Orange squares: I178 and F62 variants. Dark blue dots: W155 variants. Light green dot: L92F/Q94Y/R204C/S250C variant. Green dot: R204C/S250C variant with a disulfide bond introduced. Yellow dot: L92F/Q94Y variant. The figure was adapted from Pfaff et al.<sup>[110]</sup>

Accordingly, the hydrolytic activity of the variants L92F/Q94Y and R204C/S250C as well as the wild-type and LCC ICCG was further examined using lcPET and high-crystallinity PET (hcPET) powder and PET-NP (Figure 8). The amorphized PET powders were obtained by a melt-quenching technique resulting in crystallinities of 33% and 26%, respectively, after crushing and ball milling. Since the L92F/Q94Y variant and the wild-type completely degraded Gf-PET film in 1 M potassium phosphate buffer (pH 8.0) within 24 h at 72 °C, the weight loss was additionally calculated after 12 h (Figure 8A). The L92F/Q94Y variant resulted in a 2.3-fold higher weight loss (37.1 mg, 62.4%) than the wild-type thereby exceeding the R204C/S250C variant as well as the LCC ICCG. These results were also visible in the hydrolysis of lcPET powder (13% crystallinity) (Figure 8B) with a 2.9-fold and 2.3-fold higher product release for the L92F/Q94Y variant than the wild-type and LCC ICCG, respectively. Therefore, PES-H1 L92F/Q94Y was identified as the most active lcPET hydrolase, under the applied reaction conditions. However, in the hydrolysis of hcPET powder, LCC ICCG outperformed all PES-H1 variants (4-fold more degradation

product) (Figure 8C,D). Nevertheless, L92F/Q94Y was still 3.4-fold more active than the wild-type. In comparison to PES-H1 and its variants, the extent of degradation was inversely related to the crystallinity of the material, which is consistent with previous research on the use of hydrolases to degrade PET with varying crystallinities.<sup>[60]</sup> Further analysis of the PET powders in terms of the weight-average ( $M_w$ ) and number-average ( $M_n$ ) molecular masses revealed that the hcPET powders contained significantly shorter polymers (or even oligomers). This indicates that the activity of PES-H1 and variants is rather influenced by crystallinity than the  $M_n$  compared to LCC ICCG and *vice versa*. The suggestion that the enzymatic hydrolysis of PET may not only be influenced by the crystallinity, but also the average polymer length, was recently confirmed.<sup>[190]</sup>

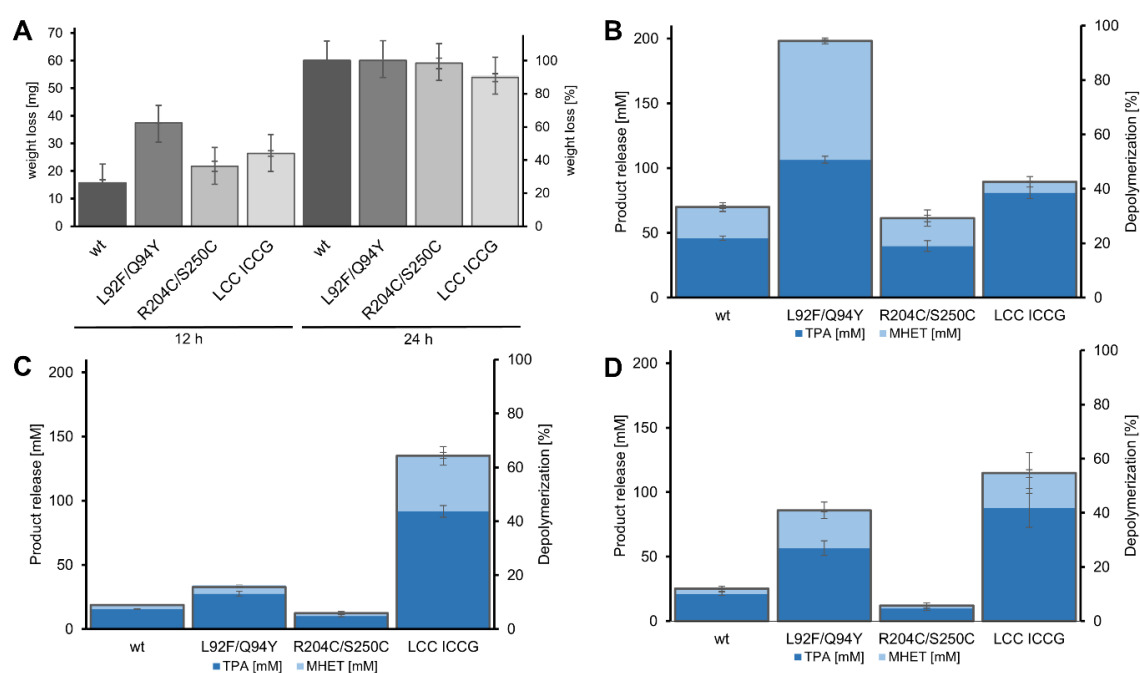


**Figure 8.** Characterisation of PET-hydrolyzing activity of PES-H1 (wt), L92F/Q94Y, R204C/S250C and LCC ICCG. (A) Weight loss (in [mg] and [%]) of Gf-PET film determined after enzymatic hydrolysis at 72 °C for 12 and 24 h in 1 M potassium phosphate buffer (pH 8.0). (B–D) Total product release [mM] is shown and used to calculate the depolymerization efficiency [%] with (B) lcPET powder (13%), (C) ball-milled hcPET powder (26%), and (D) grinder-crushed hcPET powder (33%) after 24 h at 72 C. The total product was defined as the sum of TPA (dark blue), MHET (light blue), and BHET (light grey). Error bars indicate the standard deviation calculated from at least three replicates. The figure was copied from Pfaff et al.<sup>[110]</sup>

Additionally, kinetic parameters evaluated for PET-NP hydrolysis in a turbidimetric assay support the results gained using PET film, lcPET powder and hcPET powder.

In summary, the variants identified in this study hold promise for future applications in biocatalytic plastic recycling.



## 2.1.2 Engineering of mesophilic *IsPETase* for higher thermostability (Article II)

The efficiency of the enzymatic degradation is highly influenced by the crystallinity of the PET material. At temperatures near the  $T_g$  of PET the accessibility of the amorphous fraction is enhanced which allows the attack of thermophilic PET hydrolases with a  $T_{opt}$  near the  $T_g$ . As already mentioned in chapter 1.3.1, the engineering of mesophilic enzymes such as the *IsPETase* is another possibility to create thermostable PET hydrolases with higher thermostability and activity.

Therefore, an ePCR-generated mutant library based on the thermostable triple mutant *IsPETase* S121E/D186H/R280A (TM)<sup>[82]</sup> was created and screened using an agar plate-based assay. The screening of ~52% of the ePCR-based mutant library (~49,000 clones) at 60 °C revealed four mutants with enhanced thermostability, namely TM K95N/F201I, TM S125N/A226T, TM Q119L and TM T51A/S125I/S207I. Characterisation of the  $T_m$  via nano differential scanning fluorimetry displayed TM K95N/F201I as the most thermostable variant with an 5.3 °C increased  $T_m$  of 61.7 °C compared to the TM (Table 1). Following this result, the mutations K95N and F201I were introduced into the previously published thermostable *IsPETase* variants TM N233C/S282C<sup>[136]</sup> (TM2) and DuraPETase<sup>[83]</sup> to identify more thermostable variants. Additionally, the influence of N233C and S282C substitution reported for the TM was studied for the DuraPETase. All variants revealed a higher  $T_m$  than the wild-type and TM (Table 1). Not surprisingly, introducing the mutations N233C/S282C led to the most thermostable variant DuraPETase N233C/S282C with a  $T_m$  of 81.1 °C in this study (Table 1). The introduction of a disulfide bond has shown to be one of the most suitable engineering strategies for thermostability as described in chapter 1.3.1.

**Table 1.** Melting points of selected *IsPETase* variants, which were generated by combining the K95N/F201I substitutions with other previously described *IsPETase* mutants. The table was adapted with permission from Brott et al.<sup>[65]</sup>

	<i>IsPETase</i> variant	$T_m \pm SD$ [°C]	$T_m$ [°C] increase compared to	
			WT	TM
WT	<i>IsPETase</i> WT	45.1 ± 0.1	-	-
TM	<i>IsPETase</i> TM	56.6 ± 1.6	11.5	-
TM1	<i>IsPETase</i> TM K95N/F201I	61.6 ± 0.1	16.6	5.1
TM2	<i>IsPETase</i> TM N233C/S282C	68.2 ± 0.1	23.2	11.6
TM3	<i>IsPETase</i> TM K95N/F201I/N233C/S282C	70.8 ± 0.1	25.8	14.3
D	DuraPETase	75.0 ± 0.1	29.9	18.4
D1	DuraPETase N233C/S282C	81.1 ± 0.1	36.1	24.6
D2	DuraPETase K95N/S121E/F201I/R280A	71.9 ± 0.1	26.9	15.3
D3	DuraPETase K95N/S121E/F201I/N233C/R280A/S282C	78.4 ± 0.1	33.3	21.8

To investigate the PET-hydrolysing activity of the selected variants, PET-NP and Gf-PET film were hydrolysed at different temperatures ranging from 30 °C to 60 °C for 24 h (Figure 9). In most cases, higher incubation temperatures resulted in a higher degradation rate and product release for the thermostabilised *IsPETase* variants, with a significant increase in performance from 30 °C to 40 °C. Better enzymatic degradation performance can be expected as the flexibility of the amorphous polymer chains increases at temperatures close to the  $T_g$  of PET. Low hydrolysis activities of PET-NP were observed for variants containing the K95N and F201I substitutions. The amino acid F201 is found deeply hidden in the hydrophobic core, which also includes positions W97, L101, M157, L199, L230, W257, and M258.<sup>[83]</sup> Since F201I is only five amino acid residues away from the catalytic D206, it is possible that the substitution has a structural influence on the active site. At 60 °C the highest product release was observed with *IsPETase*<sup>TM</sup> N233C/S282C (TM2) with a 15-fold increased relative activity in comparison to the wild-type.

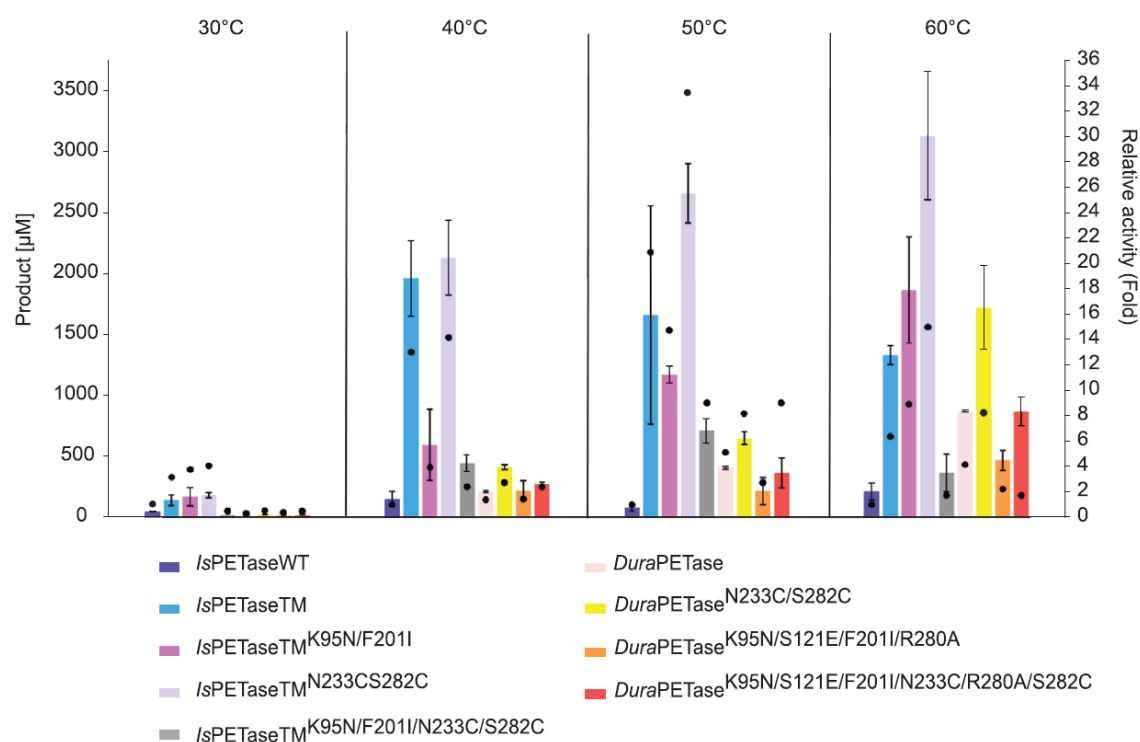


**Figure 9.** Total product release after degradation of PET-NP using selected *IsPETase* variants after 24 h and an incubation temperature of 60 °C. Black dots represent the relative activity compared to wild-type *IsPETase*. Biocatalysis with PET-NP was performed with 30 nM *IsPETase* variant in 50 mM sodium phosphate buffer (pH 7.5) at the incubation temperature of 60 °C and a constant agitation of 1000 rpm for 24 h. A final PET-NP concentration of 0.2 mg mL<sup>-1</sup> was used. The total product release refers to the sum of released MHET, TPA, and BHET. The measurements were performed in triplicates and the mean values and standard deviations are given in the figure. The figure was copied with permission from by Brott et al.<sup>[65]</sup>

Furthermore, the degradation of Gf-PET film was performed at 60 °C for 72 h (Figure 10). All thermostable variants, except for wild-type and D2, show higher relative activities than

the TM. Surprisingly, TM3, which exhibited a strongly reduced relative activity in PET-NP hydrolysis, had one of the highest relative activities compared to WT (120-fold increase, Figure 10) and TM (10 to 20-fold increase). Due to the high thermostability of TM3 and D1 both variants could release the highest product amount thereby showing the advantage of a high  $T_m$  for PET hydrolysis. The loss of enzymatic activity, as demonstrated for *IsPETase* variants containing the K95N and F201I substitution, may be compensated by the increased polymer substrate accessibility at higher  $T_{opt}$ .

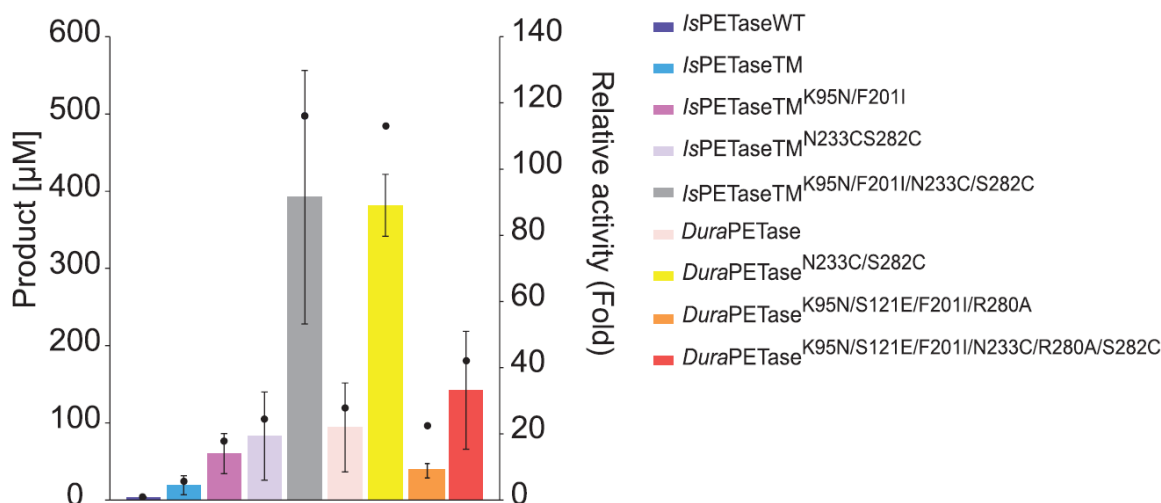


**Figure 10.** Total product release after degradation of amorphous PET film for selected *IsPETase* variants after 72 h at an incubation temperature of 60 °C. Black dots represent the relative activity compared to wild-type *IsPETase*. For biocatalysis with amorphous PET film, an enzyme concentration of 50nM was used. The reaction was carried out in 50 mM glycine-NaOH buffer (pH 9.0). The PET film was incubated at 60 °C and a constant agitation of 1000 rpm for 3 days. The total product release refers to the sum of released MHET, TPA, and BHET. The measurements were performed in triplicates and the mean values and standard deviations are given. The figure was copied with permission from Brott et al.<sup>[65]</sup>

## 2.2 High-Throughput Screening of PET Hydrolase Activity

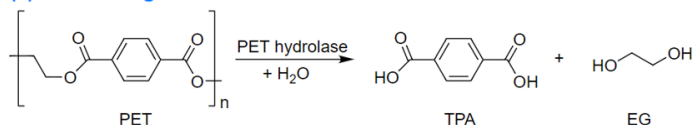
Although most modern HPLC devices are equipped with autosamplers, sequential measurements of the hydrolysis products, TPA, MHET and BHET, are time-consuming and thus complicate the analysis of metagenome and large mutant libraries as discussed in chapter 1.3.3. To overcome this problem rapid HT detection methods must be developed. In this chapter the application of HT screening assays based on fluorimetry, and a biosensor specifically targeting TPA content are described. **Articles III and IV** both provide a proof-of-concept for the identification of novel thermostable PET hydrolases from metagenomes or protein engineering efforts under HT conditions.

## 2.2.1 Fluorimetric High-Throughput Screening in Crude Cell Lysate using PET-NP (Article III)

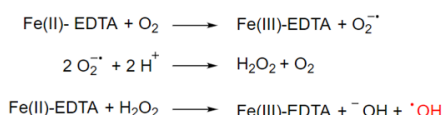
As a result of the fragmentation of larger plastic debris, nanoplastics (<100 nm) are ubiquitous pollutants in natural environments causing a serious risk to human and animal health.<sup>[92,130,191–193]</sup> Consequently, not only investigations on the hydrolysis of PET packaging material in their native form, but also as PET-NPs, are of great importance.

For the preparation of PET-NPs low-crystallinity postconsumer PET packaging material was diluted in HFIP. HFIP droplets containing dissolved PET were rapidly distributed in ultrapure water using an Ultra-Turrax mixer resulting in a homogeneous suspension. To remove large aggregates of the precipitated polymer the PET-NP suspension was filtered, and the volume was reduced to a third of the initial volume using a rotary evaporator, subsequently. Analysis via dynamic light scattering (DLS) and scanning electron microscopy (SEM) revealed an average size of 76.6 nm and the spherical shape of the PET-NP validating this method as a suitable approach for PET-NP generation.

### (1) PET NP degradation



### (2) Fenton-like reaction: formation of hydroxyl radicals



### (3) Hydroxylation of terephthalate to fluorescent 2-hydroxyterephthalate

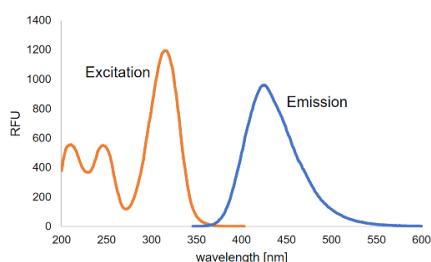
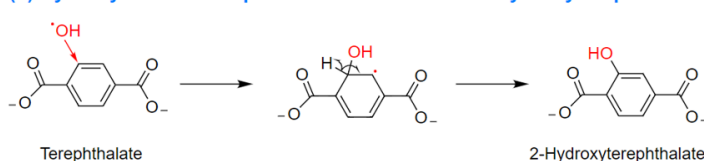


**Figure 11.** Terephthalate was detected fluorimetrically as the PET hydrolysis product. (1) TPA and EG are monomeric products of PET enzymatic hydrolysis. (2) The Fe(II)-EDTA complex mediates the formation of hydroxyl radicals. (3) Terephthalate hydroxylation to fluorescent 2-HOTP in the presence of hydroxyl radicals. The maxima of excitation and emission of 2-HOTP are 315nm and 421nm, respectively. RFU stands for relative fluorescence units. The figure was copied from by Pfaff et al.<sup>[128]</sup> Copyright (2021) Elsevier Inc.

As a proof-of-concept, the PET hydrolysis of the produced PET-NPs was performed at 60 °C for 30 min and 60 min in a 96-well microtiter plate format using crude cell lysates of recombinantly expressed thermophilic PET hydrolase TfCut2 and its inactive variant TfCut2 S130A obtained by a repeated freeze-thaw cycles.

Following the PET-NP degradation, 150  $\mu$ L soluble supernatants were extracted and added to a 96-well microtiter plate to fluorimetrically estimate the release of TPA. This fluorimetric assay was already established by Wei et al. and has demonstrated its high sensitivity in the monitoring of TPA produced by PET using purified TfCut2.<sup>[120]</sup> In alkaline buffer (pH>8.0), TPA appears in its deprotonated form as terephthalate allowing the monohydroxylation into 2-HOTP in the presence of hydroxyl radicals which results in a strong fluorescence signal at 421 nm upon excitation at 315 nm (Figure 11). The hydroxyl radicals were generated by a Fenton-like reaction of the chelator ethylenediaminetetraacetic acid (EDTA) and iron(II) sulphate (final concentration of 625  $\mu$ M) and incubated with the hydrolysis supernatant at room temperature for 10 min prior to the fluorimetric analysis.

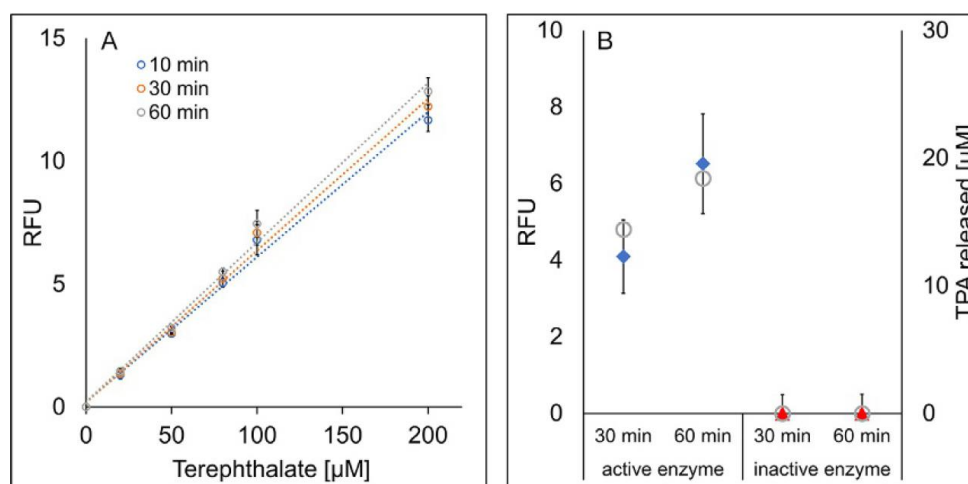


**Figure 12.** Terephthalate concentrations were estimated using fluorimetry. (A) Calibration curves determined using cell lysates after 60 min incubation at 60 °C and subsequent hydroxylation of various terephthalate standards in the presence of Fe(II)-EDTA (0.625mM) at room temperature for 10-60 min. The incubation time with Fe(II)-EDTA had no significant effect, thus 10 min were used for further assay development. (B) An example of identifying hits is a comparison of the RFU determined in the supernatants of enzyme-catalyzed hydrolysis of PET NPs (after 30 and 60 min shaking at 60 °C, respectively). Significantly higher RFU values (blue diamonds) were monitored with the active TfCut2 in good agreement with the terephthalic acid (TPA) amounts determined by reverse phase (RP)-HPLC (grey circles, secondary y-axis) than with the inactive enzyme (red triangles). The standard deviations obtained with at least three independent measurements are indicated by the error bars. The figure was copied from by Pfaff et al.<sup>[128]</sup> Copyright (2021) Elsevier Inc.

The TPA amount in each hydrolysis sample was calculated based on the linear calibration curve ( $R^2 > 0.992$ ) obtained from the TPA standard solutions (Figure 12A). By subtracting the background autofluorescence caused by the TfCut2 S130A, the RFU determined with TfCut2 are in good agreement with the respective reverse phase (RP)-HPLC measurements (Figure 12B).

This validates the applicability of the fluorimetric assay as a HT screening method presented in this book chapter (Figure 13). Furthermore, it allows the rapid identification of possible PET hydrolases by using PET-NP which are more likely to be degraded faster due to their increased specific surface area. Additionally, the use of non-purified enzymes in comparison to purified enzymes in this HT approach is of great advantage since the very cost-intensive HT purification can be avoided.

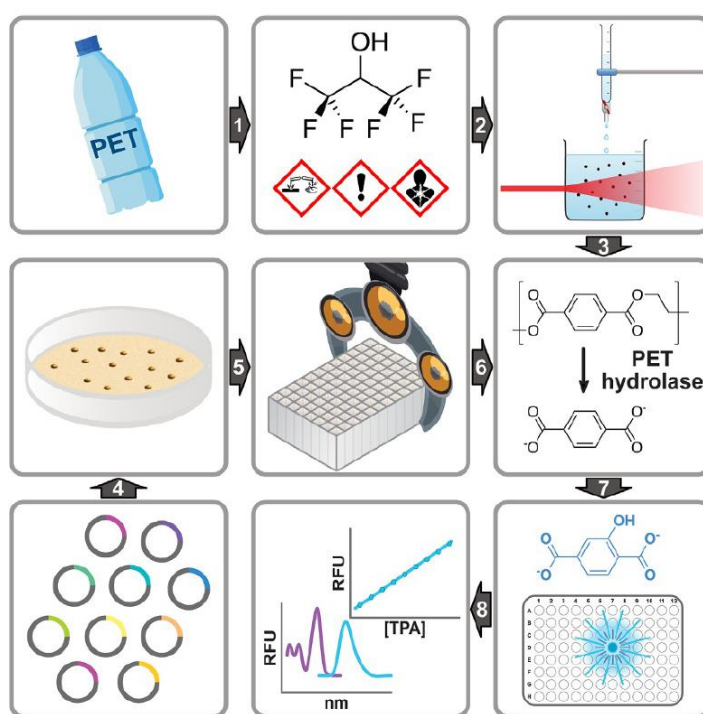


**Figure 13.** The fluorimetric HT screening method is used to detect PET hydrolase activity. (1) Pre-consumer PET is cut and dissolved in HFIP. (2) Dissolved PET is dropped into rapidly stirring ultrapure water, resulting in the formation of nanoparticles that can be identified using SEM and DLS. (3) The NP are ready to use in the enzymatic assays after the solvent has been removed. (4) A plasmid library is transformed into a strain of expression, such as *E. coli* BL21 (DE3). (5) The resulting colonies are used to inoculate 96-deep-well plates for protein expression, after which crude cell lysates are prepared. (6) To test PET-hydrolyzing activity, crude cell lysates are mixed with PET-NP. (7-8) The formation of the product terephthalate is detected by a Fenton-like reaction with hydroxyl radicals. Terephthalate is converted to 2-HOTP and measured using fluorescence (excitation at 315nm and emission at 421nm). The figure was copied from Pfaff et al.<sup>[128]</sup> Copyright (2021) Elsevier Inc.

## 2.2.2 Biosensor-based High-Throughput Screening in Living Cells and Efforts towards a Circular Economy (Article IV)

As described in chapter 1.3.3 developing biosensors specifically assaying the PET hydrolysis product TPA show high potentials for the application as HT methods. Previously, the luciferase LuxAB from *Photorhabdus luminescens*, expressed in *E. coli* K12 MG1655 RARE (*E. coli* RARE), was introduced as a reliable detection method of structurally diverse aldehydes that were synthesised by co-expression of the carboxyl acid reductase CAR<sub>Mm</sub> in living cells in a 96-well microtiter plate format.<sup>[149]</sup> The structural similarity of the synthesised aromatic aldehydes such as benzaldehyde, cuminaldehyde and 2-phenylacetaldehyde (2-PAA) from carboxyl acid substrates to TPA-derived aldehydes, prompted investigations towards the capabilities of CAR<sub>Mm</sub> and LuxAB to detect TPA.

First, resting cells (RCs) of *E. coli* BL21 (DE3) co-expressing CAR<sub>Mm</sub> and a phosphopantetheinyl transferase from *Nocardia iowensis* (PPT<sub>Ni</sub>) were investigated for the possibility of biotransformation of TPA. Although TPA could not be detected in untransformed RCs by gas chromatography equipped with a flame ionization detector (GC/FID) the formation of 4-(hydroxymethyl) benzaldehyde (4-HMBAL) and 1,4-benzenedimethanol (1,4-BDM; 32.7±3.5% combined yields) confirms the activity of CAR<sub>Mm</sub>/PPT<sub>Ni</sub> toward TPA and the possibility of further reduction by endogenous host enzymes. Additionally, whole cell biotransformations with *E. coli* RARE and *E. coli* BL21 (DE3) Δlpp were investigated demonstrating that the bioreduction of TPA with the latter *E. coli* strain is significantly enhanced with a suspension mixture of TPA (31.1±5.9%), 4-carboxybenzaldehyde (4-CBAL) (36.8±9.9%), 4-HMBAL (6.5±2.2%), 1,4-BDM (13.7±5.7%) and traces of terephthalaldehyde (TAL) according to GC/FID (Figure 14A).

As a result, RCs of *E. coli* RARE and *E. coli* BL21 (DE3) Δlpp were prepared expressing only LuxAB or LuxAB together with CAR<sub>Mm</sub>/PPT<sub>Ni</sub>. *E. coli* RARE exhibits lower aromatic aldehyde-reducing activity to prevent the rapid metabolisation of the cytotoxic aldehydes.<sup>[194]</sup> Previously established HT assay conditions were applied for the biotransformation of TPA resulting in bioluminescence in the presence of TPA-derived aldehydes in both *E. coli* strains expressing LuxAB.

The highest fold-increase in bioluminescence was observed in the presence of TAL and 4-CBAL at a final concentration of 1 mM. Both displaying bioluminescence about 8-fold above background in RCs of *E. coli* BL21(DE3) Δlpp after 15 min, followed by 4-HMBAL (4-fold) (Figure 14B). TPA increased the signal of more than 4-fold when LuxAB and

$CAR_{Mm}/PPT_{Ni}$  were co-expressed in the same cell (Figure 14C) but not in RCs that only expressed the biosensor. Similar results were obtained in RCs of *E. coli* RARE but with a drastically higher sensitivity (0.1 mM final concentration) thus preventing the accumulation of high cytotoxic aldehyde concentrations.<sup>[194]</sup>

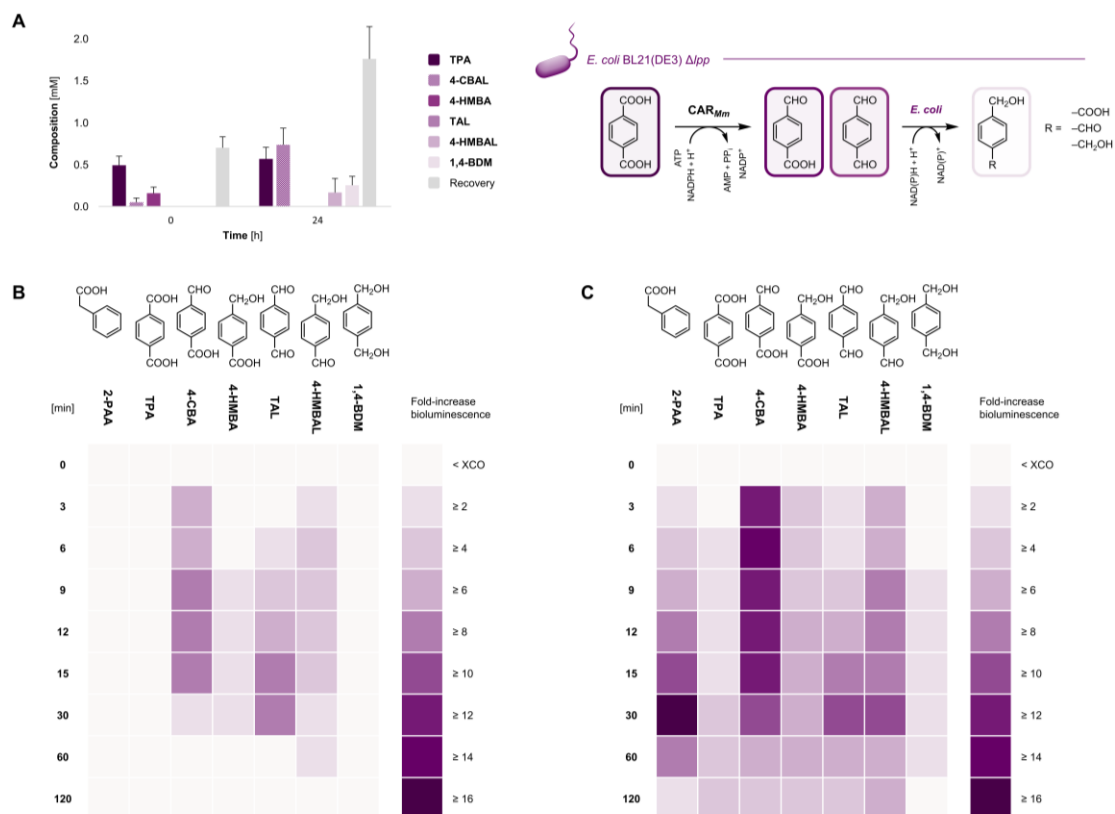


**Figure 14.** Enzyme-coupled biosensor assembly in *E. coli* BL21(DE3)  $\Delta lpp$ . (A)  $CAR_{Mm}$  reduces TPA to 4-CBAL and TAL, which are then further reduced *in vivo* by endogenous enzymes to 4-HMBA, 4-HMBAL, and 1,4-BDM;  $PPT_{Ni}$  for posttranslational modification of  $CAR_{Mm}$  is omitted for clarity. Experiments were carried out in RCs of *E. coli* BL21(DE3)  $\Delta lpp$  (OD<sub>600</sub>~10.0) co-expressing enzymes from pACYCDuet-1/ $car_{Mm};ppt_{Ni}$ <sup>[148]</sup> with 2 mM TPA and 5% (n/n) DMSO as organic cosolvent. 0 h (after TPA addition and mixing) and 24 h sampling. The low solubility of TPA in resting cell medium (RCM) and the volatility of reaction compounds hampered recovery. GC yields are shown as mean values + standard deviation (SD) [mM] of biological replicates (n = 3); (B) Direct detection of aldehydes (1 mM) in RCs of *E. coli* BL21(DE3)  $\Delta lpp$  expressing LuxAB from pLuxAB by increasing bioluminescence over time. (C) *In situ* aldehyde production from carboxylates (1 mM) in *E. coli* BL21(DE3)  $\Delta lpp$  RCs co-expressing LuxAB and  $CAR_{Mm}/PPT_{Ni}$ ; 2-PAA was used as a control. Experiments were carried out under HT assay conditions with 1% (n/n) DMSO, as previously described<sup>[148]</sup>; data are presented as mean fold-increase bioluminescence obtained from biological replicates (n= 3). The figure was copied with permission from Bayer et al.<sup>[151]</sup>

Following these findings, PET hydrolysates of the enzymatic degradation of Gf-PET by LCC, LCC ICCG and PES-H1 were utilised to adapt the LuxAB/ $CAR_{Mm}$  biosensor system under HT conditions for a real-world scenario. In presence of 1 mM TPA, the bioluminescence increased from 5-fold to 17-fold in RCs of *E. coli* RARE within 4 hours.



After 4 hours, bioluminescence signals increased >7-fold in LCC-ICCG samples compared to PET hydrolysates obtained by PES-H1 and LCC (Figure 15) which could be explained by a higher concentration of potassium terephthalate salts in the LCC-ICCG PET hydrolysates compared to LCC, for example. TPA yields in the supernatants of the three hydrolysates were calculated based on the fold increase of the bioluminescence  $38.3 \pm 3.8$  mM,  $39.3 \pm 1.3$  mM, and  $95.5 \pm 10.7$  mM for PES-H1, LCC, and LCC-ICCG, respectively, and are in good agreement with the TPA concentrations determined by RP-HPLC.

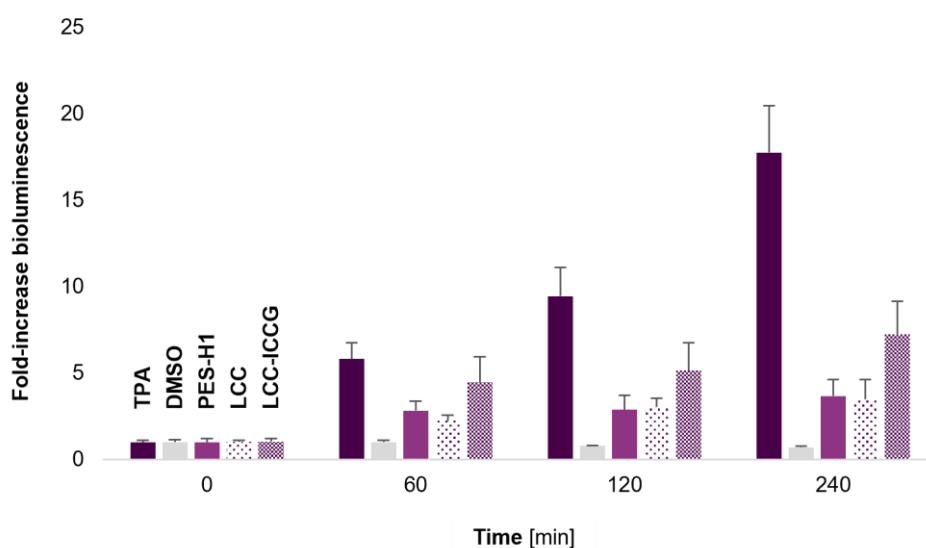


**Figure 15.** PET hydrolysis samples analyzed under HT conditions in *E. coli* RARE. The enzyme-coupled biosensor system produced bioluminescence in the presence of 1 mM TPA (positive control) and hydrolysates obtained by the enzymatic degradation of Gf-PET films by PES-H1, LCC, and LCC-ICCG; however, the bioluminescence did not increase over time in the presence of 1% (n/n) DMSO. Experiments were carried out in RCs of *E. coli* RARE under HT assay conditions previously described<sup>[148]</sup>; data are presented as mean values of the fold-increase in bioluminescence + SD of biological replicates (n > 3). The figure was copied with permission from Bayer et al.<sup>[151]</sup>

Additionally, in a proof-of-concept study, benzoic acid and TPA were converted into benzaldehyde and highly reactive TAL and further into their corresponding primary diamines benzylamine (BAM;  $35.3 \pm 0.7\%$ ) (Fig.4A) and 1,4-bis-(aminomethyl) benzene (1,4-BDM;  $15.0 \pm 5.0\%$ ) (Fig.4B). Structurally related diamines find application in the synthesis of polyurethanes and polyamides<sup>[195]</sup> which supports efforts toward a circular plastic economy.

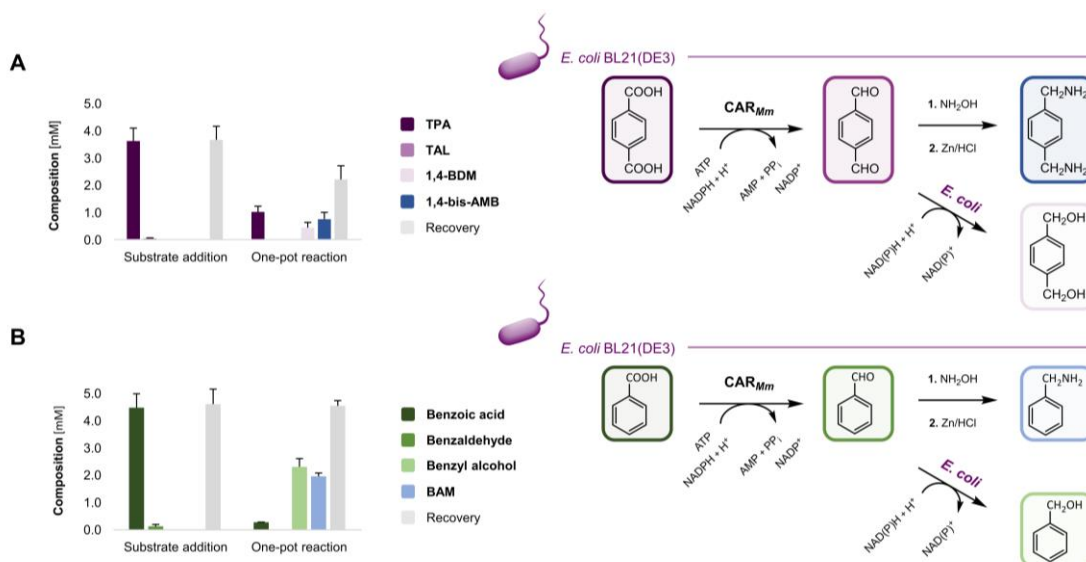


**Figure 16.** Chemo-enzymatic one-pot cascades. CAR<sub>Mm</sub> reduces carboxylates to the corresponding aldehydes in RCs of *E. coli* BL21(DE3); PPT<sub>M</sub> is omitted for clarity. The oximes (not shown) are formed in the presence of NH<sub>2</sub>OH-HCl and are reduced to the primary amines (shades of blue) after the addition of Zn/HCl to the same reaction vessel. (A) The TAL intermediate produces the desired 1,4-bis-AMB as well as 1,4-BDM as a significant by-product. Recoveries were reduced due to TPA's low solubility in RCM containing 5% (n/n) DMSO as an organic co-solvent, reaction compound volatility, and the formation of yet-to-be-identified by-products such as imines.<sup>[196,197]</sup> (B) Benzoic acid was reduced to benzaldehyde in the presence of 5% (n/n) ethanol, yielding the desired BAM after reductive amination and benzyl alcohol as the sole by-product. Experiments were carried out in RCs (OD<sub>600</sub>~10.0) co-expressing pACYCDuet-1/car<sub>Mm</sub>:ppt<sub>Ni</sub> enzymes.<sup>[148]</sup> Sampling: (1) after adding NH<sub>2</sub>OH-HCl and carboxylic acid (2.2 and 1.1 equivalent for TPA and benzoic acid, respectively) and mixing; (2) after performing the reductive amination in one pot. The mean values + SD [mM] of biological replicates (n= 3) are used to calculate the GC yields. The performance of *E. coli* RARE RCs was comparable, with 27.2±6.6% BAM and 13.1±8.0% 1,4-bis-AMB produced (n= 2). The figure was copied with permission from Bayer et al.<sup>[151]</sup>

### 3 Conclusions

The global production of PET, the most abundant synthetic polyester, in the packaging and textile industry and its inappropriate disposal significantly contributes to the global solid waste stream and environmental plastic pollution. The application of thermophilic PET hydrolases in the biocatalytic recycling on industrial scale has emerged as a promising technology for a sustainable circular plastic economy. However, in the last two decades only a handful of benchmark enzymes were described and extensively engineered for this purpose.

The use of HT screening methods, as shown in **Articles II, III and IV**, facilitates the identification of new thermostable enzymes, e.g. from metagenomes or mutant libraries. The ePCR based mutant library created in **Article II** was investigated using an agar plate-based assay allowing the HT screening of approximately 49,000 clones. **Articles I and II** describe two different engineering strategies using either a known thermophilic metagenome-derived PET hydrolase PES-H1 or the thermostabilised mesophilic *IsPETase* TM. In both cases, thermostable variants with higher hydrolytic activities towards different PET materials were created and – not surprisingly – the improvement in thermostability for the *IsPETase* is higher than for PES-H1 as PES-H1 is already highly thermophilic whereas *IsPETase* wild-type has only activity around 30°C. This proves that both strategies are viable options for the creation of thermostable variants with the potential for further assessments under industrially relevant conditions.

The reaction mechanism of the interfacial enzymatic PET hydrolysis including the adsorption and desorption of biocatalysts onto the polymer surface is not yet fully understood. The elucidation of the crystal structures of PES-H1 and PES-H2 in complex with MHETA and BHET (**Article I**) shed light on the binding mechanism by identifying different noncovalent ligand binding modes. These understandings, in combination with MD simulations and mutation strategies described in literature contributed to the design of efficient PET hydrolases. PES-H1 L92F/Q94Y was identified as the most active *IsPETase* hydrolase at 72 °C even outperforming (under the applied conditions) LCC ICCG, the previously reported most active PET hydrolase in literature, thus being a good candidate for future applications in industrial plastic recycling processes.

The Fenton-chemistry mediated fluorimetric screening assay (**Article III**) as well as the LuxAB-biosensor system-based methods (**Article IV**), both of which can directly detect free terephthalate in the supernatant after PET hydrolysis, were investigated towards their applicability as a HT screening method for PET hydrolase. The applicability was confirmed

in proof-of-concept reactions revealing the LuxAB biosensor system as the first and only TPA-biosensor system in living cells to date. Furthermore, the reaction of the aldehydes to their corresponding diamines provided a new option for the bio-based conversion of polymer building blocks to other chemicals with potentially higher values (upcycling).

## 4 References

- [1] M. Carus, L. Dammer, A. Raschka, P. Skoczinski, *Greenhouse Gas. Sci. Technol.* **2020**, *10*, 488–505.
- [2] L. D. Ellis, N. A. Rorrer, K. P. Sullivan, M. Otto, J. E. McGeehan, Y. Román-Leshkov, N. Wierckx, G. T. Beckham, *Nat. Catal.* **2021**, *4*, 539–556.
- [3] S. Kakadellis, G. Rosetto, *Science* **2021**, *373*, 49–50.
- [4] G. W. Coates, Y. D. Y. L. Getzler, *Nat. Rev. Mater.* **2020**, *5*, 501–516.
- [5] R. Wei, T. Tiso, J. Bertling, K. O'Connor, L. M. Blank, U. T. Bornscheuer, *Nat. Catal.* **2020**, *3*, 867–871.
- [6] P. Skoczinski, L. Krause, A. Raschka, L. Dammer, M. Carus, in *Methods in Enzymology*, Elsevier, **2021**, pp. 1–26.
- [7] V. Goel, P. Luthra, G. S. Kapur, S. S. V. Ramakumar, *J. Polym. Environ.* **2021**, *29*, 3079–3104.
- [8] A. P. Fantilli, R. Calvi, E. Quieti, P. L. Radavelli, in *International Conference on Raw Materials and Circular Economy*, MDPI, **2021**, p. 2.
- [9] R. A. Tufa, D. Chanda, M. Ma, D. Aili, T. B. Demissie, J. Vaes, Q. Li, S. Liu, D. Pant, *Appl. Energy* **2020**, *277*, 115557.
- [10] P. Ruiz, A. Raschka, P. Skoczinski, J. Ravenstijn, M. Carus, *Carbon Dioxide (CO<sub>2</sub>) as Chemical Feedstock for Polymers – Technologies, Polymers, Developers and Producers*, Nova-Institut GmbH, **2021**.
- [11] K. Ravindranath, R. A. Mashelkar, *Chem. Eng. Sci.* **1986**, *41*, 2197–2214.
- [12] J. E. McIntyre, in *Wiley Series in Polymer Science* (Eds.: J. Scheirs, T.E. Long), John Wiley & Sons, Ltd, Chichester, UK, **2004**, pp. 1–28.
- [13] J. R. Whinfield, *Nature* **1946**, *158*, 930–931.
- [14] W. T. Astbury, C. J. Brown, *Nature* **1946**, *158*, 871–871.
- [15] W. McMahan, H. A. Birdsall, G. R. Johnson, C. T. Camilli, *J. Chem. Eng. Data* **1959**, *4*, 57–79.
- [16] L. E. Amborski, D. W. Flierl, *Ind. Eng. Chem.* **1953**, *45*, 2290–2295.
- [17] Th. Rieckmann, S. Völker, in *Wiley Series in Polymer Science* (Eds.: J. Scheirs, T.E. Long), John Wiley & Sons, Ltd, Chichester, UK, **2004**, pp. 29–115.
- [18] Olagoke Olabisi, Kolapo Adewale, *Handbook of Thermoplastics, Second Edition*, CRC Press, Taylor & Francis Group, **2015**.
- [19] F. Awaja, D. Pavel, *Eur. Polym. J.* **2005**, *41*, 1453–1477.
- [20] F. Pacheco-Torgal, Y. Ding, S. Jalali, *Constr. Build. Mater.* **2012**, *30*, 714–724.
- [21] W. Reddish, *Trans. Faraday Soc.* **1950**, *46*, 459.
- [22] S. Berkowitz, *J. Appl. Polym. Sci.* **1984**, *29*, 4353–4361.
- [23] A. Singh, N. A. Rorrer, S. R. Nicholson, E. Erickson, J. S. DesVeaux, A. F. T. Avelino, P. Lamers, A. Bhatt, Y. Zhang, G. Avery, L. Tao, A. R. Pickford, A. C. Carpenter, J. E. McGeehan, G. T. Beckham, *Joule* **2021**, *5*, 2479–2503.
- [24] M. Alisch, A. Feuerhack, H. Müller, B. Mensak, J. Andreaus, W. Zimmermann, *Biocatal. Biotransformation* **2004**, *22*, 347–351.
- [25] S. H. Zeronian, M. J. Collins, *Text. Progr.* **1989**, *20*, 1–26.
- [26] M. Alisch-Mark, A. Herrmann, W. Zimmermann, *Biotechnol Lett* **2006**, *28*, 681–685.
- [27] T. Brueckner, A. Eberl, S. Heumann, M. Rabe, G. M. Guebitz, *J. Polym. Sci. A. Polym. Chem.* **2008**, *46*, 6435–6443.
- [28] A. Eberl, S. Heumann, T. Brückner, R. Araujo, A. Cavaco-Paulo, F. Kaufmann, W. Kroutil, G. M. Guebitz, *J. Biotechnol.* **2009**, *143*, 207–212.
- [29] G. Fischer-Colbrie, S. Heumann, S. Liebming, E. Almansa, A. Cavaco-Paulo, G. M. Guebitz, *Biocatal. Biotransformation* **2004**, *22*, 341–346.
- [30] A. Feuerhack, M. Alisch-Mark, A. Kisner, S. H. Pezzin, W. Zimmermann, J. Andreaus, *Biocatal. Biotransformation* **2008**, *26*, 357–364.
- [31] D. Paszun, T. Szychaj, *Ind. Eng. Chem. Res.* **1997**, *36*, 1373–1383.
- [32] S. Joo, I. J. Cho, H. Seo, H. F. Son, H.-Y. Sagong, T. J. Shin, S. Y. Choi, S. Y. Lee, K.-J. Kim, *Nat. Commun.* **2018**, *9*, 382.

- [33] R. Ambrosini, R. S. Azzoni, F. Pittino, G. Diolaiuti, A. Franzetti, M. Parolini, *Environ. Pollut.* **2019**, *253*, 297–301.
- [34] M. Bergmann, M. Klages, *Mar. Pollut. Bull.* **2012**, *64*, 2734–2741.
- [35] P. Benyathiar, P. Kumar, G. Carpenter, J. Brace, D. K. Mishra, *Polymers* **2022**, *14*, 2366.
- [36] D. S., L. Andriotis, I. A., D. A., N. P., P. Sifaka, I. Tsagkalias, G. Tsintzou, in *Material Recycling - Trends and Perspectives* (Ed.: D. Achilias), InTech, **2012**.
- [37] B. Sethi, in *Recycling of Polymers* (Ed.: R. Francis), Wiley, **2016**, pp. 55–114.
- [38] M. Frounchi, *Macromol. Symp.* **1999**, *144*, 465–469.
- [39] M. Häußler, M. Eck, D. Rothauer, S. Mecking, *Nature* **2021**, *590*, 423–427.
- [40] S. M. Al-Salem, *Waste Manage.* **2009**, *29*, 479–484.
- [41] H. Mori, Y. Maeda, S. Kubota, K. Yamaguchi, O. Ito, T. Maeda, *Polym. J.* **2002**, *34*, 687–691.
- [42] C. Sammon, J. Yarwood, N. Everall, *Polym. Degrad. Stab.* **2000**, *67*, 149–158.
- [43] V. Tournier, C. M. Topham, A. Gilles, B. David, C. Folgoas, E. Moya-Leclair, E. Kamionka, M.-L. Desrousseaux, H. Texier, S. Gavalda, M. Cot, E. Guémard, M. Dalibey, J. Nomme, G. Cioci, S. Barbe, M. Chateau, I. André, S. Duquesne, A. Marty, *Nature* **2020**, *580*, 216–219.
- [44] S. R. Shukla, A. M. Harad, *Polymer Degradation and Stability* **2006**, *91*, 1850–1854.
- [45] T. Oeser, R. Wei, T. Baumgarten, S. Billig, C. Föllner, W. Zimmermann, *J. Biotechnol.* **2010**, *146*, 100–104.
- [46] A. Eberl, S. Heumann, T. Brückner, R. Araujo, A. Cavaco-Paulo, F. Kaufmann, W. Kroutil, G. M. Guebitz, *J. Biotechnol.* **2009**, *143*, 207–212.
- [47] S. Sulaiman, S. Yamato, E. Kanaya, J.-J. Kim, Y. Koga, K. Takano, S. Kanaya, *Appl. Environ. Microbiol.* **2012**, *78*, 1556–1562.
- [48] E. Herrero Acero, D. Ribitsch, G. Steinkellner, K. Gruber, K. Greimel, I. Eiteljoerg, E. Trotscha, R. Wei, W. Zimmermann, M. Zinn, A. Cavaco-Paulo, G. Freddi, H. Schwab, G. Guebitz, *Macromolecules* **2011**, *44*, 4632–4640.
- [49] S. Chen, X. Tong, R. W. Woodard, G. Du, J. Wu, J. Chen, *J. Biol. Chem.* **2008**, *283*, 25854–25862.
- [50] R. Wei, D. Breite, C. Song, D. Gräsing, T. Ploss, P. Hille, R. Schwerdtfeger, J. Matysik, A. Schulze, W. Zimmermann, *Adv. Sci.* **2019**, *6*, 1900491.
- [51] I. Taniguchi, S. Yoshida, K. Hiraga, K. Miyamoto, Y. Kimura, K. Oda, *ACS Catal.* **2019**, *9*, 4089–4105.
- [52] W. Zimmermann, S. Billig, in *Biofunctionalization of Polymers and Their Applications* (Eds.: G.S. Nyanhongo, W. Steiner, G. Guebitz), Springer Berlin Heidelberg, Berlin, Heidelberg, **2010**, pp. 97–120.
- [53] G. M. Guebitz, A. Cavaco-Paulo, *Trends Biotechnol.* **2008**, *26*, 32–38.
- [54] D. Ribitsch, S. Heumann, E. Trotscha, E. Herrero Acero, K. Greimel, R. Leber, R. Birner-Gruenberger, S. Deller, I. Eiteljoerg, P. Remler, T. Weber, P. Siegert, K.-H. Maurer, I. Donelli, G. Freddi, H. Schwab, G. M. Guebitz, *Biotechnol. Prog.* **2011**, *27*, 951–960.
- [55] M. Barth, A. Honak, T. Oeser, R. Wei, M. R. Belisário-Ferrari, J. Then, J. Schmidt, W. Zimmermann, *J. Biotechnol.* **2016**, *11*, 1082–1087.
- [56] E. de Q. Eugenio, I. S. P. Campisano, A. M. de Castro, M. A. Z. Coelho, M. A. P. Langone, *J. Polym. Environ.* **2021**, DOI 10.1007/s10924-021-02301-4.
- [57] U. Witt, M. Yamamoto, U. Seeliger, R.-J. Müller, V. Warzelhan, *Angew. Chem. Int. Ed.* **1999**, *38*, 1438–1442.
- [58] E. Marten, R.-J. Müller, W.-D. Deckwer, *Polym. Degrad. Stab.* **2005**, *88*, 371–381.
- [59] R.-J. Müller, H. Schrader, J. Profe, K. Dresler, W.-D. Deckwer, *Macromol. Rapid Commun.* **2005**, *26*, 1400–1405.
- [60] R. Wei, G. von Haugwitz, L. Pfaff, J. Mican, C. P. S. Badenhorst, W. Liu, G. Weber, H. P. Austin, D. Bednar, J. Damborsky, U. T. Bornscheuer, *ACS Catal.* **2022**, *12*, 3382–3396.

- [61] R. Bianchi, P. Chiavacci, R. Vosa, G. Guerra, *J. Appl. Polym. Sci.* **1991**, *43*, 1087–1089.
- [62] D. Langevin, J. Grenet, J. M. Saiter, *Europ. Polym. J.* **1994**, *30*, 339–345.
- [63] S. Yoshida, K. Hiraga, T. Takehana, I. Taniguchi, H. Yamaji, Y. Maeda, K. Toyohara, K. Miyamoto, Y. Kimura, K. Oda, *Science* **2016**, *351*, 1196–1199.
- [64] Å. M. Ronkvist, W. Xie, W. Lu, R. A. Gross, *Macromolecules* **2009**, *42*, 5128–5138.
- [65] S. Brott, L. Pfaff, J. Schuricht, J. Schwarz, D. Böttcher, C. P. S. Badenhorst, R. Wei, U. T. Bornscheuer, *Eng. Life Sci.* **2022**, *22*, 192–203.
- [66] F. Kawai, *Catalysts* **2021**, *11*, 206.
- [67] P. J. Baker, C. Poultney, Z. Liu, R. Gross, J. K. Montclare, *Appl. Microbiol. Biotechnol.* **2012**, *93*, 229–240.
- [68] D. Danso, C. Schmeisser, J. Chow, W. Zimmermann, R. Wei, C. Leggewie, X. Li, T. Hazen, W. R. Streit, *Appl. Environ. Microbiol.* **2018**, *84*, e02773-17.
- [69] S. Sulaiman, D.-J. You, E. Kanaya, Y. Koga, S. Kanaya, *Biochemistry* **2014**, *53*, 1858–1869.
- [70] J. Then, R. Wei, T. Oeser, A. Gerdts, J. Schmidt, M. Barth, W. Zimmermann, *FEBS Open Bio* **2016**, *6*, 425–432.
- [71] J. Then, R. Wei, T. Oeser, M. Barth, M. R. Belisário-Ferrari, J. Schmidt, W. Zimmermann, *J. Biotechnol.* **2015**, *10*, 592–598.
- [72] T. Miyakawa, H. Mizushima, J. Ohtsuka, M. Oda, F. Kawai, M. Tanokura, *Appl. Microbiol. Biotechnol.* **2015**, *99*, 4297–4307.
- [73] M. Oda, Y. Yamagami, S. Inaba, T. Oida, M. Yamamoto, S. Kitajima, F. Kawai, *Appl. Microbiol. Biotechnol.* **2018**, *102*, 10067–10077.
- [74] N. Numoto, N. Kamiya, G.-J. Bekker, Y. Yamagami, S. Inaba, K. Ishii, S. Uchiyama, F. Kawai, N. Ito, M. Oda, *Biochemistry* **2018**, *57*, 5289–5300.
- [75] A. Nakamura, N. Kobayashi, N. Koga, R. Iino, *ACS Catal.* **2021**, *11*, 8550–8564.
- [76] W. Zeng, X. Li, Y. Yang, J. Min, J.-W. Huang, W. Liu, D. Niu, X. Yang, X. Han, L. Zhang, L. Dai, C.-C. Chen, R.-T. Guo, *ACS Catal.* **2022**, 3033–3040.
- [77] R. Wei, C. Song, D. Gräsing, T. Schneider, P. Bielytskyi, D. Böttcher, J. Matysik, U. T. Bornscheuer, W. Zimmermann, *Nat. Commun.* **2019**, *10*, 5581.
- [78] X. Xi, K. Ni, H. Hao, Y. Shang, B. Zhao, Z. Qian, *Enzyme Microb. Technol.* **2021**, *143*, 109715.
- [79] A. N. Shirke, C. White, J. A. Englaender, A. Zwarycz, G. L. Butterfoss, R. J. Linhardt, R. A. Gross, *Biochemistry* **2018**, *57*, 1190–1200.
- [80] U. T. Bornscheuer, *Science* **2016**, *351*, 1154–1155.
- [81] G. J. Palm, L. Reisky, D. Böttcher, H. Müller, E. A. P. Michels, M. C. Walczak, L. Berndt, M. S. Weiss, U. T. Bornscheuer, G. Weber, *Nat. Commun.* **2019**, *10*, 1717.
- [82] H. F. Son, I. J. Cho, S. Joo, H. Seo, H.-Y. Sagong, S. Y. Choi, S. Y. Lee, K.-J. Kim, *ACS Catal.* **2019**, *9*, 3519–3526.
- [83] Y. Cui, Y. Chen, X. Liu, S. Dong, Y. Tian, Y. Qiao, R. Mitra, J. Han, C. Li, X. Han, W. Liu, Q. Chen, W. Wei, X. Wang, W. Du, S. Tang, H. Xiang, H. Liu, Y. Liang, K. N. Houk, B. Wu, *ACS Catal.* **2021**, *11*, 1340–1350.
- [84] H. Lu, D. J. Diaz, N. J. Czarnecki, C. Zhu, W. Kim, R. Shroff, D. J. Acosta, B. R. Alexander, H. O. Cole, Y. Zhang, N. A. Lynd, A. D. Ellington, H. S. Alper, *Nature* **2022**, *604*, 662–667.
- [85] E. L. Bell, R. Smithson, S. Kilbride, J. Foster, F. J. Hardy, S. Ramachandran, A. A. Tedstone, S. J. Haigh, A. A. Garforth, P. J. R. Day, C. Levy, M. P. Shaver, A. P. Green, *Nat. Catal.* **2022**, *5*, 673–681.
- [86] A. M. de Castro, A. Carniel, J. Nicomedes Junior, A. da Conceição Gomes, É. Valoni, *J. Ind. Microbiol. Biotechnol.* **2017**, *44*, 835–844.
- [87] A. Carniel, A. da C. Gomes, M. A. Z. Coelho, A. M. de Castro, *Bioprocess Biosyst. Eng.* **2021**, *44*, 507–516.
- [88] S. Kaabel, J. P. D. Therien, C. E. Deschênes, D. Duncan, T. Frišćić, K. Auclair, *Proc. Nat. Acad. Sci. USA* **2021**, 118, No. e2026452118.
- [89] L. N. Woodard, M. A. Grunlan, *ACS Macro Lett.* **2018**, *7*, 976–982.

- [90] J. Kari, M. Andersen, K. Borch, P. Westh, *ACS Catal.* **2017**, *7*, 4904–4914.
- [91] E. Erickson, T. J. Shakespeare, F. Bratti, B. L. Buss, R. Graham, M. A. Hawkins, G. König, W. E. Michener, J. Miscall, K. J. Ramirez, N. A. Rorrer, M. Zahn, A. R. Pickford, J. E. McGeehan, G. T. Beckham, *ChemSusChem* **2022**, *15*, No. e202101932.
- [92] K. Vogel, R. Wei, L. Pfaff, D. Breite, H. Al-Fathi, C. Ortmann, I. Estrela-Lopis, T. Venus, A. Schulze, H. Harms, U. T. Bornscheuer, T. Maskow, *Sci. Total Environment.* **2021**, *773*, 145111.
- [93] J. A. Bååth, K. Borch, K. Jensen, J. Brask, P. Westh, *ChemBioChem* **2021**, *22*, 1627–1637.
- [94] C. Silva, S. Da, N. Silva, T. Matamá, R. Araújo, M. Martins, S. Chen, J. Chen, J. Wu, M. Casal, A. Cavaco-Paulo, *J. Biotechnol.* **2011**, *6*, 1230–1239.
- [95] R. Wei, T. Oeser, J. Schmidt, R. Meier, M. Barth, J. Then, W. Zimmermann, *Biotechnol. Bioeng.* **2016**, *113*, 1658–1665.
- [96] R. Wei, T. Oeser, J. Then, N. Kühn, M. Barth, J. Schmidt, W. Zimmermann, *AMB Expr.* **2014**, *4*, 44.
- [97] R. Wei, T. Oeser, M. Barth, N. Weigl, A. Lübs, M. Schulz-Siegmund, M. C. Hacker, W. Zimmermann, *J. Mol. Catal. B: Enzym* **2014**, *103*, 72–78.
- [98] R. Xue, Y. Chen, H. Rong, R. Wei, Z. Cui, J. Zhou, W. Dong, M. Jiang, *Front. Bioeng. Biotechnol.* **2021**, *9*, 762854.
- [99] D. Ribitsch, A. O. Yebra, S. Zitzenbacher, J. Wu, S. Nowitsch, G. Steinkellner, K. Greimel, A. Doliska, G. Oberdorfer, C. C. Gruber, K. Gruber, H. Schwab, K. Stana-Kleinschek, E. H. Acero, G. M. Guebitz, *Biomacromolecules* **2013**, *14*, 1769–1776.
- [100] M. T. Zumstein, H.-P. E. Kohler, K. McNeill, M. Sander, *Environ. Sci. Technol.* **2016**, *50*, 197–206.
- [101] S. Weinberger, K. Haernvall, D. Scaini, G. Ghazaryan, M. T. Zumstein, M. Sander, A. Pellis, G. M. Guebitz, *Green Chem.* **2017**, *19*, 5381–5384.
- [102] Y. Zhang, L. Wang, J. Chen, J. Wu, *Carbohydrate Polymers* **2013**, *97*, 124–129.
- [103] J. Arnlung Bååth, V. Novy, L. V. Carneiro, G. M. Guebitz, L. Olsson, P. Westh, D. Ribitsch, *Biotechnol. Bioeng.* **2022**, *119*, 470–481.
- [104] S. F. Badino, J. A. Bååth, K. Borch, K. Jensen, P. Westh, *Enzyme Microb. Technol.* **2021**, *152*, 109937.
- [105] S. Feng, Y. Yue, M. Zheng, Y. Li, Q. Zhang, W. Wang, *ACS Sustain. Chem. Eng.* **2021**, *9*, 9823–9832.
- [106] M. Zheng, Y. Li, W. Dong, S. Feng, Q. Zhang, W. Wang, *J. Hazard. Mater.* **2022**, *423*, 127017.
- [107] S. Boneta, K. Arafet, V. Moliner, *J. Chem. Inf. Model.* **2021**, *61*, 3041–3051.
- [108] C. Jerves, R. P. P. Neves, M. J. Ramos, S. da Silva, P. A. Fernandes, *ACS Catal.* **2021**, *11*, 11626–11638.
- [109] X. Han, W. Liu, J.-W. Huang, J. Ma, Y. Zheng, T.-P. Ko, L. Xu, Y.-S. Cheng, C.-C. Chen, R.-T. Guo, *Nat. Commun.* **2017**, *8*, 2106.
- [110] L. Pfaff, J. Gao, Z. Li, A. Jäckering, G. Weber, J. Mican, Y. Chen, W. Dong, X. Han, C. G. Feiler, Y.-F. Ao, C. P. S. Badenhorst, D. Bednar, G. J. Palm, M. Lammers, J. Damborsky, B. Strodel, W. Liu, U. T. Bornscheuer, R. Wei, *ACS Catal.* **2022**, *12*, 9790–9800.
- [111] Z. Li, Y. Zhao, P. Wu, H. Wang, Q. Li, J. Gao, H.-M. Qin, H. Wei, U. T. Bornscheuer, X. Han, R. Wei, W. Liu, *Biochem. Biophys. Res. Commun.* **2022**, *626*, 100–106.
- [112] H. P. Austin, M. D. Allen, B. S. Donohoe, N. A. Rorrer, F. L. Kearns, R. L. Silveira, B. C. Pollard, G. Dominick, R. Duman, K. El Omari, V. Mykhaylyk, A. Wagner, W. E. Michener, A. Amore, M. S. Skaf, M. F. Crowley, A. W. Thorne, C. W. Johnson, H. L. Woodcock, J. E. McGeehan, G. T. Beckham, *Proc. Natl. Acad. Sci. USA* **2018**, *115*, E4350–E4357.
- [113] T. Fecker, P. Galaz-Davison, F. Engelberger, Y. Narui, M. Sotomayor, L. P. Parra, C. A. Ramírez-Sarmiento, *Biophys. J.* **2018**, *114*, 1302–1312.



- [114] C. Roth, R. Wei, T. Oeser, J. Then, C. Föllner, W. Zimmermann, N. Sträter, *Appl. Microbiol. Biotechnol.* **2014**, *98*, 7815–7823.
- [115] C. H. S. Costa, A. M. Santos, C. N. Alves, S. Martí, V. Moliner, K. Santana, J. Lameira, *Proteins* **2021**, *89*, 1340–1352.
- [116] D. Yi, T. Bayer, C. P. S. Badenhorst, S. Wu, M. Doerr, M. Höhne, U. T. Bornscheuer, *Chem. Soc. Rev.* **2021**, *50*, 8003–8049.
- [117] U. Markel, K. D. Essani, V. Besirlioglu, J. Schiffels, W. R. Streit, U. Schwaneberg, *Chem. Soc. Rev.* **2020**, *49*, 233–262.
- [118] D. Danso, C. Schmeisser, J. Chow, W. Zimmermann, R. Wei, C. Leggewie, X. Li, T. Hazen, W. R. Streit, *Appl. Environ. Microbiol.* **2018**, *84*, e02773-17.
- [119] A. Meyer, R. Pellaux, S. Potot, K. Becker, H.-P. Hohmann, S. Panke, M. Held, *Nature Chem.* **2015**, *7*, 673–678.
- [120] R. Wei, T. Oeser, M. Barth, N. Weigl, A. Lübs, M. Schulz-Siegmund, M. C. Hacker, W. Zimmermann, *J. Mol. Catal. B: Enzym* **2014**, *103*, 72–78.
- [121] R. Wei, T. Oeser, J. Then, N. Kühn, M. Barth, J. Schmidt, W. Zimmermann, *AMB Expr.* **2014**, *4*, 44.
- [122] M. Barth, T. Oeser, R. Wei, J. Then, J. Schmidt, W. Zimmermann, *Biochem. Eng. J.* **2015**, *93*, 222–228.
- [123] R. Wei, T. Oeser, S. Billig, W. Zimmermann, *Biotechnol. Journal* **2012**, *7*, 1517–1521.
- [124] Weigert, S.; Gagsteiger, A.; Menzel, T.; Höcker, B. A Versatile Assay Platform for Enzymatic Poly(Ethylene-Terephthalate) Degradation. *Protein Eng. Des. Sel.* **2021**, *34*, No. gzab022
- [125] J. D. Unciti-Broceta, V. Cano-Cortés, P. Altea-Manzano, S. Pernagallo, J. J. Díaz-Mochón, R. M. Sánchez-Martín, *Sci. Rep.* **2015**, *5*, 10091.
- [126] F. Kawai, M. Oda, T. Tamashiro, T. Waku, N. Tanaka, M. Yamamoto, H. Mizushima, T. Miyakawa, M. Tanokura, *Appl. Microbiol. Biotechnol.* **2014**, *98*, 10053–10064.
- [127] J. Schmidt, R. Wei, T. Oeser, L. Dedavid e Silva, D. Breite, A. Schulze, W. Zimmermann, *Polymers* **2017**, *9*, 65.
- [128] L. Pfaff, D. Breite, C. P. S. Badenhorst, U. T. Bornscheuer, R. Wei, in *Methods in Enzymology*, Elsevier, **2021**, pp. 253–270.
- [129] K. Welzel, R.-J. Müller, W.-D. Deckwer, *Chemie Ingenieur Technik* **2002**, *74*, 1496–1500.
- [130] A. G. Rodríguez-Hernández, J. A. Muñoz-Tabares, J. C. Aguilar-Guzmán, R. Vazquez-Duhalt, *Environ. Sci.: Nano* **2019**, *6*, 2031–2036.
- [131] R. Molitor, A. Bollinger, S. Kubicki, A. Loeschcke, K. Jaeger, S. Thies, *Microb. Biotechnol.* **2020**, *13*, 274–284.
- [132] J. Liu, J. He, R. Xue, B. Xu, X. Qian, F. Xin, L. M. Blank, J. Zhou, R. Wei, W. Dong, M. Jiang, *Biotechnol. Adv.* **2021**, *48*, 107730.
- [133] C. Charnock, *J. Microbiol. Methods* **2021**, *185*, 106222.
- [134] V. Pirillo, L. Pollegioni, G. Molla, *FEBS J.* **2021**, *288*, 4730–4745.
- [135] A. Carniel, V. de A. Waldow, A. M. de Castro, *Biotechnol. Adv.* **2021**, *52*, 107811.
- [136] E. Z. L. Zhong-Johnson, C. A. Voigt, A. J. Sinskey, *Sci. Rep.* **2021**, *11*, 928.
- [137] E. Herrero Acero, D. Ribitsch, G. Steinkellner, K. Gruber, K. Greimel, I. Eiteljoerg, E. Trotscha, R. Wei, W. Zimmermann, M. Zinn, A. Cavaco-Paulo, G. Freddi, H. Schwab, G. Guebitz, *Macromolecules* **2011**, *44*, 4632–4640.
- [138] A. O'Neill, A. Cavaco-Paulo, *Biocatal. Biotransform.* **2004**, *22*, 353–356.
- [139] Å. M. Ronkvist, W. Xie, W. Lu, R. A. Gross, in *ACS Symposium Series* (Eds.: H.N. Cheng, R.A. Gross), American Chemical Society, Washington, DC, **2010**, pp. 385–404.
- [140] J. Lusty Beech, R. Clare, W. M. Kincannon, E. Erickson, J. E. McGeehan, G. T. Beckham, J. L. DuBois, *RSC Adv.* **2022**, *12*, 8119–8130.
- [141] D. Reyes-Duarte, C. Coscolín, M. Martínez-Martínez, M. Ferrer, H. García-Arellano, in *Lipases and Phospholipases* (Ed.: G. Sandoval), Springer New York, New York, NY, **2018**, pp. 109–117.

- [142] P. Halonen, T. Reinikainen, A. Nyyssölä, J. Buchert, *Enzym. Microbiol. Technol.* **2009**, *44*, 394–399.
- [143] L. Linxiang, Y. Abe, Y. Nagasawa, R. Kudo, N. Usui, K. Imai, T. Mashino, M. Mochizuki, N. Miyata, *Biomed. Chromatogr.* **2004**, *18*, 470–474.
- [144] M. Gimeno-Pérez, J. D. Finnigan, C. Echeverria, S. J. Charnock, A. Hidalgo, D. M. Mate, *ChemSusChem* **2022**, *15*, No. e202102750
- [145] Y. Qiao, R. Hu, D. Chen, L. Wang, Y. Fu, C. Li, Z. Dong, Y. Weng, W. Du, *Microbiology*, **2021**.
- [146] H. Eshghi, N. Mirzaie, A. Asoodeh, *Dyes Pigm.* **2011**, *89*, 120–126.
- [147] I. Pardo, R. K. Jha, R. E. Bermel, F. Bratti, M. Gaddis, E. McIntyre, W. Michener, E. L. Neidle, T. Dale, G. T. Beckham, C. W. Johnson, *Metabol. Eng.* **2020**, *62*, 260–274.
- [148] J. Li, M. R. H. Nina, X. Zhang, Y. Bai, *ACS Synth. Biol.* **2022**, *11*, 1106–1113.
- [149] T. Bayer, A. Becker, H. Terholsen, I. J. Kim, I. Menyes, S. Buchwald, K. Balke, S. Santala, S. C. Almo, U. T. Bornscheuer, *Catalysts* **2021**, *11*, 953.
- [150] D. Kasai, M. Kitajima, M. Fukuda, E. Masai, *Appl. Environ. Microbiol.* **2010**, *76*, 6047–6055.
- [151] T. Bayer, L. Pfaff, Y. Branson, A. Becker, S. Wu, U. T. Bornscheuer, R. Wei, *iScience* **2022**, *25*, 104326.
- [152] S. M. Clarkson, R. J. Giannone, D. M. Kridelbaugh, J. G. Elkins, A. M. Guss, J. K. Michener, *Appl. Environ. Microbiol.* **2017**, *83*, e01313-17.
- [153] P. Tufvesson, J. Lima-Ramos, N. A. Haque, K. V. Gernaey, J. M. Woodley, *Org. Process Res. Dev.* **2013**, *17*, 1233–1238.
- [154] S. Lutz, U. T. Bornscheuer, Eds., *Protein Engineering Handbook*, Wiley-VCH, **2012**.
- [155] G. A. Behrens, A. Hummel, S. K. Padhi, S. Schätzle, U. T. Bornscheuer, *Adv. Synth. Catal.* **2011**, *353*, 2191–2215.
- [156] U. Bornscheuer, R. J. Kazlauskas, *Curr. Protoc. Protein Sci.* **2011**, *66*, DOI 10.1002/0471140864.ps2607s66.
- [157] W. M. Dawson, G. G. Rhys, D. N. Woolfson, *Curr. Opin. Chem. Biol.* **2019**, *52*, 102–111.
- [158] H. Kries, R. Blomberg, D. Hilvert, *Curr. Opin. Chem. Biol.* **2013**, *17*, 221–228.
- [159] B. Seelig, J. W. Szostak, *Nature* **2007**, *448*, 828–831.
- [160] R. J. Kazlauskas, U. T. Bornscheuer, *Nat. Chem. Biol.* **2009**, *5*, 526–529.
- [161] U. T. Bornscheuer, *Phil. Trans. R. Soc. A.* **2018**, *376*, 20170063.
- [162] U. T. Bornscheuer, G. W. Huisman, R. J. Kazlauskas, S. Lutz, J. C. Moore, K. Robins, *Nature* **2012**, *485*, 185–194.
- [163] H. Jochens, U. T. Bornscheuer, *Chem. Eur. J. of Chem. Bio.* **2010**, *11*, 1861–1866.
- [164] U. T. Bornscheuer, B. Hauer, K. E. Jaeger, U. Schwaneberg, *Angew. Chem. Int. Ed.* **2019**, *58*, 36–40.
- [165] R. C. Cadwell, G. F. Joyce, *Genome Res.* **1992**, *2*, 28–33.
- [166] S. Chusacultanchai, Y. Yuthavong, in *Parasite Genomics Protocols*, Humana Press, New Jersey, **2004**, pp. 319–334.
- [167] W. P. C. Stemmer, *Nature* **1994**, *370*, 389–391.
- [168] T. Davids, M. Schmidt, D. Böttcher, U. T. Bornscheuer, *Curr. Opin. Chem. Biol.* **2013**, *17*, 215–220.
- [169] L. Weng, J. E. Spoonamore, *Micromachines* **2019**, *10*, 734.
- [170] M. Dörr, M. P. C. Fibinger, D. Last, S. Schmidt, J. Santos-Aberturas, D. Böttcher, A. Hummel, C. Vickers, M. Voss, U. T. Bornscheuer, *Biotechnol. Bioeng.* **2016**, *113*, 1421–1432.
- [171] K. K. Yang, Z. Wu, F. H. Arnold, *Nat. Methods* **2019**, *16*, 687–694.
- [172] S. K. Burley, H. M. Berman, C. Bhikadiya, C. Bi, L. Chen, L. Di Costanzo, C. Christie, K. Dalenberg, J. M. Duarte, S. Dutta, Z. Feng, S. Ghosh, D. S. Goodsell, R. K. Green, V. Guranović, D. Guzenko, B. P. Hudson, T. Kalro, Y. Liang, R. Lowe, H. Namkoong, E. Peisach, I. Periskova, A. Prlić, C. Randle, A. Rose, P. Rose, R. Sala, M. Sekharan, C. Shao, L. Tan, Y.-P. Tao, Y. Valasatava, M. Voigt, J. Westbrook, J.

- Woo, H. Yang, J. Young, M. Zhuravleva, C. Zardecki, *Nucleic Acids Res.* **2019**, *47*, D464–D474.
- [173] D. S. Goodsell, C. Zardecki, L. Di Costanzo, J. M. Duarte, B. P. Hudson, I. Persikova, J. Segura, C. Shao, M. Voigt, J. D. Westbrook, J. Y. Young, S. K. Burley, *Protein Sci.* **2020**, *29*, 52–65.
- [174] R. K. Kuipers, H.-J. Joosten, W. J. H. van Berkel, N. G. H. Leferink, E. Rooijen, E. Ittmann, F. van Zimmeren, H. Jochens, U. Bornscheuer, G. Vriend, V. A. P. Martins dos Santos, P. J. Schaap, *Proteins* **2010**, NA-NA.
- [175] C. Camacho, G. Coulouris, V. Avagyan, N. Ma, J. Papadopoulos, K. Bealer, T. L. Madden, *BMC Bioinformatics* **2009**, *10*, 421.
- [176] J. Stourac, J. Dubrava, M. Musil, J. Horackova, J. Damborsky, S. Mazurenko, D. Bednar, *Nucleic Acids Res.* **2021**, *49*, D319–D324.
- [177] M. Musil, J. Stourac, J. Bendl, J. Brezovsky, Z. Prokop, J. Zendulka, T. Martinek, D. Bednar, J. Damborsky, *Nucleic Acids Res.* **2017**, *45*, W393–W399.
- [178] J. Stourac, O. Vavra, P. Kokkonen, J. Filipovic, G. Pinto, J. Brezovsky, J. Damborsky, D. Bednar, *Nucleic Acids Res.* **2019**, *47*, W414–W422.
- [179] E. Chovancova, A. Pavelka, P. Benes, O. Strnad, J. Brezovsky, B. Kozlikova, A. Gora, V. Sustr, M. Klvana, P. Medek, L. Biedermannova, J. Sochor, J. Damborsky, *PLoS Comput. Biol.* **2012**, *8*, No. e1002708.
- [180] A. Pavelka, E. Chovancova, J. Damborsky, *Nucleic Acids Res.* **2009**, *37*, W376–W383.
- [181] L. Sumbalova, J. Stourac, T. Martinek, D. Bednar, J. Damborsky, *Nucleic Acids Res.* **2018**, *46*, W356–W362.
- [182] H. J. Wijma, R. J. Floor, P. A. Jekel, D. Baker, S. J. Marrink, D. B. Janssen, *Protein Eng. Des. Sel.* **2014**, *27*, 49–58.
- [183] A. S. Bommarius, J. K. Blum, M. J. Abrahamson, *Curr. Opin. Chem. Biol.* **2011**, *15*, 194–200.
- [184] E. Callaway, *Nature* **2020**, *588*, 203–204.
- [185] R. A. Chica, N. Doucet, J. N. Pelletier, *Curr. Opin. Chem. Biol.* **2005**, *16*, 378–384.
- [186] S. Lutz, *Curr. Opin. Chem. Biol.* **2010**, *21*, 734–743.
- [187] R. Wei, T. Oeser, W. Zimmermann, in *Adv. Appl. Microbiol.*, Elsevier, **2014**, pp. 267–305.
- [188] P. Falkenstein, R. Wei, J. Matysik, C. Song, in *Methods in Enzymology*, Elsevier, **2021**, pp. 231–252.
- [189] M. Furukawa, N. Kawakami, A. Tomizawa, K. Miyamoto, *Sci. Rep.* **2019**, *9*, 16038.
- [190] R. K. Brizendine, E. Erickson, S. J. Haugen, K. J. Ramirez, J. Miscall, D. Salvachúa, A. R. Pickford, M. J. Sobkowicz, J. E. McGeehan, G. T. Beckham, *ACS Sustain. Chem. Eng.* **2022**, *10*, 9131–9140.
- [191] R. Lehner, C. Weder, A. Petri-Fink, B. Rothen-Rutishauser, *Environ. Sci. Technol.* **2019**, *53*, 1748–1765.
- [192] S. Wagner, T. Reemtsma, *Nat. Nanotechnol.* **2019**, *14*, 300–301.
- [193] J. Liu, Y. Ma, D. Zhu, T. Xia, Y. Qi, Y. Yao, X. Guo, R. Ji, W. Chen, *Environ. Sci. Technol.* **2018**, *52*, 2677–2685.
- [194] A. M. Kunjapur, Y. Tarasova, K. L. J. Prather, *J. Am. Chem. Soc.* **2014**, *136*, 11644–11654.
- [195] X. Wang, S. Gao, J. Wang, S. Xu, H. Li, K. Chen, P. Ouyang, *Chin. J. Chem. Eng.* **2021**, *30*, 4–13.
- [196] A. Simion, C. Simion, T. Kanda, S. Nagashima, Y. Mitoma, T. Yamada, K. Mimura, M. Tashiro, *J. Chem. Soc., Perkin Trans. 1* **2001**, 2071–2078.
- [197] C. Godoy-Alcántar, A. K. Yatsimirsky, J.-M. Lehn, *J. Phys. Org. Chem.* **2005**, *18*, 979–985.



## 5 Author Contributions

### Article I **Multiple Substrate Binding Mode-Guided Engineering of a Thermophilic PET Hydrolase**

L. Pfaff, J. Gao, Z. Li, A. Jäckering, G. Weber, J. Mican, Y. Chen, W. Dong, X. Hu, C. G. Feiler, Y. Ao, C. P. S. Badenhorst, D. Bednar, G. J. Palm, M. Lammers, J. Damborsky, B. Strodel, W. Liu, U. T. Bornscheuer, R. Wei, *ACS Catal.* **2022**, *12*, 9790-9800.

Conceptualization: R.W., W.L., and U.T.B. Protein crystallographic studies: J.G., Z.L., X.H., C.G.F., G.J.P., M.L., and W.L. Computational simulations: A.J., G.W., J.M., Y.-F.A., D.B., J.D., B.S., and W.L. Protein engineering and characterization: L.P., J.G., and Z.L. Polymer treatment and characterization: Y.C. and W.D. Writing-original draft: L.P., A.J., G.W., C.P.S.B., W.L., and R.W. Writing-review and editing: all authors. Supervision and funding acquisition: W.D., J.D., B.S., W.L., U.T.B., and R.W. All authors read and approved the manuscript.

### Article II **Engineering and evaluation of thermostable *Is*PETase variants for PET degradation**

S. Brott, L. Pfaff, J. Schuricht, J. Schwarz, D. Böttcher, C. P. S. Badenhorst, R. Wei, U. T. Bornscheuer, *Eng. Life Sci.* **2021**, *22*, 192-203.

Conceptualization: U.T.B, R.W., D.B. Protein engineering and characterization: S.B., L.P., J.S., J.S., D.B. Polymer preparation and characterization: S.B. and L.P. Writing-original draft: S.B., R.W., U.T.B. Writing-review and editing: all authors. Supervision: U.T.B, R.W., D.B., C.P.S.B. Funding Acquisition U.T.B, R.W., C.P.S.B. All authors read and approved the manuscript.

### Article III **Fluorimetric High-Throughput Screening Method for Polyester Hydrolase Activity Using Polyethylene Terephthalate Nanoparticles**

L. Pfaff, D. Breite, C. P. S. Badenhorst, U. T. Bornscheuer, R. Wei, in *Methods in Enzymology*, Elsevier, **2021**, Vol. 648, 253-270.

Conceptualization: U.T.B, R.W., C.P.S.B. Polymer production and characterization: L.P., D.B. Protein characterization: L.P., C.P.S.B. Writing-original draft: all authors. Writing-review and editing: all authors. Supervision: U.T.B, R.W.,C.P.S.B. All authors read and approved the manuscript.

**Article IV      Biosensor and chemo-enzymatic one-pot cascade applications to detect and transform PET-derived terephthalic acid in living cells**

T. Bayer, L. Pfaff, Y. Branson, A. Becker, S. Wu, U. T. Bornscheuer, R. Wei, *iScience* **2022**, 25, 104326.

Conceptualization, T.B. and R.W.; Methodology, T.B. and R.W.; Investigation, T.B., A.B., Y.B., L.P., and S.W.; Resources, U.T.B. and R.W.; Data Curation, T.B. and L.P.; Writing – Original Draft, T.B.; Writing- Reviewing & Editing, A.B., U.T.B., Y.B., L.P., R.W., and S.W.; Visualization, T.B. and A.B.; Supervision, T.B., U.T.B., and R.W.; Project Administration, T.B., U.T.B., and R.W.; Funding Acquisition, T.B., U.T.B., R.W., and S.W. All authors read and approved the manuscript.

---

Lara Pfaff

---

Prof. Dr. Uwe T. Bornscheuer

# Articles





# Article I



# Multiple Substrate Binding Mode-Guided Engineering of a Thermophilic PET Hydrolase

Lara Pfaff, Jian Gao, Zhishuai Li, Anna Jäckering, Gert Weber, Jan Mican, Yingping Chen, Weiliang Dong, Xu Han, Christian G. Feiler, Yu-Fei Ao, Christoffel P. S. Badenhorst, David Bednar, Gottfried J. Palm, Michael Lammers, Jiri Damborsky, Birgit Strodel, Weidong Liu,\* Uwe T. Bornscheuer,\* and Ren Wei\*



Cite This: *ACS Catal.* 2022, 12, 9790–9800



Read Online

ACCESS |



Metrics & More



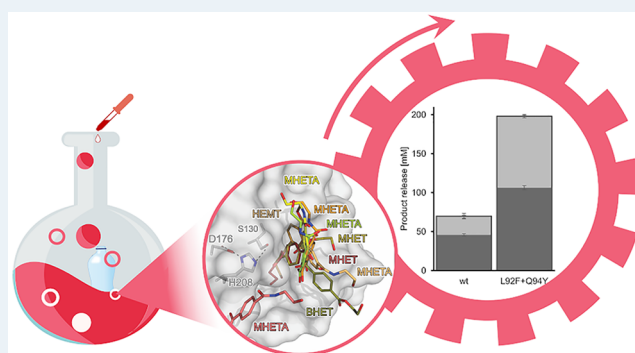
Article Recommendations



Supporting Information

**ABSTRACT:** Thermophilic polyester hydrolases (PES-H) have recently enabled biocatalytic recycling of the mass-produced synthetic polyester polyethylene terephthalate (PET), which has found widespread use in the packaging and textile industries. The growing demand for efficient PET hydrolases prompted us to solve high-resolution crystal structures of two metagenome-derived enzymes (PES-H1 and PES-H2) and notably also in complex with various PET substrate analogues. Structural analyses and computational modeling using molecular dynamics simulations provided an understanding of how product inhibition and multiple substrate binding modes influence key mechanistic steps of enzymatic PET hydrolysis. Key residues involved in substrate-binding and those identified previously as mutational hotspots in homologous enzymes were subjected to mutagenesis. At 72 °C, the L92F/Q94Y variant of PES-H1 exhibited 2.3-fold and 3.4-fold improved hydrolytic activity against amorphous PET films and pretreated real-world PET waste, respectively. The R204C/S250C variant of PES-H1 had a 6.4 °C higher melting temperature than the wild-type enzyme but retained similar hydrolytic activity. Under optimal reaction conditions, the L92F/Q94Y variant of PES-H1 hydrolyzed low-crystallinity PET materials 2.2-fold more efficiently than LCC ICCG, which was previously the most active PET hydrolase reported in the literature. This property makes the L92F/Q94Y variant of PES-H1 a good candidate for future applications in industrial plastic recycling processes.

**KEYWORDS:** polyethylene terephthalate (PET), PET hydrolysis, thermophilic polyester hydrolase, enzyme engineering, crystallization, molecular dynamics, binding modes, kinetics



## INTRODUCTION

Polyethylene terephthalate (PET), the most abundant synthetic polyester, is widely used in the packaging and textile industries. The global production of PET recently reached 82 million metric tons per year.<sup>1</sup> This contributes significantly to the global solid waste stream and environmental plastic pollution. Biocatalytic recycling of PET has emerged as a promising technology that allows the recovery of monomeric building blocks at both laboratory and pilot plant scales.<sup>2–5</sup> Although PET hydrolases from a wide range of microorganisms have been identified, only a handful of benchmark enzymes have been extensively engineered for industrial applications.<sup>6</sup>

As an interfacial biocatalytic reaction, the efficiency of PET degradation is limited by the number of accessible ester bonds at the polymer surface. Amorphous PET polymer chains become more accessible to enzymatic hydrolysis at temperatures approaching the glass transition temperature of PET ( $T_g$ , 65–71 °C).<sup>6</sup> In aqueous environments, water serves as a plasticizer that lowers the  $T_g$  of PET by up to 16 °C.<sup>6–8</sup> This

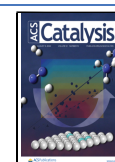
effect increases the flexibility of polymer chains at the PET surface layer, allowing degradation at ambient temperatures by mesophilic PET hydrolases, like *IsPETase* from *Ideonella sakaiensis*, which have optimal operating temperatures ( $T_{opt}$ ) of approximately 40 °C.<sup>9</sup> Nonetheless, thermophilic and thermostable PET hydrolases have superior degradation activity because of increased substrate accessibility at elevated temperatures.<sup>10–12</sup>

LCC, a cutinase isolated from a leaf-branch compost metagenome library, is one of the most extensively investigated thermophilic PET hydrolases.<sup>13–15</sup> Structure-based protein engineering of LCC has resulted in an F243I/D238C/S283C/

Received: May 8, 2022

Revised: July 6, 2022

Published: July 27, 2022



Y127G variant (LCC ICCG) that can efficiently depolymerize pretreated postconsumer PET bottles within 10 h at 72 °C. This enables the biocatalytic recycling of PET waste at industrially relevant scales.<sup>5</sup> Calcium ions ( $\text{Ca}^{2+}$ ) can boost the thermostability of many bacterial PET hydrolases (changes in  $T_m$  ( $\Delta T_m$ ) = 10–16 °C and  $\Delta T_{\text{opt}} \geq 10$  °C).<sup>13,16–18</sup> Engineering of residues in the  $\text{Ca}^{2+}$  binding sites has proven to be a useful approach for increasing the  $T_m$  of several PET hydrolases by up to 26 °C.<sup>5,11,17,19–22</sup> Introduction of a disulfide bridge at this site (D238C/S283C) markedly increased the melting point ( $T_m$ ) of LCC from 84.7 to 94.5 °C. In a recent study, LCC ICCG was further engineered to obtain an A59K/V63I/N248P variant with a  $T_m$  of 98.9 °C.<sup>23</sup> Nonetheless, the  $T_{\text{opt}}$  of this variant for degrading low-crystallinity PET (lcPET, <15% crystallinity) was 74 °C, only 2 °C higher than that for the precursor LCC ICCG.<sup>5</sup> At reaction temperatures above 70 °C, water-plasticized lcPET rapidly crystallizes to high-crystallinity PET (hcPET), which is much harder to hydrolyze.<sup>6,24,25</sup> The 20% crystallinity threshold for enzymatic hydrolysis can be reached within 3 h at 75 °C.<sup>5</sup> This competitive physical aging process of amorphous polymers can therefore considerably reduce the efficiency of enzymatic PET depolymerization, which limits the maximum extent of degradation that can be achieved.<sup>25</sup> Therefore, biocatalysts with  $T_{\text{opt}}$  in the range 72–74 °C, rather than with extremely high  $T_m$  values, are desired.<sup>6</sup> The mesophilic IsPETase ( $T_m$  of 48.7 °C) has also been subjected to protein engineering to improve its thermostability. For example, Cui et al. used a computational strategy to design DuraPETase, a variant with a 31 °C higher  $T_m$  and considerably improved PET hydrolysis activity than the wild-type enzyme.<sup>26</sup> More recently, a machine-learning-aided approach was used to engineer IsPETase to produce Fast-PETase, a variant with a  $T_m$  of 67.1 °C and increased depolymerization efficiency.<sup>27</sup>

In-depth understanding of the binding mechanisms and noncovalent interactions of insoluble polymeric substrates with biocatalysts can contribute to the design of more efficient PET hydrolases. So far, only two studies have reported structures of crystals soaked with PET analogues. Han et al. reported a structure of the inactive R103G/S131A IsPETase mutant complexed with 1-(2-hydroxyethyl) 4-methyl terephthalate (HEMT).<sup>28</sup> Zeng et al. reported the structure of an inactive S165A mutant of LCC ICCG complexed with mono-(2-hydroxyethyl) terephthalate (MHET).<sup>23</sup> Consequently, more structures of PET hydrolases with bound substrate analogues are needed. This would enable more precise computational simulations for elucidating the mechanisms of enzymatic depolymerization and predicting more efficient mutants. So far, studies mostly relied on computationally modeled PET substrate conformations.<sup>15,29–32</sup> Therefore, we solved crystal structures of two PET hydrolases in complex with PET analogues.

Two highly similar thermophilic PET hydrolases (PES-H1 and PES-H2), derived from a compost metagenome library, were recently disclosed in a patent application.<sup>33</sup> PES-H1 demonstrated exceptional hydrolytic activity on amorphous PET films, outperforming wild-type LCC under identical conditions.<sup>13,15</sup> Nearly complete depolymerization was achieved after incubation at 70 °C for 24 h.<sup>33</sup> We first solved high-resolution structures of both enzymes in their apo form (PDB codes: 7CUV for PES-H1 and 7W69 for PES-H1). While this work was in progress, another crystal structure of PES-H1 (called PHL7 in the publication, PDB code: 7NEI)

was solved.<sup>34</sup> By soaking with various PET substrate analogues, structures of both PES-H1 and PES-H2 in complex with these ligands were obtained by us. These structures were used for exploring substrate binding modes by molecular dynamics (MD) simulations. Finally, we generated PES-H1 variants with significantly improved activity on both amorphous Goodfellow PET (Gf-PET) films and pretreated postconsumer (‘real-world’) PET waste. These variants outperformed both the wild-type PES-H1 and LCC ICCG.<sup>5</sup>

## RESULTS AND DISCUSSION

**Structures of PES-H1 and PES-H2.** The crystal structures of PES-H1 and PES-H2 were solved at atomic resolutions of 1.45 Å (PDB code: 7CUV) and 1.56 Å (PDB code: 7W69), in the space groups  $P2_1$  and  $C2$ , respectively (Figure S1; Tables S1 and S2). PES-H1 and PES-H2 differ in only four residues (A/E1, L/F209, D/N232, and S/A254), of which only the L/F209 residues are in close vicinity to the catalytic triad (Figure 1). The two hydrolases have similar structures that adopt the

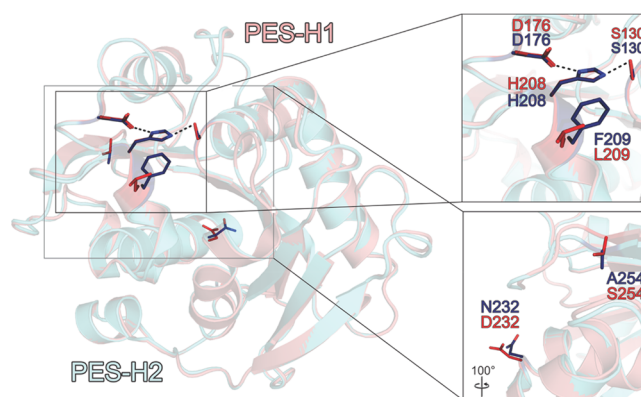


**Figure 1.** Structural comparison of PES-H1 (salmon, PDB code: 7CUV) and PES-H2 (light blue, PDB code: 7W69). The locations of the variable residues L/F209, D/N232, and S/A254 are indicated. The variable position A/E1 is located at the flexible N-terminal ends of PES-H1 and PES-H2 and are therefore not visible. The S130–H208–D176 catalytic triad is also shown. The amino acid residues are shown as sticks in red for PES-H1 and in dark blue for PES-H2. The inset in the right upper panel demonstrates the close vicinity of the variable position L/F209 to the catalytic triad.

canonical  $\alpha/\beta$ -hydrolase fold with a core consisting of nine  $\beta$ -sheets and ten  $\alpha$ -helices (Figure S1). Comparison of the apo structure of PES-H1 with the structures of other bacterial PET hydrolases resulted in low root-mean-square deviation (RMSD) values for the protein backbone (Table S3). These highly conserved structures form a distinct subclass of the  $\alpha/\beta$ -hydrolase superfamily.<sup>6</sup> PES-H1 has a catalytic triad consisting of S130, H208, and D176 (Figure 1). The nucleophile S130 is located within hydrogen bond distance to be polarized by the base H208, which is in turn stabilized by the acid D176. PES-H1 forms an intramolecular disulfide bridge like structurally similar homologous enzymes (e.g., PDB codes: 5XH3, 3VIS, 4CGI, 4EB0, 4WFJ, and 1JFR). This conserved disulfide bridge (C241/C256) connects two loops between the last  $\beta$ -sheet (Figure S1).

**Binding Modes of Substrate Analogues and Degradation Intermediates.** Although more than 70 crystal structures of bacterial PET-degrading enzymes are available in the PDB database, the majority of them are apo structures

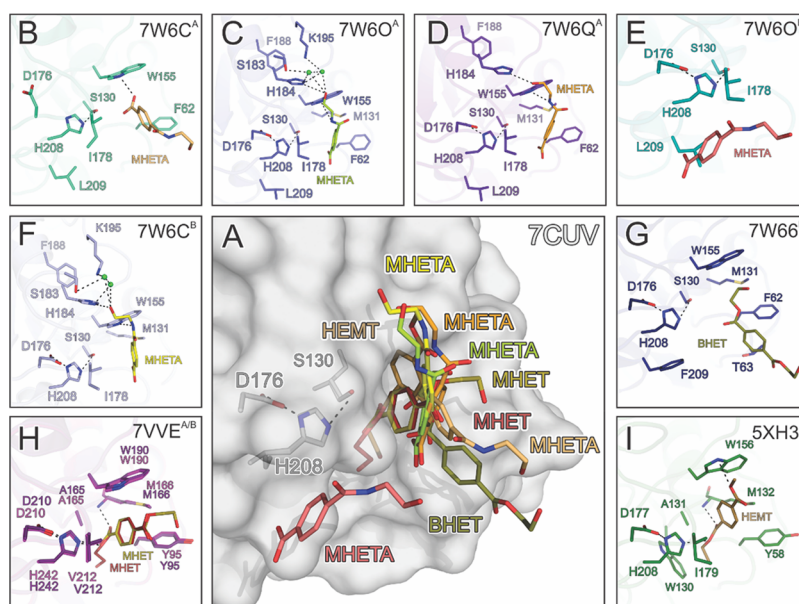


**Figure 2.** Comparison of the PET substrate analogue binding modes in the structures of PES-H1, PES-H2, LCC ICCG S165A, and *IsPETase* R103G/S131A. Single chains (superscripts for chain A or chain B) were extracted from the deposited structures in the PDB database to identify individual binding modes of the soaked ligands within an asymmetric unit. Dashed lines indicate hydrogen bonds (H-bond cut off of 3.5 Å). Interacting residues are shown as sticks and are colored by element: carbon, as for the respective molecule; nitrogen, blue; oxygen, red; sulfur, yellow. Green spheres represent water oxygens. (A) Superimposed structures show the overlapping binding modes of the substrate analogues with the apo structure of PES-H1 (PDB code: 7CUV). (B–F) PES-H1 in complex with MHETA: (B) 7W6C<sup>A</sup>; (C) 7W6O<sup>A</sup>; (D) 7W6Q<sup>A</sup>; (E) 7W6O<sup>B</sup>; and (F) 7W6C<sup>B</sup>. (G) PES-H2 in complex with BHET (7W66). (H) LCC ICCG S165A in complex with MHET (7VVE<sup>A</sup>, 7VVE<sup>B</sup>). (I) *IsPETase* R103G/S131A in complex with HEMT (5XH3).

with no substrate bound.<sup>6</sup> In order to investigate the mechanism of PET hydrolysis, we solved the structures of PES-H1 in complex with citrate (PDB code: 7E30) and also in complex with the nonhydrolyzable substrate analogue 4-(2-hydroxyethylcarbamoyl) benzoic acid (MHETA) (PDB codes: 7W6C, 7W6O, and 7W6Q; Figure 2B–F), to better understand changes in the protein structure upon binding a PET substrate based on this analogue. We also solved the structures of PES-H2 in complex with polyethylene glycol (PEG) 6000 (PDB code: 7E31) and in complex with bis(2-hydroxyethyl) terephthalate (BHET) (PDB code: 7W66; Figure 2G) (Tables S1 and S2). Based on the structures of PES-H1 (with bound MHETA) and PES-H2 (with bound BHET), six ligand-binding modes were identified. The orientations of the ligands in the substrate binding cavities are distinct but similar to those observed for HEMT bound to *IsPETase* R103G/S131A<sup>28</sup> (PDB code: 5XH3; Figure 2I) and MHET bound to the S165A variant of LCC ICCG<sup>23</sup> (PDB code: 7VVE; Figure 2H).

While the structures of LCC ICCG S165A (PDB code: 7VVE; Figure 2H) and *IsPETase* R103G/S131A (PDB code: 5XH3; Figure 2I) exhibited productive ligand conformations with the ester carbonyl carbons interacting with the oxygen of the catalytic serine residue, the PES-H structures revealed multiple noncatalytic intermediate binding modes (IBMs) with the ester bonds (or amide bond in MHETA) positioned too far from S130 for nucleophilic attack. This supports the previous hypothesis that PET hydrolysis may involve dynamic reorientation of polymer chains in the active sites of PET hydrolases.<sup>15,35</sup> MHET and BHET have frequently been found to inhibit enzymatic PET depolymerization.<sup>36,37</sup> The multiple IBMs suggest an enhanced residence likelihood of these inhibitory degradation intermediates in the substrate-binding

groove, where they may prevent productive binding of polyester segments.

The conformational flexibility of predominantly hydrophobic residues surrounding the active site may help to recognize and bind bulky PET substrates during biocatalysis. In the enzyme–substrate complex structures of LCC ICCG S165A (Figure 2H) and *IsPETase* R103G/S131A (Figure 2I), the aromatic rings of the substrate analogues are T-stacked to W190 and W156, respectively. This effect has been proposed to be very important for PET binding.<sup>38</sup> Similar  $\pi$ -stacking interactions with the equivalent W155 were discovered in the PES-H1 structures 7W6C (Figure 2B, F), 7W6O<sup>A</sup> (Figure 2C), and 7W6Q<sup>A</sup> (Figure 2D). In most IBMs of MHETA ligands (Figure 2B–F), the hydroxyl end of the ethanolamine moiety points away from the catalytic triad. This is partly in agreement with the MHET conformation shown in 7VVE (Figure 2H), which is different from the position of the ethylene glycol (EG) moiety of HEMT bound to *IsPETase* R103G/S131A (5XH3; Figure 2I). MHETA ligands also interacted with other hydrophobic residues like F62, I178, and L209 in the binding groove of PES-H1. The backbone amide NH groups of M131 and F62 form an oxyanion hole, which is a characteristic shared by many  $\alpha/\beta$ -hydrolases. Terephthalate (TPA) moieties in our structures are found in close vicinity to F62 (equivalent to Y95 in LCC ICCG S165A and Y58 in *IsPETase* R103G/S131A), rather than close to the catalytic triads as in *IsPETase* R103G/S131A (Figure 2I) and LCC ICCG S165A (7VVE<sup>A</sup>; Figure 2H). Furthermore, the hydroxyl end of the ethanolamine moiety forms a hydrogen bond with H184 (Figure 2C,D). The only distinct MHETA binding mode in PES-H1 was observed in 7W6O<sup>B</sup> (Figure 2E), in which MHETA is bound at the surface of PES-H1, slightly outside the catalytic cavity. This binding mode suggests that

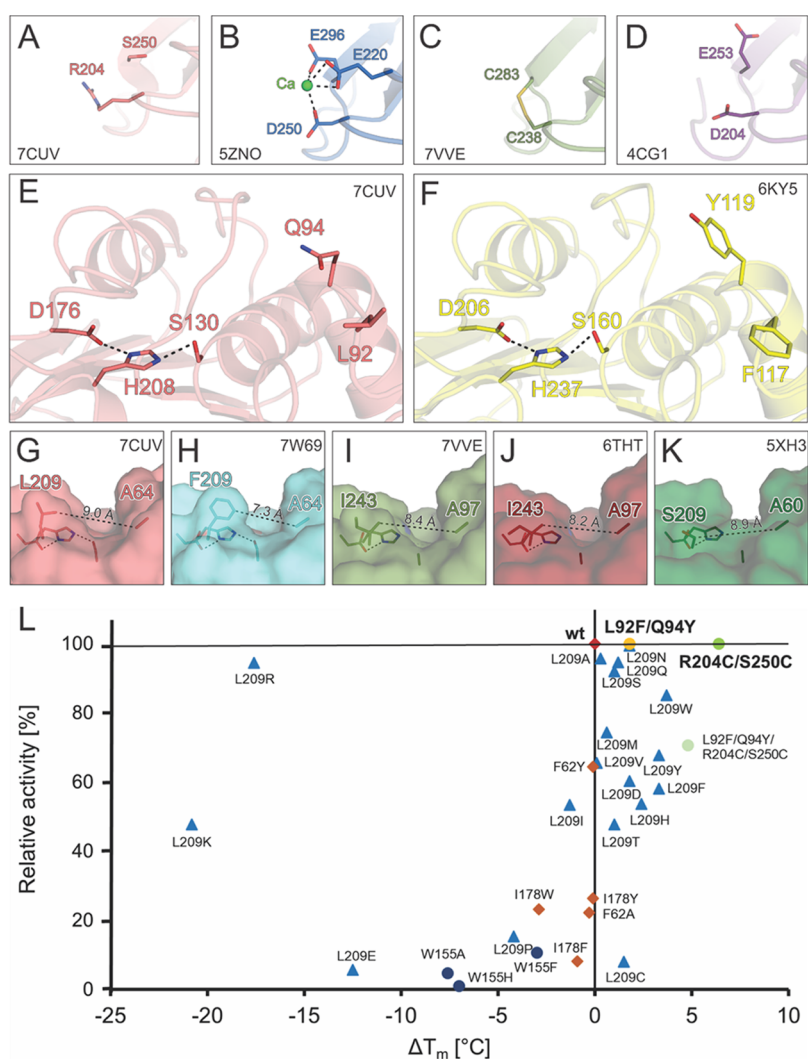


**Figure 3.** Overview of selected engineering hotspots in PES-H1 for enhancing PET hydrolysis activity and thermostability. (A) A disulfide bridge (R204/S250) is introduced into PES-H1 (PDB code: 7CUV) where a putative Ca<sup>2+</sup> binding site (D250/E296) is found in (B) the homologous Cut190. (C) Similarly engineered disulfide bridges in LCC ICCG (C238/C283; PDB codes: 7VVE and 6THT) and (D) TfCut2 (D204/E253; PDB code: 4CG1). (E) The L92F and Q94Y substitutions of PES-H1 were based on the corresponding residues in (F) DuraPETase (F117 and Y119; PDB code: 6KY5). (G–K) Variable amino acid residues were found at the site equivalent to L209 in PES-H1: (G) PES-H1, PDB code 7CUV; (H) PES-H2, PDB code 7W69; (I, J) LCC ICCG S165A, PDB codes 7VVE and 6THT; and (K) *IsPETase* R103G/S131A, PDB code 5XH3. These residues influence the width of the substrate-binding groove. (L) A number of PES-H1 variants had different PET hydrolyzing activities and thermostabilities. Changes in  $T_m$  compared to the wild-type enzyme ( $\Delta T_m$  (°C)) are shown. The percentage relative activity compared to the wild-type enzyme was calculated based on the weight loss of Gf-PET film after 24 h at 72 °C. Red square: wild-type PES-H1. Blue triangles: L209 variants. Orange squares: I178 and F62 variants. Dark blue dots: W155 variants. Light green dot: L92F/Q94Y/R204C/S250C variant. Green dot: R204C/S250C variant with a disulfide bond introduced. Yellow dot: L92F/Q94Y variant.

substrates can bind at the surface prior to entering deeper into the active site cavity. BHET is more loosely bound to PES-H2 (7W66<sup>B</sup>; Figure 2G). It is embedded in a groove consisting of S130, H207, W155, I178, H129, F62, and M131. The ester bond between the TPA and EG moieties is closer to S130 but is still outside the catalytic distance, in contrast to the positioning of MHETA in PES-H1. The TPA moiety is close to F62 but far from W155. The second EG moiety is completely exposed to the solvent and has no obvious interactions with any residue.

**MD Simulations to Study the Interactions of PES-H1 with a PET Oligomer.** To better understand the mechanism of PET hydrolysis, we performed MD simulations of PES-H1 in complex with a modeled oligomer consisting of three repeating PET units (3PET) (Figure S3C) to resemble the

binding of a longer polymer segment. PES-H1 remained stable in MD simulations at a time scale of 100 ns as indicated by the steady low backbone RMSD of less than 1 Å compared to the crystal structure (Figure S2). The modeled PES-H1-3PET complex corresponds to a productive state with short distances between the oxyanion hole amides and the central 3PET carbonyl oxygen atom (2.32 and 1.80 Å), and between the carbonyl carbon of an ester in 3PET and the side chain oxygen of the catalytic S130 (2.32 Å). Unfluctuating distances of the 3PET carbonyl carbons to the catalytic S130 verified the productive state of the modeled oligomer during three independent 100 ns MD simulations (Figure S3). Nonetheless, 3PET was slightly flexible in the PES-H1 binding site (Figure S3A). To identify the most favorable 3PET binding modes, we concatenated the trajectories and clustered the 3PET

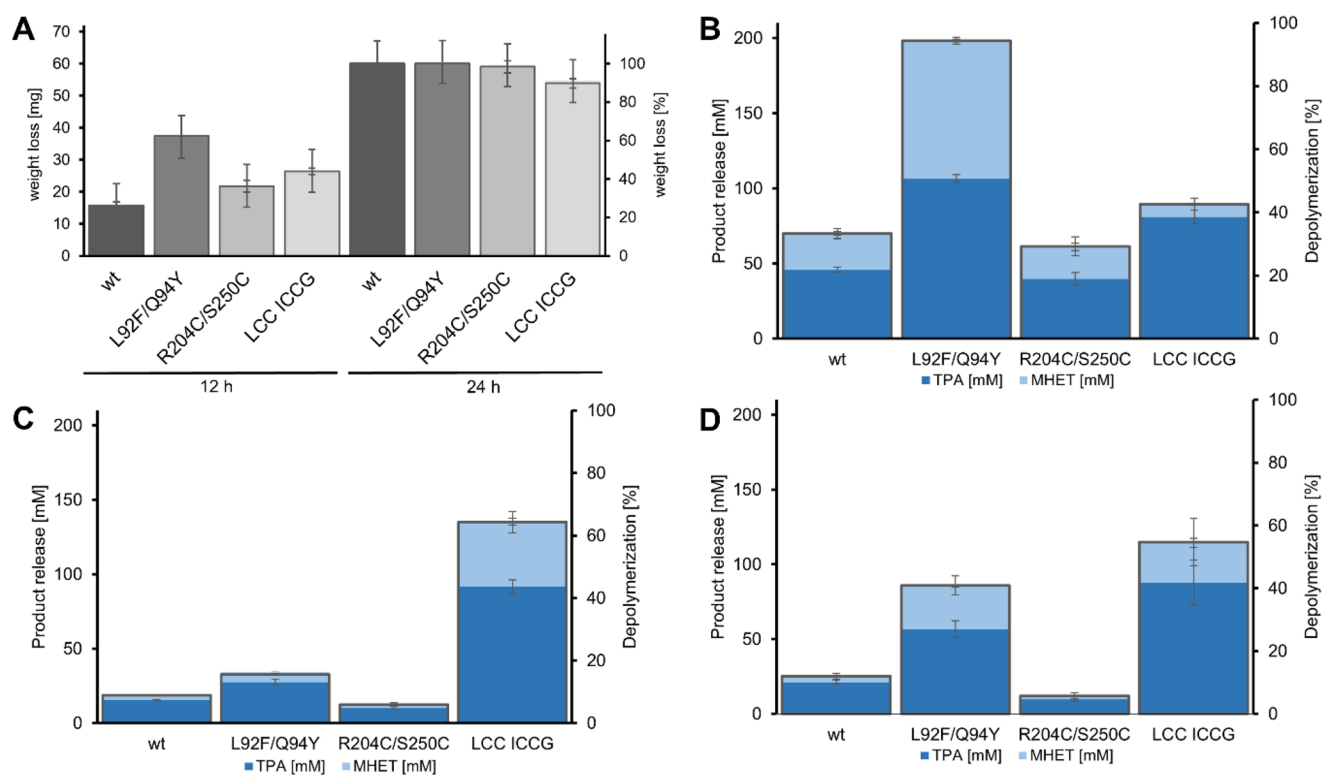


**Figure 4.** Characterization of PET-hydrolyzing activity of PES-H1 (wt), the L92F/Q94Y and R204C/S250C variants, and LCC ICCG. (A) Weight loss (in [mg] and [%]) of Gf-PET film determined after enzymatic hydrolysis at 72 °C for 12 and 24 h in 1 M potassium phosphate buffer (pH 8.0). (B–D) Total product release [mM] is shown and used to calculate the depolymerization efficiency [%] with (B) lcPET powder (13%), (C) ball-milled hcPET powder (26%), and (D) grinder-crushed hcPET powder (33%) after 24 h at 72 °C. The total product was defined as the sum of TPA (dark blue), MHET (light blue), and BHET (light gray). Error bars indicate the standard deviation calculated from at least three replicates.

conformations. The four most populated clusters correspond to the four preferred binding modes, each including >5% of all ligand conformations (Figure S4). Cluster 1 represents the 3PET binding mode adopted in about 28% of the conformations (Table S4, Figure S4C). After superimposing the PES-H1 (PDB code: 7CUV) and LCC ICCG S165A structures (PDB code: 7VVE), the central PET unit of cluster 1 and the MHET overlap well with an RMSD of 2.95 Å, while the binding mode of cluster 3 (found in about 8% of all conformations) deviates the most from that of MHET, with an RMSD of 4.01 Å (Figure S4D). This suggests that being adjacent to S130 results in multiple beneficial interactions between PET and the surrounding residues. Evaluating the interaction energies of the four binding poses demonstrated that hydrophobic Lennard-Jones (LJ) interactions between the side chains and the central 3PET unit had a predominant influence on binding. F62, W155, and I178 formed strong LJ interactions ( $<-10$  kJ mol<sup>-1</sup>), in agreement with their close interactions with soaked MHETA ligands (Figure 2B–D,F,G). H208 and M131 also formed strong LJ interactions ( $<-7$  kJ mol<sup>-1</sup>) (Figures 1 and 3; Figure S4C). Additionally, T63, A64, and L209 mediate strong LJ interactions ( $<-7$  kJ mol<sup>-1</sup>) with all three units of 3PET. The side chains of F62 and W155 form stable aromatic interactions with the aromatic rings of 3PET. The orientation of the TPA moieties suggest T-stacking interactions with W155, in agreement with the orientation of MHETA bound to PES-H1 (PDB codes: 7W6C<sup>A</sup>, 7W6C<sup>B</sup>, 7W6O<sup>A</sup>, and 7W6Q<sup>A</sup>) and with earlier studies on other PET hydrolases.<sup>12,23</sup> Furthermore, the strong LJ interactions with F62 are in agreement with the close proximity between

MHETA and F62. The Coulomb interactions involve fewer residues and are often mediated by backbone atoms of residues, like F62 and M131 from the oxyanion hole, and L92, but can also involve side chains of residues like Q94, H208, N212, and the catalytic S130 ( $<-7$  kJ mol<sup>-1</sup>). It should be emphasized that the significant contributions by L92 and Q94 are the result of hydrogen bonding with the terminal carboxyl group of the first PET unit, which should only occur when exocission of polymeric PET substrates takes place. When the total interaction energy is considered, G61, H129, and T157 are also identified as strong PET-binding residues ( $<-7$  kJ mol<sup>-1</sup>).

**Engineering PES-H1 for Improved Thermostability and Activity on Amorphous PET Film.** Elevated reaction temperatures of up to 75 °C increase polymer chain mobility, making the amorphous fractions of PET more accessible to enzymatic hydrolysis. We investigated enzymatic PET degradation at 72 °C because it is the optimal temperature for the hydrolysis of amorphized PET waste by the reference enzyme LCC ICCG.<sup>5</sup> Empirical data have shown that the  $T_m$  of a PET hydrolase is usually at least 12 °C higher than its  $T_{opt}$ .<sup>5,11,13,17</sup> Hence, biocatalysts with a  $T_m$  over 85 °C are preferred for efficient PET degradation. When determined in buffers with low ionic strengths (Table S5), PES-H1 had a  $T_m$  of 77.1 °C, as determined by nano differential scanning fluorimetry (NanoDSF) and differential scanning calorimetry (DSC). This is in agreement with previously published data.<sup>34</sup> In the 1 M potassium phosphate buffer demonstrated by previous studies to be optimal for PET degradation by selected enzymes,<sup>33,34,39</sup> the  $T_m$  of PES-H1 was increased to 85 °C

(Table S5), thereby enabling its application at 72 °C (Figure S5). Because high salt concentrations are not ideal for industrial processes, we investigated the degradation of Gf-PET film by PES-H1 in the presence of lower phosphate buffer concentrations (Figure S6). The results demonstrated a positive correlation between the buffer concentration and the PET degradation performance of wild-type PES-H1 at 72 °C. This is most likely due to the decreased thermostability of PES-H1 at lower buffer concentrations (Table S5).

Many homologous PET hydrolases, including PES-H1 itself, have been found to be stabilized in the presence of Ca<sup>2+</sup> ions, as indicated by increased  $T_m$ , improved PET-hydrolyzing activity, or both.<sup>13,17,18</sup> Ca<sup>2+</sup> binding can be mediated by several negatively charged residues. For example, D250 and E296 in the homologous Cut190 from *Saccharomonospora viridis* were identified by crystallographic investigations to be involved in Ca<sup>2+</sup> binding (Figure 3B).<sup>40</sup> Ca<sup>2+</sup> can be precipitated by buffer ions like phosphate and also by the PET hydrolysis product terephthalate,<sup>6,41</sup> making the dependence of PET hydrolase stability on Ca<sup>2+</sup> undesirable. This dependence can be significantly mitigated by replacing the Ca<sup>2+</sup> binding residues by a disulfide bridge to generate variants that are thermostable in the absence of Ca<sup>2+</sup>.<sup>5,19,11,17,20–22</sup> Accordingly, we generated an R204C/S250C variant of PES-H1 and confirmed disulfide bond formation using Ellman's reagent (Figure S7). The  $T_m$  of this variant was increased by 6.4 °C (Figure 3L, Table S5). Previous studies reported that introducing disulfide bridges at equivalent positions of homologous PET hydrolases resulted in higher increases in  $T_m$  (TfCut2,  $\Delta T_m = 24.9$  °C; IsPETase,  $\Delta T_m = 22.3$  °C; LCC,  $\Delta T_m = 9.8$  °C; Cut190,  $\Delta T_m = 23.1$  °C).<sup>5,17,19,21</sup> While more negatively charged amino acids like D250 and E296 in Cut190 (Figure 3B), D238 and S283 in LCC (Figure 3C), and D204 and E253 in TfCut2 (Figure 3D) are frequently observed at these sites, wild-type IsPETase (N204 and S253) and PES-H1 (R204 and S250, Figure 3A) lack these negatively charged residues. This suggests that the generic thermostabilizing effect of an engineered disulfide bridge at this position might be due to a variety of interactions rather than just replacing the Ca<sup>2+</sup> binding site. After 24 h at 72 °C, both the wild-type and the R204C/S250C variant of PES-H1 hydrolyzed Gf-PET film (98% depolymerization) almost completely (Figure 4A).

Recently, Nakamura et al. reported an R47C/G89C variant of the homologous hydrolase PET2 and validated the formation of a disulfide bridge by X-ray crystallography.<sup>22</sup> Compared to wild-type PET2, the  $T_m$  of the R47C/G89C variant of PET2 was increased by 3.1 °C, and its PET hydrolysis activity was 1.3-fold higher. We created a R6C/S49C variant in an attempt to form an equivalent disulfide bridge in PES-H1. This variant was inactive and was therefore not further investigated.

The PES-H1 structure (PDB code: 7CUV, Figure 3E) was compared to the thermostabilized DuraPETase (PDB code: 6KYS, Figure 3F) for identifying additional mutation hotspots. Using Rosetta energy calculations, an L92F/Q94Y variant of PES-H1 was constructed based on the L117F/Q119Y mutations present in DuraPETase. The L92F/Q94Y variant of PES-H1 had a 1.8 °C higher  $T_m$  and could almost completely depolymerize Gf-PET film after 24 h at 72 °C (Figures 3L and 4A). Interestingly, the aromatic amino acids that we introduced (L92F/Q94Y) correspond to equivalent residues (F125 and Y127) in LCC ICC.<sup>5</sup> Interestingly, LCC ICC was converted to the more active LCC ICCG by removal

of the tyrosine residue (Y127G), while introduction of the equivalent tyrosine into PES-H1 (Q94Y) in combination with L92F resulted in increased activity. The L92F/Q94Y variant of PES-H1 outperformed LCC ICCG in the hydrolysis of various PET materials under conditions optimal for PES-H1 (Figure 4A,B). Cui et al. also observed synergistic effects between the equivalent L117F (L92F in PES-H1) and Q119Y (Q94Y in PES-H1) substitutions.<sup>26</sup> They argued that these aromatic residues interact with other residues (S214, W185, and Y87) to form an “aromatic tunnel” that facilitates the binding of PET chains to the active site. The hydrophobic nature of the mutations enhances noncovalent interactions with the substrate and improves the overall hydrophobic packing and stability of DuraPETase. The same effect could explain the increased activity and stability of the L92F/Q94Y variant of PES-H1. We introduced the previously discussed disulfide bridge (R204C/S250C) to the L92F/Q94Y variant to generate the L92F/Q94Y/R204C/S250C variant of PES-H1. Although the  $T_m$  of this variant was increased by 4.8 °C, it was not further characterized because it hydrolyzed Gf-PET film less efficiently than wild-type PES-H1 (Figure 3L).

Of the four residues that differ between PES-H1 and PES-H2, only L209 is located close to the active site (Figures 1 and 3G). This site has repeatedly been recognized as an engineering hotspot in other homologous PET hydrolases due to its potential interactions with polymeric substrates. Variants with increased specific activity on PET have been created by replacing F at this position with A (TfCut2: F208A), W (LCC WCCG: F243W), or I (LCC ICCG: F243I; Figure 3I,J).<sup>5,42</sup> The equivalent S of IsPETase (Figure 3K) has also been replaced with F, but an additional W159H substitution was required for improved PET hydrolysis activity.<sup>43</sup> It was recently shown that exchanging L209 in PES-H1 (called PHL7 by Sonnendecker et al.<sup>34</sup>) to the F found in PES-H2 (Fig 3G,H) reduced PET hydrolysis activity by half. We obtained similar results for the hydrolysis of Gf-PET film by the L209F variant of PES-H1 (Figure 3L). We subjected position L209 to saturation mutagenesis and found that most variants (except L209K, L209R, L209E, L209P, and L209I) resulted in enhanced thermostability. For the L209W, L209F, and L209Y variants, the highest  $\Delta T_m$  in 50 mM phosphate buffer ranged from 3.3 to 3.7 °C (Figure 3L). However, the PET hydrolysis activities of these variants were decreased by more than 15%. Several earlier studies<sup>43,44</sup> suggested that the S238F substitution (equivalent to L209F in PES-H1) in the W159H/S238F variant of IsPETase narrowed the active site cleft, potentially enhancing  $\pi$ -stacking between PET and F238. In contrast, Furukawa et al.<sup>42</sup> suggested that the corresponding F of TfCut2 restricts access to lcPET, attributing the influence of this residue on catalytic activity to side-chain volume rather than hydrophobicity. Therefore, the role of this important residue is still not fully understood, and it may play different roles in different PET hydrolases.

In addition, we engineered several key residues potentially involved in strong interactions with PET as indicated by structures of PES-H1 and PES-H2 in complex with PET analogues (Figure 2) and MD simulations (Figure S4). These include F62 (Figure 2B–D,G), W155 (Figure 2B–D,F,G), and I178 (Figure 2E). F62 is part of the oxyanion hole. Except for PES-H1, Cut190,<sup>18</sup> and Tcur1278,<sup>45</sup> other known homologous PET hydrolases have a tyrosine at this position. Introducing this tyrosine into PES-H1 (F62Y) lowered the hydrolytic



activity drastically but had no influence on  $T_m$  (Figure 3L). The same effects were observed for the F62A variant.

The W155 residue of PES-H1 is equivalent to the W185 residue of *IsPETase*. The W185 of *IsPETase* (W130 in Figure 2I due to different residue numbering in the 5XH3 crystal structure) is flexible and can move to open or close access to the active site.<sup>43</sup> This wobbling is beneficial for mesophilic PET hydrolases because the PET polymer chain has lower chain mobility at ambient temperatures, and a flexible W185 may facilitate substrate binding.<sup>15</sup> This dynamic tryptophan is conserved in many homologous PET hydrolases and is involved in strong interactions with the aromatic rings of PET. We replaced the W155 of PES-H1 to A, F or H, resulting in almost complete loss of activity and considerably reduced stability (Figure 3L). Austin et al. reported similarly reduced activity for the equivalent W185A variant of *IsPETase*.<sup>43</sup> In contrast, the conformation of the corresponding W190 (Figure 2H) in the thermophilic LCC ICCG is fixed by interactions with H218 and F222 (H184 and F188 in PES-H1, Figure 2C,D,F). As a result, LCC ICCG has a more rigid substrate-binding groove, yet it still allows PET binding at elevated temperatures as a result of increased polymer chain mobility.<sup>23</sup>

The I178 residue is located near the catalytic triad of PES-H1 (Figure 2B–D,F). Previous studies have reported substitutions of this I178 residue in homologous *Thermobifida fusca* cutinases to smaller residues like S or A, which resulted in PET hydrolyzing activities comparable to that of the wild-type enzyme.<sup>46,47</sup> Therefore, we instead substituted I178 to large aromatic residues. However, the I178W, I178F, and I178Y variants lost significant PET hydrolysis activity, and their  $T_m$  decreased slightly, suggesting that additional aromatic interactions may hinder productive binding of PET chains. Therefore, we did not further investigate the I178 residue of PES-H1.

**Comparing the Hydrolytic Activity of Selected PES-H1 Variants on Different PET Materials.** The L92F/Q94Y and R204C/S250C variants of PES-H1 were further investigated using different PET materials. The crystallinity of real-world postconsumer PET waste depends on its thermal history and life cycle.<sup>6</sup> Therefore, for biocatalytic recycling at the industrial scale, pretreatment by thermomechanical amorphization and micronization is essential to provide uniformly degradable substrates (in terms of comparable crystallinity, particle size, etc.).<sup>5,48</sup> In this study, we used a melt-quenching technique to amorphize postconsumer PET bottles, which were then micronized by various methods. Crystallinity of the PET bottle waste was decreased from 27% to 19% after melt-quenching and increased again to 33% and 26%, respectively, after crushing or ball milling (Table S6). The crystallinity values determined with differently micronized PET powders are in good agreement with two previous studies.<sup>48,49</sup> However, the crystallinities of our samples were markedly higher than that reported by Tournier et al., who used other techniques.<sup>5</sup> We determined the average molecular masses of selected PET samples by gel permeation chromatography (GPC) and found that values decreased after melt-quenching and micronization (Table S6). Since the particle size can influence the biocatalytic degradability of PET powders, it was important to use similarly sized particles for all assays. Therefore, we sieved all micronized PET samples using a 177  $\mu\text{m}$  mesh to obtain more homogeneous powders.

LCC ICCG and the wild-type PES-H1 were used as reference enzymes. The distinct distribution of charged amino

acids at the surfaces of these two enzymes may explain the differences in their buffer requirements (Figure S8). Compared to PES-H1, LCC ICCG does not lose its thermostability and PET degrading activity at a low phosphate buffer concentration (100 mM).<sup>5</sup> However, higher phosphate concentrations (up to 1 M) do not reduce the PET hydrolysis activity of wild-type LCC.<sup>15,39,50</sup> Since 1 M phosphate buffer is optimal for the activity and stability of PES-H1 while not negatively influencing LCC, we used this buffer for all subsequent PET degradation experiments. As shown in Figure 4A, wild-type PES-H1 and the L92F/Q94Y variant completely depolymerized Gf-PET film in 24 h at 72 °C. Therefore, we also determined the weight loss after 12 h of incubation. The highest weight loss of 37.1 mg (62.4%) was obtained with the L92F/Q94Y variant, and this was 2.3-fold higher than with wild-type PES-H1. The L92F/Q94Y variant also significantly outperformed both the R204C/S250C variant and LCC ICCG in the hydrolysis of Gf-PET film (Figure 4A). Averaged conversion rates of 2.5  $\text{mg}_{\text{PET}} \text{h}^{-1}$  and 2.3  $\text{mg}_{\text{PET}} \text{h}^{-1}$  were obtained using wild-type PES-H1 and LCC ICCG, respectively. While the value for PES-H1 is similar to that previously determined by Sonnendecker et al.,<sup>34</sup> the value for LCC ICCG is markedly lower than that reported by Tournier et al.<sup>5</sup> As explained above, this may in part be due to differences between the PET materials used in different studies. Based on the information provided by the manufacturer, Gf-PET films differ considerably in terms of crystallinity, thickness, molecular mass, and many other polymer parameters, making a direct comparison of data generated in different studies impossible.<sup>6</sup>

After 24 h at 72 °C, the degradation performance of PES-H1, L92F/Q94Y, R204C/S250C, and LCC ICCG on low-crystallinity (13%) micronized waste PET powder was comparable to that on Gf-PET film. The L92F/Q94Y variant yielded 2.9-fold and 2.2-fold more degradation products than wild-type PES-H1 and LCC ICCG, respectively (Figure 4B). This indicated that, under the applied degradation conditions, the L92F/Q94Y variant was the most active lcPET hydrolase. The R204C/S250C variant was as active as the wild-type PES-H1 in hydrolyzing lcPET materials (Figure 4A,B). However, the R204C/S250C variant was significantly less active than the wild-type against hcPET materials (Figure 4C,D). In contrast, the L92F/Q94Y variant was more active than the wild-type PES-H1 against hcPET powders, forming up to 3.4-fold more degradation products (Figure 4D). For hydrolyzing hcPET powders (Figure 4C,D) generated by different pretreatment methods, LCC ICCG outperformed all PES-H1 variants and yielded up to 4.0-fold more degradation products than the L92F/Q94Y variant (Figure 4C,D). While the crystallinities of the crushed and ball-milled PET powders were clearly higher than the degradable threshold value of approximately 20% suggested by Wei et al.<sup>25</sup> and Thomsen et al.,<sup>24</sup> LCC ICCG surprisingly released more degradation products from these substrates than from lcPET powder (13% crystallinity) (Figure 4B–D). By comparison with PES-H1 and its variants, the extent of degradation was inversely correlated to the material crystallinity, which is in agreement with previous research on using hydrolases to degrade PET with varying crystallinities.<sup>6</sup>

In addition to the crystallinity values obtained by DSC, we also determined the number-average ( $M_n$ ) and weight-average ( $M_w$ ) molecular masses of the PET powders used for the enzymatic degradation experiments (Table S6). The lower  $M_n$  values determined for the hcPET powders derived from ball-milled and grinder-crushed PET bottle waste than that with

the grinder-crushed PET film means that the PET bottle powders contained significantly shorter polymers (or even oligomers). When the degradation by PES-H1, its variants, and LCC ICCG (Figure 4B–D) is interpreted in terms of the molecular masses of the PET powders, it appears that  $M_n$  had a larger influence on the degradation by LCC ICCG than by PES-H1 and its variants. LCC ICCG seems to hydrolyze shorter polymers more efficiently, while the degradation by PES-H1 and its variants seems to be more influenced by crystallinity. Tournier et al.<sup>5</sup> found that LCC ICCG could not efficiently depolymerize the hcPET obtained by their pretreatment methods, but they did not report the molecular masses of their materials. Therefore, a direct comparison of our data to that reported by Tournier et al.<sup>5</sup> cannot be made, but our data suggest that not only crystallinity but also average polymer length may influence the enzymatic degradation of PET. This suggests that crystallinity might be only one of several important polymer characteristics that influence enzymatic degradation and that polymer properties should be more extensively characterized in future studies. The superiority of the L92F/Q94Y variant of PES-H1 in degrading lcPET is important since industrially amorphized PET waste has crystallinities below 15%.<sup>5</sup> The L92F/Q94Y variant of PES-H1 could therefore be investigated as an alternative to LCC ICCG for PET hydrolysis.

A heterogeneous kinetic model described by the following equation has been widely used for evaluating enzymatic PET hydrolysis.<sup>12,45,46,51–53</sup>

$$v_0 = k_h[S_0] \frac{K_A[E_0]}{1 + K_A[E_0]} \quad (1)$$

In this equation,  $v_0$  describes the initial reaction rate,  $k_h$  the hydrolysis rate constant,  $[S_0]$  the initial substrate concentration,  $[E_0]$  the enzyme concentration, and  $K_A$  the adsorption equilibrium constant. We used PET nanoparticles (PET-NP) prepared using previously published protocols<sup>51,54</sup> as the substrate to characterize the hydrolysis kinetics catalyzed by PES-H1, its variants, and LCC ICCG. The rates of turbidity change measured at 600 nm as a result of PET-NP degradation were determined in a microplate reader at 70 °C (Figures S9 and S10). The kinetic constants determined according to eq 1 are summarized in Table 1. The initial reaction velocity  $v_0$  was

**Table 1. Kinetic Parameters for PET-NP Hydrolysis by PES-H1, Its Variants, and LCC ICCG**

	$K_A$ [ $\mu\text{M}^{-1}$ ]	$k_h$ [ $\text{mL mg}^{-1} \text{min}^{-1}$ ]
PES-H1 wild-type	$4.710 \pm 0.087$	$0.054 \pm 0.001$
L92F/Q94Y	$8.259 \pm 0.028$	$0.065 \pm 0.002$
R204C/S250C	$4.063 \pm 0.191$	$0.064 \pm 0.001$
LCC ICCG	$5.953 \pm 0.032$	$0.048 \pm 0.001$

defined as the turbidity decrease over a reaction time of 40 min using 0.5 mg mL<sup>-1</sup> PET-NP (Figure S9). The L92F/Q94Y variant resulted in the highest hydrolysis rate constant ( $k_h$ ) of 0.065 mL mg<sup>-1</sup> min<sup>-1</sup>, followed by R204C/S250C (0.064 mL mg<sup>-1</sup> min<sup>-1</sup>), wild-type PES-H1 (0.054 mL mg<sup>-1</sup> min<sup>-1</sup>), and LCC ICCG (0.048 mL mg<sup>-1</sup> min<sup>-1</sup>). The adsorption equilibrium constant  $K_A$  is a parameter to evaluate the enzyme affinity to PET-NP. The R204C/S250C variant had the lowest affinity to PET, while the L92F/Q94Y variant had the highest affinity, which was 1.8-fold higher than that of wild-type PES-H1 and 1.4-fold higher than that of LCC ICCG. The high

affinity of the L92F/Q94Y variant to PET nanoparticles demonstrates the importance of the adsorption of enzymes to the surface of PET-NP for efficient hydrolysis. The  $K_A$  values determined in this study fall in the same range as those determined for many homologous PET hydrolases by other procedures.<sup>12,45,46,51,52</sup> In general, the kinetic data, depicted in Table 1 and Table S7 support the observations made using other PET materials (Figure 4A,B). Additionally, we measured the initial hydrolysis rate as a function of the substrate concentration in the range 0–0.5 mg mL<sup>-1</sup> using a constant enzyme concentration of 0.7  $\mu\text{M}$ . This enzyme concentration was selected to ensure substrate-saturated conditions (Figure S9). The experimental data fit well to the kinetic model (Figures S9 and S10), demonstrating that under these conditions the model describes the experimental data accurately.

## CONCLUSIONS

In this study, we solved crystal structures of the thermophilic enzymes PES-H1 and PES-H2 in apo form and notably also in complexes with the PET monomer analogues MHETA and BHET. This enabled the identification of six intermediate binding modes and several key residues involved in binding to PET. MD simulations supported the involvement of these residues in PET binding. Structural analyses and previously identified mutational hotspots were used to select PES-H1 residues for mutagenesis. Several PES-H1 variants with improved thermostability and PET hydrolysis activity were identified. The most active L92F/Q94Y variant outperformed the reference enzyme LCC ICCG in hydrolyzing lcPET materials (<15% crystallinity). Its superior activity over wild-type PES-H1 was also evident with other hcPET materials derived from real-world PET bottle waste. Our detailed structural analyses provide a better understanding of the mechanisms of interfacial biocatalysis, and our engineered variants hold promise for future applications in biocatalytic plastic recycling.

## ASSOCIATED CONTENT

### Supporting Information

The Supporting Information is available free of charge at <https://pubs.acs.org/doi/10.1021/acscatal.2c02275>.

Materials and methods; data collection of crystal structures of PES-H1 and PES-H2 in apo form and in complex with MHETA and BHET; RMSD of selected PET hydrolases; MD simulations; changes in  $T_m$ ; crystallinities and molecular masses of PET substrates; kinetic parameters of PET-NP hydrolysis; oligonucleotides; structure of PES-H1; stability of PES-H1 in MD simulations; RMSD of 3PET during MD simulations; binding positions of 3PET clusters; degradation of PET at 70 and 72 °C; phosphate dependence; cysteine calibration curve; electrostatic surface display; hydrolysis of PET-NP with varying enzyme concentrations; and hydrolysis of PET-NP with varying substrate concentrations (PDF)

GAFF parameters for each PET unit in 3PET (TXT)

## AUTHOR INFORMATION

### Corresponding Authors

Weidong Liu – Tianjin Institute of Industrial Biotechnology, Chinese Academy of Sciences, Tianjin 300308, China;

National Technology Innovation Center of Synthetic Biology, Tianjin 300308, China; University of Chinese Academy of Sciences, Beijing 100049, China; [orcid.org/0000-0001-7954-7700](https://orcid.org/0000-0001-7954-7700); Email: [liu\\_wd@tib.cas.cn](mailto:liu_wd@tib.cas.cn)

**Uwe T. Bornscheuer** – Department of Biotechnology & Enzyme Catalysis, Institute of Biochemistry, University of Greifswald, 17487 Greifswald, Germany; [orcid.org/0000-0003-0685-2696](https://orcid.org/0000-0003-0685-2696); Email: [uwe.bornscheuer@uni-greifswald.de](mailto:uwe.bornscheuer@uni-greifswald.de)

**Ren Wei** – Department of Biotechnology & Enzyme Catalysis, Institute of Biochemistry, University of Greifswald, 17487 Greifswald, Germany; [orcid.org/0000-0003-3876-1350](https://orcid.org/0000-0003-3876-1350); Email: [ren.wei@uni-greifswald.de](mailto:ren.wei@uni-greifswald.de)

## Authors

**Lara Pfaff** – Department of Biotechnology & Enzyme Catalysis, Institute of Biochemistry, University of Greifswald, 17487 Greifswald, Germany; [orcid.org/0000-0002-1529-8917](https://orcid.org/0000-0002-1529-8917)

**Jian Gao** – Tianjin Institute of Industrial Biotechnology, Chinese Academy of Sciences, Tianjin 300308, China; National Technology Innovation Center of Synthetic Biology, Tianjin 300308, China

**Zhishuai Li** – Tianjin Institute of Industrial Biotechnology, Chinese Academy of Sciences, Tianjin 300308, China; University of Chinese Academy of Sciences, Beijing 100049, China

**Anna Jäckering** – Institute of Biological Information Processing: Structural Biochemistry (IBI-7), Forschungszentrum Jülich, 52428 Jülich, Germany; Institute of Theoretical and Computational Chemistry, Heinrich Heine University, 40225 Düsseldorf, Germany; [orcid.org/0000-0003-0031-159X](https://orcid.org/0000-0003-0031-159X)

**Gert Weber** – Helmholtz-Zentrum Berlin für Materialien und Energie, 14109 Berlin, Germany; [orcid.org/0000-0003-3624-1060](https://orcid.org/0000-0003-3624-1060)

**Jan Mican** – Loschmidt Laboratories, Department of Experimental Biology and RECETOX, Faculty of Science, Masaryk University, 625 00 Brno, Czech Republic; [orcid.org/0000-0002-8877-163X](https://orcid.org/0000-0002-8877-163X)

**Yinping Chen** – State Key Laboratory of Materials-Oriented Chemical Engineering, College of Biotechnology and Pharmaceutical Engineering, Nanjing Tech University, Nanjing 211816, China

**Weiliang Dong** – State Key Laboratory of Materials-Oriented Chemical Engineering, College of Biotechnology and Pharmaceutical Engineering, Nanjing Tech University, Nanjing 211816, China; [orcid.org/0000-0002-8556-5689](https://orcid.org/0000-0002-8556-5689)

**Xu Han** – Tianjin Institute of Industrial Biotechnology, Chinese Academy of Sciences, Tianjin 300308, China; National Technology Innovation Center of Synthetic Biology, Tianjin 300308, China

**Christian G. Feiler** – Helmholtz-Zentrum Berlin für Materialien und Energie, 14109 Berlin, Germany

**Yu-Fei Ao** – Department of Biotechnology & Enzyme Catalysis, Institute of Biochemistry, University of Greifswald, 17487 Greifswald, Germany; CAS Key Laboratory of Molecular Recognition and Function, Institute of Chemistry, Chinese Academy of Sciences, Beijing 100190, China

**Christoffel P. S. Badenhorst** – Department of Biotechnology & Enzyme Catalysis, Institute of Biochemistry, University of

Greifswald, 17487 Greifswald, Germany; [orcid.org/0000-0002-5874-4577](https://orcid.org/0000-0002-5874-4577)

**David Bednar** – Loschmidt Laboratories, Department of Experimental Biology and RECETOX, Faculty of Science, Masaryk University, 625 00 Brno, Czech Republic; International Clinical Research Center, St. Anne's University Hospital, 656 91 Brno, Czech Republic

**Gottfried J. Palm** – Department Synthetic and Structural Biochemistry, Institute of Biochemistry, University of Greifswald, 17487 Greifswald, Germany; [orcid.org/0000-0003-0329-0413](https://orcid.org/0000-0003-0329-0413)

**Michael Lammers** – Department Synthetic and Structural Biochemistry, Institute of Biochemistry, University of Greifswald, 17487 Greifswald, Germany

**Jiri Damborsky** – Loschmidt Laboratories, Department of Experimental Biology and RECETOX, Faculty of Science, Masaryk University, 625 00 Brno, Czech Republic; International Clinical Research Center, St. Anne's University Hospital, 656 91 Brno, Czech Republic

**Birgit Strodel** – Institute of Biological Information Processing: Structural Biochemistry (IBI-7), Forschungszentrum Jülich, 52428 Jülich, Germany; Institute of Theoretical and Computational Chemistry, Heinrich Heine University, 40225 Düsseldorf, Germany; [orcid.org/0000-0002-8734-7765](https://orcid.org/0000-0002-8734-7765)

Complete contact information is available at: <https://pubs.acs.org/10.1021/acscatal.2c02275>

## Author Contributions

Conceptualization: R.W., W.L., and U.T.B. Protein crystallographic studies: J.G., Z.L., X.H., C.G.F., G.J.P., M.L., and W.L. Computational simulations: A.J., G.W., J.M., Y.-F.A., D.B., J.D., B.S., and W.L. Protein engineering and characterization: L.P., J.G., and Z.L. Polymer treatment and characterization: Y.C. and W.D. Writing—original draft: L.P., A.J., G.W., C.P.S.B., W.L., and R.W. Writing—review and editing: all authors. Supervision and funding acquisition: W.D., J.D., B.S., W.L., U.T.B., and R.W.

## Funding

The authors W.L., J.G., Z.L., X.H., and W.D. acknowledge the financial support provided by the National Key Research and Development Program of China (2021YFC2103600 and 2021YFA0910200). The authors U.T.B., R.W., L.P., D.B., J.M., and J.D. gratefully acknowledge the financial support received from the European Union's Horizon 2020 research and innovation program (MIX-UP, grant 870294; upPE-T, grant 953214; CETOCOEN Excellence, grant 857560) and from the Czech Ministry of Education (CZ.02.1.01/0.0/0.0/16\_026/0008451). A.J. is financially supported by the German Federal Environmental Foundation. The authors J.G., X.H., and W.L. also thank the Tianjin Synthetic Biotechnology Innovation Capacity Improvement Project (TSBICIP-PTJJ-008, TSBICIP-IJCP-003, TSBICIP-KJGG-009-01, and TSBICIP-KJGG-002-06), the Youth Innovation Promotion Association CAS, and the China Scholarship Council for financial support. The authors W.D. and Y.C. acknowledge the financial support provided by the National Natural Science Foundation of China (31961133017).

## Notes

The authors declare no competing financial interest.

## ACKNOWLEDGMENTS

A.J. and B.S. gratefully acknowledge the computing time granted through JARA-HPC (project PETaseMD) on the supercomputer JURECA at Forschungszentrum Jülich,<sup>55</sup> the hybrid computer cluster purchased from funding by the Deutsche Forschungsgemeinschaft (DFG, German Research Foundation) project number INST 208/704-1 FUGG, and the Centre for Information and Media Technology at Heinrich Heine University Düsseldorf. Furthermore, we thank the staff from BL10U2/BL17B/BL17B/BL18U1/BL19U1 beamline of the National Facility for Protein Science in Shanghai (NFPS) at Shanghai Synchrotron Radiation Facility (SSRF) and staff from Beamline 14.1 at BESSY, for assistance during data collection.

## REFERENCES

- (1) Singh, A.; Rorrer, N. A.; Nicholson, S. R.; Erickson, E.; DesVeaux, J. S.; Avelino, A. F. T.; Lamers, P.; Bhatt, A.; Zhang, Y.; Avery, G.; Tao, L.; Pickford, A. R.; Carpenter, A. C.; McGeehan, J. E.; Beckham, G. T. Techno-Economic, Life-Cycle, and Socioeconomic Impact Analysis of Enzymatic Recycling of Poly(Ethylene Terephthalate). *Joule* **2021**, *5* (9), 2479–2503.
- (2) Wei, R.; Tiso, T.; Bertling, J.; O'Connor, K.; Blank, L. M.; Bornscheuer, U. T. Possibilities and Limitations of Biotechnological Plastic Degradation and Recycling. *Nat. Catal.* **2020**, *3* (11), 867–871.
- (3) Tiso, T.; Winter, B.; Wei, R.; Hee, J.; de Witt, J.; Wierckx, N.; Quicker, P.; Bornscheuer, U. T.; Bardow, A.; Nogales, J.; Blank, L. M. The Metabolic Potential of Plastics as Biotechnological Carbon Sources – Review and Targets for the Future. *Metab. Engin.* **2022**, *71*, 77–98.
- (4) Jönsson, C.; Wei, R.; Biundo, A.; Landberg, J.; Schwarz Bour, L.; Pezzotti, F.; Toca, A.; Jacques, L. M.; Bornscheuer, U. T.; Syrén, P. Biocatalysis in the Recycling Landscape for Synthetic Polymers and Plastics towards Circular Textiles. *ChemSusChem* **2021**, *14* (19), 4028–4040.
- (5) Tournier, V.; Topham, C. M.; Gilles, A.; David, B.; Folgoas, C.; Moya-Leclair, E.; Kamionka, E.; Desrousseaux, M.-L.; Texier, H.; Gavalda, S.; Cot, M.; Guémard, E.; Dalibey, M.; Nomme, J.; Cioci, G.; Barbe, S.; Chateau, M.; André, I.; Duquesne, S.; Marty, A. An Engineered PET Depolymerase to Break down and Recycle Plastic Bottles. *Nature* **2020**, *580* (7802), 216–219.
- (6) Wei, R.; von Haugwitz, G.; Pfaff, L.; Mican, J.; Badenhorst, C. P. S.; Liu, W.; Weber, G.; Austin, H. P.; Bednar, D.; Damborsky, J.; Bornscheuer, U. T. Mechanism-Based Design of Efficient PET Hydrolases. *ACS Catal.* **2022**, *12* (6), 3382–3396.
- (7) Bianchi, R.; Chiavacci, P.; Vosa, R.; Guerra, G. Effect of Moisture on the Crystallization Behavior of PET from the Quenched Amorphous Phase. *J. Appl. Polym. Sci.* **1991**, *43* (6), 1087–1089.
- (8) Langevin, D.; Grenet, J.; Saiter, J. M. Moisture Sorption in PET Influence on the Thermokinetic Parameters. *Eur. Polym. J.* **1994**, *30* (3), 339–345.
- (9) Yoshida, S.; Hiraga, K.; Takehana, T.; Taniguchi, I.; Yamaji, H.; Maeda, Y.; Toyohara, K.; Miyamoto, K.; Kimura, Y.; Oda, K. A Bacterium That Degrades and Assimilates Poly(Ethylene Terephthalate). *Science* **2016**, *351* (6278), 1196–1199.
- (10) Kawai, F. The Current State of Research on PET Hydrolyzing Enzymes Available for Biorecycling. *Catalysts* **2021**, *11* (2), 206.
- (11) Brott, S.; Pfaff, L.; Schuricht, J.; Schwarz, J.; Böttcher, D.; Badenhorst, C. P. S.; Wei, R.; Bornscheuer, U. T. Engineering and Evaluation of Thermostable IsPETase Variants for PET Degradation. *Eng. Life Sci.* **2022**, *22* (3–4), 192–203.
- (12) Ronkvist, Å. M.; Xie, W.; Lu, W.; Gross, R. A. Cutinase-Catalyzed Hydrolysis of Poly(Ethylene Terephthalate). *Macromolecules* **2009**, *42* (14), 5128–5138.
- (13) Sulaiman, S.; You, D.-J.; Kanaya, E.; Koga, Y.; Kanaya, S. Crystal Structure and Thermodynamic and Kinetic Stability of Metagenome-Derived LC-Cutinase. *Biochemistry* **2014**, *53* (11), 1858–1869.
- (14) Sulaiman, S.; Yamato, S.; Kanaya, E.; Kim, J.-J.; Koga, Y.; Takano, K.; Kanaya, S. Isolation of a Novel Cutinase Homolog with Polyethylene Terephthalate-Degrading Activity from Leaf-Branch Compost by Using a Metagenomic Approach. *Appl. Environ. Microbiol.* **2012**, *78* (5), 1556–1562.
- (15) Wei, R.; Song, C.; Gräning, D.; Schneider, T.; Bielytskyi, P.; Böttcher, D.; Matysik, J.; Bornscheuer, U. T.; Zimmermann, W. Conformational Fitting of a Flexible Oligomeric Substrate Does Not Explain the Enzymatic PET Degradation. *Nat. Commun.* **2019**, *10* (1), 5581.
- (16) Miyakawa, T.; Mizushima, H.; Ohtsuka, J.; Oda, M.; Kawai, F.; Tanokura, M. Structural Basis for the Ca<sup>2+</sup>-Enhanced Thermostability and Activity of PET-Degrading Cutinase-like Enzyme from *Saccharomonospora viridis* AHK190. *Appl. Microbiol. Biotechnol.* **2015**, *99* (10), 4297–4307.
- (17) Then, J.; Wei, R.; Oeser, T.; Gerds, A.; Schmidt, J.; Barth, M.; Zimmermann, W. A Disulfide Bridge in the Calcium Binding Site of a Polyester Hydrolase Increases Its Thermal Stability and Activity against Polyethylene Terephthalate. *FEBS Open Bio* **2016**, *6* (5), 425–432.
- (18) Oda, M.; Yamagami, Y.; Inaba, S.; Oida, T.; Yamamoto, M.; Kitajima, S.; Kawai, F. Enzymatic Hydrolysis of PET: Functional Roles of Three Ca<sup>2+</sup> Ions Bound to a Cutinase-like Enzyme, Cut190\*, and Its Engineering for Improved Activity. *Appl. Microbiol. Biotechnol.* **2018**, *102* (23), 10067–10077.
- (19) Zhong-Johnson, E. Z. L.; Voigt, C. A.; Sinskey, A. J. An Absorbance Method for Analysis of Enzymatic Degradation Kinetics of Poly(Ethylene Terephthalate) Films. *Sci. Rep.* **2021**, *11* (1), 928.
- (20) Then, J.; Wei, R.; Oeser, T.; Barth, M.; Belisário-Ferrari, M. R.; Schmidt, J.; Zimmermann, W. Ca<sup>2+</sup> and Mg<sup>2+</sup> Binding Site Engineering Increases the Degradation of Polyethylene Terephthalate Films by Polyester Hydrolases from *Thermobifida fusca*. *Biotechnol. J.* **2015**, *10* (4), 592–598.
- (21) Emori, M.; Numoto, N.; Senga, A.; Bekker, G.; Kamiya, N.; Kobayashi, Y.; Ito, N.; Kawai, F.; Oda, M. Structural Basis of Mutants of PET-degrading Enzyme from *Saccharomonospora viridis* AHK190 with High Activity and Thermal Stability. *Proteins* **2021**, *89* (5), 502–511.
- (22) Nakamura, A.; Kobayashi, N.; Koga, N.; Iino, R. Positive Charge Introduction on the Surface of Thermostabilized PET Hydrolase Facilitates PET Binding and Degradation. *ACS Catal.* **2021**, *11* (14), 8550–8564.
- (23) Zeng, W.; Li, X.; Yang, Y.; Min, J.; Huang, J.-W.; Liu, W.; Niu, D.; Yang, X.; Han, X.; Zhang, L.; Dai, L.; Chen, C.-C.; Guo, R.-T. Substrate-Binding Mode of a Thermophilic PET Hydrolase and Engineering the Enzyme to Enhance the Hydrolytic Efficacy. *ACS Catal.* **2022**, *12* (5), 3033–3040.
- (24) Thomsen, T. B.; Hunt, C. J.; Meyer, A. S. Influence of Substrate Crystallinity and Glass Transition Temperature on Enzymatic Degradation of Polyethylene Terephthalate (PET). *N. Biotechnol.* **2022**, *69*, 28–35.
- (25) Wei, R.; Breite, D.; Song, C.; Gräning, D.; Ploss, T.; Hille, P.; Schwerdtfeger, R.; Matysik, J.; Schulze, A.; Zimmermann, W. Biocatalytic Degradation Efficiency of Postconsumer Polyethylene Terephthalate Packaging Determined by Their Polymer Microstructures. *Adv. Sci.* **2019**, *6* (14), 1900491.
- (26) Cui, Y.; Chen, Y.; Liu, X.; Dong, S.; Tian, Y.; Qiao, Y.; Mitra, R.; Han, J.; Li, C.; Han, X.; Liu, W.; Chen, Q.; Wei, W.; Wang, X.; Du, W.; Tang, S.; Xiang, H.; Liu, H.; Liang, Y.; Houk, K. N.; Wu, B. Computational Redesign of a PETase for Plastic Biodegradation under Ambient Condition by the GRAPE Strategy. *ACS Catal.* **2021**, *11* (3), 1340–1350.
- (27) Lu, H.; Diaz, D. J.; Czarnecki, N. J.; Zhu, C.; Kim, W.; Shroff, R.; Acosta, D. J.; Alexander, B. R.; Cole, H. O.; Zhang, Y.; Lynd, N. A.; Ellington, A. D.; Alper, H. S. Machine Learning-Aided Engineering of Hydrolases for PET Depolymerization. *Nature* **2022**, *604* (7907), 662–667.

- (28) Han, X.; Liu, W.; Huang, J.-W.; Ma, J.; Zheng, Y.; Ko, T.-P.; Xu, L.; Cheng, Y.-S.; Chen, C.-C.; Guo, R.-T. Structural Insight into Catalytic Mechanism of PET Hydrolase. *Nat. Commun.* **2017**, *8* (1), 2106.
- (29) Boneta, S.; Arafet, K.; Moliner, V. QM/MM Study of the Enzymatic Biodegradation Mechanism of Polyethylene Terephthalate. *J. Chem. Inf. Model.* **2021**, *61* (6), 3041–3051.
- (30) Feng, S.; Yue, Y.; Zheng, M.; Li, Y.; Zhang, Q.; Wang, W. Is PETase- and Is MHETase-Catalyzed Cascade Degradation Mechanism toward Polyethylene Terephthalate. *ACS Sustain. Chem. Eng.* **2021**, *9* (29), 9823–9832.
- (31) Jerves, C.; Neves, R. P. P.; Ramos, M. J.; da Silva, S.; Fernandes, P. A. Reaction Mechanism of the PET Degrading Enzyme PETase Studied with DFT/MM Molecular Dynamics Simulations. *ACS Catal.* **2021**, *11* (18), 11626–11638.
- (32) Zheng, M.; Li, Y.; Dong, W.; Feng, S.; Zhang, Q.; Wang, W. Computational Biotransformation of Polyethylene Terephthalate by Depolymerase: A QM/MM Approach. *J. Hazard. Mater.* **2022**, *423*, 127017.
- (33) Zimmermann, W.; Wei, R.; Hille, P.; Oeser, T.; Schmidt, J. New Polypeptides Having a Polyester Degrading Activity and Uses Thereof. EP3517608A1, July 31, 2019.
- (34) Sonnendecker, C.; Oeser, J.; Richter, P. K.; Hille, P.; Zhao, Z.; Fischer, C.; Lippold, H.; Blázquez-Sánchez, P.; Engelberger, F.; Ramírez-Sarmiento, C. A.; Oeser, T.; Lihanova, Y.; Frank, R.; Jahnke, H.; Billig, S.; Abel, B.; Sträter, N.; Matysik, J.; Zimmermann, W. Low Carbon Footprint Recycling of Post-Consumer PET Plastic with a Metagenomic Polyester Hydrolase. *ChemSusChem* **2022**, *15* (9), No. e202101062.
- (35) Falkenstein, P.; Wei, R.; Matysik, J.; Song, C. Mechanistic Investigation of Enzymatic Degradation of Polyethylene Terephthalate by Nuclear Magnetic Resonance. In *Methods in Enzymology*; Elsevier, 2021; Vol. 648, pp 231–252.
- (36) Barth, M.; Honak, A.; Oeser, T.; Wei, R.; Belisário-Ferrari, M. R.; Then, J.; Schmidt, J.; Zimmermann, W. A Dual Enzyme System Composed of a Polyester Hydrolase and a Carboxylesterase Enhances the Biocatalytic Degradation of Polyethylene Terephthalate Films. *J. Biotechnol.* **2016**, *11* (8), 1082–1087.
- (37) Eugenio, E. de Q.; Campisano, I. S. P.; de Castro, A. M.; Coelho, M. A. Z.; Langone, M. A. P. Kinetic Modeling of the Post-Consumer Poly(Ethylene Terephthalate) Hydrolysis Catalyzed by Cutinase from *Humicola insolens*. *J. Polym. Environ.* **2022**, *30*, 1627–1637.
- (38) Chen, C.; Han, X.; Ko, T.; Liu, W.; Guo, R. Structural Studies Reveal the Molecular Mechanism of PETase. *FEBS J.* **2018**, *285* (20), 3717–3723.
- (39) Schmidt, J.; Wei, R.; Oeser, T.; Belisário-Ferrari, M. R.; Barth, M.; Then, J.; Zimmermann, W. Effect of Tris, MOPS, and Phosphate Buffers on the Hydrolysis of Polyethylene Terephthalate Films by Polyester Hydrolases. *FEBS Open Bio* **2016**, *6* (9), 919–927.
- (40) Numoto, N.; Kamiya, N.; Bekker, G.-J.; Yamagami, Y.; Inaba, S.; Ishii, K.; Uchiyama, S.; Kawai, F.; Ito, N.; Oda, M. Structural Dynamics of the PET-Degrading Cutinase-like Enzyme from *Saccharomonospora viridis* AHK190 in Substrate-Bound States Elucidates the Ca<sup>2+</sup>-Driven Catalytic Cycle. *Biochemistry* **2018**, *57* (36), 5289–5300.
- (41) Baker, P. J.; Poultney, C.; Liu, Z.; Gross, R.; Montclare, J. K. Identification and Comparison of Cutinases for Synthetic Polyester Degradation. *Appl. Microbiol. Biotechnol.* **2012**, *93* (1), 229–240.
- (42) Furukawa, M.; Kawakami, N.; Tomizawa, A.; Miyamoto, K. Efficient Degradation of Poly(Ethylene Terephthalate) with *Thermobifida fusca* Cutinase Exhibiting Improved Catalytic Activity Generated Using Mutagenesis and Additive-Based Approaches. *Sci. Rep.* **2019**, *9* (1), 16038.
- (43) Austin, H. P.; Allen, M. D.; Donohoe, B. S.; Rorrer, N. A.; Kearns, F. L.; Silveira, R. L.; Pollard, B. C.; Dominick, G.; Duman, R.; El Omari, K.; Mykhaylyk, V.; Wagner, A.; Michener, W. E.; Amore, A.; Skaf, M. S.; Crowley, M. F.; Thorne, A. W.; Johnson, C. W.; Woodcock, H. L.; McGeehan, J. E.; Beckham, G. T. Characterization and Engineering of a Plastic-Degrading Aromatic Polyesterase. *Proc. Natl. Acad. Sci. U.S.A.* **2018**, *115* (19), E4350–E4357.
- (44) Erickson, E.; Shakespeare, T. J.; Bratti, F.; Buss, B. L.; Graham, R.; Hawkins, M. A.; König, G.; Michener, W. E.; Miscall, J.; Ramirez, K. J.; Rorrer, N. A.; Zahn, M.; Pickford, A. R.; McGeehan, J. E.; Beckham, G. T. Comparative Performance of PETase as a Function of Reaction Conditions, Substrate Properties, and Product Accumulation. *ChemSusChem* **2022**, *15* (1), No. e202101932.
- (45) Wei, R.; Oeser, T.; Then, J.; Kühn, N.; Barth, M.; Schmidt, J.; Zimmermann, W. Functional Characterization and Structural Modeling of Synthetic Polyester-Degrading Hydrolases from *Thermomonospora curvata*. *AMB Expr.* **2014**, *4* (1), 44.
- (46) Wei, R.; Oeser, T.; Schmidt, J.; Meier, R.; Barth, M.; Then, J.; Zimmermann, W. Engineered Bacterial Polyester Hydrolases Efficiently Degrade Polyethylene Terephthalate Due to Relieved Product Inhibition: Engineered Polyester Hydrolases. *Biotechnol. Bioeng.* **2016**, *113* (8), 1658–1665.
- (47) Silva, C.; Da, S.; Silva, N.; Matamá, T.; Araújo, R.; Martins, M.; Chen, S.; Chen, J.; Wu, J.; Casal, M.; Cavaco-Paulo, A. Engineered *Thermobifida fusca* Cutinase with Increased Activity on Polyester Substrates. *J. Biotechnol.* **2011**, *6* (10), 1230–1239.
- (48) Gamerith, C.; Zartl, B.; Pellis, A.; Guillaumot, F.; Marty, A.; Acero, E. H.; Guebitz, G. M. Enzymatic Recovery of Polyester Building Blocks from Polymer Blends. *Process. Biochem.* **2017**, *59*, 58–64.
- (49) Bai, C. Structural Changes in Poly(Ethylene Terephthalate) Induced by Mechanical Milling. *Polymer* **2000**, *41* (19), 7147–7157.
- (50) Falkenstein, P.; Gräsing, D.; Bielytskiy, P.; Zimmermann, W.; Matysik, J.; Wei, R.; Song, C. UV Pretreatment Impairs the Enzymatic Degradation of Polyethylene Terephthalate. *Front. Microbiol.* **2020**, *11*, 689.
- (51) Vogel, K.; Wei, R.; Pfaff, L.; Breite, D.; Al-Fathi, H.; Ortmann, C.; Estrela-Lopis, I.; Venus, T.; Schulze, A.; Harms, H.; Bornscheuer, U. T.; Maskow, T. Enzymatic Degradation of Polyethylene Terephthalate Nanoplastics Analyzed in Real Time by Isothermal Titration Calorimetry. *Sci. Total Environ.* **2021**, *773*, 145111.
- (52) Wei, R.; Oeser, T.; Barth, M.; Weigl, N.; Lübs, A.; Schulz-Siegmund, M.; Hacker, M. C.; Zimmermann, W. Turbidimetric Analysis of the Enzymatic Hydrolysis of Polyethylene Terephthalate Nanoparticles. *J. Mol. Catal. B: Enzym.* **2014**, *103*, 72–78.
- (53) Scandola, M.; Focarete, M. L.; Frisoni, G. Simple Kinetic Model for the Heterogeneous Enzymatic Hydrolysis of Natural Poly(3-Hydroxybutyrate). *Macromolecules* **1998**, *31* (12), 3846–3851.
- (54) Pfaff, L.; Breite, D.; Badenhorst, C. P. S.; Bornscheuer, U. T.; Wei, R. Fluorimetric High-Throughput Screening Method for Polyester Hydrolase Activity Using Polyethylene Terephthalate Nanoparticles. In *Methods in Enzymology*; Elsevier, 2021; Vol. 648, pp 253–270.
- (55) Krause, D.; Thörnig, P. JURECA: Modular Supercomputer at Jülich Supercomputing Centre. *JLSRF* **2018**, *4*, A132.

# Supporting Information

## Multiple Substrate Binding Mode-Guided Engineering of a Thermophilic PET Hydrolase

*Lara Pfaffl*<sup>1</sup>, *Jian Gao*<sup>2,3</sup>, *Zhishuai Li*<sup>2,4</sup>, *Anna Jäckering*<sup>5,6</sup>, *Gert Weber*<sup>7</sup>, *Jan Mican*<sup>8</sup>, *Yinping Chen*<sup>9</sup>, *Weiliang Dong*<sup>9</sup>, *Xu Han*<sup>2,3</sup>, *Christian G. Feiler*<sup>7</sup>, *Yu-Fei Ao*<sup>1,10</sup>, *Christoffel P.S. Badenhorst*<sup>1</sup>, *David Bednar*<sup>8,11</sup>, *Gottfried J. Palm*<sup>12</sup>, *Michael Lammers*<sup>12</sup>, *Jiri Damborsky*<sup>8,11</sup>, *Birgit Strodel*<sup>5,6</sup>, *Weidong Liu*<sup>2,3,4\*</sup>, *Uwe T. Bornscheuer*<sup>1\*</sup>, *Ren Wei*<sup>1\*</sup>

<sup>1</sup>Department of Biotechnology & Enzyme Catalysis, Institute of Biochemistry, University of Greifswald, Felix-Hausdorff-Str. 4, 17487 Greifswald, Germany

<sup>2</sup>Tianjin Institute of Industrial Biotechnology, Chinese Academy of Sciences, 32 West 7th Avenue, Tianjin Airport Economic Area, Tianjin 300308, China

<sup>3</sup>National Technology Innovation Center of Synthetic Biology, 32 West 7th Avenue, Tianjin Airport Economic Area, Tianjin 300308, China

<sup>4</sup>University of Chinese Academy of Sciences, 19A Yuquan Road, Beijing, 100049 China

<sup>5</sup>Institute of Biological Information Processing: Structural Biochemistry (IBI-7),  
Forschungszentrum Jülich, Wilhelm-Johnen-Straße, 52428 Jülich, Germany

<sup>6</sup>Institute of Theoretical and Computational Chemistry, Heinrich Heine University, Düsseldorf,  
Universitätsstr. 1, 40225 Düsseldorf, Germany

<sup>7</sup>Helmholtz-Zentrum Berlin für Materialien und Energie, Hahn-Meitner-Platz 1, 14109 Berlin,  
Germany

<sup>8</sup>Loschmidt Laboratories, Department of Experimental Biology and RECETOX, Faculty of  
Science, Masaryk University, Kamenice 5/C13, 625 00 Brno, Czech Republic

<sup>9</sup>State Key Laboratory of Materials-Oriented Chemical Engineering, College of Biotechnology  
and Pharmaceutical Engineering, Nanjing Tech University, Nanjing, China

<sup>10</sup>CAS Key Laboratory of Molecular Recognition and Function, Institute of Chemistry, Chinese  
Academy of Sciences, Zhongguancun North First Street 2, 100190 Beijing, China

<sup>11</sup>International Clinical Research Center, St. Anne's University Hospital, Pekarska 53, 656 91  
Brno, Czech Republic

<sup>12</sup>Department Synthetic and Structural Biochemistry, Institute of Biochemistry, University of  
Greifswald, Felix-Hausdorff-Str. 4, 17487 Greifswald, Germany

\*Email: liu\_wd@tib.cas.cn; uwe.bornscheuer@uni-greifswald.de; ren.wei@uni-greifswald.de

## **Materials and Methods**

### **Materials**

Chemicals and consumables were purchased from Merck KGaA (Darmstadt, Germany), Sigma-Aldrich (Steinheim, Germany), Carl Roth (Karlsruhe, Germany), TCI (Tokyo, Japan), Thermo Fisher Scientific (Waltham, MA, USA) and New England Biolabs GmbH (Frankfurt am Main, Germany). Oligonucleotides (Table S8) were ordered from Thermo Fisher Scientific (Waltham, MA, USA) and Eurofins (Ebersberg, Germany). Amorphous PET film (250  $\mu$ m thickness, product number ES301445) was purchased from Goodfellow GmbH (Bad Nauheim, Germany).

### **Protein production for crystallization, structure determination, and refinement**

The genes encoding PES-H1 and PES-H2 were synthesized by GENE ray Biotech Co. (Shanghai, China) and cloned into the pET-32a vector between the EcoRI and NotI restriction sites. Detailed nucleotide sequences encoding the enzymes are given after the Material and Methods. The pET-32a-*pes-h1* and pET-32a-*pes-h2* plasmids were transformed into *Escherichia coli* BL21trxB (DE3). Cells from single colonies were used to inoculate 5 mL lysogeny broth (LB) medium and grown at 37 °C to an optical density at 600 nm ( $OD_{600}$ ) of approximately 0.8 before induction using 0.5 mM isopropyl  $\beta$ -D-thiogalactopyranoside (IPTG) at 16 °C for 18 h. Cells were harvested by centrifugation at 5,000 g for 15 min and then resuspended in lysis buffer consisting of 25 mM Tris-HCl (pH 7.5), 150 mM sodium chloride (NaCl), and 20 mM imidazole, followed by disruption using a French Press (800-1200 bar, 2-5 cycles). Cell debris were removed by centrifugation at 17,000 g for 1 h at 4 °C. The supernatant was then applied to a 5 mL Ni-NTA column on an FPLC system (GE Healthcare, Chicago, USA) for protein purification. Target proteins were eluted at 100 mM imidazole when a 20-250 mM imidazole



gradient was applied. Each protein was dialyzed against 25 mM Tris-HCl (pH 7.5) containing 150 mM NaCl, and subjected to tobacco etch virus (TEV) protease digestion overnight to remove the hexahistidine (His<sub>6</sub>)-tag. The solutions were then passed through an Ni-NTA column again. The untagged target protein was eluted with 25 mM Tris-HCl (pH 7.5) containing 150 mM NaCl. The purity of each protein (>95%) was confirmed by sodium dodecyl sulfate polyacrylamide gel electrophoresis (SDS-PAGE) analysis. The purified proteins were concentrated to ~20 mg mL<sup>-1</sup> for screening crystallization conditions.

### **Crystallization, data collection, structure determination, and refinement**

All crystallization experiments were conducted at 25 °C using the sitting-drop vapor-diffusion method. In general, 1 µL of a PES-H1 or PES-H2 containing solution (15 mg mL<sup>-1</sup> in 25 mM Tris-HCl (pH 7.5) containing 150 mM NaCl) were mixed with 1 µL of reservoir solution in 48-well Cryschem plates and equilibrated against 100 µL of the reservoir solution. The two optimized crystallization conditions for PES-H1 were: 17% w/v polyethylene glycol (PEG) 6000, 0.1 M citric acid (cit) (pH 5.0), 30% 2-methylpentane-2,4-diol (MPD) and 8% Tacsimate (pH 4.0), 0.1 M citric acid (pH 5.0), 20% PEG3350.

The two optimized crystallization conditions for PES-H2 were: 32% PEG 2000 MME, 0.1 M KBr and 24% PEG4000, 0.1 M citric acid (pH 5.6), and 9% isopropanol. Within one week, the crystals reached sizes suitable for X-ray diffraction. The crystals in complex with 4-(2-hydroxyethylcarbamoyl) benzoic acid (MHETA) or bis(2-hydroxyethyl) terephthalate (BHET) were obtained by soaking them with their respective mother liquor containing substrate powder for 72 h. All X-ray diffraction data sets were collected at the Beamlines BL10U2(BL17U1)/BL17B/BL18U1/BL19U1 of the National Facility for Protein Science in

Shanghai (NFPS) at the Shanghai Synchrotron Radiation Facility (SSRF), and Beamline 14.1 at Berlin using the third-generation synchrotron radiation source (BESSY). The crystals were mounted in a CryoLoop and soaked with cryoprotectant solution prior to data collection at 100 K. The diffraction images were processed by using HKL2000.<sup>1</sup> All crystal structures were solved by the molecular replacement (MR) method with the Phaser program<sup>2</sup> from the Phenix<sup>3</sup> suite using the structure of the *IsPETase* from *Ideonella sakaiensis* 201-F6 (PDB code: 5XG0) as the search model.<sup>4</sup> Further refinement was carried out using the programs phenix.refine<sup>5</sup> and Coot.<sup>6</sup> Prior to the structural refinements, 5% randomly selected reflections were set aside for calculating  $R_{\text{free}}$ <sup>7</sup> as a monitor. Data collection and refinement statistics are summarized in Tables S1 and S2. All figures were prepared using PyMOL (<http://pymol.sourceforge.net>).

### **Molecular dynamics simulations**

To model and analyze the PET-PES-H1 interactions, we used a PET trimer (3PET) to mimic the polymeric substrate of PES-H1. For correctly placing 3PET into the binding cleft, PyMOL<sup>8</sup> was used to superimpose the central 3PET unit with the position of 1-2(-hydroxyethyl) 4-methyl terephthalate (HEMT) in complex with *IsPETase* (PDB code 5XH3).<sup>4</sup> Generalized AMBER force field (GAFF) parameters<sup>9</sup> were derived for 3PET by performing quantum mechanics calculations at the HF6-31G\* level using Gaussian 09<sup>10</sup>. The partial charges were determined by restrained electrostatic potential (RESP) calculations<sup>11,12</sup> using the antechamber tool of the Antechamber package<sup>9,13,14</sup> available in AmberTools 21<sup>15</sup> and redistributed to yield a net charge of zero for each 3PET unit using the Antechamber tool Prepgen (see GAFF parameters). All molecular dynamics (MD) simulations were carried out using GROMACS 2020.4<sup>16</sup> using the AMBER14SB<sup>17</sup> protein force field with Parmbsc1 parameters<sup>18</sup> and the newly derived PET parameters to determine the

potential energy and forces. After determining the pKa of titratable residues using Propka3 3.4.0, hydrogens were added to or removed from the PES-H1 crystal structure to mimic a protonation state at pH 7. The PES-H1-3PET complex was centered in a periodic dodecahedron box with at least 1 nm distance to the box edges, solvated with water described by the TIP3P water model<sup>19</sup> and neutralized by adding Na<sup>+</sup> ions, resulting in a system containing 32,990 atoms in total. Energy minimization of the system was conducted using the steepest descent algorithm<sup>20</sup> prior to a two-step equilibration, first in the NVT ensemble for 0.2 ns, followed by a 1 ns equilibration simulation in the NpT ensemble to set the temperature to 303 K (30 °C, Nosé-Hoover thermostat)<sup>21,22</sup> and the pressure at 1.0 bar (Parrinello-Rahman barostat).<sup>23</sup> The final 100 ns production run was performed in triplicates using different randomly generated initial velocities. The electrostatic interactions were calculated using the particle-mesh Ewald method<sup>24,25</sup> and a cutoff of 8 Å was applied to both the electrostatic and Lennard-Jones (LJ) interactions. The bonds were constrained using the LINCS algorithm<sup>26</sup>, which allows for a time step of 2 fs. Coordinates were saved every 20 ps.

The three trajectories were concatenated and the 3PET conformations were clustered using the algorithm described by Daura et al.<sup>27</sup> together with a cutoff of 2 Å applied to the root-mean-square deviation (RMSD) to assign the cluster membership. This resulted in the identification of four particularly stable binding poses corresponding to the four most populated clusters (Figure S3C). All MD snapshots belonging to each of the four clusters were retrieved and submitted to further analysis per binding pose. The protein residues putatively interacting with 3PET were identified using the Visual Molecular Dynamics (VMD)<sup>28</sup> software and the strength of these residue-3PET interactions was energetically quantified.

## **Enzyme production and purification for the enzymatic hydrolysis of PET substrates**

The genes encoding PES-H1 and the reference enzyme LCC ICCG were codon-optimized for expression in *E. coli*, synthesized and cloned into the pET-28a(+) vector and the pET-26b(+) vector by BioCat GmbH (Heidelberg, Germany) between the NcoI (for PES-H1) or NdeI (for LCC ICCG) and XhoI restriction sites. The plasmids (pET-28a(+)-*pes-h1* and variants) were used to transform competent *E. coli* SHuffle® T7 Express or *E. coli* BL21 (DE3). For the expression in *E. coli* SHuffle® T7 Express, the cells were grown in LB medium supplemented with kanamycin ( $50 \mu\text{g mL}^{-1}$ ) at  $30 \text{ }^\circ\text{C}$  to  $\text{OD}_{600}$  of  $\sim 1$  and then induced using  $1 \text{ mM}$  IPTG at  $16 \text{ }^\circ\text{C}$  for 12 h. LCC ICCG and PES-H1 variants were expressed in autoinduction medium (ZYM-5052) supplemented with kanamycin ( $50 \mu\text{g mL}^{-1}$ ) at  $21 \text{ }^\circ\text{C}$  for 23 h and 20 h, respectively, as described previously.<sup>29</sup> Cells were harvested by centrifugation at  $10,000 \text{ g}$  for 30 min, resuspended in lysis buffer ( $50 \text{ mM}$  sodium phosphate (pH 8.0),  $300 \text{ mM}$  NaCl) and lysed by ultrasonication ( $2 \times 3 \text{ min}$ ,  $50\%$  power,  $50\%$  amplitude). Cell debris were removed by centrifugation at  $10,000 \text{ g}$  for 30 min and the enzymes were purified using cobalt-ion affinity chromatography (ROTI®Garose-His/Co Beads, Carl Roth, Karlsruhe, Germany). Unbound proteins were removed using lysis buffer (pH 8.0) supplemented with  $20 \text{ mM}$  or  $50 \text{ mM}$  imidazole. PES-H1 and LCC ICCG were eluted with elution buffer ( $50 \text{ mM}$  sodium phosphate (pH 8.0),  $300 \text{ mM}$  NaCl, and  $100 \text{ mM}$  or  $250 \text{ mM}$  imidazole, respectively). The target proteins were desalted with  $50 \text{ mM}$  sodium phosphate buffer (pH 8.0) and concentrated using Vivaspin™ ultrafiltration devices ( $10 \text{ kDa}$  MWCO, Cytiva, Freiburg, Germany). Enzyme purities were verified by SDS-PAGE analysis.

### **Site-directed mutagenesis**

Enzyme variants were generated using the Q5<sup>®</sup> Site-Directed Mutagenesis Kit (New England Biolabs GmbH, Frankfurt am Main, Germany). The sequences of the mutagenesis oligonucleotides are listed in Table S8. Mutagenesis was verified by Sanger sequencing (Eurofins Genomics Germany GmbH, Ebersberg, Germany).

### **Melting temperature measurements**

The  $T_m$  values of the PES-H1 variants were determined by nano differential scanning fluorimetry (NanoDSF) using the Prometheus NT.48 (NanoTemper Technologies, Munich, Germany) and differential scanning calorimetry (DSC; TA Instruments, Newcastle, USA). The measurements were conducted using protein concentrations of 0.5 mg mL<sup>-1</sup> or 0.3 mg mL<sup>-1</sup> to determine temperature profiles from 20 °C to 95 °C and 20 °C to 100°C at 1 °C per minute, respectively. The nanoDSF instrument has a fixed excitation wavelength of 285 nm and records emitted light at 330 nm and 350 nm.

### **Enzymatic hydrolysis of PET film and PET powder**

The degradation of amorphous Gf-PET PET film (7% crystallinity) was performed using an enzyme concentration of 0.5 mg<sub>enzyme</sub> g<sub>PET</sub><sup>-1</sup>, 1 mg<sub>enzyme</sub> g<sub>PET</sub><sup>-1</sup>, or 2 mg<sub>enzyme</sub> g<sub>PET</sub><sup>-1</sup> in 1.5 mL potassium phosphate buffer (1 M, pH 8.0) by shaking at 1,000 rpm and 72 °C on a ThermoMixer C (Eppendorf, Hamburg, Germany) for 12 h or 24 h. The reaction conditions were adapted from a published patent application.<sup>30</sup> The hydrolysis reactions were performed in triplicate. Gf-PET films were cut into small pieces of ~2 cm × 1 cm and washed with 0.1% SDS solution, ultrapure H<sub>2</sub>O and absolute ethanol before drying at room temperature for 24 h. Weight loss as a result of

enzymatic degradation was determined gravimetrically. The degradation of PET powder (13%, 26%, or 33% crystallinity) was conducted in the same way with an enzyme concentration of  $1 \text{ mg}_{\text{enzyme}} \text{ g}_{\text{PET}}^{-1}$  for 24 h. The degradation products were analyzed by reversed-phase high-performance liquid chromatography (HPLC) on a VWR Hitachi LaChrom Elite system (VWR International, Radnor, USA) equipped with a Kinetex<sup>®</sup> column (5  $\mu\text{M}$  EVO C18 100 Å, 150x4.6 mm; Phenomenex<sup>®</sup>, Aschaffenburg, Germany).<sup>31</sup> Samples (10  $\mu\text{l}$ ) were injected and separated at 30 °C with a gradient of acetonitrile in water containing 0.1% (v/v) formic acid. Acetonitrile was increased from 5% to 44% over 12 min and then to 70% over 3 min, after which the ratio remained constant for a further 3 min, using a flow rate of 0.8 mL min<sup>-1</sup>. Terephthalate (TPA), mono-(2-hydroxyethyl) terephthalate (MHET), and BHET were detected by UV absorbance at 240 nm and quantified based on a calibration curve obtained with commercially available TPA in the concentration range from 0 to 1 mM.

### **Kinetic analysis**

For the kinetic analysis of PET nanoparticle (PET-NP) degradation by PES-H1 and its variants, PET-NPs were produced as previously described.<sup>32-34</sup> For determining the kinetic parameters, a turbidimetric assay was applied as described before.<sup>35</sup> A mixture of 3 mL ROTIPHORESE<sup>®</sup> gel 40, 3 mL potassium phosphate buffer (1 M, pH 8.0), 120  $\mu\text{L}$  tetramethylethylenediamine and PET-NP suspension (1.7 mg mL<sup>-1</sup>) was prepared and filled up to a final volume of 15 mL with ultrapure H<sub>2</sub>O. Ammonium persulfate (2  $\mu\text{L}$  of a 40% (w/v) solution) and the enzyme solution were added to a total volume of 50  $\mu\text{L}$  and mixed with 150  $\mu\text{L}$  of the substrate- and acrylamide-containing mixture. The turbidimetric assay monitoring the enzymatic hydrolysis of PET-NP was performed at 600 nm in a microtiter plate at 70 °C for 40 min with 0.5 mg mL<sup>-1</sup> PET-NP and varying enzyme

concentrations in the range of 0-2  $\mu\text{M}$ . In addition, the degradation of PET-NP was also carried out with a constant enzyme concentration of 0.7  $\mu\text{M}$  and substrate concentrations ranging from 0 to 0.5  $\text{mg mL}^{-1}$ . All determinations were performed in triplicate.

A kinetic model (equation 1) based on previous studies,<sup>36-38</sup> was used to analyze the heterogenous kinetics of the PET-NP degradation, where  $v_0$  is the initial reaction rate;  $k_h$ , the hydrolysis rate constant;  $[\text{S}_0]$ , the initial substrate concentration;  $[\text{E}_0]$ , enzyme concentration, and  $K_A$  the adsorption equilibrium constant.

$$v_0 = k_h [\text{S}_0] \frac{K_A [\text{E}_0]}{1 + K_A [\text{E}_0]} \quad (1)$$

## **PET powder production and analysis**

### ***Pretreatment of waste PET bottles***

The bottle wall part of collected post-consumer PET plastic bottles was cut into small flakes of about 5 cm  $\times$  5 cm for more even melting and crushing processes. PET flakes were washed with ultrapure water and then dried in the drying oven. Before the melting experiment, the dried PET flakes were placed in an aluminum tray and sealed with tin foil to prevent oxidation. Then, the temperature was set to 280  $^{\circ}\text{C}$  in the high-temperature reactor for 40 min. This temperature exceeds the  $T_m$  of PET (250-260  $^{\circ}\text{C}$ ) and can thus result in homogeneous melts of PET. Low-crystallinity PET (lcPET) can be obtained by rapidly cooling the molten PET with ice-cold water within 10 s (quenching step). The melt quenched PET was crushed into powders using a portable herb grinder (Model 800Y, Yongkang Boou Hardware Products Co., Ltd., Yongkang, China) for 5 min or a planetary ball mill (Model PM2L, Shanghai Droide Instruments Ltd., Shanghai, China) for 30 min. The herb grinder uses a rotating blade to mechanically grind the melt-quenched PET. The temperature of the portable herb grinder could not be controlled and increased above room

temperature during grinding. In the ball milling process, the melt-quenched PET is mixed with steel milling balls, followed by continuous rotation at a speed of 400 rpm to grind the plastics through the collision of the beads. The temperature of the ball mill was constantly maintained at room temperature. Finally, PET powders with different particle sizes were collected and sieved with different mesh sizes. Similarly, Gf-PET films were crushed using the herb grinder and sieved in the same manner to produce lcPET powders for enzymatic degradation.

### *Characterization of PET samples*

The crystallinity of PET was measured by differential scanning calorimetry (DSC) on an TAQ2000 instrument (TA instruments, Newcastle, USA). Thermograms were monitored from the first heating process from 50 to 300 °C at a rate of 10 °C min<sup>-1</sup> under a nitrogen atmosphere. Under these conditions, the crystallinity of virgin PET (waste PET bottles and commercial PET films), melt-quenched PET, and PET powders obtained by different pulverization methods were determined as described in a previous publication.<sup>39</sup>

Additionally, gel permeation chromatography (GPC) measurements were performed using an Agilent PL-GPC50 (Agilent, California, USA) device to detect the molecular weight distributions of various PET samples dissolved in hexafluoro-2-propanol.

The crystallinity, the number average molecular weight (M<sub>n</sub>), and the weight average molecular weight (M<sub>w</sub>) of the PET samples are summarized in Table S6.



### **Using Ellman's reagent to determine the presence of a disulfide bond**

To quantify the number of free cysteine residues, Ellman's reagent (5,5'-dithiobis-(2-nitrobenzoic acid, DNTB) was used. 25  $\mu\text{L}$  of 1  $\text{mg mL}^{-1}$  R204C/S250C were incubated with 255  $\mu\text{L}$  of freshly prepared Ellman's reaction solution (2  $\text{mg mL}^{-1}$  DTNB in 0.1 M sodium phosphate buffer, pH 8.0) and 250  $\mu\text{L}$  0.1 M sodium phosphate buffer (pH 8.0) containing 0.1 M EDTA and incubated for 15 min. The absorption of TBN<sup>2-</sup> was measured at 412 nm. To calculate the concentration of free cysteine residues, a calibration curve prepared with cysteine solutions at concentrations from 0 to 1.5 mM was used.

## Nucleotide sequences

### PES-H1

Codon-optimized nucleotide sequence of PES-H1 cloned between the NcoI and XhoI restriction sites of the pET-28b(+) bacterial expression plasmid and between the EcoRI and NotI restriction sites of the pET-32a bacterial expression plasmid.

```
ATGGCTAACCCGTATGAACGCGGCCCGGATCCGACCGAAAGCAGCATTGAAGCGGT
GCGCGGCCCGTTTGCGGTGGCGCAGACCACCGTCAGCCGTCTGCAGGCGGATGGCT
TTGGCGGCGGCACCATTTATTATCCGACCGATAACCAGCCAGGGCACCTTTGGCGCGG
TGCGCATCAGCCCGGGCTTTACCGCCGGTCAGGAAAGCATTGCCTGGCTGGGCCCCG
CGTATTGCCAGCCAGGGCTTTGTGGTGATTACCATTGATACCATCACCCGTCTGGAT
CAGCCGGACAGCCGCGGTCGTCAGTTGCAGGCGGCGCTGGATCATCTGCGTACCAA
CAGCGTGGTGCGTAACCGTATTGATCCGAACCGTATGGCGGTGATGGGTTCACAGCAT
GGGCGGCGGCGGCGCGCTGTCGGCGGCGGCGAATAACACCAGCCTGGAAGCGGCG
ATTCCGCTGCAGGGCTGGCATAACCCGCAAAAACCTGGAGCAGCGTGCGCACGCCGAC
GCTGGTGGTTGGCGCGCAGCTGGATAACCATTGCGCCGGTTTCCAGCCACAGCGAAG
CGTTTTATAACAGCCTGCCGAGCGATCTGGATAAAGCCTATATGGAACCTGCGCGGTG
CCAGCCATCTGGTCAGCAATACGCCGGATACCACCACCGCCAAATACAGCATTGCCT
GGCTGAAACGCTTTGTCGATGATGATCTGCGTTATGAACAGTTCCTGTGCCCGGCGC
CGGATGATTTTGCCATCAGCGAATATCGCAGCACCTGCCCGTTTTAA
```

## **PES-H2**

Codon-optimized nucleotide sequence of PES-H2 cloned between the EcoRI and NotI restriction sites of the pET-32a bacterial expression plasmid.

```
ATGGAAAACCCGTATGAACGTGGCCCCGGATCCGACCGAAAGCAGCATTGAAGCAGT
TCGCGGCCCGTTTGCAGTGGCCCAGACCACCGTGAGTCGCTTACAGGCAGATGGTTT
TGGTGGCGGCACTATTTATTATCCGACCGATACCTCTCAGGGGACGTTTGGTGCCGT
GGCCATTTCTCCGGGCTTTACCGCAGGCCAGGAAAGTATTGCCTGGTTAGGTCCGCG
TATTGCCTCTCAGGGCTTTGTTGTGATTACCATTGATACCATTACCCGCTTAGATCAG
CCGGATTCACGCGGTCGTCAGTTACAGGCAGCACTGGATCATCTGCGCACCAATTCT
GTTGTTTCGTAATCGTATTGATCCGAATCGCATGGCAGTTATGGGTCATAGCATGGGT
GGCGGCGGCGCCTTAAGTGCAGCCGCCAATAATACCTCTTTAGAAGCCGCAATTCCG
TTACAGGGCTGGCATAACCCGTAAAAATTGGAGTAGCGTTCGCACCCCGACCTTAGTT
GTGGGCGCCCAGCTGGATACCATTGCTCCCGTGTCAAGTCATAGTGAAGCATTTTAT
AATTCACTGCCGAGCGATTTAGATAAAGCCTATATGGAACTGCGTGGTGCATCACAT
TTTGTGTCTAATAACCCCGGATACCACCACCGCCAAATATAGTATTGCCTGGCTGAAA
CGCTTTGTTGATAATGATCTGCGCTATGAACAGTTTCTGTGTCCGGCCCCGGATGATT
TTGCAATTAGCGAATATCGTGCAACCTGTCCGTTTTAA
```

**Table S1.** Data collection and refinement statistics of PES-H1-apo, PES-H1-cit, PES-H2-apo and PES-H2-PEG crystals.

	<b>PES-H1-apo</b>	<b>PES-H1-cit</b>	<b>PES-H2-apo</b>	<b>PES-H2-PEG</b>
PDB code	7CUV	7E30	7W69	7E31
Data collection				
space group	P2 <sub>1</sub>	P2 <sub>1</sub> 2 <sub>1</sub> 2 <sub>1</sub>	C2	P2 <sub>1</sub> 2 <sub>1</sub> 2 <sub>1</sub>
-cell				
a [Å]	52.01	55.97	105.52	55.34
b [Å]	69.54	97.08	55.34	94.86
c [Å]	74.85	99.11	51.15	105.5
$\alpha / \beta / \gamma$ (°)	90/90/90	90/90/90	90/93.36/90	90/90/90
resolution [Å]	25.0-1.45 (1.50-1.45)	25.0-1.56 (1.62-1.56)	22.9-1.56 (1.62-1.56)	24.3-1.38 (1.43-1.38)
unique reflections	89271 (8550)	77551 (7586)	41976 (4156)	114425 (11157)
redundancy	6.8 (3.8)	5.0 (3.2)	9.4 (6.4)	7.5 (4.3)
completeness [%]	96.9 (93.5)	99.9 (99.6)	99.86 (99.43)	99.78 (98.39)
average I/ $\sigma$ (I)	15.1 (2.5)	18.5 (3.02)	22.4 (2.80)	49.3 (2.64)
Rmeans	0.18 (0.53)	0.084 (0.48)	0.12 (0.65)	0.056 (0.52)
CC 1/2	0.994 (0.872)	0.993 (0.838)	0.993 (0.853)	0.992 (0.829)
Refinement				
no. reflections of	89157 (8383)	77449 (7581)	41964 (4156)	114421 (11157)
	4457(419)	3866 (373)	2101 (210)	5721 (557)
Rwork[a] (95 % of data)	0.163 (0.214)	0.152 (0.203)	0.1838 (0.2487)	0.1672 (0.2244)

Rfree[a] (5 % of data)	0.180 (0.246)	0.172 (0.225)	0.1928 (0.2475)	0.1772 (0.2426)
RMSD bonds [Å]	0.009	0.013	0.013	0.008
RMSD angles [°]	1.534	1.649	1.64	1.41
dihedral angles				
most favored [%]	98.2	97.8	97.66	98.24
allowed [%]	1.8	2.2	2.34	1.76
disallowed [%]	0	0	0	0
Average B-factor/ Number of non-hydrogen atoms				
Protein	16.25/3912	18.29/3924	20.37/3936	14.61/1968
Ion/ligands		32.35/47	43.23/20	29.84/10
solvent	31.10/653	32.03/555	33.86/773	29.75/313

Values in parentheses are for the highest resolution shell.

**Table S2.** Data collection and refinement statistics of PES-H1-MHETA, PES-H1-MHETA2, PES-H2-MHETA3 and PES-H2-BHET crystals.

	<b>PES-H1-MHETA1</b>	<b>PES-H1-MHETA2</b>	<b>PES-H1-MHETA3</b>	<b>PES-H2-BHET</b>
PDB code	7W6C	7W6O	7W6Q	7W66
Data collection				
space group	P2 <sub>1</sub>	P2 <sub>1</sub>	P2 <sub>1</sub>	P2 <sub>1</sub> 2 <sub>1</sub> 2 <sub>1</sub>
-cell				
a [Å]	52.51	52.67	52.71	105.84
b [Å]	56.01	56.19	56.22	55.62
c [Å]	102.31	100.03	108.62	95.88
$\alpha / \beta / \gamma$ (°)	90/94.41/90	90/93.91/90	90/93.78/90	90/90/90
resolution [Å]	29.5-2.3 (2.382-2.3)	25.8-2.2 (2.279-2.2)	27.1-2.2 (2.279-2.2)	49.2-1.96 (2.03-1.96)
unique reflections	26497 (2642)	29919 (2947)	30069 (2951)	39103 (4057)
redundancy	5.6 (5.4)	6.4 (6.7)	6.3 (6.3)	6.2 (5.2)
completeness [%]	99.45 (98.80)	99.84 (100.00)	99.83 (99.97)	94.36 (99.78)
average I/ $\sigma$ (I)	9.2 (6.0)	22.2 (18.6)	22.7 (17.6)	13.0 (2.5)
Rmeans	0.19 (0.35)	0.09 (0.12)	0.083 (0.105)	0.109 (0.75)
CC 1/2	0.979 (0.911)	0.995 (0.985)	0.996 (0.987)	0.998 (0.797)
Refinement				
no. of reflections	26482 (2642)	29906 (2947)	30051 (2952)	39072 (4056)
	1352 (122)	1479 (144)	1517 (147)	1954 (202)
Rwork[a] (95 % of data)	0.2487 (0.2789)	0.2224 (0.2575)	0.2250 (0.2567)	0.1976 (0.2879)

Rfree[a] (5 % of data)	0.2791 (0.2733)	0.2657 (0.3247)	0.2550 (0.2916)	0.2281 (0.3240)
RMSD bonds [Å]	0.013	0.006	0.006	0.005
RMSD. angles [°]	1.82	0.90	0.96	0.81
dihedral angles				
most favored [%]	94.71	95.49	94.51	97.65
allowed [%]	5.29	4.51	5.49	2.35
disallowed [%]	0.00	0.00	0.00	0.00
Average B-factor/ Number of non-hydrogen atoms				
Protein	18.35/3912	15.09/3912	16.21/3912	24.89/3916
Ion/ligands	38.57/30	30.84/15	31.07/15	36.50/18
solvent	17.78/169	21.14/347	22.78/382	32.81/363

Values in parentheses are for the highest resolution shell.

**Table S3.** Backbone RMSD values calculated based on the crystal structures of selected homologous PET hydrolases to that of PES-H1 (PDB code: 7CUV). *BurPL*: IsPETase-like enzyme from *Burkholderiales bacterium* RIFCSPLOWO2\_02\_ FULL\_57\_36. RgPETase: PETase from *Rhizobacter gummiphilus*.

Enzyme	PDB ID	Main chain RMSD (Å)
PES-H1	7CUV	0.000
PES-H1-cit	7E30	0.259
PES-H1-MHETA1	7W6C	0.358
PES-H1-MHETA2	7W6O	0.209
PES-H1-MHETA3	7W6Q	0.232
PES-H2	7W69	0.207
PES-H2-PEG	7E31	0.208
PES-H2-BHET	7W66	0.258
lipase	1JFR	0.388
Est119	3VIS	0.541
TfCut2	4CG1	0.457
LC-cutinase	6THT	0.644
Cut190 <sup>S226P</sup>	4WFI	0.471
<i>Thermobifida fusca</i> cutinase	5ZOA	0.459
IsPETase	5XG0	0.512
<i>BurPL</i>	7CWQ	0.578
LCC cutinase from <i>Biortus</i>	7DS7	0.655
PE-H	6SBN	0.732
PET2 F105R/E110K	7EC8	0.766
RgPETase	7DZT	0.605
PHL-7	7NEI	0.285



**Table S4.** Characteristics of the four binding positions observed by clustering. In total, 252 clusters were found. The distance between the catalytic S130 and the carbonyl carbon of the central PET unit was averaged over all frames belonging to the respective cluster.

	<b>Total / 1-4</b>	<b>Cluster 1</b>	<b>Cluster 2</b>	<b>Cluster 3</b>	<b>Cluster 4</b>
frames	15003 / 8765	4253	2592	1136	784
	100% / 58.40%	28.35%	17.28%	7.57%	5.23%
Fraction 1 <sup>st</sup>	5001 / 3746	2074	101	1133	438
	100% / 42.74%	48.77%	3.90%	99.74%	55.87%
Fraction 2 <sup>nd</sup>	5001 / 2836	2041	790	3	2
	100% / 32.36%	47.99%	30.48%	0.26%	0.26%
Fraction 3 <sup>rd</sup>	5001 / 2183	138	1701	0	344
	100% / 24.91%	3.24%	65.63%	0%	43.88%
Distance [ Å ]					
Ser130-O - PET-C		3.27 ± 0.30	4.12 ± 0.31	4.48 ± 0.34	3.58 ± 0.26

**Table S5.** Melting temperatures of PES-H1 and variants in potassium phosphate buffer. Values which were not determined are abbreviated with "n.d.".

Buffer	T <sub>m</sub> [°C]		
	PES-H1	L92F/Q94Y	R204C/S250C
0.05 M potassium phosphate	77.1	78.2	76.8
0.1 M potassium phosphate	n.d.	n.d.	79.6
0.5 M potassium phosphate	n.d.	n.d.	88.2
1 M potassium phosphate	84.9	86.7	91.3

**Table S6.** Crystallinity and molecular mass of PET materials before and after pretreatments determined by DSC and GPC, respectively. Values which were not determined are abbreviated with "n.d."  $M_w$ : weight average molecular mass,  $M_n$ : number average molecular mass.

<b>Sample name</b>	<b>Crystallinity (%) by DSC</b>	<b>Molecular mass by GPC</b>
Goodfellow PET film untreated	7%	$M_w$ :39872 $M_n$ :19652
PET nanoparticles prepared with Gf PET film	n.d.	$M_w$ :8864 $M_n$ :5770
Crushed PET film powder (particle size: 177 $\mu$ M mesh)	13%	$M_w$ :26197 $M_n$ :20874
Post-consumer PET bottle (untreated)	27%	$M_w$ :32304 $M_n$ :14885
PET bottle after melt-quenching	19%	$M_w$ :30214 $M_n$ :14542
crushed PET bottle powder (particle size: 177 $\mu$ M mesh)	33%	$M_w$ :26667 $M_n$ :13290
ball-milled PET bottle powder (particle size: 177 $\mu$ M mesh)	26%	$M_w$ :22266 $M_n$ :16224

**Table S7.** Kinetic parameters for PET-NP hydrolysis by PES-H1, its variants, and LCC ICCG.

$K_A$ = adsorption equilibrium constant.  $k_h$ = hydrolysis rate constant,  $k_h \times K_A$ = pseudo-catalytic efficiency.

	$K_A$ [ $\mu\text{M}^{-1}$ ]	$k_h$ [mL mg <sup>-1</sup> min <sup>-1</sup> ]	$k_h \times K_A$ [mL $\mu\text{M}^{-1}$ mg <sup>-1</sup> min <sup>-1</sup> ]*
PES-H1 wild-type	4.710 ± 0.087	0.054 ± 0.001	0.254
L92F/Q94Y	8.259 ± 0.028	0.065 ± 0.002	0.537
R204C/S250C	4.063 ± 0.191	0.064 ± 0.001	0.260
LCC ICCG	5.953 ± 0.032	0.048 ± 0.001	0.286

\*We can clearly show a 2.1-fold higher “pseudo-catalytic efficiency” value (mathematically equivalent to the catalytic efficiency described by  $k_{\text{cat}}/K_M$  based on the conventional Michaelis-Menten kinetics) with L92F/Q94Y compared to the wild-type enzyme. In addition, the ranking of the enzymes in terms of this value is remarkably consistent with that determined in the hydrolysis of amorphous PET materials as shown in Figures 4A and 4B. However, this pseudo-catalytic efficiency parameter based on the Langmuir-isotherm-based model is not yet properly defined and fully understood, which does not allow us to give a clear statement in the main text.

**Table S8.** Oligonucleotide primers used for the generation of PES-H1 variants.

<b>Variant</b>	<b>Sequence (5' → 3')</b>
L92F/Q94Y_fw	TTATCCGGACAGCCGCGGTCGT
L92F/Q94Y_rv	TCAAAACGGGTGATGGTATCAATGGTAATCACCAC
S204C_fw	TATGGAAGTGTGCGGTGCCAGCC
S204C_rv	TAGGCTTTATCCAGATCGCTCGG
S250C_fw	TTTTGCCATCTGCGAATATCGCAGCACCTGC
S250C_rv	TCATCCGGCGCCGGGCAC

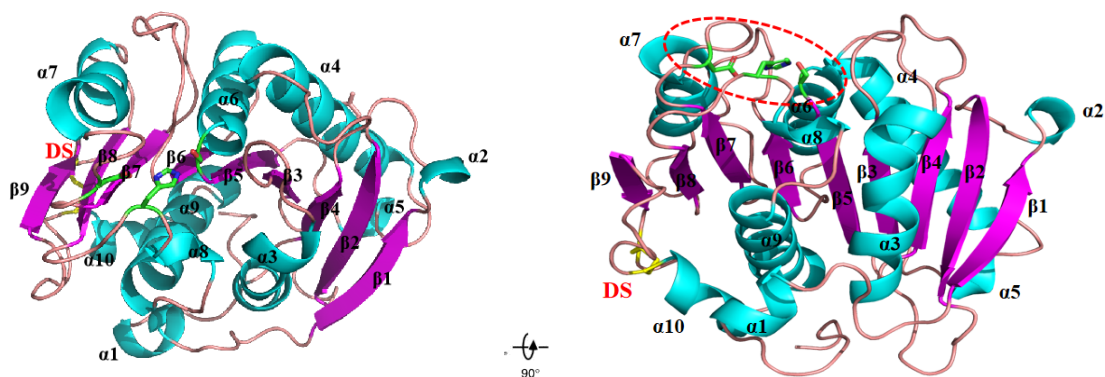


**Figure S1.** Structure of PES-H1. The structure of PES-H1 is represented as a cartoon. The catalytic triad (red dashed circle, top left) and disulfide bridge (red labels) are shown as sticks. The  $\alpha$ -helices,  $\beta$ -sheets and loops are shown in light blue, purple, and cyan, respectively.

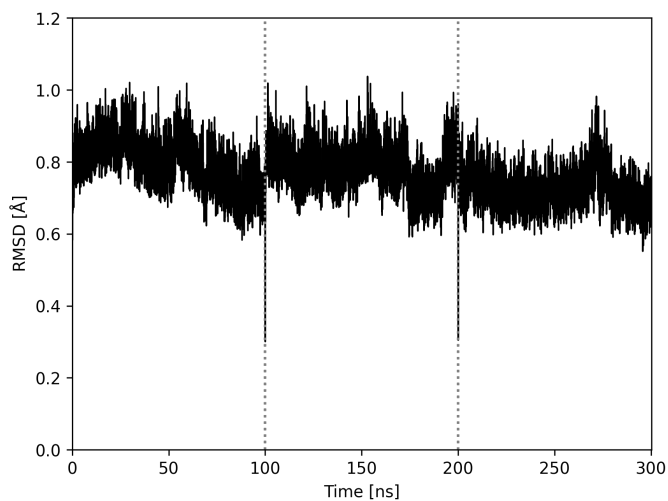


**Figure S2.** RMSD of the PES-H1 calculated against its crystal structure during the  $3 \times 100$  ns MD simulations. The protein backbone atoms were used for this calculation. The three simulations were concatenated for this analysis and the start of the second and third simulation is indicated by vertical dotted lines. The RMSD values below  $1 \text{ \AA}$  confirm the stability of the protein in the simulations.

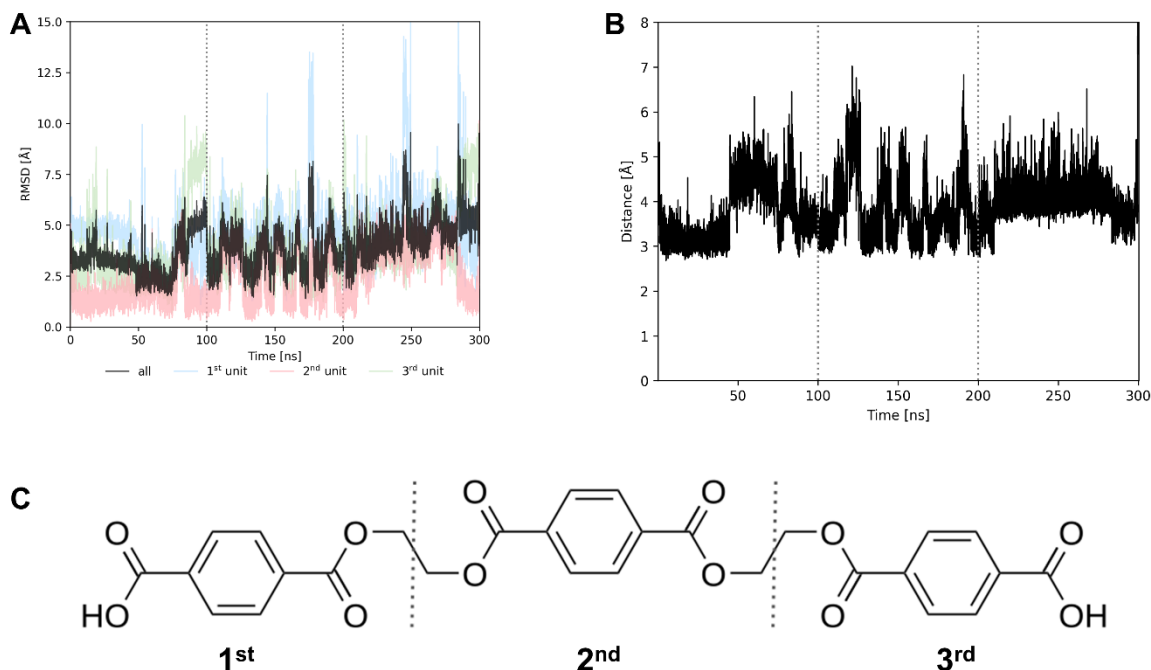


**Figure S3.** RMSD of 3PET from its starting structure and the minimum distance between the catalytic S130 and the second carbonyl carbon of the 2<sup>nd</sup> repeating unit during the  $3 \times 100$  ns MD simulations. (A) The RMSD values were determined for the whole 3PET substrate (black: all) as well as each 3PET unit (blue: 1<sup>st</sup>, red: 2<sup>nd</sup> and green: 3<sup>rd</sup> unit), respectively, after alignment of the protein structures. This provides a measure for the change in binding position of 3PET. (B) The evolution of the minimum distance between the  $\gamma$ -O atom of the catalytic S130 and the closest carbonyl carbon atom of the central repeating unit in 3PET was calculated. This analysis revealed that 3PET adopted a hydrolysis-competent orientation. Three simulations were concatenated for this analysis and the start of the second and third simulation is indicated by vertical dotted lines. (C) 3PET oligomer structure with the 1<sup>st</sup>, 2<sup>nd</sup>, and 3<sup>rd</sup> PET repeating units labeled from left to right and divided by dotted lines

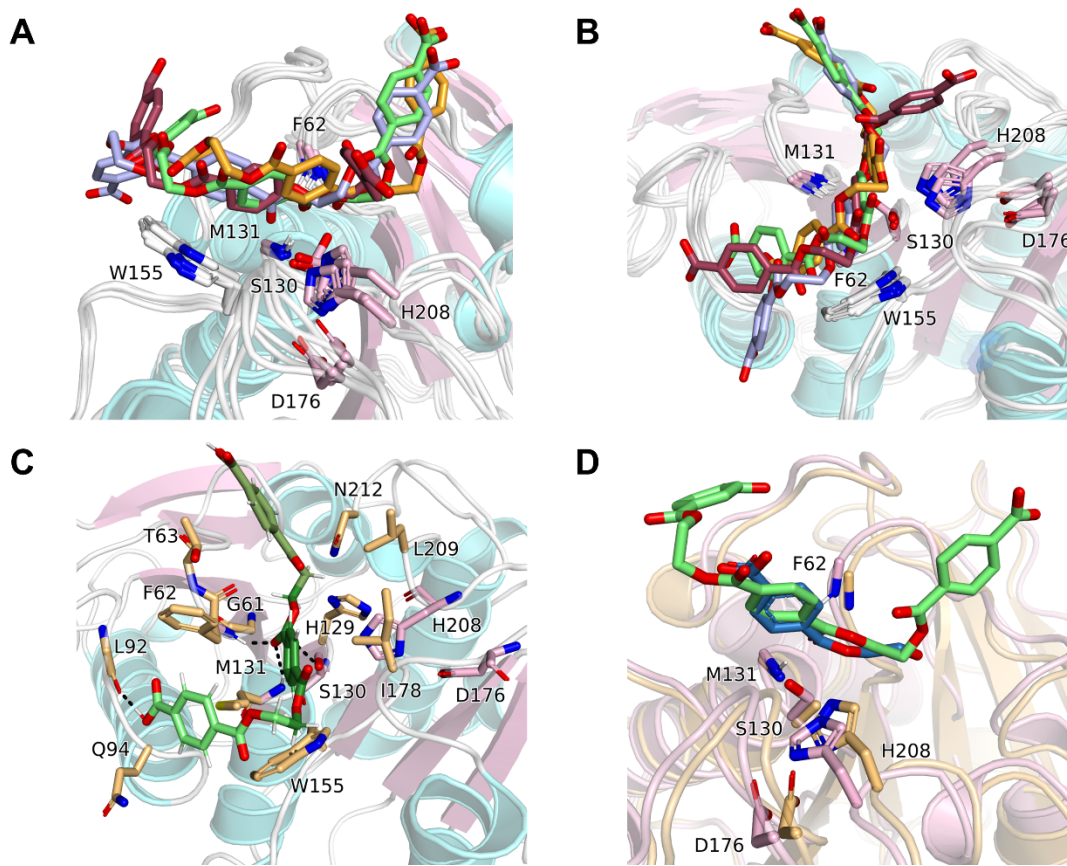


**Figure S4.** Binding positions of the 3PET clusters. Binding positions of all four clusters are given from a side view (A) and top view (B). The 3PET ligands are shown in green (cluster 1), orange (cluster 2), blue (cluster 3) and red (cluster 4). As an orientation marker, W155 is additionally shown as white sticks. The binding mode of cluster 1 (C) is colored from light green (1<sup>st</sup> unit) to dark green (3<sup>rd</sup> unit) and the most prominent interacting residues (sidechain/ backbone) are shown as orange sticks. (D) Superposition of the PES-H1 (light pink) and LCC ICCG with bound MHET (light orange, PDB code: 7VVE) structures. The 3PET ligand in the binding pose of cluster 1 is shown in light green, while MHET is colored in deep teal. For all images, the catalytic triad residues (S130, D176, and H208) and the oxyanion hole (F62 and M131) of PES-H1 are shown in light magenta. Nitrogen atoms are colored blue and oxygen atoms are colored red. The images were generated using PyMOL.



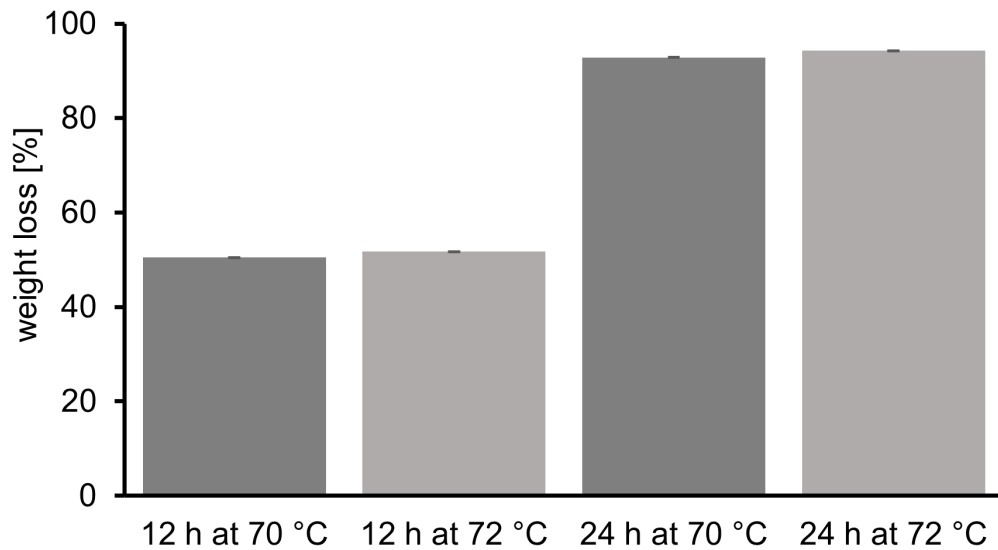


**Figure S5.** PET film degradation catalyzed by PES-H1 at 70 °C and 72 °C. Error bars indicate the standard deviations calculated from three replicates

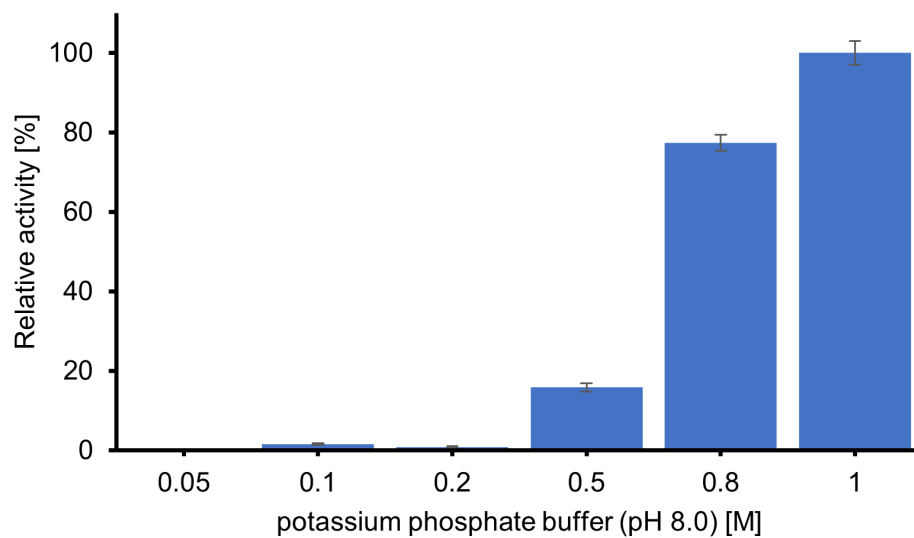


**Figure S6.** Phosphate dependence of PES-H1. PES-H1 was used to catalyze hydrolysis of Gf-PET film at 72 °C for 24 h in potassium phosphate buffer (pH 8.0). Phosphate concentrations ranged from 0.05 M to 1 M. Error bars indicate the standard deviations calculated from three replicates..

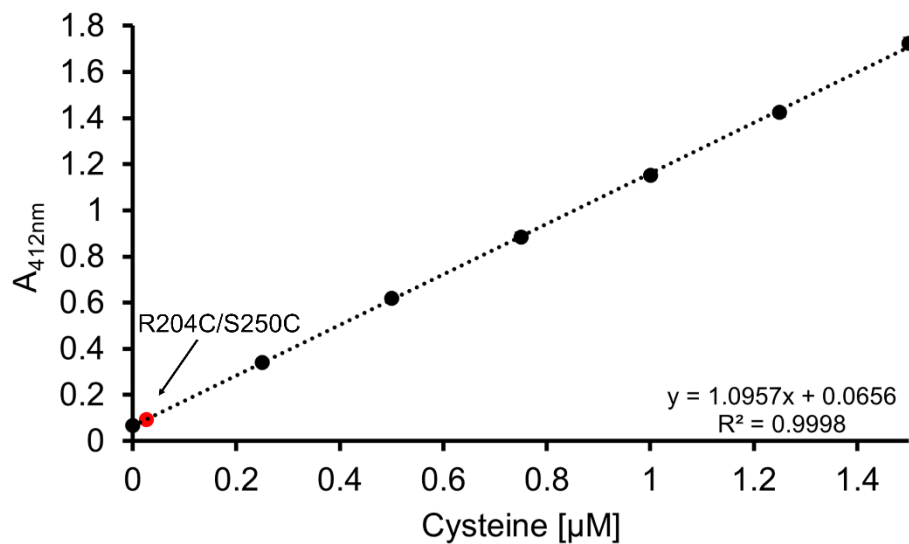


**Figure S7.** Cysteine calibration curve to determine the amount of free sulfhydryl-groups and confirm the disulfide bond formation. The concentration of free cysteines in the R204C/S250C variant of PES-H1 ( $0.02 \pm 0 \mu\text{M}$ ; red dot) was calculated based on the dotted calibration line obtained with linearly fitted absorbance data according to the experimentally determined absorbance values at 412 nm. No absorbance was measured for the R204C/S250C variant, demonstrating the formation of a new disulfide bond.

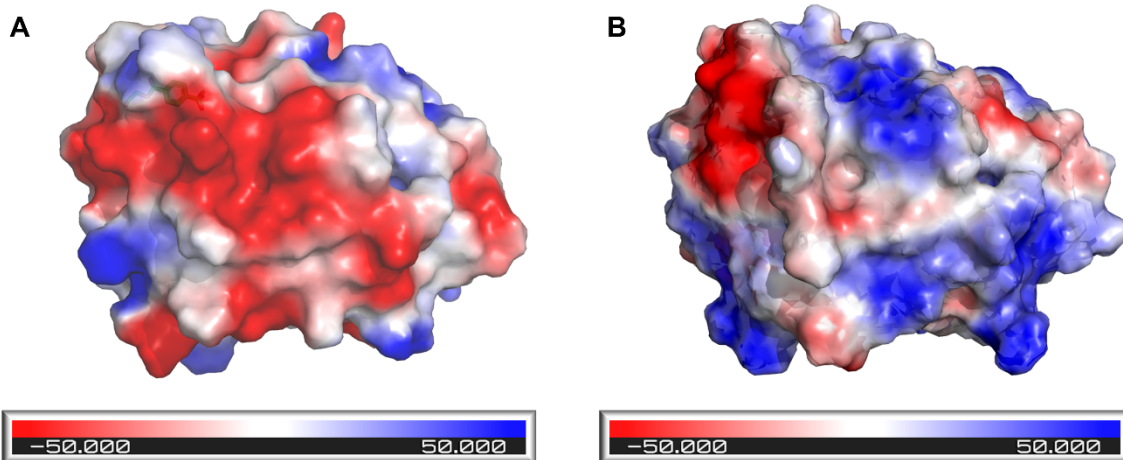


**Figure S8.** Electrostatic surfaces of PES-H1 (A) and LCC ICCG (B). Red areas indicate negatively charged residues whereas blue areas represent positively charged residues (-50 kT/e to +50 kT/e). The images were generated using PyMOL.

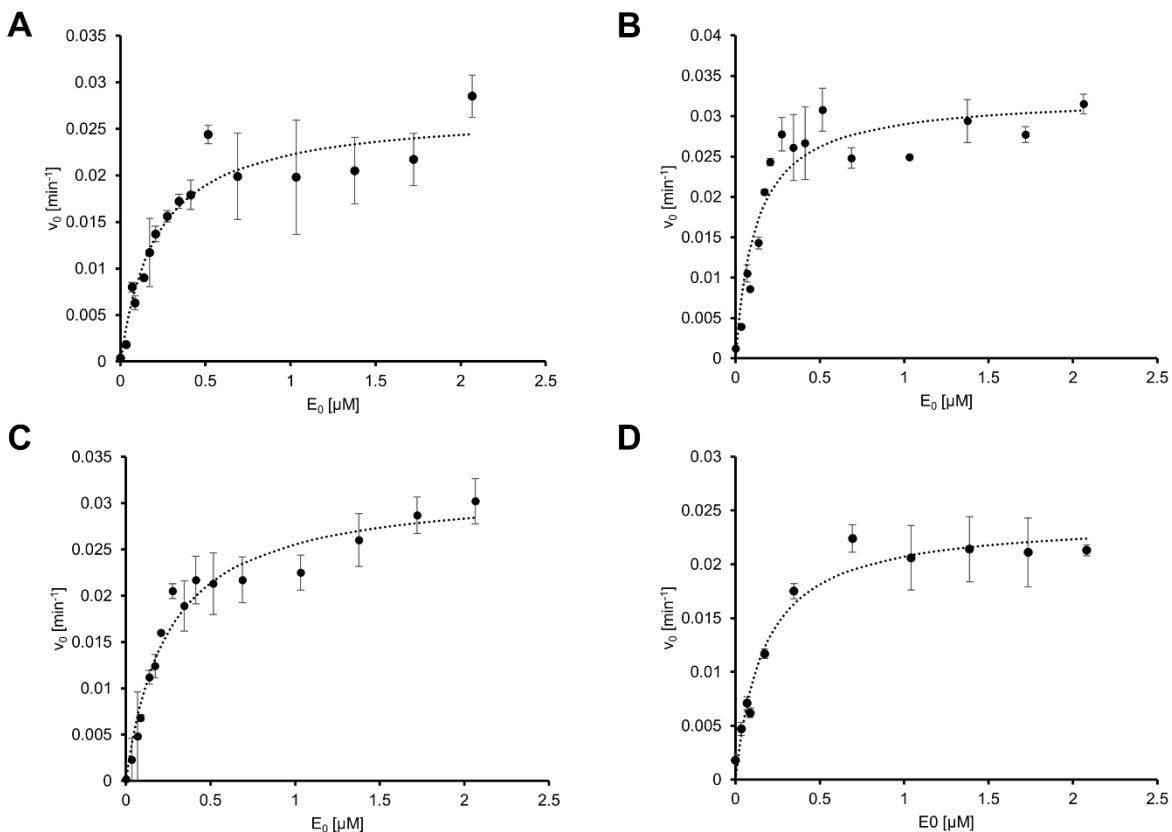


**Figure S9.** Hydrolysis of PET-NP by (A) PES-H1, (B) the L92F/Q94Y variant, (C) the R204C/S250C variant, and (D) LCC ICCG. The initial PET hydrolysis rates were determined by a turbidimetric assay by measuring apparent absorbance of light at 600 nm in a microtiter plate reader. Reactions in 1 M potassium phosphate buffer (pH 8.0) contained  $0.5 \text{ mg mL}^{-1}$  PET-NP and  $0\text{-}2 \text{ }\mu\text{M}$  enzyme and were incubated at  $70 \text{ }^\circ\text{C}$ . Data points represent the averages and error bars the standard deviations calculated from three replicates. The fitted data are shown as dotted curves.

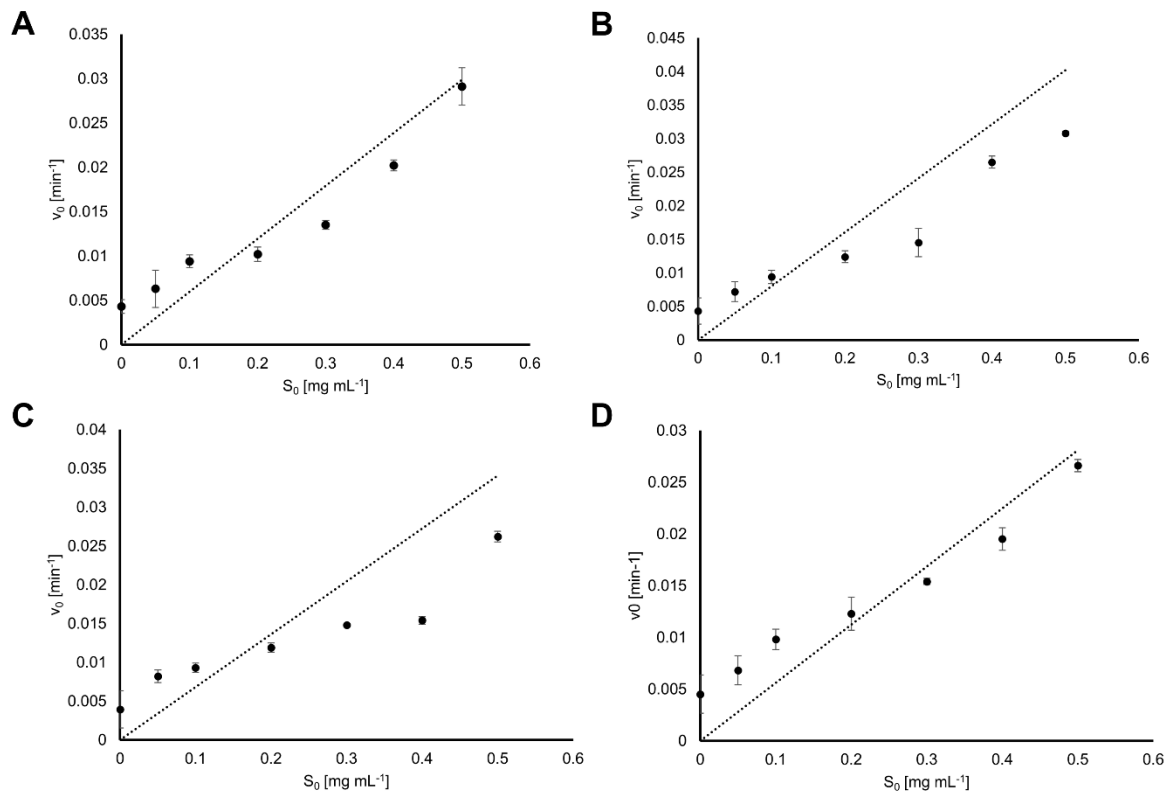


**Figure S10.** Hydrolysis of PET-NP by (A) PES-H1, (B) the L92F/Q94Y variant, (C) the R204C/S250C variant, and (D) LCC ICCG. The initial PET hydrolysis rates were determined by a turbidimetric assay by measuring apparent absorbance of light at 600 nm in a microtiter plate reader. Reactions in 1 M potassium phosphate buffer (pH 8.0) contained  $0.7 \mu\text{M}$  enzyme and  $0\text{-}0.5 \text{ mg mL}^{-1}$  PET-NP and were incubated at  $70 \text{ }^\circ\text{C}$ . Data points represent the averages and error bars the standard deviations calculated from three replicates. The fitted data are shown as dotted lines.

## REFERENCES

- (1) Otwinowski, Z.; Minor, W. [20] Processing of X-Ray Diffraction Data Collected in Oscillation Mode. In *Methods in Enzymology*; Elsevier, **1997**; Vol. 276, pp 307–326.
- (2) McCoy, A. J.; Grosse-Kunstleve, R. W.; Adams, P. D.; Winn, M. D.; Storoni, L. C.; Read, R. J. *Phaser Crystallographic Software. J. Appl. Crystallogr.* **2007**, *40* (4), 658–674.
- (3) Liebschner, D.; Afonine, P. V.; Baker, M. L.; Bunkóczi, G.; Chen, V. B.; Croll, T. I.; Hintze, B.; Hung, L.-W.; Jain, S.; McCoy, A. J.; Moriarty, N. W.; Oeffner, R. D.; Poon, B. K.; Prisant, M. G.; Read, R. J.; Richardson, J. S.; Richardson, D. C.; Sammito, M. D.; Sobolev, O. V.; Stockwell, D. H.; Terwilliger, T. C.; Urzhumtsev, A. G.; Videau, L. L.; Williams, C. J.; Adams, P. D. Macromolecular Structure Determination Using X-Rays, Neutrons and Electrons: Recent Developments in *Phenix. Acta Crystallogr. D. Struct. Biol.* **2019**, *75* (10), 861–877.
- (4) Han, X.; Liu, W.; Huang, J.-W.; Ma, J.; Zheng, Y.; Ko, T.-P.; Xu, L.; Cheng, Y.-S.; Chen, C.-C.; Guo, R.-T. Structural Insight into Catalytic Mechanism of PET Hydrolase. *Nat. Commun.* **2017**, *8* (1), 2106.
- (5) Afonine, P. V.; Grosse-Kunstleve, R. W.; Echols, N.; Headd, J. J.; Moriarty, N. W.; Mustyakimov, M.; Terwilliger, T. C.; Urzhumtsev, A.; Zwart, P. H.; Adams, P. D. Towards Automated Crystallographic Structure Refinement with *Phenix.Refine. Acta Crystallogr. D. Biol. Crystallogr.* **2012**, *68* (4), 352–367.
- (6) Emsley, P.; Cowtan, K. *Coot*: Model-Building Tools for Molecular Graphics. *Acta Crystallogr. D. Biol. Crystallogr.* **2004**, *60* (12), 2126–2132.
- (7) Brünger, A. T.; Adams, P. D.; Clore, G. M.; DeLano, W. L.; Gros, P.; Grosse-Kunstleve, R. W.; Jiang, J. S.; Kuszewski, J.; Nilges, M.; Pannu, N. S.; Read, R. J.; Rice, L. M.; Simonson,

- T.; Warren, G. L. Crystallography & NMR System: A New Software Suite for Macromolecular Structure Determination. *Acta Crystallogr. D. Biol. Crystallogr.* **1998**, *54* (5), 905–921.
- (8) *The PyMOL Molecular Graphics System, Version 1.8*, **2015**. Schrödinger, LLC.
- (9) Wang, J.; Wolf, R. M.; Caldwell, J. W.; Kollman, P. A.; Case, D. A. Development and Testing of a General Amber Force Field. *J. Comput. Chem.* **2004**, *25* (9), 1157–1174.
- (10) M.J. Frisch, G.W. Trucks, H.B. Schlegel, G.E. Scuseria, M.A. Robb, J.R. Cheeseman, G. Scalmani, V. Barone, B. Mennucci, G.A. Petersson, H. Nakatsuji, M. Caricato, X. Li, H.P. Hratchian, A.F. Izmaylov, J. Bloino, G. Zheng, J.L. Sonnenberg, M. Hada, M. Ehara, K. Toyota, R. Fukuda, J. Hasegawa, M. Ishida, T. Nakajima, Y. Honda, O. Kitao, H. Nakai, T. Vreven, J.A. Montgomery, J.E. Peralta, F. Ogliaro, M. Bearpark, J.J. Heyd, E. Brothers, K.N. Kudin, V.N. Staroverov, R. Kobayashi, J. Normand, K. Raghavachari, A. Rendell, J.C. Burant, S.S. Iyengar, J. Tomasi, M. Cossi, N. Rega, J.M. Millam, M. Klene, J.E. Knox, J.B. Cross, V. Bakken, C. Adamo, J. Jaramillo, R. Gomperts, R.E. Stratmann, O. Yazyev, A.J. Austin, R. Cammi, C. Pomelli, J.W. Ochterski, R.L. Martin, K. Morokuma, V.G. Zakrzewski, G.A. Voth, P. Salvador, J.J. Dannenberg, S. Dapprich, A.D. Daniels, Ö. Farkas, J.B. Foresman, J.V. Ortiz, J. Cioslowski, and D.J. Fox. Gaussian 09. Revision E.01, Gaussian Inc., Wallingford CT. **2009**.
- (11) Bayly, C. I.; Cieplak, P.; Cornell, W.; Kollman, P. A. A Well-Behaved Electrostatic Potential Based Method Using Charge Restraints for Deriving Atomic Charges: The RESP Model. *J. Phys. Chem.* **1993**, *97* (40), 10269–10280.

- (12) Cornell, W. D.; Cieplak, P.; Bayly, C. I.; Kollman, P. A. Application of RESP Charges to Calculate Conformational Energies, Hydrogen Bond Energies, and Free Energies of Solvation. *J. Am. Chem. Soc.* **1993**, *115* (21), 9620–9631.
- (13) Wang, J.; Wang, W.; Kollman, P. A.; Case, D. A. Antechamber, An Accessory Software Package For Molecular Mechanical Calculations. *J. Am. Chem. Soc.* **2001**, *222*.
- (14) Wang, J.; Wang, W.; Kollman, P. A.; Case, D. A. Automatic Atom Type and Bond Type Perception in Molecular Mechanical Calculations. *J. Mol. Graph. Model.* **2006**, *25* (2), 247–260.
- (15) K. Belfon, I.Y. Ben-Shalom, S.R. Brozell, D.S. Cerutti, T.E. Cheatham III, G.A. Cisneros, V.W.D. Cruzeiro, T.A. Darden, R.E. Duke, G. Giambasu, M.K. Gilson, H. Gohlke, A.W. Goetz, R. Harris, S. Izadi, S.A. Izmailov, C. Jin, K. Kasavajhala, M.C. Kaymak, E. King, A. Kovalenko, T. Kurtzman, T.S. Lee, S. LeGrand, P. Li, C. Lin, J. Liu, T. Luchko, R. Luo, M. Machado, V. Man, M. Manathunga, K.M. Merz, Y. Miao, O. Mikhailovskii, G. Monard, H. Nguyen, K.A. O’Hearn, A. Onufriev, F. Pan, S. Pantano, R. Qi, A. Rahnamoun, D.R. Roe, A. Roitberg, C. Sagui, S. Schott-Verdugo, J. Shen, C.L. Simmerling, N.R. Skrynnikov, J. Smith, J. Swails, R.C. Walker, J. Wang, H. Wei, R.M. Wolf, X. Wu, Y. Xue, D.M. York, S. Zhao, P.A. Kollman, D.A. Case, H.M. Aktulga. *Amber 2021*; University of California, San Francisco, **2021**.
- (16) Abraham, M. J.; Murtola, T.; Schulz, R.; Páll, S.; Smith, J. C.; Hess, B.; Lindahl, E. GROMACS: High Performance Molecular Simulations through Multi-Level Parallelism from Laptops to Supercomputers. *SoftwareX* **2015**, *1–2*, 19–25.



- (17) Maier, J. A.; Martinez, C.; Kasavajhala, K.; Wickstrom, L.; Hauser, K. E.; Simmerling, C. Ff14SB: Improving the Accuracy of Protein Side Chain and Backbone Parameters from Ff99SB. *J. Chem. Theory Comput.* **2015**, *11* (8), 3696–3713.
- (18) Ivani, I.; Dans, P. D.; Noy, A.; Pérez, A.; Faustino, I.; Hospital, A.; Walther, J.; Andrio, P.; Goñi, R.; Balaceanu, A.; Portella, G.; Battistini, F.; Gelpí, J. L.; González, C.; Vendruscolo, M.; Laughton, C. A.; Harris, S. A.; Case, D. A.; Orozco, M. Parmbsc1: A Refined Force Field for DNA Simulations. *Nat. Methods* **2016**, *13* (1), 55–58.
- (19) Jorgensen, W. L.; Chandrasekhar, J.; Madura, J. D.; Impey, R. W.; Klein, M. L. Comparison of Simple Potential Functions for Simulating Liquid Water. *J. Chem. Phys.* **1983**, *79* (2), 926–935.
- (20) Cauchy, M. A. Méthode Générale Pour La Résolution Des Systemes d'équations Simultanées. *CR Hebd. Acad. Sci.* **1847**, No. 25, 536–538.
- (21) Nosé, S. A Molecular Dynamics Method for Simulations in the Canonical Ensemble. *Mol. Phys.* **1984**, *52* (2), 255–268.
- (22) Hoover, W. G. Canonical Dynamics: Equilibrium Phase-Space Distributions. *Phys. Rev. A* **1985**, *31* (3), 1695–1697.
- (23) Parrinello, M.; Rahman, A. Polymorphic Transitions in Single Crystals: A New Molecular Dynamics Method. *J. Appl. Phys.* **1981**, *52* (12), 7182–7190.
- (24) Darden, T.; York, D.; Pedersen, L. Particle Mesh Ewald: An  $N \cdot \log(N)$  Method for Ewald Sums in Large Systems. *J. Chem. Phys.* **1993**, *98* (12), 10089–10092.
- (25) Essmann, U.; Perera, L.; Berkowitz, M. L.; Darden, T.; Lee, H.; Pedersen, L. G. A Smooth Particle Mesh Ewald Method. *J. Chem. Phys.* **1995**, *103* (19), 8577–8593.

- (26) Hess, B.; Bekker, H.; Berendsen, H. J. C.; Fraaije, J. G. E. M. LINCS: A Linear Constraint Solver for Molecular Simulations. *J. Comput. Chem.* **1997**, *18* (12), 1463–1472.
- (27) Daura, X.; Gademann, K.; Jaun, B.; Seebach, D.; van Gunsteren, W. F.; Mark, A. E. Peptide Folding: When Simulation Meets Experiment. *Angew. Chem. Int. Ed.* **1999**, *38* (1–2), 236–240.
- (28) Humphrey, W.; Dalke, A.; Schulten, K. VMD: Visual Molecular Dynamics. *J. Mol. Graph.* **1996**, *14* (1), 33–38.
- (29) Studier, F. W. Protein Production by Auto-Induction in High-Density Shaking Cultures. *Protein Expression Purif.* **2005**, *41* (1), 207–234.
- (30) Zimmermann, W.; Wei, R.; Hille, P.; Oeser, T.; Schmidt, J. New Polypeptides Having a Polyester Degrading Activity and Uses Thereof. EP3517608A1, July 31, **2019**.
- (31) Palm, G. J.; Reisky, L.; Böttcher, D.; Müller, H.; Michels, E. A. P.; Walczak, M. C.; Berndt, L.; Weiss, M. S.; Bornscheuer, U. T.; Weber, G. Structure of the Plastic-Degrading *Ideonella sakaiensis* MHETase Bound to a Substrate. *Nat. Commun.* **2019**, *10* (1), 1717.
- (32) Brott, S.; Pfaff, L.; Schuricht, J.; Schwarz, J.; Böttcher, D.; Badenhorst, C. P. S.; Wei, R.; Bornscheuer, U. T. Engineering and Evaluation of Thermostable IsPETase Variants for PET Degradation. *Eng. Life Sci.* **2021**, *22* (3-4), 192-203
- (33) Pfaff, L.; Breite, D.; Badenhorst, C. P. S.; Bornscheuer, U. T.; Wei, R. Fluorimetric High-Throughput Screening Method for Polyester Hydrolase Activity Using Polyethylene Terephthalate Nanoparticles. In *Methods in Enzymology*; Elsevier, 2021; Vol. 648, pp 253–270.
- (34) Vogel, K.; Wei, R.; Pfaff, L.; Breite, D.; Al-Fathi, H.; Ortmann, C.; Estrela-Lopis, I.; Venus, T.; Schulze, A.; Harms, H.; Bornscheuer, U. T.; Maskow, T. Enzymatic Degradation of

- Polyethylene Terephthalate Nanoplastics Analyzed in Real Time by Isothermal Titration Calorimetry. *Sci. Total Environ.* **2021**, *773*, 145111.
- (35) Belisário-Ferrari, M. R.; Wei, R.; Schneider, T.; Honak, A.; Zimmermann, W. Fast Turbidimetric Assay for Analyzing the Enzymatic Hydrolysis of Polyethylene Terephthalate Model Substrates. *Biotechnol. J.* **2019**, *14* (4), 1800272.
- (36) Ronkvist, Å. M.; Xie, W.; Lu, W.; Gross, R. A. Cutinase-Catalyzed Hydrolysis of Poly(Ethylene Terephthalate). *Macromolecules* **2009**, *42* (14), 5128–5138.
- (37) Scandola, M.; Focarete, M. L.; Frisoni, G. Simple Kinetic Model for the Heterogeneous Enzymatic Hydrolysis of Natural Poly(3-Hydroxybutyrate). *Macromolecules* **1998**, *31* (12), 3846–3851.
- (38) Wei, R.; Oeser, T.; Barth, M.; Weigl, N.; Lübs, A.; Schulz-Siegmund, M.; Hacker, M. C.; Zimmermann, W. Turbidimetric Analysis of the Enzymatic Hydrolysis of Polyethylene Terephthalate Nanoparticles. *J. Mol. Catal., B-Enzym* **2014**, *103*, 72–78.
- (39) Wei, R.; Breite, D.; Song, C.; Gräsing, D.; Ploss, T.; Hille, P.; Schwerdtfeger, R.; Matysik, J.; Schulze, A.; Zimmermann, W. Biocatalytic Degradation Efficiency of Postconsumer Polyethylene Terephthalate Packaging Determined by Their Polymer Microstructures. *Adv. Sci.* **2019**, *6* (14), 1900491.

GAFF parameters for each PET unit (HPT: 1st unit, PET: 2nd unit, TPT: 3rd unit). The distinction into these three residues allows to use the same parameters for longer PET oligomers.

[ moleculetype ]

```
; Name          nrexcl
PET_all         3
```

[ atoms ]

```
; nr          type  resnr residue  atom   cgnr    charge      mass  typeB
chargeB      massB
```

```
; residue 301 HPT rtp HPT  q  0.0
```

nr	type	resnr	residue	atom	cgnr	charge	mass	typeB
1	ca	301	HPT	CG	1	-0.182603	12.01	
2	ca	301	HPT	CD1	2	-0.080671	12.01	
3	ha	301	HPT	HD1	3	0.138091	1.008	
4	ca	301	HPT	CD2	4	-0.080671	12.01	
5	ha	301	HPT	HD2	5	0.138091	1.008	
6	ca	301	HPT	CE1	6	-0.161565	12.01	
7	ha	301	HPT	HE1	7	0.163596	1.008	
8	ca	301	HPT	CE2	8	-0.161565	12.01	
9	ha	301	HPT	HE2	9	0.163596	1.008	
10	ca	301	HPT	CZ	10	-0.001699	12.01	
11	c	301	HPT	C1	11	0.95232	12.01	
12	c	301	HPT	C2	12	0.767006	12.01	
13	c3	301	HPT	C3	13	0.234898	12.01	
14	h1	301	HPT	H31	14	0.041201	1.008	
15	h1	301	HPT	H32	15	0.041201	1.008	
16	o	301	HPT	O11	16	-0.616653	16	
17	os	301	HPT	O12	17	-0.571755	16	
18	o	301	HPT	O21	18	-0.592326	16	
19	oh	301	HPT	O22	19	-0.658644	16	
20	ho	301	HPT	H22	20	0.468152	1.008	;qtot 0

```
; residue 302 PET rtp PET  q  0.0
```

nr	type	resnr	residue	atom	cgnr	charge	mass	typeB
21	ca	302	PET	CG	21	-0.137174	12.01	
22	ca	302	PET	CD1	22	-0.108708	12.01	
23	ha	302	PET	HD1	23	0.143188	1.008	
24	ca	302	PET	CD2	24	-0.108708	12.01	
25	ha	302	PET	HD2	25	0.143188	1.008	
26	ca	302	PET	CE1	26	-0.108708	12.01	
27	ha	302	PET	HE1	27	0.143188	1.008	
28	ca	302	PET	CE2	28	-0.108708	12.01	
29	ha	302	PET	HE2	29	0.143188	1.008	
30	ca	302	PET	CZ	30	-0.137174	12.01	
31	c	302	PET	C1	31	0.84416	12.01	
32	c	302	PET	C2	32	0.84416	12.01	
33	c3	302	PET	C3	33	0.257521	12.01	
34	h1	302	PET	H31	34	0.043825	1.008	
35	h1	302	PET	H32	35	0.043825	1.008	
36	c3	302	PET	C4	36	0.257521	12.01	
37	h1	302	PET	H41	37	0.043825	1.008	
38	h1	302	PET	H42	38	0.043825	1.008	
39	o	302	PET	O11	39	-0.583255	16	
40	os	302	PET	O12	40	-0.537862	16	
41	o	302	PET	O21	41	-0.583255	16	
42	os	302	PET	O22	42	-0.537862	16	;qtot 0

```

; residue 303 TPT rtp TPT q 0.0
 43      ca   303   TPT   CG    43  -0.001699   12.01
 44      ca   303   TPT   CD1   44  -0.161565   12.01
 45      ha   303   TPT   HD1   45   0.163596   1.008
 46      ca   303   TPT   CD2   46  -0.161565   12.01
 47      ha   303   TPT   HD2   47   0.163596   1.008
 48      ca   303   TPT   CE1   48  -0.080671   12.01
 49      ha   303   TPT   HE1   49   0.138091   1.008
 50      ca   303   TPT   CE2   50  -0.080671   12.01
 51      ha   303   TPT   HE2   51   0.138091   1.008
 52      ca   303   TPT    CZ   52  -0.182603   12.01
 53      c    303   TPT    C1   53   0.767006   12.01
 54      c    303   TPT    C2   54   0.95232    12.01
 55      c3   303   TPT    C4   55   0.234898   12.01
 56      h1   303   TPT   H41   56   0.041201   1.008
 57      h1   303   TPT   H42   57   0.041201   1.008
 58      o    303   TPT   O11   58  -0.592326    16
 59      oh   303   TPT   O12   59  -0.658644    16
 60      ho   303   TPT   H12   60   0.468152   1.008
 61      o    303   TPT   O21   61  -0.616653    16
 62      os   303   TPT   O22   62  -0.571755    16 ;qtot 0

```

```
[ bondtypes ]
```

```

; i   j   func      b0      kb
ca ca      1   0.13984  385850
ca c       1   0.14906  289450
ca ha      1   0.10860  289370
c o       1   0.12183  533630
c os      1   0.13584  327020
c oh      1   0.13513  334800
c3 os     1   0.14316  258240
c3 h1     1   0.10969  276650
c3 c3     1   0.15375  251790
oh ho     1   0.09730  310790

```

```
[ angletypes ]
```

```

; i   j   k   func      th0      cth
ca ca ca      1   120.02   557.31
ca ca ha      1   119.88   403.34
ca c o       1   122.60   574.88
ca c os      1   112.44   579.90
ca ca c      1   120.33   538.06
ca c oh      1   113.45   579.07
c os c3     1   115.98   529.69
c oh ho     1   106.55   417.56
c3 c3 os    1   107.97   569.02
c3 c3 h1    1   109.56   388.28
o c os     1   123.25   630.11
os c3 h1    1   109.78   425.09
o c oh     1   122.10   635.13
h1 c3 h1    1   108.46   328.03

```

```

[ dihedraltypes ] ; improper
;i j k l func phase kd pn
ca ca ca ha 4 180.00 4.60240 2
ca o c os 4 180.00 4.60240 2
ca ca ca c 4 180.00 4.60240 2
ca o c oh 4 180.00 4.60240 2
c ca ca ca 4 180.00 4.60240 2

```

```

[ dihedraltypes ]
;i j k l func phase kd pn
ca ca ca ca 9 180.0 15.16700 2
ca ca ca ha 9 180.0 15.16700 2
ca c os c3 9 180.0 11.29680 2
ca ca c o 9 180.0 4.18400 2
ca ca c os 9 180.0 4.18400 2
ca ca ca c 9 180.0 15.16700 2
ca ca c oh 9 180.0 4.18400 2
ca c oh ho 9 180.0 9.62320 2
c ca ca ca 9 180.0 15.16700 2
c ca ca ha 9 180.0 15.16700 2
c os c3 h1 9 0.0 1.60387 3
c os c3 c3 9 0.0 1.60247 3
c os c3 c3 9 180.0 3.34720 1
c3 os c o 9 180.0 5.85760 1
c3 os c o 9 180.0 11.29680 2
os c3 c3 os 9 0.0 0.60250 3
os c3 c3 os 9 0.0 4.91620 2
os c3 c3 h1 9 0.0 0.00000 0
os c3 c3 h1 9 0.0 1.04600 1
o c oh ho 9 0.0 7.94960 1
o c oh ho 9 180.0 9.62320 2
ha ca ca ha 9 180.0 15.16700 2
h1 c3 c3 h1 9 0.0 0.65084 3

```








## Article II





## RESEARCH ARTICLE

# Engineering and evaluation of thermostable *IsPETase* variants for PET degradation

Stefan Brott  | Lara Pfaff  | Josephine Schuricht | Jan-Niklas Schwarz  |  
 Dominique Böttcher  | Christoffel P. S. Badenhorst  | Ren Wei  |  
 Uwe T. Bornscheuer 

Department of Biotechnology & Enzyme Catalysis, University of Greifswald  
 Institute of Biochemistry, Greifswald, Germany

## Correspondence

Uwe T. Bornscheuer, Department of Biotechnology & Enzyme Catalysis, University of Greifswald Institute of Biochemistry, Felix-Hausdorff-Straße 4, 17489 Greifswald, Germany.

Email:

[uwe.bornscheuer@uni-greifswald.de](mailto:uwe.bornscheuer@uni-greifswald.de)

Dedicated to Prof. Thomas Scheper on the occasion of his retirement.

## Abstract

Polyethylene terephthalate (PET) is a mass-produced petroleum-based synthetic polymer. Enzymatic PET degradation using, for example, *Ideonella sakaiensis* PETase (*IsPETase*) can be a more environmentally friendly and energy-saving alternative to the chemical recycling of PET. However, *IsPETase* is a mesophilic enzyme with an optimal reaction temperature lower than the glass transition temperature ( $T_g$ ) of PET, where the amorphous polymers can be readily accessed for enzymatic breakdown. In this study, we used error-prone PCR to generate a mutant library based on a thermostable triple mutant (TM) of *IsPETase*. The library was screened against the commercially available polyester-polyurethane Impranil DLN W 50 for more thermostable *IsPETase* variants, yielding four variants with higher melting points. The most promising *IsPETase*<sup>TM<sup>K95N/F201I</sup></sup> variant had a 5.0°C higher melting point than *IsPETase*<sup>TM</sup>. Although this variant showed a slightly lower activity on PET at lower incubation temperatures, its increased thermostability makes it a more active PET hydrolase at higher reaction temperatures up to 60°C. Several other variants were compared and combined with selected previously published *IsPETase* mutants in terms of thermostability and hydrolytic activity against PET nanoparticles and amorphous PET films. Our findings indicate that thermostability is one of the most important characteristics of an effective PET hydrolase.

## KEYWORDS

PET hydrolysis, PETase, polyethylene terephthalate, protein engineering, thermostability

**Abbreviations:** BHET, bis-(2-hydroxyethyl) terephthalate; EG, ethylene glycol; *IsPETase*, PETase from *Ideonella sakaiensis*; LCC, leaf-branch compost cutinase; MHET, mono-(2-hydroxyethyl) terephthalate; PET, polyethylene terephthalate; TA, terephthalic acid;  $T_m$ , melting point; TM, triple mutant

This is an open access article under the terms of the [Creative Commons Attribution](https://creativecommons.org/licenses/by/4.0/) License, which permits use, distribution and reproduction in any medium, provided the original work is properly cited.

© 2021 The Authors. *Engineering in Life Sciences* published by Wiley-VCH GmbH

## 1 | INTRODUCTION

The combination of mass production of single-use plastic products, plastic longevity, and insufficient waste management has resulted in an accumulation of plastic in the environment over the last few decades [1]. Globally, approximately 368 million tons of plastic were produced in 2019 alone [2]. Polyethylene terephthalate (PET), a semi-crystalline thermoplastic composed of the two monomeric units terephthalic acid (TA) and ethylene glycol (EG), linked by ester bonds, is one of the mass-produced petroleum-based synthetic polymers [3, 4]. More than 50 million tons of PET are annually produced globally, with the main applications being synthetic fibers in the textile industry and beverage bottles in the packaging sector [5, 6].

Recycling is a viable disposal solution for existing plastic waste in terms of energy savings, material efficiency and circularity, for which the use of enzymes can be an alternative option [7]. PET has hydrolysable ester backbones and is thus more susceptible to enzymatic degradation than petrochemical vinyl plastics with solely carbon-carbon backbones [8, 9]. Several enzymes capable of cleaving PET have been discovered in recent years [10]. These PET hydrolases belong to the enzyme classes of carboxylesterases [11], lipases [12] and cutinases [13–16]. When compared to chemical recycling methods, the use of enzymes provides an environmentally friendly and energy-saving alternative that also reduces the use of hazardous chemicals [7]. Although the industrially-relevant use of enzymes in PET degradation is still in its early stages, an engineered variant of the leaf-branch compost cutinase (LCC) has already enabled nearly complete depolymerization of pre-treated PET bottle waste and virgin polymers were re-synthesized using the recovered TA [17]. A significant milestone in PET breakdown was the identification of the Gram-negative aerobic  $\beta$ -proteobacterium *Ideonella sakaiensis* by screening of 250 environmental samples obtained from a PET bottle recycling site in Japan [18]. The bacterium utilized PET as its main energy and carbon source, and it was able to grow on low-crystallinity PET film and degrade it almost completely after 6 weeks at an incubation temperature of 30°C under controlled laboratory conditions [18]. Two enzymes, designated as *IsPETase* and *IsMHETase*, are involved in the breakdown of PET by *Ideonella sakaiensis* [18]. *IsPETase* catalyzes the depolymerization of PET to the main product mono-(2-hydroxyethyl) terephthalate (MHET) and the side products bis-(2-hydroxyethyl) terephthalate (BHET), TA, and EG [18]. *IsMHETase* then hydrolyzes MHET to TA and EG [18].

In recent years, the crystal structures of *IsPETase* and *IsMHETase* have been elucidated and published [19–25].

### PRACTICAL APPLICATION

In this work, an error-prone PCR-generated mutant library was screened using an agar plate assay based on the commercially available polyester-polyurethane Impranil DLN W 50. With this type of screening, finding multiple thermostable polyester hydrolase variants within a mutant library was possible. Recycling plastics such as PET with enzymes is one of the recently developed methods to mitigate the plastic pollution and to promote the circularity of material flow for a sustainable plastic economy. The enzymatic degradation of polyethylene terephthalate is more feasible at higher incubation temperatures. Therefore, mesophilic enzymes such as the *IsPETase* from *Ideonella sakaiensis* need to be engineered, revealing higher thermostability and activity by protein engineering methods such as directed evolution.

Despite this, only one *IsPETase* structure has been solved so far with a co-crystallized ligand analogous to MHET [19]. *IsPETase* exhibits a typical  $\alpha/\beta$ -hydrolase fold consisting of seven  $\alpha$ -helices and nine  $\beta$ -strands forming a central twisted  $\beta$ -sheet [21], which is highly conserved among many other cutinase-like PET-hydrolyzing enzymes [26]. The catalytic triad of *IsPETase*, located on the protein surface, is composed of the amino acids S160-D206-H237 [22]. The enzyme has two intramolecular disulfide bridges, whereas the structurally homologous cutinases TfCut2 from *Thermobifida fusca* and LCC only have one [19, 27]. The strictly conserved disulfide bridge (C273-C289) connects the last loop and the C-terminal helix [19]. The *IsPETase*-specific disulfide bridge (C203-C239) is located near the active site and connects two loops containing the residues of the catalytic triad [19]. This disulfide bridge is thought to be responsible for the high room temperature flexibility of the *IsPETase* active site and the resulting high activity against PET [27]. Methods such as structure-based sequence alignment of *IsPETase* with structural homologues or molecular docking experiments followed by biochemical characterization have also contributed to the elucidation of important residues in the enzyme [19, 20, 23, 24]. For example, a tryptophan residue crucial for substrate binding was discovered in *IsPETase* [19]. This amino acid W185 is located near the catalytic center and can adopt three different conformations, which is why it is also referred as a wobbling tryptophan [19, 23]. In a proposed substrate binding, W185 forms  $\pi$ - $\pi$ -stacking

interactions with the phenylene units of PET, allowing interactions with the substrate and facilitating binding [19, 23]. The wobbling of W185 in *IsPETase* is based on a serine at position 214 and an isoleucine at 218, which allow the tryptophan to rotate [28]. In homologous enzymes, these serine and isoleucine residues are replaced by histidine or phenylalanine, respectively, restricting the movement of the tryptophan and thus lowering the activity for PET degradation [28].

Unlike LCC or TfCut2 from *T. fusca*, *IsPETase* is a mesophilic enzyme with a melting point ( $T_m$ ) of approximately 45°C, and it is thus thermally unstable for applications at higher temperatures [16, 29, 30]. The crystallinity of PET influences the efficiency of enzymatic PET degradation [16, 31]. The presence of highly ordered crystalline content in a specific PET sample reduces the overall mobility of the polymer chains and their accessibility to enzymatic hydrolysis [29, 32]. In comparison, the less-ordered amorphous fraction is significantly more susceptible to enzymatic attack at a reaction temperature close to the glass transition temperature ( $T_g$ ) of PET [29]. Because enzymatic PET hydrolysis is carried out in aqueous environments, the  $T_g$  of PET is notably reduced to below 60°C due to the plasticization effect of water [33, 34]. As a result, increasing the thermal stability of a desired PET hydrolase for use at temperatures above 60°C has proven to be useful for making better PET-degrading enzymes [26].

In order to achieve effective PET degradation by *IsPETase*, the activity and thermostability of the enzyme has been improved by protein engineering in previous studies [19, 20, 22–24]. For instance, an improvement of *IsPETase* activity was achieved by the R280A substitution [20]. Docking studies showed that the polar arginine residue in the binding pocket of *IsPETase* hinders stable binding of PET, therefore the substitution of the arginine residue by small hydrophobic amino acid residues leads to increased activity [20]. Son et al. generated an *IsPETase* triple mutant (TM = *IsPETase*<sup>S121E/D186H/R280A</sup>) by combining the R280A mutation with the  $\beta$ 6- $\beta$ 7-connecting loop-stabilizing mutations S121E and D186H. The resulting triple mutant exhibited a 14-fold improved PET hydrolysis activity and its  $T_m$  was increased by 8.81°C [21]. The addition of another disulfide bridge to this triple mutant via N233C and S282C substitutions resulted in a  $T_m$  of 69.4°C and a further 5 to 7-fold increase in activity [35]. The equivalent disulfide bond has been shown to have similar thermostabilizing and activating effects with the homologous PET hydrolyzing enzymes LCC [17] and TfCut2 [36]. Cui et al. used a computer-assisted strategy called GRAPE (greedy accumulated strategy for protein engineering) to create another *IsPETase* variant [37]. This variant (*IsPETase*<sup>L117F/Q119Y/T140D/W159H/G165A/I168R/A180I/S188Q/S214H/</sup>

R280A) was named *DuraPETase* because its  $T_m$  was increased by 31°C and it had increased degradation activity against highly crystalline PET film [37].

In this study, we used error-prone PCR to generate a mutant library based on the triple mutant of *IsPETase* [21]. The library was screened for thermostable *IsPETase* variants against the commercially available polyester-polyurethane Impranil DLN W 50. Selected variants were then combined with other previously published promising *IsPETase* mutants (Table 1) and investigated in terms of thermostability and hydrolytic activity against PET nanoparticles and amorphous PET films.

## 2 | MATERIALS AND METHODS

Chemicals and consumables were purchased from Sigma Aldrich (Steinheim, Germany), Carl Roth (Karlsruhe, Germany), Fermentas (St. Leon-Rot, Germany), Fluka (Buchs, Switzerland), Thermo Fisher Scientific (Waltham, MA, USA), Merck KGaA (Darmstadt, Germany), ChiroBlock GmbH (Wolfen, Germany) and New England Biolabs GmbH (Frankfurt am Main, Germany). Oligonucleotide primers (Table S1) were ordered from Thermo Fisher Scientific (Waltham, MA, USA). The polyester-polyurethane emulsion Impranil DLN W 50 was a kind gift provided by CSC JÄKLECHEMIE GmbH & Co. (Hamburg, Germany).

### 2.1 | Generation of *IsPETase* variants

Synthetic genes, codon optimized for expression in *Escherichia coli*, encoding the wild-type *IsPETase* from *I. sakaiensis*, *DuraPETase*, and *DuraPETase*<sup>K95N/S121E/D186H/F201I</sup>, were synthesized and cloned into the pET-21b vector by BioCat GmbH (Heidelberg, Germany). The constructs encoded the recombinant proteins as fusions to C-terminal His<sub>6</sub>-tags for affinity purification, for purification method see Supporting Information. The TM was generated based on the wild-type gene using the Q5 Site-Directed Mutagenesis Kit (New England Biolabs GmbH, Frankfurt am Main, Germany). For the generation of the mutant library based on the triple mutant, the GeneMorph II Random Mutagenesis Kit (Agilent Technologies Inc., Santa Clara, CA, USA) was used. The error-prone PCR amplicon was cleaned up using the NucleoSpin Gel and PCR Clean-up kit (MACHEREY-NAGEL GmbH & Co. KG, Düren, Germany) and used as a MegaPrimer for MEGAWHOP cloning [38] using *Pfu*Plus! DNA Polymerase (EURx, Gdansk, Poland). To remove the template plasmid from

**TABLE 1** Overview of previously published promising *IsPETase* variants which have served as templates for this study

<i>IsPETase</i> variant	Amino acid substitutions	References
<i>IsPETase</i> TM	<i>IsPETase</i> <sup>S121E/D186H/R280A</sup>	[21]
<i>IsPETase</i> TM <sup>N233C/S282C</sup>	<i>IsPETase</i> <sup>S121E/D186H/N233C/R280A/S282C</sup>	[35]
<i>DuraPETase</i>	<i>IsPETase</i> <sup>L117F/Q119Y/T140D/W159H/G165A/I168R/A180I/S188Q/S214H/R280A</sup>	[37]

the library, the MEGAWHOP PCR product was digested with DpnI (New England Biolabs GmbH, Frankfurt am Main, Germany). The library was transformed into electrocompetent *E. coli* TOP10 (Thermo Fisher Scientific, Waltham, MA, USA) and 0.1% of it was sequenced to investigate the mutation spectrum. Sanger Sequencing was performed using Mix2Seq Kits from Eurofins Genomics Germany GmbH (Ebersberg, Germany). Substitutions of K95N/F201I and/or N233C/S282C in wild-type *IsPETase*, *DuraPETase*, and *DuraPETase*<sup>K95N/S121E/F201/R280A</sup> were introduced by QuikChange using *Pfu*Plus! DNA Polymerase, followed by DpnI digestion and transformation into chemically competent *E. coli* TOP10. The expression of active *IsPETase* variants is described in the Supporting Information.

## 2.2 | Screening based on Impranil agar plates

Impranil DLN W 50 agar plates were used for the screening of the *IsPETase*TM mutant library. The lysogeny broth (LB) agar plates contained 0.5 mM isopropyl- $\beta$ -D-thiogalactopyranoside (IPTG), 100  $\mu$ g mL<sup>-1</sup> ampicillin, and 0.5% Impranil DLN W 50, diluted from a 40% suspension. The mutant library was used to transform chemically competent *E. coli* SHuffle T7 Express (New England Biolabs GmbH, Frankfurt am Main, Germany) cells which were then spread onto LB agar plates containing 100  $\mu$ g mL<sup>-1</sup> ampicillin. After the cells were incubated overnight at 30°C, colonies were picked and transferred to another LB-ampicillin agar plate (storage plate) and in parallel to the Impranil agar plate (assay plate). The storage and assay plates were first incubated overnight at 30°C, the assay plates were subsequently incubated at 60°C for 24 h. Degradation of Impranil leads to formation of clear zones around colonies expressing active *IsPETase* variants. An increased size of the haloes formed, relative to the TM as control, was used as a preliminary indication of increased thermostability. Selected colonies were picked from the storage plate and used to inoculate an overnight culture for plasmid isolation using the innuPREP Plasmid Mini Kit (Analytik Jena GmbH, Jena, Germany). Increased thermostability was then experimentally verified by pro-

tein expression, purification and nanoDSF, as described below.

## 2.3 | Determination of protein concentration

Protein concentrations were determined using the Pierce BCA Protein Assay Kit (Thermo Fisher Scientific, Waltham, MA, USA).

## 2.4 | Measurement of melting points

Determination of the  $T_m$  for each *IsPETase* variant was performed by nanoDSF using the Prometheus NT.48 (NanoTemper Technologies, Munich, Germany). The measurement was performed in 50 mM sodium phosphate (pH 7.5) using a protein concentration of 0.5 mg mL<sup>-1</sup>. Temperature was scanned at 1°C per minute between 20°C and 95°C. The instrument has a fixed excitation wavelength of 285 nm in combination with emission wavelengths of 330 and 350 nm.

## 2.5 | Degradation of PET nanoparticles and PET film

PET nanoparticles were prepared based on previous publications [39, 40]. The degradation of PET nanoparticles (0.2 mg mL<sup>-1</sup>) was performed with an *IsPETase* concentration of 30 nM in 200  $\mu$ L of 50 mM sodium phosphate buffer (pH 7.5). Enzymatic hydrolysis was performed at different incubation temperatures ranging from 30°C to 60°C and a constant agitation of 1000 rpm for 24 h. For the biocatalysis with amorphous PET film (Goodfellow GmbH, Bad Nauheim, Germany), the film was cut into 1  $\times$  2 cm<sup>2</sup> pieces (~60 mg) and washed with a solution containing sodium dodecyl sulfate (SDS), distilled water, and ethanol. The PET film was then dried at 50°C for 24 h. The degradation of PET film was performed in 50 mM glycine-NaOH buffer (pH 9.0) with an *IsPETase* concentration of 50 nM in a reaction volume of 1.5 mL at 60°C and constant agitation of 1000 rpm for 72 h. To quench the reaction, PET nanoparticles were first removed by centrifugation at 17,000  $\times$  g

for 10 min at 4°C. Next, 100  $\mu$ L of the supernatant was added to an equal volume of 200 mM sodium phosphate (pH 2.5) containing 20% v/v dimethyl sulfoxide (DMSO). This mixture was then incubated at 95°C for 10 min. To quench the reaction with amorphous PET film, the PET film was removed. Then, the same quenching protocol as for PET nanoparticles, without the centrifugation step, was performed. Samples were stored at -20°C until measurement by high-performance liquid chromatography with the Hitachi LaChrom Elite HPLC System (Hitachi, Chiyoda, Japan). Analysis of MHET, BHET, and TA by HPLC was performed according to Palm et al. [25]. Briefly, PET degradation products were analyzed on a Kinetex 5  $\mu$ m EVO C18 100 Å, 150  $\times$  4.6 mm column (Phenomenex, Aschaffenburg, Germany) with a gradient of acetonitrile and 0.1% v/v formic acid in water at 30°C. Ten microliters of sample was injected and the flow rate was 0.8 mL min<sup>-1</sup>. Acetonitrile was increased from 5% to 44% over 12 min and then to 70% over 15 min, after which the ratio remained constant at 70% acetonitrile for 3 min. MHET, BHET, and TA were detected at 240 nm, and quantification was performed based on calibration curves.

### 3 | RESULTS

#### 3.1 | Screening for thermostable *IsPETase* variants

Approximately 49,000 clones were screened on Impranil agar plates, accounting for approximately ~52% of the error-prone PCR-based mutant library with ~95,000 clones. *IsPETase* activity was assessed by observing the halo formation around the bacterial colony. At higher incubation temperatures ( $\geq 60^\circ\text{C}$ ), the size of the clear zones was thought to be dependent on the thermostability of the recombinant variants. Four colonies with significantly increased halo sizes, compared to that of the TM, were selected for further experiments. These were TM<sup>K95N/F201I</sup>, TM<sup>S125N/A226T</sup>, TM<sup>Q119L</sup> and TM<sup>T51A/S125I/S207I</sup> (Figure S1). Based on structural analysis of *IsPETase* (Figure S2), six substitutions were present on the surface of the TM. In contrast, the F201I mutation was located deeply inside the enzyme. After expression and purification (Figure S3), the  $T_m$  of these four variants as well as the wild-type *IsPETase* (WT) and TM were determined by nanoDSF (Figure 1A). For WT and TM,  $T_m$  of 45.1°C and 56.6°C, respectively, were measured. Most of the variants displayed an improvement in  $T_m$  of approximately 2°C compared to TM (Table S2). The most thermostable variant was *IsPETase*TM<sup>K95N/F201I</sup> (TM1) with an increased  $T_m$  of 61.7°C which is 5.3°C higher than that of *IsPETase*TM.

#### 3.2 | Engineering of more thermostable *IsPETase* variants

With the aim of generating further more thermostable variants, the most promising stabilizing K95N and F201I substitutions were incorporated into previously published *IsPETase* variants including *IsPETase*TM<sup>N233C/S282C</sup> (TM2) and *DuraPETase* (D). For *DuraPETase* variants, the S121E and R280A substitutions were also investigated simultaneously, since these substitutions in combination with the K95N and F201I substitution led to the high  $T_m$  in the discovered TM1 variant. At the same time the influence of the N233C and S282C substitutions, which were previously described by Zhong-Johnson et al. [35] exclusively for the *IsPETase*TM, were also investigated with *DuraPETase*. After expression and purification, the  $T_m$  was determined via nanoDSF for selected *IsPETase* variants (Figure 1B). An increase in  $T_m$  of 2.6°C from 68.2°C to 70.9°C was observed for the *IsPETase*TM<sup>K95N/F201I/N233C/S282C</sup> (TM3) variant (Table 2). Introduction of the substitutions K95N, S121E, R280A and F201I led to a decrease of the  $T_m$  by 3°C from 75.0°C to 71.9°C in *DuraPETase*<sup>K95N/S121E/F201I/R280A</sup> (D2). In comparison, by introducing the double cysteine residues, the  $T_m$  of *DuraPETase* variants were further increased, to 81.1°C for *DuraPETase*<sup>N233C/S282C</sup> (D1) and 78.4°C for *DuraPETase*<sup>K95N/S121E/F201I/N233C/R280A/S282C</sup> (D3). Consequently,  $T_m$  has been increased by 36.1°C from 45.1°C to 81.1°C for D1 compared to the WT by incorporating the previously reported N233C and S282C substitutions.

#### 3.3 | Influence of substitutions on PET nanoparticle and amorphous PET film hydrolysis

The hydrolysis of PET nanoparticles with aforementioned *IsPETase* variants was investigated at different temperatures ranging from 30°C to 60°C for 24 h. With increasing temperature, an increased degradation rate of PET nanoparticles in terms of higher product release could be observed for each variant (Figure 2). A notably improved performance in PET hydrolysis was observed with all variants when the incubation temperature was increased from 30°C to 40°C. Even the WT showed increased activity at higher temperatures, although the  $T_m$  is only 45°C (Table 2) and the overall yield of degradation products was markedly lower than with the other variants. Comparing the TM related variants, it can be observed that the introduction of the K95N and F201I substitution into the existing TM2 variant as well as into the TM resulted in a decrease in total product release, defined

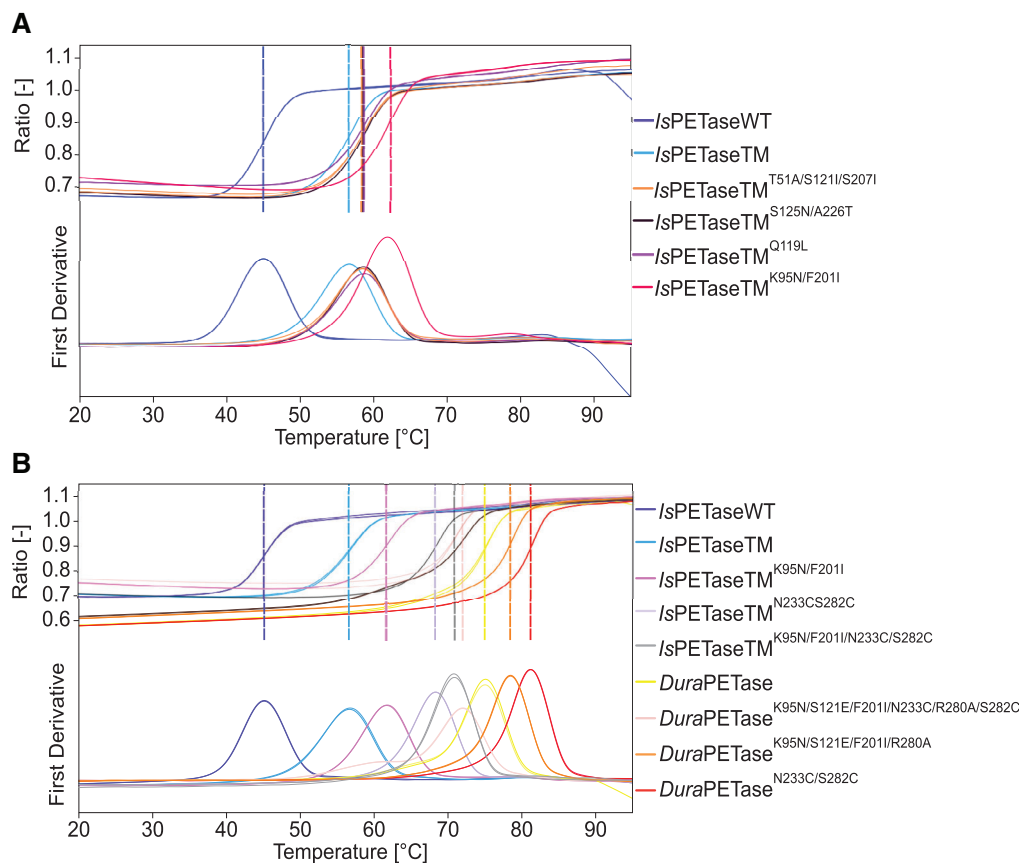


**FIGURE 1** Melting point determination of selected *IsPETase* variants by nanoDSF. (A) Discovered *IsPETase* variants from the screening and (B) constructed *IsPETase* variants by combining different mutations with previously published amino acid substitutions (B). The  $T_m$  can be determined from the position of the curve maximum. The measurement was performed in 50 mM sodium phosphate buffer (pH 7.5) with purified enzymes ( $0.5 \text{ mg mL}^{-1}$ ). The measurements were performed in duplicates

**TABLE 2** Melting points of selected *IsPETase* variants, which were generated by combining the K96N/F201I substitutions with other previously described *IsPETase* mutants

<i>IsPETase</i> variant		Melting point $\pm$ SD [ $^{\circ}\text{C}$ ]	$T_m$ [ $^{\circ}\text{C}$ ] increase compared to	
			<i>IsPETase</i> WT	<i>IsPETase</i> TM
WT	<i>IsPETase</i> WT	$45.1 \pm 0.1$	–	–
TM	<i>IsPETase</i> TM	$56.6 \pm 1.6$	11.5	–
TM1	<i>IsPETase</i> TM <sup>K95N/F201I</sup>	$61.6 \pm 0.1$	16.6	5.1
TM2	<i>IsPETase</i> TM <sup>N233C/S282C</sup>	$68.2 \pm 0.1$	23.2	11.6
TM3	<i>IsPETase</i> TM <sup>K95N/F201I/N233C/S282C</sup>	$70.8 \pm 0.1$	25.8	14.3
D	<i>DuraPETase</i>	$75.0 \pm 0.1$	29.9	18.4
D1	<i>DuraPETase</i> <sup>N233C/S282C</sup>	$81.1 \pm 0.1$	36.1	24.6
D2	<i>DuraPETase</i> <sup>K95N/S121E/F201I/R280A</sup>	$71.9 \pm 0.1$	26.9	15.3
D3	<i>DuraPETase</i> <sup>K95N/S121E/F201I/N233C/R280A/S282C</sup>	$78.4 \pm 0.1$	33.3	21.8

Data were determined by nanoDSF with purified enzymes ( $0.5 \text{ mg mL}^{-1}$ ) in 50 mM sodium phosphate buffer (pH 7.5). The measurements were performed in duplicates. The mean values and the standard deviations (SD) are given.

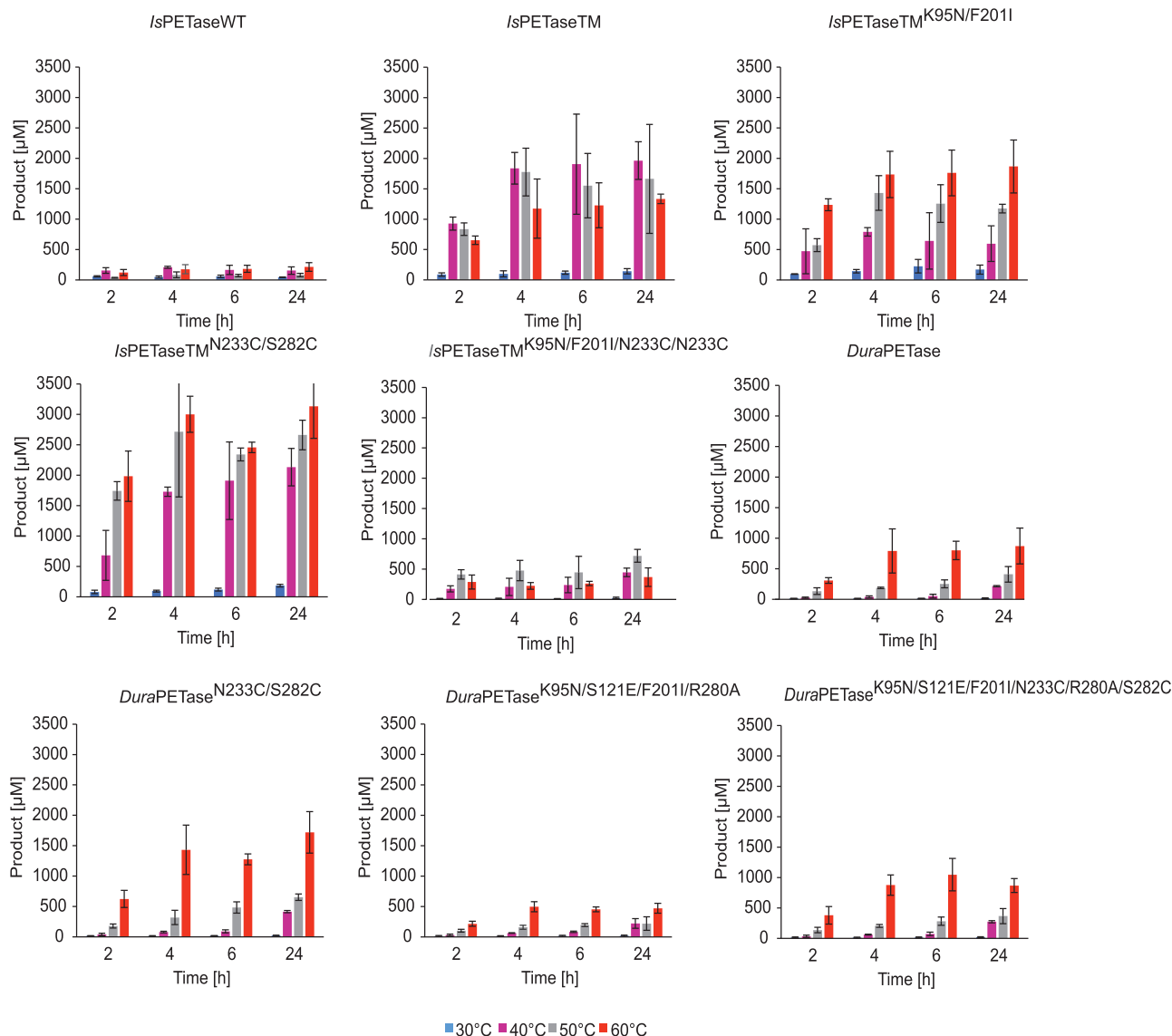


**FIGURE 2** Time course of total product release at different incubation temperatures. The total product released refers to the sum of released MHET, TA, and BHET. Biocatalysis with PET nanoparticles was performed with 30 nM *IsPETase* variant in 50 mM sodium phosphate buffer (pH 7.5) at the respective incubation temperatures and a constant agitation of 1000 rpm for 24 h. A final PET nanoparticle concentration of 0.2 mg mL<sup>-1</sup> was used. The measurements were performed in triplicates and the mean values and standard deviations are given

as the sum of released MHET, TA, and BHET, for PET nanoparticle hydrolysis (Figure 3). The relative activity compared to the TM decreased by approximately 70% for TM1 when incubated at 40°C (Table S3). Whereas at 50°C a reduction in the relative activity of only 30% was observed. However, it was also shown that at 60°C, more product was released from the TM1 variant compared to the TM. Comparable relative activities were observed at 60°C for TM and TM1. At this incubation temperature, an 8-fold enhancement was observed for TM1 in relative activity compared with wild-type *IsPETase* (Figure 3) making TM1 possessing the second largest increase after TM2. Most product formation was observed at 60°C with the TM2 variant (Figure 3). For the combination

of K95N/F201I and N233C/S282C substitutions (TM4), a strongly reduced relative activity (-70%) compared to TM at 60°C (Table S3) and a low level of total product release were observed. The K95N/S121E/F201I/R280A substitutions in the *DuraPETase* (D2) also resulted in a reduced product release during the hydrolysis of PET nanoparticles compared to other *DuraPETase* variants at 60°C. However, the degradation of PET nanoparticles was improved with the *DuraPETase* variants containing the N233C/S282C mutations. A two-fold increase in relative activity was observed as a result of this substitution for D1 at both 50°C and 60°C (Figure 3). In particular, for the *DuraPETase* variants, increased degradation of PET was shown at 60°C compared to the other incubation temperatures (Figure 2).

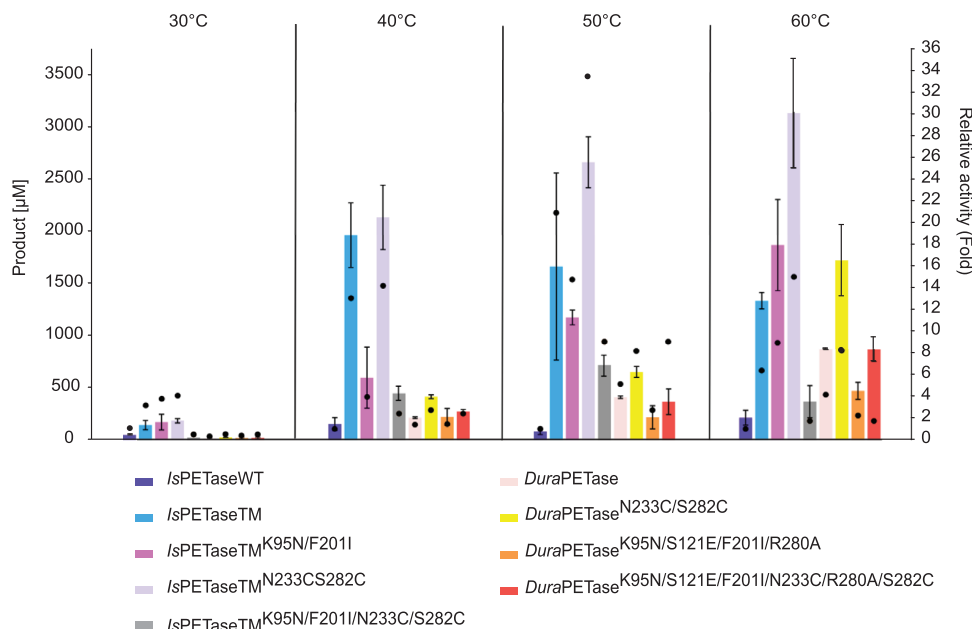


**FIGURE 3** Total product release after degradation of PET nanoparticles using selected *IsPETase* variants after 24 h and an incubation temperature of 60°C. Black dots represent the relative activity compared to wild-type *IsPETase*. Biocatalysis with PET nanoparticles was performed with 30 nM *IsPETase* variant in 50 mM sodium phosphate buffer (pH 7.5) at the incubation temperature of 60°C and a constant agitation of 1000 rpm for 24 h. A final PET nanoparticle concentration of 0.2 mg mL<sup>-1</sup> was used. The total product released refers to the sum of released MHET, TA, and BHET. The measurements were performed in triplicates and the mean values and standard deviations are given

The main product formed during the hydrolysis of PET nanoparticles was MHET (Figure S4). TA and very low BHET concentrations were also detected.

The degradation of amorphous PET film was carried out at an incubation temperature of 60°C for 72 h. Under these conditions, almost no product formation was observed for WT. Except for D2, almost all thermostable variants led to higher total product concentration when compared to unstable variants like TM (Figure 4). In addition, higher relative activities than TM were observed for all variants except for WT and D2 (Table S4). Surprisingly, compared to the degradation performance obtained with PET nanoparticles, the combination variant (TM3) exhibited one of the highest relative activities compared to WT (120-fold increase, Figure 4) and TM (10 to 20-fold increase, Table S4). The highest total product was yielded with D1 and the TM3 variant. However, unlike the hydrolysis of PET nanoparticles, the main product this time was TA rather than MHET (Figure 5).

## 4 | DISCUSSION

Screening methods based on agar plate assays containing PET or polycaprolactone nanoparticles have been developed to identify polyesterses from metagenomic libraries [41]. However, these nanoparticles can precipitate during agar plate preparation, interfering with uniform distribu-

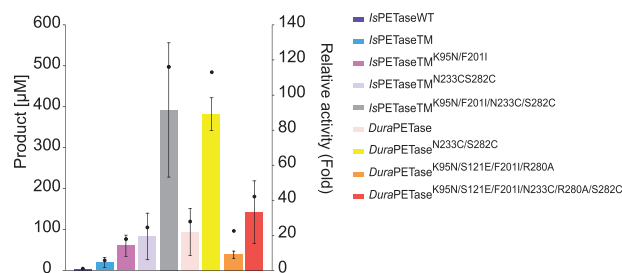


**FIGURE 4** Total product release after degradation of amorphous PET film for selected *IsPETase* variants after 72 h at an incubation temperature of 60°C. Black dots represent the relative activity compared to wild-type *IsPETase*. For biocatalysis with amorphous PET film, an enzyme concentration of 50 nM was used. The reaction was carried out in 50 mM glycine-NaOH buffer (pH 9.0). The PET film was incubated at 60°C and a constant agitation of 1000 rpm for 3 days. The total product released refers to the sum of released MHET, TA, and BHET. The measurements were performed in triplicates and the mean values and standard deviations are given

tion in the agar. Therefore, a suspension of the aliphatic polyester-polyurethane Impranil DLN W 50 can be applied instead [41]. The formation of clear zones on the agar plate around bacterial colonies indicates the functional expression of catalytically active polyester hydrolases.

All *IsPETase* variants discovered here with the Impranil agar plate screening showed an increased  $T_m$  compared the



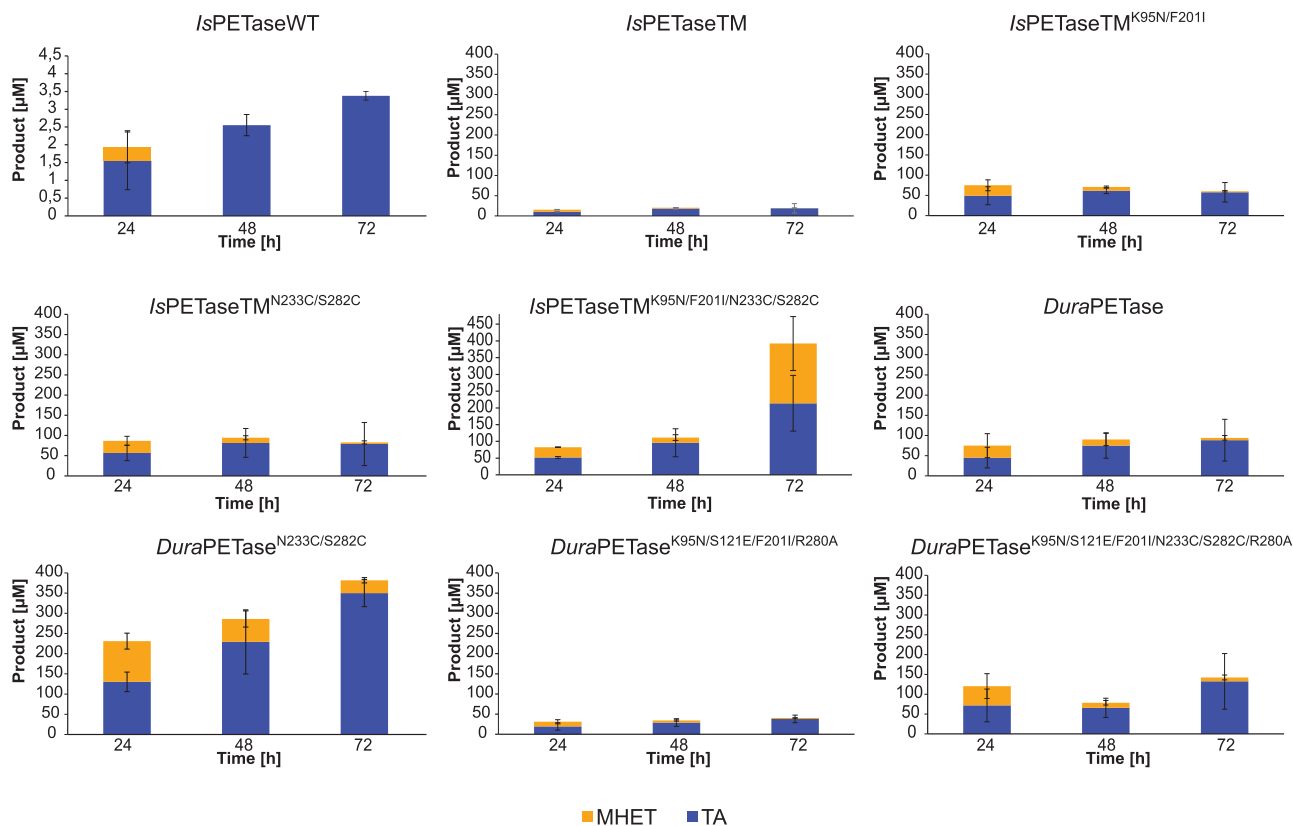


**FIGURE 5** Comparison of degradation products for amorphous PET film hydrolysis catalyzed by selected *IsPETase* variants over the time course of 72 h at an incubation temperature of 60°C. Biocatalysis with amorphous PET film was performed with 50 nM of each *IsPETase* variant in glycine-NaOH buffer (pH 9.0). The PET film was incubated at 60°C with constant agitation at 1000 rpm for 3 days. The measurement was performed in triplicates and the mean values and standard deviations are given

wild-type enzyme, thereby validating the criterium based on halo size. An improvement of 16.9°C compared to the wild-type was observed for the *IsPETase*TM<sup>K95N/F201I</sup> variant. Thermostability strongly depends on the flexibility of the protein. A variety of interactions, such as ionic interactions, disulfide bonds, hydrogen bonds, and hydrophobic interactions, affect the flexibility and thus the thermostability of the protein [42]. An increase in stability can be mediated either by stabilization of the folded form or by destabilization of the unfolded form [43]. The substitution of an amino acid must thereby affect the folded and unfolded forms differently [43]. Finding an explanation for increased thermostability is therefore usually very difficult.

For the WT and the TM,  $T_m$  of 45.1°C and 56.6°C, respectively, could be measured by nanoDSF. The  $T_m$  determined with nanoDSF have small deviations in the range of about 2°C compared to the reported  $T_m$  for WT, TM, TM2 and D. For instance, in this work a  $T_m$  increase of 29.9°C was observed for the *DuraPETase*, whereas in the publication by Cui et al. [37] an increase of 31°C was mentioned. As summarized in Table S5, the methods and exact equipment

used for the  $T_m$  measurement in different studies may be responsible for these small discrepancies.

The combination of the S125N and A226T substitutions showed an increase in thermostability in this study. However, the computationally predicted single mutations S125R and A226P for WT did not cause an increase or even a decrease in  $T_m$  as reported by Cui et al. [37]. The impact of a substitution is highly dependent on the type and number of mutations already present in an enzyme [44]. This could also be the reason for the lack of an increase and the decrease in  $T_m$  observed for the *DuraPETase* variants, which already contain the K95N/S121E/F201I and R280A substitutions. The K95 position was already evaluated in the publication reporting *DuraPETase*, where a K95A mutation only led to an increase of 2.5°C in  $T_m$  for the WT [37]. The K95N substitution could have the same influence on the thermostability as the K95A substitution, additional increase in thermostability would possibly result from the F201I substitution.

The introduction of additional disulfide bridges into an enzyme is one possible strategy to increase thermostability [43]. The main goal of these cross-links is to reduce

the flexibility of certain thermolabile folds [43]. Crosslinking results in a reduced entropic state during the unfolding process, shifting the equilibrium toward the folded form [43]. The selection of the correct positions for amino acid substitution is crucial, the substitution should have no effect on the catalytic properties of the enzyme. For the identification of suitable positions for disulfide bridges in PET degrading enzymes, the structures of homologous cutinases can be helpful [17, 45]. For Cut190 from *Saccharomonospora viridis*, which is homologous to *IsPETase* [35], the  $T_m$  could be increased by more than 20°C through replacing calcium-binding sites with disulfide bridges [45]. This led, for instance, to the discovery of the N233C and S282C substitutions in *IsPETase* [35]. However, since no crystal structure was described for the *IsPETase*<sup>N233C/S282C</sup> variant, it can only be speculated on the formation of the disulfide bridge in the *IsPETase* variants. In this study the insertion of the N233C and S282C substitutions into the *DuraPETase* also led to an increase in  $T_m$  of approximately 6.1°C. This D1 variant revealed indeed the highest  $T_m$  of 81.1°C among the so far described *IsPETase* variants.

At higher incubation temperatures, a higher product release was observed in most cases for the thermostabilized *IsPETase* variants. As the flexibility of the amorphous polymer chains will significantly increase at temperatures close to the  $T_g$  of PET, better enzymatic degradation performance can be expected [16, 29]. Increased thermostability is therefore advantageous for the *IsPETase*-catalyzed degradation of PET. A good example in this study is the comparison of the TM and TM1 variants. In the degradation of PET nanoparticles, the TM variant showed a higher total product formation at 40°C than TM1. This variant also possessed only a relative activity of 30.4% compared to TM at this incubation temperature. Only when the degradation was carried out at 60°C, a similar relative activity was observed between TM and TM1 (Table S3). The influence on PET degradation due to increased thermostability is better observed for the TM1 variant when degrading amorphous PET film. There, this variant showed an approximately two-fold increase in relative activity compared to TM (Table S4). Since TM only has a  $T_m$  of 56.5°C, it is highly probable that this variant is inactivated much faster over the period of 72 h than TM1 and therefore less product was released (Figure 4).

For variants containing the K95N and F201I substitutions, low activities for hydrolysis of PET nanoparticles were observed. The amino acid F201 is located in a deeply hidden hydrophobic core of *IsPETase*, which additionally consists of positions W97, L101, M157, L199, L230, W257 and M258 [37]. Potentially, the F201I substitution has a structural influence on the active site, since D206 is located only five amino acid residues away from this substitution. By contrast, the high thermostability of TM4 ( $T_m = 70.8^\circ\text{C}$ ) in

combination with the prolonged incubation time of 72 h may be responsible for the increased product release in the degradation of amorphous PET film. Only the D1 variant with the  $T_m$  of 81.1°C possessed a similar relative activity to TM4. Both variants support the principle that an increased  $T_m$  brings a substantial advantage for the degradation of PET.

MHET was formed as the main product of PET nanoparticle hydrolysis. This is consistent with the observations by Yoshida et al. who also showed that MHET was the major product for *IsPETase*-catalyzed hydrolysis of PET [18]. According to Yoshida et al., degradation of MHET by *IsPETase* should not be possible [18]. However, in the degradation of amorphous PET film, TA is the main product, since MHET is degraded by *IsPETase* with extended incubation time. The same reaction has already been described elsewhere [46]. A prolonged incubation of the PET at high temperatures can lead to a slow transformation of mobile amorphous fractions to rigid amorphous fractions, which are less degradable by the enzyme [16]. This process is called physical aging and can therefore be considered as a competitive reaction to the enzymatic degradation of the amorphous PET [16]. Since an amorphous PET film has much less accessible surface area and much longer polymer chains compared to the PET nanoparticles [47], *IsPETase* and its variants, which cannot take part in the effective degradation of the polymers, will be more likely to degrade the MHET. This effect is further enhanced by the prolonged incubation time of 72 h. Only very low concentrations of BHET were observed for each variant in biocatalysis (Figure S4). It is known that *IsPETase* can catalyze the hydrolysis of BHET to TA and EG [18].

Several more thermostable *IsPETase* variants were discovered in this study. Higher thermostability could also be achieved by combination of four stabilizing substitutions with already promising published variants. For the effective degradation of PET by enzymes, the right balance between hydrolytic activity and thermostability is essential. As demonstrated with *IsPETase* variants containing the K95N and F201I substitutions, even a slightly negative influence of a mutation on the activity of PET hydrolysis can be compensated by the simultaneous increase of  $T_m$  for degradation reaction at higher incubation temperatures. This led to an improved effectiveness in PET degradation by these *IsPETase* variants. An increase in thermostability is possibly accompanied by an increase in rigidity [42] which may cause an activity reduction [48]. Specifically, for PET degradation, the enzymatic activity loss may be compensated by the increased polymer substrate accessibility at higher temperatures. Nonetheless, thermostabilized *IsPETase* variants without significant loss of hydrolytic activity will be of greater interest. The same approach of combining substitutions that increase

thermostability without significantly affecting PET hydrolysis activity with mutations that increase activity has been also recently verified by Tournier et al. with LCC to be useful for engineering efficient PET hydrolases.

## ACKNOWLEDGMENTS

C.P.S.B., R.W., and U.T.B. acknowledge funding from the European Union's Horizon 2020 research and innovation programme under grant agreement no. 870294 for the project MIX-UP.

Open access funding enabled and organized by Projekt DEAL.

## CONFLICT OF INTEREST

The authors declare no conflict of interest. No experiments involving animals or humans were performed in the context of this study.


## DATA AVAILABILITY STATEMENT

Data available on request from the authors.

## ORCID

Stefan Brott  <https://orcid.org/0000-0003-2346-7706>


Lara Pfaff  <https://orcid.org/0000-0002-1529-8917>

Jan-Niklas Schwarz  <https://orcid.org/0000-0001-6319-0647>

Dominique Böttcher  <https://orcid.org/0000-0001-9981-014X>

Christoffel P. S. Badenhorst  <https://orcid.org/0000-0002-5874-4577>

Ren Wei  <https://orcid.org/0000-0003-3876-1350>

Uwe T. Bornscheuer  <https://orcid.org/0000-0003-0685-2696>

## REFERENCES

- Barnes, D. K. A., Galgani, F., Thompson, R. C. and Barlaz, M., *Philos. Trans. R. Soc. B., Biol. Sci.* 2009;364:1985–1998.
- PlasticEurope-Association of Plastics Manufactures (2020) Plastic- The facts. Plastic Europe. <https://plasticseurope.org/knowledge-hub/plastics-the-facts-2020/>. Accessed 10 Aug 2021.
- Wei, R. and Zimmermann, W., *Microb. Biotechnol.* 2017;10:1302–1307.
- Sinha, V., Patel, M. R. and Patel, J. V., *J. Polym. Environ.* 2010;18:8–25.
- Bornscheuer, U. T., *Science.* 2016;351:1154–1155.
- Andrady, A. L. and Neal, M. A., *Philos. Trans. R. Soc. B Biol. Sci.* 2009, 364, 1977–1984.
- Wei, R., Tiso, T., Bertling, J., O'connor, K., et al. *Nat. Catal.* 2020;3:867–871.
- Webb, H., Arnott, J., Crawford, R. and Ivanova, E., *Polymers.* 2013;5:1–18.
- Wei, R. and Zimmermann, W., *Microb. Biotechnol.* 2017;10:1308–1322.
- Taniguchi, I., Yoshida, S., Hiraga, K., Miyamoto, K., et al. *ACS Catal.* 2019;9:4089–4105.
- Oeser, T., Wei, R., Baumgarten, T., Billig, S., et al. *J. Biotechnol.* 2010;146:100–104.
- Eberl, A., Heumann, S., Brückner, T., Araujo, R., et al. *J. Biotechnol.* 2009, 143, 207–212.
- Sulaiman, S., Yamato, S., Kanaya, E., Kim, J. - J., et al. *Appl. Environ. Microbiol.* 2012;78:1556–1562.
- Herrero Acero, E., Ribitsch, D., Steinkellner, G., Gruber, K., et al. *Macromolecules* 2011, 44, 4632–4640.
- Chen, S., Tong, X., Woodard, R. W., Du, G., et al. *J. Biol. Chem.* 2008;283:25854–25862.
- Wei, R., Breite, D., Song, C., Gräsing, D., et al. *Adv. Sci.* 2019;6:1900491.
- Tournier, V., Topham, C. M., Gilles, A., David, B., et al. *Nature* 2020;580:216–219.
- Yoshida, S., Hiraga, K., Takehana, T., Taniguchi, I., et al. *Science* 2016;351:1196–1199.
- Han, Xu, Liu, W., Huang, J. - W., Ma, J., et al. *Nat. Commun.* 2017;8:2106.
- Joo, S., Cho, I. J., Seo, H., Son, H. F., et al. *Nat. Commun.* 2018;9:382.
- Son, H. F., Cho, I. J., Joo, S., Seo, H., et al. *ACS Catal.* 2019;9:3519–3526.
- Austin, H. P., Allen, M. D., Donohoe, B. S., Rorrer, N. A., et al. *Proc. Natl. Acad. Sci. U. S. A.* 2018;115:E4350–E4357.
- Chen, C. - C., Han, Xu, Ko, T. - P., Liu, W., et al. *Guo, R. - T., FEBS J.* 2018;285:3717–3723.
- Liu, B., He, L., Wang, L., Li, T., et al. *ChemBioChem* 2018;19:1471–1475.
- Palm, G. J., Reisky, L., Böttcher, D., Müller, H., et al. *Nat. Commun.* 2019;10:1717.
- Kawai, F., Kawabata, T. and Oda, M., *ACS Sustain. Chem. Eng.* 2020;8:8894–8908.
- Fecker, T., Galaz-Davison, P., Engelberger, F., Narui, Y., et al. *Biophys. J.* 2018;114:1302–1312.
- Chen, C. - C., Han, X., Li, X., Jiang, P., et al. *Nat. Catal.* 2021;4:425–430.
- Wei, R., Song, C., Gräsing, D., Schneider, T., et al. *Nat. Commun.* 2019;10:5581.
- Kawai, F., Kawabata, T. and Oda, M., *Appl. Microbiol. Biotechnol.* 2019;103:4253–4268.
- Ronkvist, Å. M., Xie, W., Lu, W. and Gross, R. A., *Macromolecules* 2009;42:5128–5138.
- Falkenstein, P., Gräsing, D., Bielytskyi, P., Zimmermann, W., et al. *Front. Microbiol.* 2020;11:689.
- Bianchi, R., Chiavacci, P., Vosa, R. and Guerra, G., *J. Appl Polym. Sci.* 1991;43:1087–1089.
- Langevin, D., Grenet, J. and Saiter, J. M., *Eur. Polym. J.* 1994;30:339–345.
- Zhong-Johnson, E. Z. L., Voigt, C. A. and Sinskey, A. J., *Sci. Rep.* 2021;11:928.
- Then, J., Wei, R., Oeser, T., Gerdt, A., et al. *FEBS Open Bio* 2016;6:425–432.
- Cui, Y., Chen, Y., Liu, X., Dong, S., et al. *ACS Catal.* 2021;11:1340–1350.
- Miyazaki, K. and Cloning, M., in: Voigt, C. (Ed.), *Methods Enzymol*, Elsevier Inc., 2011;498:399–406.
- Vogel, K., Wei, R., Pfaff, L., Breite, D., et al. *Sci. Total Environ.* 2021;773:145111.
- Pfaff, L., Breite, D., Badenhorst, C. P. S., Bornscheuer, U. T., et al., in: Weber, G., Bornscheuer, U. T., Wei, R. (Ed.), *Methods Enzy-*

- mol. Enzymatic Plastic Degradation, Elsevier, 2021;648:253–270.
41. Molitor, R., Bollinger, A., Kubicki, S., Loeschcke, A., et al. Microb. Biotechnol. 2019;13:274–284.
  42. Bornscheuer, U. T., Kourist, R. and Höhne, M., Chemie Unserer Zeit 2009;43:132–142.
  43. Kazlauskas, R., Chem. Soc. Rev. 2018;47:9026–9045.
  44. Jones, B. J., Lim, H. Y., Huang, J. and Kazlauskas, R. J., Biochemistry 2017;56:6521–6532.
  45. Oda, M., Yamagami, Y., Inaba, S., Oida, T., et al. Appl. Microbiol. Biotechnol. 2018;102:10067–10077.
  46. Moog, D., Schmitt, J., Senger, J., Zarzycki, J., et al. Microb. Cell Fact. 2019;18:171.
  47. Wei, R., Oeser, T., Barth, M., Weigl, N., et al. J. Mol. Catal. B Enzym. 2014;103:72–78.
  48. Siddiqui, K. S., Crit. Rev. Biotechnol. 2017;37:309–322.

## SUPPORTING INFORMATION

Additional supporting information may be found in the online version of the article at the publisher's website.

**How to cite this article:** Brott, S., Pfaff, L., Schuricht, J., Schwarz, J.-N., et al. Engineering and evaluation of thermostable *IsPETase* variants for PET degradation. Eng Life Sci. 2022, 22, 192–203. <https://doi.org/10.1002/elsc.202100105>

# Supporting information

## Engineering and evaluation of thermostable *IsPETase* variants for PET degradation

Stefan Brott, Lara Pfaff, Josephine Schuricht, Jan-Niklas Schwarz, Dominique Böttcher, Christoffel P. S. Badenhorst, Ren Wei, Uwe T. Bornscheuer

Department of Biotechnology & Enzyme Catalysis, University of Greifswald Institute of Biochemistry, Greifswald, Germany

**Correspondence:** Prof. Dr. Uwe T. Bornscheuer ([uwe.bornscheuer@uni-greifswald.de](mailto:uwe.bornscheuer@uni-greifswald.de)). Department of Biotechnology & Enzyme Catalysis, University of Greifswald Institute of Biochemistry, Felix-Hausdorff-Straße 4, 17489 Greifswald, Germany.

## Oligonucleotide primers

**Table S1:** Used Oligonucleotide primers (5'→3') for generation of *IsPETase* variants.

<b>Oligonucleotide primers for generating <i>IsPETase</i><sup>TM</sup> per Q5<sup>®</sup> Site-Directed Mutagenesis Kit</b>	
Fw_ <i>IsPETase</i> _S121E	ggatcagccggagagccgtagcag
Rv_ <i>IsPETase</i> _S121E	agggtgctgttggtgca
Fw_ <i>IsPETase</i> _D186H	agcgcctggcatagcagcaccaac
Rv_ <i>IsPETase</i> _D186H	tgcggcgccgcccgttcc
Fw_ <i>IsPETase</i> _R280A	gaatagcaccgcggtgagcgacttcc
Rv_ <i>IsPETase</i> _R280A	ggatttgcgacgcaaag
<b>Oligonucleotide primers for error-prone PCR</b>	
Fw_ <i>IsPETase</i> _ep	cagaccaatccgtatgccc
RV_ <i>IsPETase</i> _ep	ctcagggtgcagttcgc
<b>Oligonucleotide primers introducing N233C and S282C substitutions per QuikChange</b>	
Fw_ <i>IsPETase</i> <sup>TM</sup> _N233C	cagttcctggaaattgcggtggcagccacag
Rv_ <i>IsPETase</i> <sup>TM</sup> _N233C	ctgtggctgccaccgcaaattccaggaactg
Fw_ <i>IsPETase</i> <sup>TM</sup> _S282C	gaatagcaccgcggtgtgcgacttccgtac
Rv_ <i>IsPETase</i> <sup>TM</sup> _S282C	gtacggaagtcgcacaccgcggtgctattc
Fw_ <i>DuraPETase</i> _N233C	caaacagtttctggaaattgcggcgccagccatagctgc
Rv_ <i>DuraPETase</i> _N233C	gcagctatggctgcccgcaaattccagaaactgtttg
Fw_ <i>DuraPETase</i> _S282C	gaatagcaccgcccgttgcgatttgcaccg
Rv_ <i>DuraPETase</i> _S282C	cggtgcgaaaatcgcaaaccggcggtgctattc
Fw_ <i>DuraPETase</i> <sup>K95N/S121E/F201I/R280A</sup> _N233C	caaacagtttctggaaattgcggtgtagccatagctgcg
Rv_ <i>DuraPETase</i> <sup>K95N/S121E/F201I/R280A</sup> _N233C	cgcagctatggctaccaccgcaaattccagaaactgtttg
Fw_ <i>DuraPETase</i> <sup>K95N/S121E/F201I/R280A</sup> _S282C	gaatagcaccgcccgtgtgcgatttgcaccg
Rv_ <i>DuraPETase</i> <sup>K95N/S121E/F201I/R280A</sup> _S282C	cggtgcgaaaatcgcacaccggcggtgctattc

## Screening

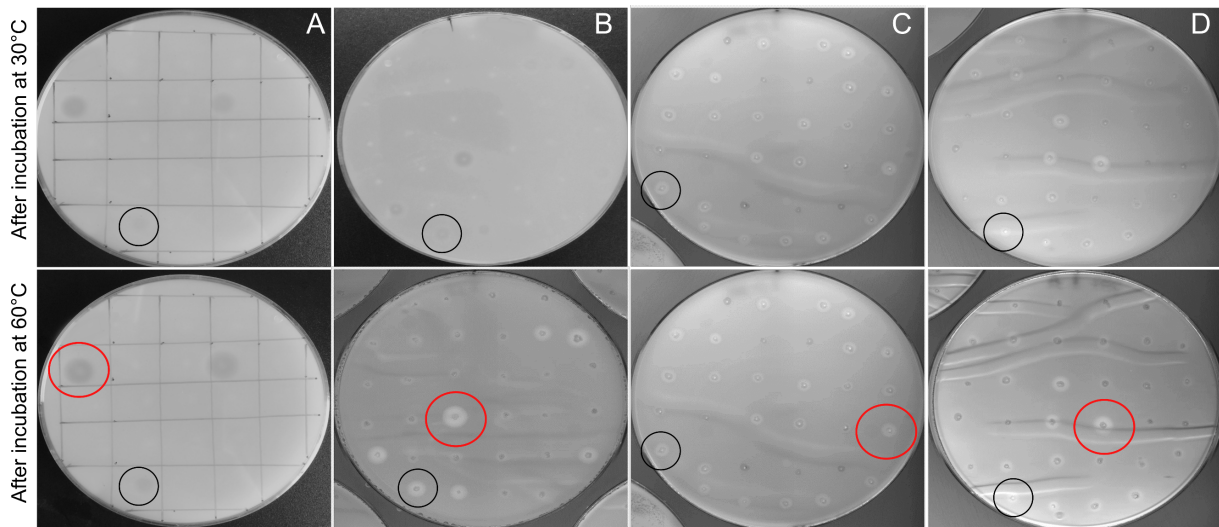


**Figure S1:** Impranil® agar plates that showed distinguishable haloes in the screening compared to the control. *IsPETase* activity is associated with a halo formation around the cell colony. Colonies expressing possibly more thermostable *IsPETase* variants are circled in red: A) *IsPETase*TM<sup>S125N/A226T</sup>, B) *IsPETase*TM<sup>K95N/F201I</sup>, C) *IsPETase*TM<sup>Q119L</sup> and D) *IsPETase*TM<sup>T51A/S125I/S207I</sup>. Each agar plate had at least one colony (outlined in black) expressing *IsPETase*TM as control. Plates were incubated for 24 hours at 30°C and then for 24 hours at 60°C. Images were colored gray for better visibility.

## Positions of discovered amino acid substitution in *IsPETase*<sup>S121E/D186H/R280A</sup>

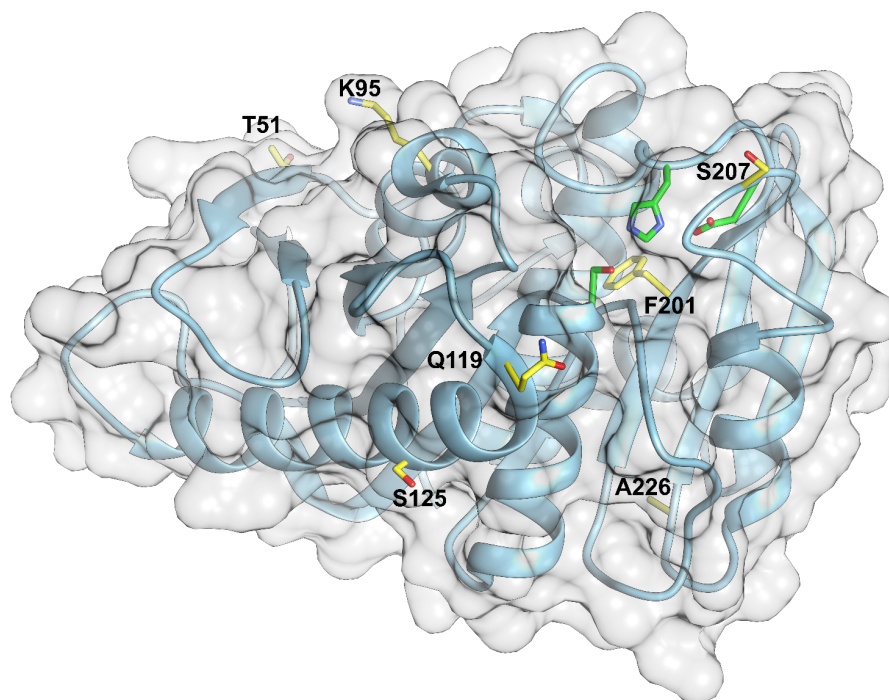


**Figure S2:** Positions of amino acid substitution within the *IsPETase* triple mutant. This figure shows only the positions of the mutations which were discovered and not the amino acids substitutions. Important amino acids are shown as sticks. The catalytic triad (S160-D206-H237) is colored green and the position of mutation sites is colored yellow. Visualization was done with UCSF Chimera [1]. The structure is based on the crystal structure (Protein Data Bank code 6IJ6) [2]. The crystal structure was not altered.

### Expression & Purification

Plasmids of the wild type *IsPETase* and variants based on the triple or quintuple mutants were transformed into chemically competent *E. coli* SHuffle<sup>®</sup> T7 Express cells (New England Biolabs GmbH, Frankfurt am Main, Germany) and spread onto LB agar plates containing 100  $\mu\text{g mL}^{-1}$  ampicillin. The plates were incubated overnight at 30°C. One colony was picked and used to inoculate an overnight culture containing 100  $\mu\text{g mL}^{-1}$  ampicillin. Cultivation was performed in 400 mL LB medium containing 100  $\mu\text{g mL}^{-1}$  ampicillin in a 1 L flask. The medium was inoculated with overnight culture and incubated at 33°C and 160 rpm until an optical density ( $\text{OD}_{600}$ ) of 1.0 was reached. Expression of the target enzyme was then induced by the addition of 1 mM IPTG. Cultivation was subsequently continued at 16°C and 160 rpm overnight. Cells were harvested by centrifugation at 3,500 g and 4°C for 50 min. The cell pellet was washed with sodium phosphate (50 mM, pH 7.5) and subsequently stored at -20°C until cells were lysed. The same protocol was used for expression of *DuraPETase* variants with the exception that the plasmids were transformed into chemically competent *E. coli* OverExpress C43(DE3) cells (Biosearch Technologies, Hoddesdon, United Kingdom). For ultrasonication using a Sonoplus HD 2070 ultrasonic homogenizer (Bandelin electronic GmbH & Co. KG, Berlin, Germany), the cell pellets were resuspended in buffer A (50 mM Tris-HCl buffer, pH 7.5, 150 mM sodium chloride, and 10 mM imidazole). Cell debris was then removed by centrifugation at 10,000 g and 4°C for 20 min. Purification was performed with the ÄktaPure chromatography system (GE Healthcare Europe GmbH, Freiburg, Germany) using a HisTrap<sup>™</sup> FF crude 5 mL column (Cytiva Europe GmbH, Freiburg, Germany). Undesired proteins were first washed away with buffer A and then with buffer A supplemented with 100 mM imidazole. Elution of *IsPETase* variants was then performed with buffer A supplemented with 200 mM imidazole. Elution fractions containing the protein of interest were pooled and concentrated using Vivaspin 6 centrifugal concentrator (10 kDa MWCO, Sartorius AG, Göttingen, Germany). PD-10 Desalting Columns (GE Healthcare, Freiburg, Germany) were used to exchange the elution buffer to 50 mM sodium phosphate buffer (pH 7.5).



A difference in expression between wild type and mutants is observed. All variants based on *IsPETase*<sup>TM</sup> have a better expression than variants based on *DuraPETase*. The differences in expression levels can also be recognized in the SDS-PAGE gels (Figure S3), for example in the lysate fractions. However, after purification, sufficient protein concentrations are present for melting point determinations and biocatalysis.

### Sodium dodecyl sulfate–polyacrylamide gel electrophoresis (SDS-PAGE)

Samples were mixed with a 5-fold stock of SDS sample buffer (Tris HCl buffer, pH 6.8, 100 mM, SDS, 4% w/v, glycerol, 20% v/v, β-mercaptoethanol, 2% v/v, EDTA, 25 mM, bromophenol blue, 0.04% w/v) and denatured by incubation at 95°C for 10 min. For the SDS-PAGE a 12.5% acrylamide gel (separating gel) and a 4.0 % loading gel was used. Electrophoresis was carried out at 200 V. Proteins were stained with Coomassie Blue (PhastGel® Blue R, Sigma Aldrich, Taufkirchen, Germany) and as reference the *Pierce*<sup>TM</sup> Unstained protein molecular weight marker (Thermo Scientific, Waltham, MA, USA) was used.

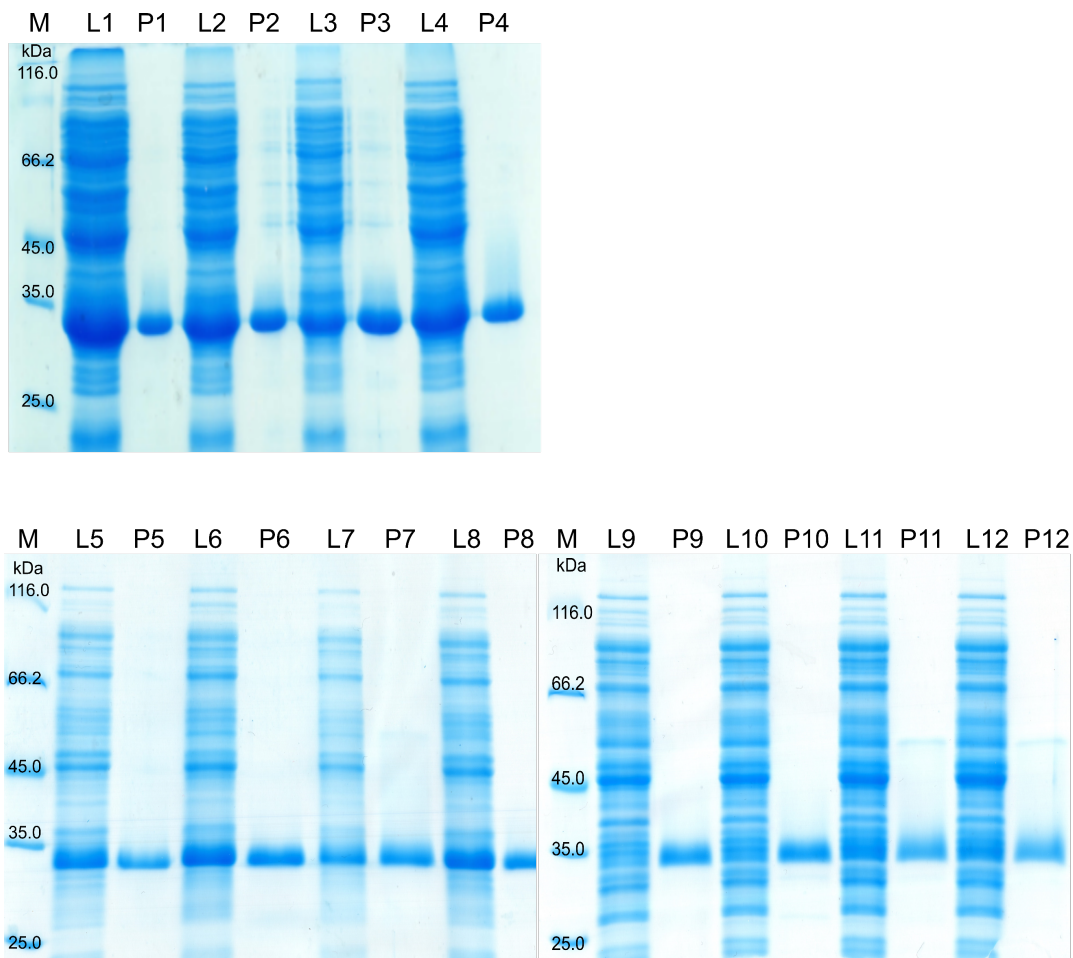


**Figure S3:** Evaluation of the purity of *IsPETase* variants after purification. Samples of the lysate (L) and the purified pooled fractions (P) were applied. Marker (M) = *Pierce*<sup>TM</sup> Unstained protein molecular weight marker. *IsPETase* has a size of approximately 30 kDa. Proteins were stained with Coomassie Blue.

- |   |   |  |
|---|---|--|
| 1 = <i>IsPETase</i> <sup>TM</sup> <sup>Q119L</sup>            | 5 = <i>IsPETase</i> <sup>WT</sup>                                   | 9 = <i>DuraPETase</i>  |
| 2 = <i>IsPETase</i> <sup>TM</sup> <sup>F51A/S125I/S207I</sup> | 6 = <i>IsPETase</i> <sup>TM</sup>                                   | 10 = <i>DuraPETase</i> <sup>N233C/S282C</sup>                        |
| 3 = <i>IsPETase</i> <sup>TM</sup> <sup>S125N/A226T</sup>      | 7 = <i>IsPETase</i> <sup>TM</sup> <sup>N233C/S282C</sup>            | 11 = <i>DuraPETase</i> <sup>K95N/S121E/F201I/R280A</sup>             |
| 4 = <i>IsPETase</i> <sup>TM</sup> <sup>K95N/F201I</sup>       | 8 = <i>IsPETase</i> <sup>TM</sup> <sup>K95N/F201I/N233C/S282C</sup> | 12 = <i>DuraPETase</i> <sup>K95N/S121E/F201I/N233C/R280A/S282C</sup> |

**Table S2:** Melting points of the *IsPETase* variants discovered in the screening with Impranil® agar plates. Data were determined by nanoDSF with purified enzymes (0.5 mg mL<sup>-1</sup>) in 50 mM sodium phosphate buffer (pH 7.5). The measurement was performed in duplicates and the mean values as well as the standard derivation are given.

Impranil® agar plate	<i>IsPETase</i> variant	Melting point ± SD [°C]
A)	<i>IsPETase</i> TM <sup>S125N/A226T</sup>	58.5 ± 0.1
B)	<i>IsPETase</i> TM <sup>K95N/F201I</sup>	61.8 ± 0.1
C)	<i>IsPETase</i> TM <sup>Q119L</sup>	58.6 ± 0.1
D)	<i>IsPETase</i> TM <sup>T51A/S125I/S207I</sup>	58.5 ± 0.1
	<i>IsPETase</i> WT	45.1 ± 0.1
	<i>IsPETase</i> TM	56.6 ± 1.6

### Preparation of PET nanoparticles

PET nanoparticles were prepared based on previous publications [3, 4]. Amorphous PET film (300 mg) (Goodfellow GmbH, Bad Nauheim, Germany) was dissolved in 20 mL of 1,1,1,3,3,3-hexafluoro-2-propanol. The dissolved PET was then added dropwise to 300 mL of Milli-Q water under vigorous stirring using an UltraTurrax T25 (IKA Werke GmbH & Co. KG, Staufen im Breisgau, Germany). Solvent was then removed from the mixture by evaporation using a rotary evaporator (Heidolph Instruments GmbH & Co. KG, Schwabach, Germany) and the aqueous suspension further concentrated under vacuum to a final volume of 50 mL. PET nanoparticle concentration was determined gravimetrically.

**Table S3:** Relative activities of selected *IsPETase* compared to the *IsPETase* triple mutant for degradation of PET nanoparticles at different incubation temperatures. Instead of the wild type the triple mutant was chosen for comparison because it was the starting point for this study. Biocatalysis with PET nanoparticles (0.2 mg mL<sup>-1</sup>) was performed with 30 nM *IsPETase* variant in 50 mM sodium phosphate buffer (pH 7.5) at different incubation temperatures and constant agitation of 1000 rpm. Relative activities are based on total product release after 24 h incubation. The mean values and standard deviations are given.

<i>IsPETase</i> variant	Relative activity [%] compared to <i>IsPETase</i> TM			
	30°C	40°C	50°C	60°C
<i>IsPETase</i> WT	32.3 ± 3.4	7.8 ± 3.1	4.9 ± 1.7	16.0 ± 5.3
<i>IsPETase</i> TM	100.0 ± 30.4	100.0 ± 15.7	100.0 ± 50.4	100.0 ± 5.8
<i>IsPETase</i> TM <sup>K95N/F201I</sup>	119.4 ± 51.5	30.4 ± 14.9	70.6 ± 4.2	139.9 ± 32.7
<i>IsPETase</i> TM <sup>N233C/S282C</sup>	128.4 ± 14.7	108.6 ± 15.7	160.0 ± 14.7	234.7 ± 39.4
<i>IsPETase</i> TM <sup>K95N/F201I/N233C/S282C</sup>	16.5 ± 9.6	18.6 ± 3.6	43.3 ± 6.4	27.5 ± 11.5
<i>DuraPETase</i>	10.9 ± 5.6	10.9 ± 0.5	24.6 ± 7.6	65.5 ± 22.0
<i>DuraPETase</i> <sup>N233C/S282C</sup>	17.4 ± 1.7	21.1 ± 0.9	39.2 ± 3.2	128.9 ± 25.6
<i>DuraPETase</i> <sup>K95N/S121E/F201I/R280A</sup>	16.6 ± 13.4	11.3 ± 4.1	13.5 ± 6.9	35.2 ± 6.1
<i>DuraPETase</i> <sup>K95N/S121E/F201I/N233C/R280A/S282C</sup>	13.6 ± 5.9	13.9 ± 0.9	22.0 ± 7.5	65.1 ± 8.6

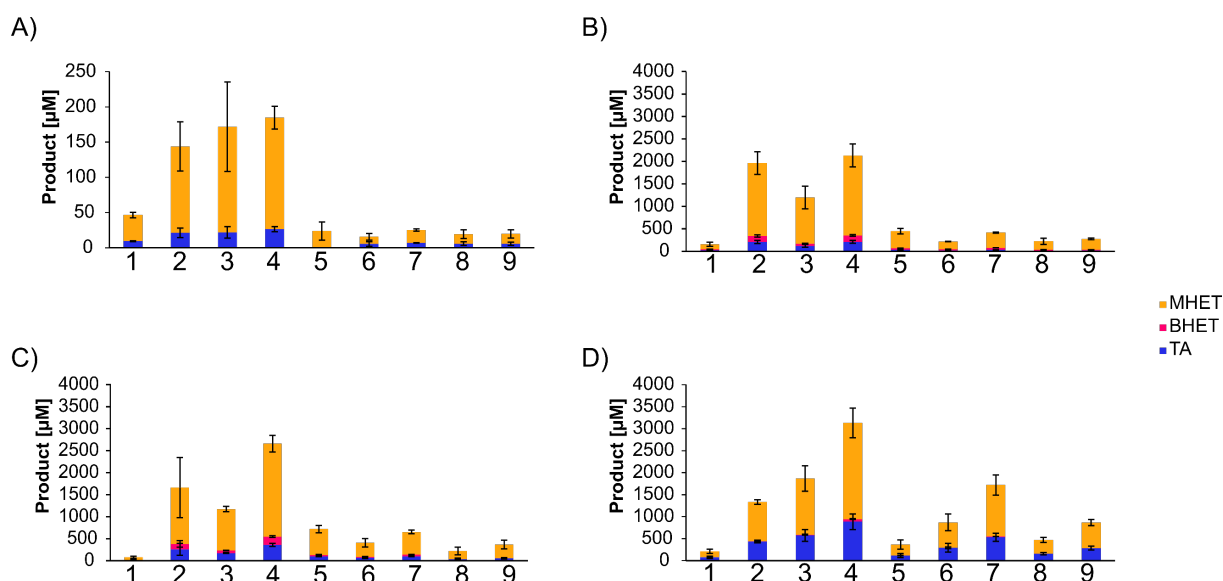


**Figure S4:** Comparison of degradation products for PET nanoparticles hydrolysis catalyzed by selected *IsPETase* variants after 24 h incubation. Biocatalysis with PET nanoparticles ( $0.2 \text{ mg mL}^{-1}$ ) was performed with 30 nM *IsPETase* variant in 50 mM sodium phosphate buffer (pH 7.5) at different incubation temperatures: A) 30°C, B) 40°C, C) 50°C and D) 60°C and a constant agitation of 1000 rpm. The investigated *IsPETase* variants: 1 = *IsPETase*WT, 2 = *IsPETase*TM, 3 = *IsPETase*TM<sup>K95N/F201I</sup>, 4 = *IsPETase*TM<sup>N233C/S282C</sup>, 5 = *IsPETase*TM<sup>K95N/F201I/N233C/S282C</sup>, 6 = *DuraPETase*, 7 = *DuraPETase*<sup>N233C/S282C</sup>, 8 = *DuraPETase*<sup>K95N/S121E/F201I/R280A</sup> and 9 = *DuraPETase*<sup>K95N/S121E/F201I/N233C/R280A/S282C</sup>. The measurement was performed in triplicates and the mean values and standard deviations are given.

**Table S4:** Relative activities of selected *IsPETase* compared to the *IsPETase* triple mutant for degradation of amorphous PET film at 60°C incubations after 72 h. Instead of the wild type the triple mutant was chosen for comparison because it was the starting point for this study. Biocatalysis was performed with 50 nM *IsPETase* variant in 50 mM glycine-NaOH buffer (pH 9.0) at 60°C incubation and constant agitation of 1000 rpm. Relative activities are based on total product release after 72 h incubation. The mean values and standard deviations are given.

<i>IsPETase</i> variant	Relative activity [%] compared to <i>IsPETase</i> TM
<i>IsPETase</i> WT	17.6 ± 3.1
<i>IsPETase</i> TM	100.0 ± 64.3
<i>IsPETase</i> TM <sup>K95N/F201I</sup>	314.3 ± 134.7
<i>IsPETase</i> TM <sup>N233C/S282C</sup>	431.6 ± 297.2
<i>IsPETase</i> TM <sup>K95N/F201I/N233C/S282C</sup>	2043.2 ± 854.4
<i>DuraPETase</i>	490.5 ± 299.7
<i>DuraPETase</i> <sup>N233C/S282C</sup>	1989.5 ± 208.7
<i>DuraPETase</i> <sup>K95N/S121E/F201I/R280A</sup>	211.1 ± 52.2
<i>DuraPETase</i> <sup>K95N/S121E/F201I/N233C/R280A/S282C</sup>	740.8 ± 398.0

**Table S5:** Compared melting points [°C] of published *IsPETase* variants.

<i>IsPETase</i> variant	This study	Son <i>et al.</i> <sup>a</sup>	Zhong-Johnson <i>et al.</i> <sup>b</sup>	Cui <i>et al.</i> <sup>c</sup>
<i>IsPETase</i> WT	45.1 ± 0.01	48.81	48.1 ± 1.3	46.0
<i>IsPETase</i> TM	56.6 ± 1.55	57.62	-	-
<i>IsPETase</i> TM <sup>N233C/S282C</sup>	68.2 ± 0.03	-	69.4 ± 0.3	-
<i>DuraPETase</i>	75.0 ± 0.11	-	-	77.0

a) in 50 mM Na<sub>2</sub>HPO<sub>4</sub>-HCl buffer (pH 7.0), determined with Applied Biosystems™ protein thermal shift™ dye [2]

b) in 50 mM glycine-NaOH buffer (pH 9.0) supplemented with 50 mM NaCl, determined with differential scanning fluorimetry with Sypro™-Orange dye [5]

c) in 50 mM Na<sub>2</sub>HPO<sub>4</sub> buffer (pH 7.5) supplemented with 100 mM NaCl, determined with differential scanning fluorimetry with Sypro™-Orange dye [6]

## References

- [1] Molecular graphics and analyses performed with UCSF Chimera, developed by the Resource for Biocomputing, Visualization, and Informatics at the University of California, San Francisco, with support from NIH P41-GM103311.
- [2] Son, H.F., Cho, I.J., Joo, S., Seo, H., et al., Rational protein engineering of thermo-stable PETase from *Ideonella sakaiensis* for highly efficient PET degradation. *ACS Catal.* 2019, 9, 3519–3526.
- [3] Vogel, K., Wei, R., Pfaff, L., Breite, D., et al., Enzymatic degradation of polyethylene terephthalate nanoplastics analyzed in real time by isothermal titration calorimetry. *Sci. Total Environ.* 2021, 773:145111.
- [4] Pfaff, L., Breite, D., Badenhorst, C.P.S; Bornscheuer, U.T., Wei, R., Fluorimetric high-throughput screening method for polyester hydrolase activity using polyethylene terephthalate nanoparticles, in: Weber, G., Bornscheuer, U.T., Wei, R. (Eds.), *Methods Enzymol. Enzymatic Plastic Degradation*, Elsevier, 2021, 648, 254-270.
- [5] Zhong-Johnson, E.Z.L., Voigt, C.A., Sinskey, A.J., An absorbance method for analysis of enzymatic degradation kinetics of poly(ethylene terephthalate) films. *Sci. Rep.* 2021, 11:928.
- [6] Cui, Y., Chen, Y., Liu, X., Dong, S., et al., Computational redesign of a PETase for plastic biodegradation under ambient condition by the GRAPE strategy. *ACS Catal.* 2021, 11, 1340–1350.

## **Article III**





# Fluorimetric high-throughput screening method for polyester hydrolase activity using polyethylene terephthalate nanoparticles

Lara Pfaff<sup>a</sup>, Daniel Breite<sup>b</sup>, Christoffel P.S. Badenhorst<sup>a</sup>,  
Uwe T. Bornscheuer<sup>a</sup>, and Ren Wei<sup>a,\*</sup>

<sup>a</sup>Department of Biotechnology & Enzyme Catalysis, Institute of Biochemistry, University of Greifswald, Greifswald, Germany

<sup>b</sup>Leibniz Institute of Surface Engineering (IOM), Leipzig, Germany

\*Corresponding author: e-mail address: ren.wei@uni-greifswald.de

## Contents

1. Introduction	254
2. PET nanoparticles: Generation, application, and characterization	255
3. Fluorimetric high-throughput screening assay	258
4. Materials, equipment, and reagents	261
4.1 PET NP production	261
4.2 PET NP characterization	262
4.3 Protein production	262
4.4 Enzymatic degradation of PET NPs	262
4.5 Determination of polyester hydrolysis activity	263
5. Protocols	264
5.1 PET NP production	264
5.2 PET NP characterization	264
5.3 Protein production	265
5.4 Enzymatic degradation of PET NP	266
5.5 Quantification of the PET degradation products	266
Acknowledgments	268
References	268

## Abstract

Biocatalysis has recently emerged as a powerful and eco-friendly technology in waste plastic recycling, especially for the widely used polyethylene terephthalate (PET). So far, however, a high-throughput screening assay specifically toward PET-hydrolyzing activity has rarely been applied. This hinders the identification of new polyester hydrolases

and their variants with adequate activities fulfilling the requirements for industrial applications. This chapter describes the detailed procedure for assaying terephthalate as a major product of enzymatic PET hydrolysis in a 96-well microtiter plate format. Using PET nanoparticles derived readily from waste food packaging as a substrate, an active thermophilic PET hydrolase was clearly distinguished from an inactive variant by a Fenton chemistry-mediated fluorimetric detection. The assay uses enzymes in crude cell lysates, obtained by a simple freeze–thaw protocol. The experimental work validates the applicability of this method for screening mutant libraries of novel PET hydrolases and will thus facilitate the identification of promising variants useful for effective plastic waste recycling.



## 1. Introduction

Plastic pollution poses a serious risk to terrestrial and aquatic ecosystems as well as human health (Eriksen et al., 2014; Rochman, Hoh, Kurobe, & Teh, 2013; Wright & Kelly, 2017). The global production of plastics, excluding synthetic fibers, reached 359 million metric tons p.a. in 2018 (PlasticsEurope, 2019) and is rapidly increasing. Therefore, efficient disposal strategies are urgently needed for sustainable treatment of plastic waste. Recycling of the existing plastic waste presents the most sustainable and viable solution in context of decreased CO<sub>2</sub> emission as well as of the fuel and energy savings (Rahimi & García, 2017; Vollmer et al., 2020). In 2015, only 9% of plastic waste was recycled worldwide (Geyer, Jambeck, & Law, 2017). Research achievements in the last two decades empowered the applicability of selected enzymes and microbes as an alternative eco-friendly plastic recycling technology (Wei et al., 2020). Especially for polyethylene terephthalate (PET), which is widely used to produce food packaging, beverage bottles, and synthetic fibers, the biotechnological recycling of plastics that allows the recovery of their monomeric building blocks has been demonstrated both at laboratory and industrially relevant scales (Kawai, Kawabata, & Oda, 2019, 2020; Tournier et al., 2020; Wei & Zimmermann, 2017). Since the identification of an efficient PET hydrolase from *Thermobifida fusca* in 2005 (Müller, Schrader, Profe, Dresler, & Deckwer, 2005), the discovery of novel PET hydrolases has become an important field of research (Kawai et al., 2020). So far, the enzymatic hydrolysis of PET has been performed using a variety of PET hydrolases obtained from both eukaryotic and prokaryotic microbes. Besides different hydrolases reported from actinomycetes, including different strains of *Thermobifida* species (Herrero Acero et al., 2011; Wei, Oeser, & Zimmermann, 2014), a commercial cutinase from the fungus



*Thermomyces insolens* (formerly *Humicola insolens*) has been reported to efficiently degrade low-crystalline PET (Ronkvist, Xie, Lu, & Gross, 2009). Another major discovery was the identification of a bacterium, *Ideonella sakaiensis*, which is able to grow on and assimilate PET at 30°C under laboratory conditions, albeit very slowly (Yoshida et al., 2016). This discovery is also interesting with respect to the speed of natural evolution of enzymes/microbes to be able to access a man-made carbon source less than 80 years after PET was first synthesized by chemists (Bornscheuer, 2016). Recently, the efficient biocatalytic depolymerization of pretreated postconsumer PET bottles within 10 h has been reported and well accepted as a breakthrough enabling the future application of biotechnological plastic recycling (Tournier et al., 2020). A variant of the plant metagenome-derived cutinase LCC which showed inherently high thermal stability and activity against amorphous PET at up to 70°C (Sulaiman et al., 2012; Sulaiman, You, Kanaya, Koga, & Kanaya, 2014; Wei, Song, et al., 2019) was generated and revealed markedly increased PET-hydrolyzing activity, compared to the wild-type enzyme. The discovery of LCC in a metagenomic library as well as further PET hydrolases found from published metagenome databases (Danso et al., 2018) emphasized the value of environmental metagenomes for the identification of more plastic-degrading hydrolases. To identify such novel polyester hydrolases, a powerful high-throughput screening (HTS) assay specifically targeting a real-world plastic substrate is required.

In this chapter, we describe the detailed procedure for assaying terephthalate, the main product from the enzymatic hydrolysis of PET nanoparticles, in a 96-well microtiter plate format (Fig. 1). This assay enables the rapid identification of outstanding PET hydrolase variants from large mutant or metagenome libraries.



## 2. PET nanoparticles: Generation, application, and characterization

Nanoplastics (size <100 nm) are omnipresent pollutants in natural environments as a result of the fragmentation of larger plastic debris. Nanoplastics may pose a serious threat to human and animal health due to their small size and larger relative surface area, which corresponds to an enhanced ability to penetrate tissues and adsorb pathogens and toxic chemicals (Lehner, Weder, Petri-Fink, & Rothen-Rutishauser, 2019; Wagner & Reemtsma, 2019). For investigations of their ecotoxicity and fate in the biological degradation

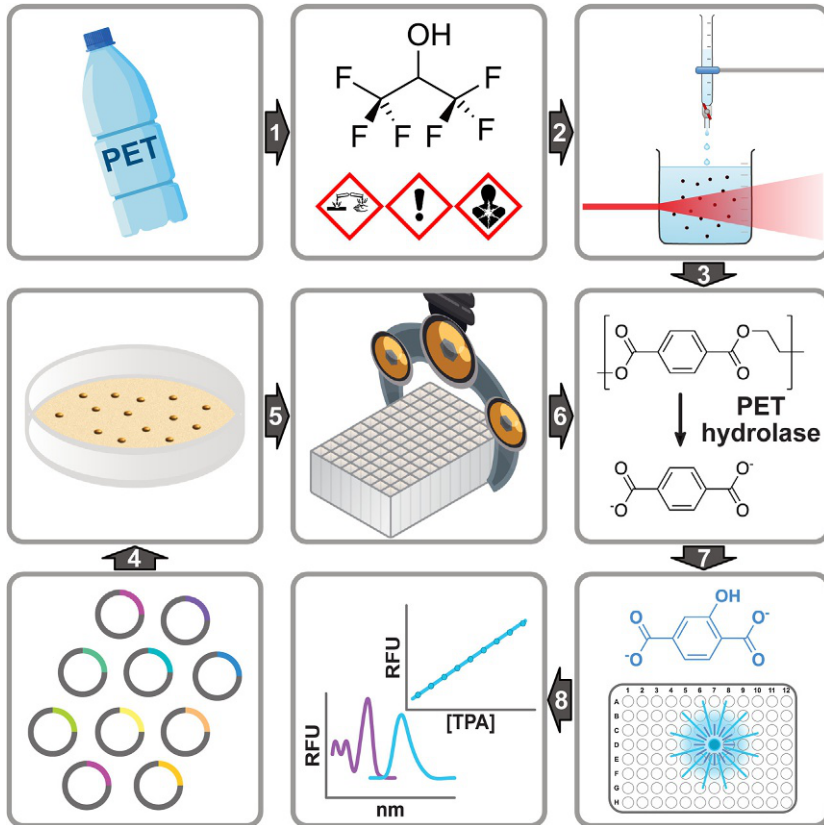


**Fig. 1** Workflow of the fluorimetric high-throughput screening method to detect PET hydrolase activity. (1) Postconsumer PET is cut and the pieces are dissolved in hexafluoro-2-propanol. (2) The dissolved PET is dropped into rapidly stirring ultrapure water, resulting in the formation of nanoparticles that are characterized by scanning electron microscopy and dynamic light scattering. (3) After removal of the solvent, the nanoparticles are ready to be used in the enzymatic assays. (4) A plasmid library is transformed into an expression strain like *Escherichia coli* BL21(DE3). (5) The resulting colonies are used to inoculate 96-deep-well plates for protein expression, which is followed by preparation of crude cell lysates. (6) The crude cell lysates are used with PET nanoparticles to assay PET-hydrolyzing activity. (7–8) Formation of the product terephthalate is detected by reaction with hydroxyl radicals, generated by a Fenton-like reaction. Terephthalate is converted to 2-hydroxyterephthalate and detected by fluorescence measurements (excitation at 315 nm and emission at 421 nm).

process, artificial polymer nanoparticles (NPs) are often utilized (Liu et al., 2018; Vogel et al., 2020). The impact of artificially generated PET NPs on human macrophages (Rodríguez-Hernández, Muñoz-Tabares, Aguilar-Guzmán, & Vazquez-Duhalt, 2019), and their degradation by various

polyester hydrolases, have been studied (Barth et al., 2015; Danso et al., 2018; Weber et al., 2019; Wei, Oeser, Barth, et al., 2014; Wei, Oeser, Billig, & Zimmermann, 2012; Wei, Oeser, Then, et al., 2014; Vogel et al., 2020).

Nanometer and submicrometer PET particles have been produced using different sources of polymers dissolved in various solvents dripped to water as an anti-solvent (Rodríguez-Hernández et al., 2019; Welzel, Müller, & Deckwer, 2002). Hexafluoro-2-propanol (HFIP) has been found to be the best solvent for PET (Berkowitz, 1984). It can rapidly dissolve PET materials with different thermal histories and crystallinities by simple incubation at room temperature (Wei, Breite, et al., 2019; Wei, Oeser, Barth, et al., 2014). Dissolved PET polymers revealed molecular weight distributions comparable to the literature value, indicating that the dissolution of PET in HFIP does not lead to significant chain scission (Wei, Breite, et al., 2019). Postconsumer PET packaging (trays, clamshells, and boxes) for fresh vegetables and fruits, which is a mass-produced low-crystalline form of PET available in the market, could be readily used to prepare PET NPs without any pre-treatment. With help of an ULTRA TURRAX mixer (Protocol 5.1), HFIP droplets containing dissolved PET were rapidly distributed in ultrapure water (Fig. 1, steps 2–3), resulting in a homogenous suspension of NPs with an average size well below the 100 nm threshold defined for nanoplastics (Fig. 2A). An average size of 76.6 nm was determined using dynamic light scattering (DLS) and verified by scanning electron microscopy (SEM; Fig. 2B), which also demonstrated the spherical shape of the PET NPs. The diameter determined by DLS is in good agreement with that previously measured by nanoparticle tracking analysis (Vogel et al., 2020).

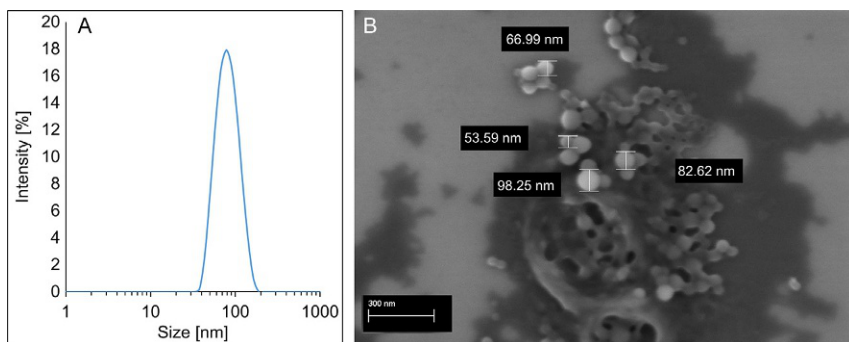


**Fig. 2** Evaluation of the size distribution of PET NPs prepared using HFIP-dissolved post-consumer PET packaging by (A) dynamic light scattering and (B) scanning electron microscopy.



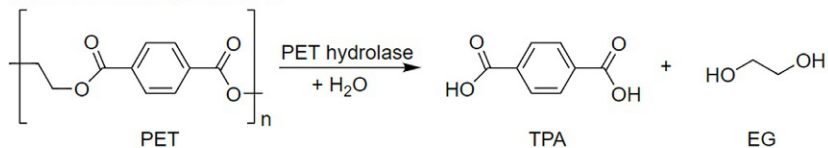
### 3. Fluorimetric high-throughput screening assay

Terephthalic acid (TPA) is one of the main products released by the enzymatic degradation of PET. Based on their characteristic absorbance at 241 nm, TPA and related esters such as mono(2-hydroxyethyl) terephthalate (MHET) and bis(2-hydroxyethyl) terephthalate (BHET) have been monitored by reversed phase high-performance liquid chromatography (RP-HPLC) with UV detection (Eberl et al., 2009; Herrero Acero et al., 2011; Palm et al., 2019). Although most modern HPLCs are equipped with autosamplers, sequential measurements are time consuming and will complicate the analysis of large mutant and metagenome libraries.

In alkaline buffer (pH above 8), TPA is present in its deprotonated species as terephthalate. Terephthalate possesses a symmetrical structure, and can thus be monohydroxylated in the presence of hydroxyl radicals to a single product, 2-hydroxyterephthalate (2-HOTP; Fig. 3), exhibiting stable fluorescence at 421 nm (excitation at 315 nm) for up to 36 h at room temperature (Saran & Summer, 1999). Dihydroxyterephthalic acid (DHT) is another fluorescent hydroxylated derivate of TPA with absorption (excitation) maximum at 375 nm (Cho et al., 2019). However, no literature has described the possibility of DHT synthesis via direct radical hydroxylation of TPA, and it will thus not interfere with this assay.

For terephthalate obtained from depolymerized PET, a high concentration (up to 30% v/v) of hydrogen peroxide and an incubation at 90°C for 30 min has been utilized in an earlier study to generate hydroxyl radicals for the conversion to fluorescent 2-HOTP (O'Neill & Cavaco-Paulo, 2004; Silva et al., 2011). It is hard to apply this temperature to microtiter plates in a high-throughput manner. Furthermore, undesirable loss of liquid by evaporation needs to be avoided, complicating sample handling. To avoid this susceptibility to interferences, the iron autoxidation-mediated hydroxylation of terephthalate has been successfully conducted at room temperature to quantify the enzymatic hydrolysis products of PET (Wei et al., 2012). The chelator ethylenediaminetetraacetic acid (EDTA) was used instead of hydrogen peroxide required for the canonical Fenton reaction. EDTA can facilitate the formation of hydroxyl radicals through stabilizing iron(III) and thus promotes the hydroxylation of terephthalate (Welch, Davis, & Aust, 2002). This Fe(II)-EDTA complex-based method has been previously established for the fluorimetric quantification of the hydroxyl radical scavenging ability of various compounds in the presence of a sodium terephthalate solution (Yang & Guo, 2001).

### (1) PET NP degradation



### (2) Fenton-like reaction: formation of hydroxyl radicals



### (3) Hydroxylation of terephthalate to fluorescent 2-hydroxyterephthalate

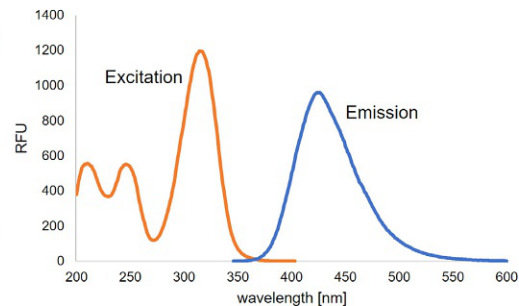
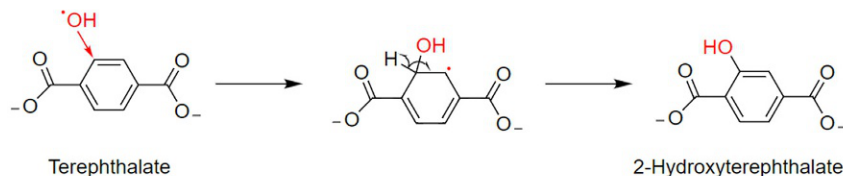


**Fig. 3** Fluorimetric detection of terephthalate as the PET hydrolysis product. (1) Enzymatic hydrolysis of PET yields TPA and EG as monomeric products. (2) The formation of hydroxyl radicals mediated by the Fe(II)-EDTA complex. (3) The hydroxylation of terephthalate to fluorescent 2-HOTP in the presence of hydroxyl radicals. The excitation and emission maxima of 2-HOTP are 315 nm and 421 nm, respectively. *RFU*: relative fluorescence units.

This fluorimetric assay has proven its high sensitivity in the monitoring of TPA resulting from PET hydrolysis using purified TfCut2, a thermophilic polyester hydrolase from *Thermobifida fusca*, in a 96-well microtiter plate format (Wei et al., 2012). The assay is robust at different phosphate buffer concentrations from 100 to 500 mM and is not inhibited by residual purified enzyme in the reaction supernatant, but is not compatible with Tris buffer, which scavenges the hydroxyl radicals. The assay was further validated by comparing the amounts of TPA determined by the fluorimetric assay and RP-HPLC, which showed an excellent agreement between the two quantification methods (Wei et al., 2012).

As high-throughput purification of target proteins (for example, in a 96-well microtiter plate format) is currently very cost-intensive, we adapted the fluorimetric assay for use with unpurified enzymes in crude cell lysates. We expressed recombinant TfCut2 as well as its inactive variant TfCut2\_S130A (Vogel et al., 2020) in ZYM-5052 autoinduction medium in 96-deep-well plates (Protocol 5.3) based on a recently published protocol (Tournier et al., 2020). Crude cell lysates obtained by repeated freeze-thaw cycles (Protocol 5.3) were directly used for the hydrolysis of PET NPs at 60°C (the optimal temperature for TfCut2). Furthermore, crude cell lysates without PET NPs were also incubated in the same manner and the resulting soluble supernatants were subjected to fluorimetric detection after adding terephthalate standards (final concentrations of 0–200 μM). As shown in Fig. 4A, linear calibration curves ( $R^2 > 0.992$ ) were obtained independent of the incubation time from 10 to 60 min for the hydroxylation of the terephthalate. Following the enzymatic hydrolysis of PET NPs with both active and inactive enzymes at 60°C for 30–60 min, 150 μL reaction supernatants were removed after centrifugation and added to a 96-well microtiter plate for the fluorimetric estimation of the terephthalate released. By subtracting the background autofluorescence resulting from the inactive enzyme, which has proven to cause no release of TPA from PET NP by RP-HPLC, the relative fluorescence units (RFU) determined with the active TfCut2 revealed a good agreement with the corresponding RP-HPLC analysis (Fig. 4B). This validates the applicability of the complete procedure schematically shown in Fig. 1 which allows sequentially the expression of enzyme libraries, the cell lysis, the hydrolysis reaction using PET NPs, as well as the final estimation of the terephthalate release by fluorimetry to be successfully performed in a 96-well microtiter plate format.

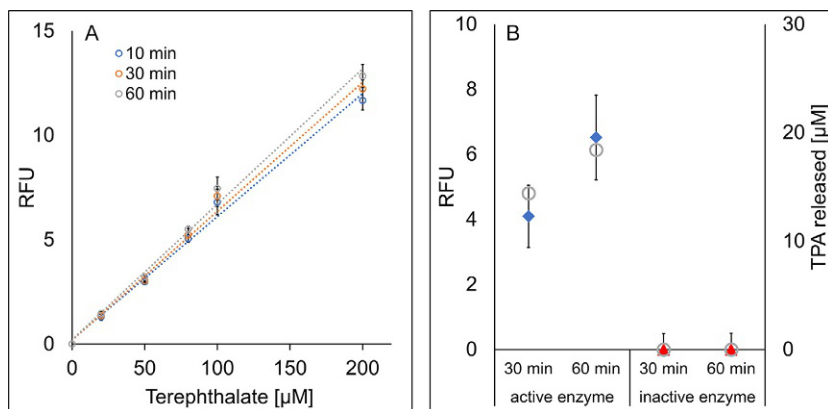


**Fig. 4** Fluorimetric estimation of the terephthalate concentrations. (A) Calibration curves determined with the cell lysates following incubation at 60°C for 60 min and the subsequent hydroxylation of various terephthalate standards in the presence of Fe(II)-EDTA (0.625 mM) for 10–60 min at room temperature. Incubation time with Fe(II)-EDTA did not have a significant effect, and 10 min was used for further assay development. (B) Comparison of the relative fluorescence units (RFU) determined in the supernatants of the enzyme-catalyzed hydrolysis of PET NPs (after 30 and 60 min shaking at 60°C, respectively) as an example for identifying hits. With the active TfCut2, significantly higher RFU values (*blue diamonds*) were monitored in a good agreement with the terephthalic acid (TPA) amounts determined by RP-HPLC (*gray circles*, secondary y-axis) than those obtained with the inactive enzyme (*red triangles*). Error bars indicate the standard deviations obtained with at least three independent measurements.



## 4. Materials, equipment, and reagents

### 4.1 PET NP production

- Postconsumer PET packaging materials (for example, clamshell boxes used as containers for fresh vegetables and fruits)
- 1,1,1,3,3,3-hexafluoro-2-propanol (HFIP)
- Ultrapure water (for example, obtained with the Milli-Q<sup>®</sup> Direct Water Purification System)
- Folded filter paper (Rotilabo<sup>®</sup> - folded filters, type 600P, Carl Roth, Karlsruhe, Germany)
- Thick-walled glass test tube with screw cap
- 1 L (narrow) glass beaker
- Glass burette
- 500 mL round-bottomed glass flask

- Disperser (IKA<sup>®</sup> ULTRA TURRAX<sup>®</sup> T-25 basic, Staufen, Germany)
- Rotary evaporator (Laborota 4000 WB, Heidolph, Schwabach, Germany)
- Centrifuge (Micro Star 17, VWR, Darmstadt, Germany)

## 4.2 PET NP characterization

- Scanning electron microscope (Ultra 55 SEM, Carl Zeiss Ltd., Göttingen, Germany)
- Chromium sputter system (Leybold LH Z400, Leybold, Hanau, Germany)
- Ethanol, technical grade
- Zetasizer Nano ZS with multipurpose titrator MPT-2 (Malvern Instruments, Worcestershire, UK)
- Disposable cuvettes (PMMA, 5 mL)

## 4.3 Protein production

- Gene of interest (for example, GenBank: [FR727681.1](#) for the wild-type TfCut2) cloned into an appropriate expression vector (for example, pET-26b(+))
- *Escherichia coli* BL21(DE3) (New England Biolabs, Ipswich, MA, US)
- ZYM-5052 medium for autoinduction ([Studier, 2005](#))
- 50 mM sodium phosphate (pH 8.0)
- Lysogeny Broth (LB)-agar plates
- Masterblock<sup>®</sup>, 96-well, 2 mL (manufactured from polypropylene), V-bottom, sterile, single-packed (Greiner Bio-One, Frickenhausen, Germany)
- Sterile toothpicks
  - Alternatively, an automated colony-picking robot can be employed
- Multichannel pipette, Transferpette<sup>®</sup>-8, 20–200  $\mu$ L (VWR, Darmstadt, Germany)
- Incubation shaker with 96-well plate tray (Infors HT Minitron, Bottmingen, Switzerland)
- Centrifuge (Heraeus<sup>®</sup> Multifuge<sup>®</sup> 3SR, Kendro Laboratory Products GmbH, Osterode, Germany)
- Low-temperature ( $-80^{\circ}\text{C}$ ) freezer
- Ice

## 4.4 Enzymatic degradation of PET NPs

- 500 mM sodium phosphate (pH 8.0)
- Ultrapure water



- PET NP suspension (1 mg/mL)
- 96-well microtiter plate
- Microtiter plate shaker (iEMS<sup>®</sup> Incubator Shaker HT, ThermoFisher Scientific, Darmstadt, Germany)

## 4.5 Determination of polyester hydrolysis activity

### 4.5.1 Fluorimetric HTS assay

- 500 mM sodium phosphate (pH 8.0)
- Terephthalic acid (TPA), reagent grade, 98% (Sigma-Aldrich, Steinheim, Germany)
- 100 mM sodium hydroxide
- 5 mM sodium EDTA solution (pH 8.0)
- 5 mM freshly prepared Fe(II)SO<sub>4</sub> solution
- FLUOTRAC<sup>™</sup> 96-well microtiter plate (manufactured from polystyrene), F-bottom (chimney well), black, medium binding (Greiner Bio-One, Frickenhausen, Germany)
- Microtiter plate reader/spectrophotometer (for example, Varioskan<sup>™</sup> LUX, ThermoFisher Scientific, Darmstadt, Germany)

### 4.5.2 RP-HPLC

- Acetonitrile, analytical grade
- Ultrapure water (degassed)
- Formic acid (FA), reagent grade, ≥95% (Sigma-Aldrich, Steinheim, Germany)
- Terephthalic acid (TPA), 98%, (Sigma-Aldrich, Steinheim, Germany)
- PET NP degradation reaction solution
- HPLC glass vials
- HPLC glass inlets
- HPLC vial lids
- Hitachi LaChrom Elite HPLC (VWR, Darmstadt, Germany)
  - Column oven: L-2300
  - Autosampler: L-2200
  - UV detector: L-2400
  - Pump: L-2130
  - HPLC Degasser 2005
- Column: Kinetex<sup>®</sup>, 5 μM EVO C18 100 Å, 150 × 4.6 mm (Phenomenex<sup>®</sup>, Aschaffenburg, Germany)



## 5. Protocols

### 5.1 PET NP production

1. Dissolve 300 mg of postconsumer PET packaging materials in 20 mL HFIP in a closed thick-walled glass test tube with screw cap and incubate at room temperature for approximately 12 h until completely dissolved.
  - a. HFIP is considered a harmful solvent, with GHS codes GHS05, GHS07, and GHS08 (GHS hazard pictograms are shown in Fig. 1).
  - b. Appropriate personal protective equipment (face shields, gloves, goggles, and a multipurpose combination respirator cartridge) should be used.
  - c. The solvent should be carefully handled in a fume hood and the waste obtained by rotary evaporation (halogenated organic waste) should be properly disposed of according to local guidelines.
  - d. It is important to use a strong and well-sealable glass vessel for incubation of HFIP.
2. Fill the solution into a burette and drip (drop speed of approximately 0.5 mL/min) into 300 mL ultrapure water under strong stirring at 13,000 rpm using the IKA<sup>®</sup> ULTRA TURRAX<sup>®</sup> (T-25 basic).
3. Remove large aggregates of the precipitated polymer by passing the liquid through a Rotilabo<sup>®</sup>-folded filter (type 600P).
4. Remove HFIP from the NP suspension using a rotary evaporator at 190 mbar and 50°C for approximately 1 h. Continue until the volume is reduced to a third of the initial volume.
5. Determine the PET NP concentration gravimetrically. Centrifuge 6 mL of suspension at room temperature and  $17,000 \times g$  for >5 min and dry the resulting pellet using a SpeedVac or by incubation at 50°C for 24 h.
6. Determine the mass of the PET nanoparticle pellet and calculate the concentration of the original suspension in mg/mL.

### 5.2 PET NP characterization

#### 5.2.1 Analysis of particle size and morphology by SEM

1. Prepare PET NP samples for SEM by diluting the PET NP suspension with ethanol (1:1).
2. Spread the suspension on a silicon wafer and leave to dry at room temperature for 24 h.
3. Mount the SEM samples on a sample holder using metal clamps.
4. Transfer the sample holder to the sputter system.

5. Apply a sputtered layer of chromium (30 nm) to ensure conductivity of the sample.
6. Transfer the sample holder to the SEM system.
7. SEM is then carried out under vacuum at different magnifications.

### 5.2.2 Analysis of particle size distribution by DLS

1. Fill a disposable cuvette (5 mL) with 2.5 mL of the PET NP suspension and mount the cuvette in the measurement system.
2. Particle size is determined following the software instructions using standard settings for DLS. Particle size can be measured based on the hydrodynamic radius, which can be calculated from the light scattering of the used laser light.
3. Use the dip cell unit (cuvette cap with two electrodes) on the cuvette in the measurement system, so that zeta potential measurements can be carried out.
4. Zeta potential is determined following the software instructions using standard settings. The zeta potential can be measured using the same solution applying the principle of ELS via the electrophoretic mobility in an applied electrical field, using the Laser-Doppler effect.

## 5.3 Protein production

The ZYM-5052 autoinduction medium (Studier, 2005) for protein production by autoinduction consists of the following components: 1% tryptone, 0.5% yeast extract, 25 mM Na<sub>2</sub>HPO<sub>4</sub>, 25 mM KH<sub>2</sub>PO<sub>4</sub>, 50 mM NH<sub>4</sub>Cl, 5 mM Na<sub>2</sub>SO<sub>4</sub>, 0.5% glycerol, 0.05% glucose, 0.2%  $\alpha$ -lactose and 2 mM MgSO<sub>4</sub>.

The recombinant expression of desired enzymes in *E. coli* BL21(DE3) is performed in ZYM-5052 autoinduction medium at 21°C for 23 h.

1. Transform the gene of interest into competent *E. coli* BL21(DE3) using either chemically competent or electrocompetent cells.
2. Add the appropriate amount of antibiotics to the ZYM-5052 medium and transfer 1 mL of medium to every well of the 96-deep-well plate.
3. Using a toothpick or colony-picking robot, transfer freshly transformed colonies from the LB-agar plate to the medium in the wells.
4. Incubate the 96-deep-well plate in an incubation shaker at 250 rpm and 21°C for 23 h.
5. Harvest *E. coli* cells by centrifugation at 3600  $\times$  g for 30 min.

The *E. coli* BL21(DE3) cells are disrupted by repeated freeze–thaw cycles (Johnson & Hecht, 1994).

1. Freeze the 96-deep-well plate containing the cell pellets at  $-80^{\circ}\text{C}$  for 30 min.
2. Incubate the plate in ice water for 10 min to thaw.
3. Repeat steps 1 and 2 three times.
4. Resuspend lysed cell pellets in 250  $\mu\text{L}$  of 50 mM sodium phosphate (pH 8.0).
5. Incubate cell suspensions at 100 rpm for 30 min at room temperature to allow the release of recombinant enzymes.
6. Centrifuge the 96-deep-well plate at  $3600 \times g$  and  $4^{\circ}\text{C}$  for 30 min to separate the insoluble debris from the soluble fraction containing recombinant enzymes.

## 5.4 Enzymatic degradation of PET NP

The enzymatic degradation of PET NP is performed in 96-well microtiter plates shaken at 900 rpm and  $60^{\circ}\text{C}$ . Recombinant TfCut2 and an inactive S130A variant are used as positive and negative controls, respectively. The reaction temperature and the duration of incubation should be adapted with respect to the optimal temperature of the applied enzyme (in the case of metagenome screening, use a temperature matching the desired properties of the polyester hydrolase to be found).

1. Mix 10  $\mu\text{L}$  of a 1 mg/mL PET NP solution (10  $\mu\text{g}$ ) with 40  $\mu\text{L}$  of 500 mM sodium phosphate (final concentration 100 mM, pH 8.0) and 50  $\mu\text{L}$  ultrapure water.
2. Incubate the assay mixture with 100  $\mu\text{L}$  crude cell lysate (final volume 200  $\mu\text{L}$ ) at  $60^{\circ}\text{C}$  for 30 and 60 min in a microtiter plate shaker (900 rpm).
3. Stop the degradation reaction by centrifugation at  $2844 \times g$  and  $4^{\circ}\text{C}$  for 15 min to remove the (precipitated) protein and unhydrolyzed NP.
4. Remove the soluble supernatant to determine the amount of degradation products using the fluorimetric HTS assay and RP-HPLC.

## 5.5 Quantification of the PET degradation products

### 5.5.1 Fluorimetric HTS assay

The emission and excitation maxima of the fluorescent product 2-HOTP are determined using a commercial standard. All measurements should be taken at least in triplicate.

1. Dissolve 1.82 mg 2-HOTP in 1 mL 100 mM sodium hydroxide to produce a 10 mM stock solution.

2. Prepare a 2-HOTP standard by diluting the 10 mM stock solution in ultrapure water to a final concentration of 100  $\mu\text{M}$ .
3. Mix 10  $\mu\text{L}$  of the 2-HOTP (100  $\mu\text{M}$ ) with 40  $\mu\text{L}$  of 500 mM sodium phosphate (pH 8.0, final buffer concentration of 100 mM) and 150  $\mu\text{L}$  ultrapure water in a black FLUOTRAC™ 96-well microtiter plate (final volume of 200  $\mu\text{L}$  in each well).
4. Determine the excitation maximum by recording fluorescence emission at 421 nm while scanning excitation wavelengths between 200 and 403 nm using a Varioskan LUX microtiter plate reader.
5. Determine the emission maximum by recording fluorescence emission between 346 and 600 nm while exciting the sample at 315 nm using a Varioskan LUX microtiter plate reader.

The fluorimetric HTS assay is performed in black FLUOTRAC™ 96-well microtiter plates at 25°C in a Varioskan LUX microtiter plate spectrophotometer.

6. Dissolve 16.6 mg TPA in 10 mL 100 mM sodium hydroxide to produce a 10 mM terephthalate stock solution
7. Prepare a terephthalate standard series by diluting the stock solution in ultrapure water to a final concentration in the range of 0–200  $\mu\text{M}$
8. Incubate 120  $\mu\text{L}$  crude cell lysates at the desired reaction temperature for the same duration to resemble the degradation reaction without the addition of PET NPs in a microtiter plate shaker
9. Mix 10  $\mu\text{L}$  of the terephthalate standard solutions with 40  $\mu\text{L}$  of 500 mM sodium phosphate (pH 8.0) and 100  $\mu\text{L}$  soluble supernatant (step 8) in a black FLUOTRAC™ 96-well microtiter plate (final volume of 150  $\mu\text{L}$  in each well)
10. Initiate hydroxylation of terephthalate by adding 25  $\mu\text{L}$  of 5 mM EDTA and 25  $\mu\text{L}$  of 5 mM  $\text{Fe(II)SO}_4$  (final concentration of 625  $\mu\text{M}$   $\text{Fe(II)-EDTA}$ ) and incubating for at least 10 min at room temperature
11. Measure the fluorescence emission at 421 nm upon excitation at 315 nm using the microtiter plate reader
12. Plot the fluorescence obtained in step 11 against the terephthalate concentrations applied to obtain a calibration curve
13. Similarly as described above in step 9, mix 150  $\mu\text{L}$  of the reaction supernatant following the enzymatic hydrolysis of PET NP instead of the terephthalate standard solution to perform the fluorimetric determination from steps 9 to 11 and estimate the amount of terephthalate based on the calibration curves obtained in step 12.

### 5.5.2 RP-HPLC

1. Separate the degradation products on a Kinetex<sup>®</sup> (5  $\mu$ M EVO C18 100  $\text{\AA}$ , 150  $\times$  4.6 mm) column by injecting 10  $\mu$ L sample.
2. Use 0.1% (v/v) formic acid in water (A) and acetonitrile (B) as mobile phases. Run a gradient from 5% to 44% (B) over 12 min, then increase to 70% (B) over 3 min. Use a flow rate of 0.8 mL/min.
3. Detect the amounts of UV-absorbing compounds by measuring absorbance at 240 nm.

## Acknowledgments

The authors acknowledge the financial support received from the European Union's Horizon 2020 research and innovation program under the grant agreement 870294 (MIX-UP project). The authors would like to thank the analytical team of the IOM (Andrea Prager, Nadja Schönherr, and Ingrid Reinhard) for their contributions to the analysis of PET NPs.

## References

- Barth, M., Oeser, T., Wei, R., Then, J., Schmidt, J., & Zimmermann, W. (2015). Effect of hydrolysis products on the enzymatic degradation of polyethylene terephthalate nanoparticles by a polyester hydrolase from *Thermobifida fusca*. *Biochemical Engineering Journal*, *93*, 222–228.
- Berkowitz, S. (1984). Viscosity–molecular weight relationships for poly(ethylene terephthalate) in hexafluoroisopropanol–pentafluorophenol using SEC–LALLS. *Journal of Applied Polymer Science*, *29*, 4353–4361.
- Bornscheuer, U. T. (2016). Feeding on plastic. *Science*, *351*, 1154–1155.
- Cho, E., Choi, J., Jo, S., Park, D.-H., Hong, Y. K., Kim, D., et al. (2019). A single-benzene-based fluorophore: Optical waveguiding in the crystal form. *ChemPlusChem*, *84*, 1130.
- Danso, D., Schmeisser, C., Chow, J., Zimmermann, W., Wei, R., Leggewie, C., et al. (2018). New insights into the function and global distribution of polyethylene terephthalate (PET)-degrading bacteria and enzymes in marine and terrestrial metagenomes. *Applied and Environmental Microbiology*, *84*, e02773–17.
- Eberl, A., Heumann, S., Brückner, T., Araujo, R., Cavaco-Paulo, A., Kaufmann, F., et al. (2009). Enzymatic surface hydrolysis of poly(ethylene terephthalate) and bis (benzoyloxyethyl) terephthalate by lipase and cutinase in the presence of surface active molecules. *Journal of Biotechnology*, *143*, 207–212.
- Eriksen, M., Lebreton, L. C. M., Carson, H. S., Thiel, M., Moore, C. J., Borerro, J. C., et al. (2014). Plastic pollution in the world's oceans: More than 5 trillion plastic pieces weighing over 250,000 tons afloat at sea. *PLoS One*, *9*, e111913.
- Geyer, R., Jambeck, J. R., & Law, K. L. (2017). Production, use, and fate of all plastics ever made. *Science Advances*, *3*, e1700782.
- Herrero Acero, E., Ribitsch, D., Steinkellner, G., Gruber, K., Greimel, K., Eiteljoerg, I., et al. (2011). Enzymatic surface hydrolysis of PET: Effect of structural diversity on kinetic properties of cutinases from *Thermobifida*. *Macromolecules*, *44*, 4632–4640.
- Johnson, B. H., & Hecht, M. H. (1994). Recombinant proteins can be isolated from *E. coli* cells by repeated cycles of freezing and thawing. *Nature Biotechnology*, *12*, 1357–1360.

- Kawai, F., Kawabata, T., & Oda, M. (2019). Current knowledge on enzymatic PET degradation and its possible application to waste stream management and other fields. *Applied Microbiology and Biotechnology*, *103*, 4253–4268.
- Kawai, F., Kawabata, T., & Oda, M. (2020). Current state and perspectives related to the polyethylene terephthalate hydrolases available for biorecycling. *ACS Sustainable Chemistry & Engineering*, *8*, 8894–8908.
- Lehner, R., Weder, C., Petri-Fink, A., & Rothen-Rutishauser, B. (2019). Emergence of nanoplastic in the environment and possible impact on human health. *Environmental Science & Technology*, *53*, 1748–1765.
- Liu, J., Ma, Y., Zhu, D., Xia, T., Qi, Y., Yao, Y., et al. (2018). Polystyrene nanoplastics-enhanced contaminant transport: Role of irreversible adsorption in glassy polymeric domain. *Environmental Science & Technology*, *52*, 2677–2685.
- Müller, R.-J., Schrader, H., Profe, J., Dresler, K., & Deckwer, W.-D. (2005). Enzymatic degradation of poly(ethylene terephthalate): Rapid hydrolyse using a hydrolase from *T. fusca*. *Macromolecular Rapid Communications*, *26*, 1400–1405.
- O'Neill, A., & Cavaco-Paulo, A. (2004). Monitoring biotransformations in polyesters. *Biocatalysis and Biotransformation*, *22*, 353–356.
- Palm, G. J., Reisky, L., Böttcher, D., Müller, H., Michels, E. A. P., Walczak, M. C., et al. (2019). Structure of the plastic-degrading *Ideonella sakaiensis* MHETase bound to a substrate. *Nature Communications*, *10*, 1717.
- PlasticsEurope. Plastics—the Facts. (2019). An analysis of European plastics production. In *Demand and waste data*. <https://www.plasticseurope.org/en/resources/publications/1804-plastics-facts-2019>.
- Rahimi, A., & García, J. M. (2017). Chemical recycling of waste plastics for new materials production. *Nature Reviews Chemistry*, *1*, 0046.
- Rochman, C. M., Hoh, E., Kurobe, T., & Teh, S. J. (2013). Ingested plastic transfers hazardous chemicals to fish and induces hepatic stress. *Scientific Reports*, *3*, 3263.
- Rodríguez-Hernández, A. G., Muñoz-Tabares, J. A., Aguilar-Guzmán, J. C., & Vazquez-Duhalt, R. (2019). A novel and simple method for polyethylene terephthalate (PET) nanoparticle production. *Environmental Science: Nano*, *6*, 2031–2036.
- Ronkvist, Å. M., Xie, W., Lu, W., & Gross, R. A. (2009). Cutinase-catalyzed hydrolysis of poly(ethylene terephthalate). *Macromolecules*, *42*, 5128–5138.
- Saran, M., & Summer, K. H. (1999). Assaying for hydroxyl radicals: Hydroxylated terephthalate is a superior fluorescence marker than hydroxylated benzoate. *Free Radical Research*, *31*, 429–436.
- Silva, C., Da, S., Silva, N., Matamá, T., Araújo, R., Martins, M., et al. (2011). Engineered *Thermobifida fusca* cutinase with increased activity on polyester substrates. *Biotechnology Journal*, *6*, 1230–1239.
- Studier, F. W. (2005). Protein production by auto-induction in high density shaking cultures. *Protein Expression and Purification*, *41*, 207–234.
- Sulaiman, S., Yamato, S., Kanaya, E., Kim, J.-J., Koga, Y., Takano, K., et al. (2012). Isolation of a novel cutinase homolog with polyethylene terephthalate-degrading activity from leaf-branch compost by using a metagenomic approach. *Applied and Environmental Microbiology*, *78*, 1556–1562.
- Sulaiman, S., You, D.-J., Kanaya, E., Koga, Y., & Kanaya, S. (2014). Crystal structure and thermodynamic and kinetic stability of metagenome-derived LC-cutinase. *Biochemistry*, *53*, 1858–1869.
- Tournier, V., Topham, C. M., Gilles, A., David, B., Folgoas, C., Moya-Leclair, E., et al. (2020). An engineered PET depolymerase to break down and recycle plastic bottles. *Nature*, *580*, 216–219.
- Vogel, K., Wei, R., Al-Fatih, H., Pfaff, L., Ortmann, C., Estrela-Lopis, I., et al. (2020). Enzymatic degradation of polyethylene terephthalate nanoplastics analyzed in real time by isothermal titration calorimetry. submitted.

- Vollmer, I., Jenks, M. J. F., Roelands, M. C. P., White, R. J., van Harmelen, T., de Wild, P., et al. (2020). Beyond mechanical recycling: Giving new life to plastic waste. *Angewandte Chemie, International Edition*, *59*, 15402–15423.
- Wagner, S., & Reemtsma, T. (2019). Things we know and don't know about nanoplastic in the environment. *Nature Nanotechnology*, *14*, 300–301.
- Weber, J., Petrović, D., Strodel, B., Smits, S. H. J., Kolkenbrock, S., Leggewie, C., et al. (2019). Interaction of carbohydrate-binding modules with poly(ethylene terephthalate). *Applied Microbiology and Biotechnology*, *103*, 4801–4812.
- Wei, R., Breite, D., Song, C., Gräsing, D., Ploss, T., Hille, P., et al. (2019). Biocatalytic degradation efficiency of postconsumer polyethylene terephthalate packaging determined by their polymer microstructures. *Advanced Science*, *6*, 1900491.
- Wei, R., Oeser, T., Barth, M., Weigl, N., Lübs, A., Schulz-Siegmund, M., et al. (2014). Turbidimetric analysis of the enzymatic hydrolysis of polyethylene terephthalate nanoparticles. *Journal of Molecular Catalysis B: Enzymatic*, *103*, 72–78.
- Wei, R., Oeser, T., Billig, S., & Zimmermann, W. (2012). A high-throughput assay for enzymatic polyester hydrolysis activity by fluorimetric detection. *Biotechnology Journal*, *7*, 1517–1521.
- Wei, R., Oeser, T., Then, J., Kühn, N., Barth, M., Schmidt, J., et al. (2014). Functional characterization and structural modeling of synthetic polyester-degrading hydrolases from *Thermomonospora curvata*. *AMB Express*, *4*, 44.
- Wei, R., Oeser, T., & Zimmermann, W. (2014). Synthetic polyester-hydrolyzing enzymes from thermophilic actinomycetes. *Advances in Applied Microbiology*, *89*, 267–305.
- Wei, R., Song, C., Gräsing, D., Schneider, T., Bielytskiy, P., Böttcher, D., et al. (2019). Conformational fitting of a flexible oligomeric substrate does not explain the enzymatic PET degradation. *Nature Communications*, *10*, 5581.
- Wei, R., Tiso, T., Bertling, J., O'Connor, K., Blank, L. M., & Bornscheuer, U. T. (2020). Possibilities and limitations of biotechnological plastic degradation and recycling. *Nature Catalysis*, *3*, 867–871.
- Wei, R., & Zimmermann, W. (2017). Biocatalysis as a green route for recycling the recalcitrant plastic polyethylene terephthalate. *Microbial Biotechnology*, *10*, 1302–1307.
- Welch, K. D., Davis, T. Z., & Aust, S. D. (2002). Iron autoxidation and free radical generation: Effects of buffers, ligands, and chelators. *Archives of Biochemistry and Biophysics*, *397*, 360–369.
- Welzel, K., Müller, R.-J., & Deckwer, W.-D. (2002). Enzymatischer Abbau von Polyester-Nanopartikeln. *Chemie Ingenieur Technik*, *74*, 1496–1500.
- Wright, S. L., & Kelly, F. J. (2017). Plastic and human health: A micro issue? *Environmental Science & Technology*, *51*, 6634–6647.
- Yang, X. F., & Guo, X. Q. (2001). Fe(II)-EDTA chelate-induced aromatic hydroxylation of terephthalate as a new method for the evaluation of hydroxyl radical-scavenging ability. *The Analyst*, *126*, 928–932.
- Yoshida, S., Hiraga, K., Takehana, T., Taniguchi, I., Yamaji, H., Maeda, Y., et al. (2016). A bacterium that degrades and assimilates poly(ethylene terephthalate). *Science*, *351*, 1196–1199.

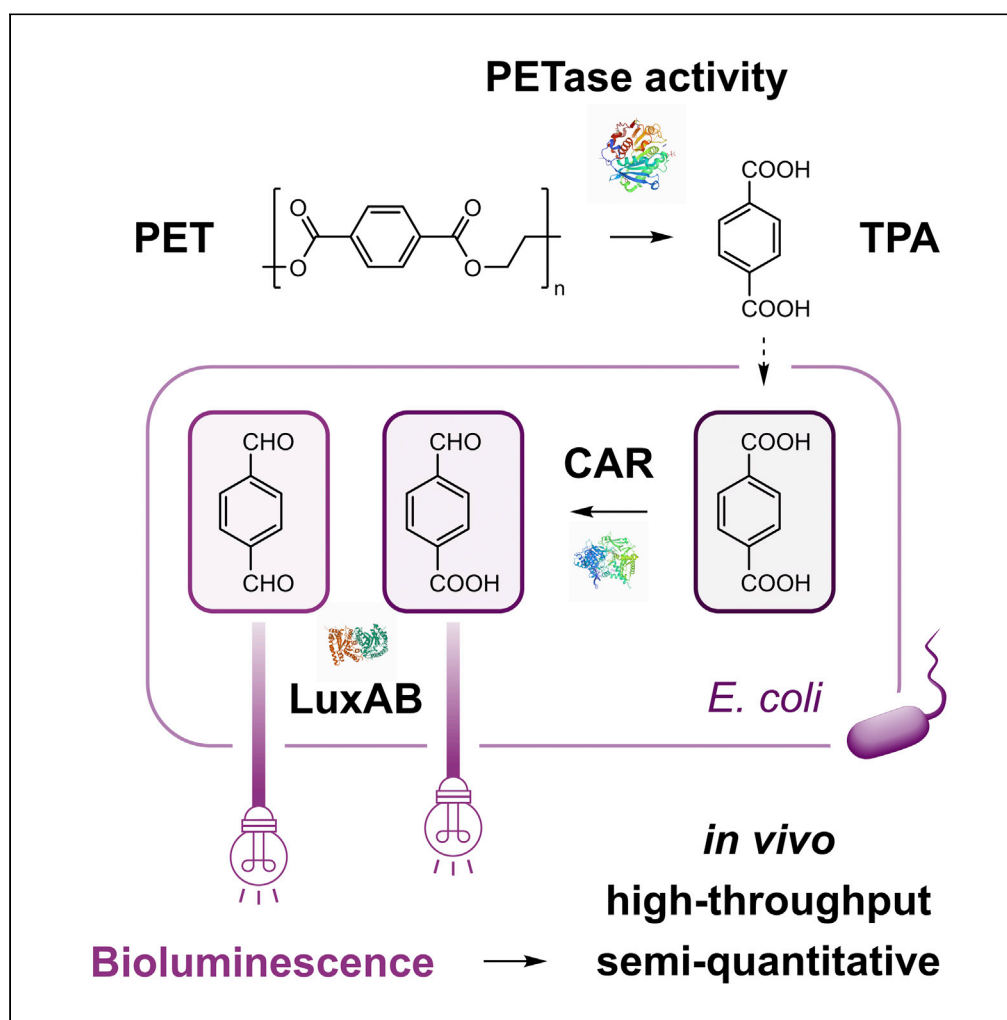


## **Article IV**



Article

Biosensor and chemo-enzymatic one-pot cascade applications to detect and transform PET-derived terephthalic acid in living cells



Thomas Bayer,  
Lara Pfaff, Yannick  
Branson, Aileen  
Becker, Shuke Wu,  
Uwe T.  
Bornscheuer, Ren  
Wei

thomas.bayer@uni-greifswald.  
de (T.B.)  
ren.wei@uni-greifswald.de  
(R.W.)

**Highlights**

First bio-reduction of  
terephthalic acid (TPA) by  
a carboxylic acid  
reductase *in vivo*

Real-time, high-  
throughput detection of  
TPA-derived aldehydes by  
luciferase LuxAB

Bioluminescence reflects  
TPA amounts, assessing  
(engineered) PET  
hydrolase activity

Transformation of TPA  
into the diamine through  
chemo-enzymatic one-pot  
cascade

Bayer et al., iScience 25,  
104326  
May 20, 2022 © 2022 The  
Authors.  
[https://doi.org/10.1016/  
j.isci.2022.104326](https://doi.org/10.1016/j.isci.2022.104326)



## Article

## Biosensor and chemo-enzymatic one-pot cascade applications to detect and transform PET-derived terephthalic acid in living cells

Thomas Bayer,<sup>1,2,4,\*</sup> Lara Pfaff,<sup>1</sup> Yannick Branson,<sup>1</sup> Aileen Becker,<sup>1</sup> Shuke Wu,<sup>1,3</sup> Uwe T. Bornscheuer,<sup>1</sup> and Ren Wei<sup>1,\*</sup>

## SUMMARY

Plastic waste imposes a serious problem to the environment and society. Hence, strategies for a circular plastic economy are demanded. One strategy is the engineering of polyester hydrolases toward higher activity for the biotechnological recycling of polyethylene terephthalate (PET). To provide tools for the rapid characterization of PET hydrolases and the detection of degradation products like terephthalic acid (TPA), we coupled a carboxylic acid reductase (CAR) and the luciferase LuxAB. CAR converted TPA into the corresponding aldehydes in *Escherichia coli*, which yielded bioluminescence that not only semiquantitatively reflected amounts of TPA in hydrolysis samples but is suitable as a high-throughput screening assay to assess PET hydrolase activity. Furthermore, the CAR-catalyzed synthesis of terephthalaldehyde was combined with a reductive amination cascade in a one-pot setup yielding the corresponding diamine, suggesting a new strategy for the transformation of TPA as a product obtained from PET biodegradation.

## INTRODUCTION

The global production of plastics is rapidly increasing. More than 8% of the global petrochemical production – 4% as source for materials and 4% to cover energy demands – were consumed by plastic manufacturing industries (Hopewell et al., 2009). However, only a fraction of discarded plastic is recycled (Geyer et al., 2017). Consequently, efficient disposal and sustainable recycling strategies for plastic waste are urgently needed to reduce the risk of pollution imposed on ecosystems and human health (Eriksen et al., 2014; Rahimi and Garcia, 2017; Vollmer et al., 2020; Wright and Kelly, 2017). Furthermore, to decrease both carbon dioxide (CO<sub>2</sub>) emissions and the dependence on fossil fuel-based resources, a circular plastic economy is regarded as the central – and vital – approach (Raoul et al., 2021; Sarah and Gloria, 2021; Simon et al., 2021; Wei et al., 2020).

Particularly, the biocatalysis-based recycling of polyethylene terephthalate (PET), which is extensively used to manufacture food packaging and beverage containers, has become a vivid field of research with the discovery of microbial PET-degrading enzymatic activities (Kawai et al., 2019, 2020; Tournier et al., 2020; Wei et al., 2020, 2022; Yoshida et al., 2016). So far, PET hydrolases from actinomycetes including different *Thermobifida* strains (Herrero Acero et al., 2011; Müller et al., 2005; Wei et al., 2014), from the bacterium *Ideonella sakaiensis* (Yoshida et al., 2016), and a commercial cutinase from the fungi *Thermomyces insolens*, formerly known as *Humicola insolens*, have been employed (Ronkvist et al., 2009). Recently, a variant of the compost metagenome-derived and highly thermostable leaf-branch compost cutinase (LCC) (Sulaiman et al., 2012) was engineered toward increased PET-hydrolyzing activity, which pushed the enzymatic depolymerization of PET from laboratory scales to industrially relevant metrics by degrading amorphized (i.e., pretreated) postconsumer PET bottles in only 10 h reaction time (Tournier et al., 2020). This and the fact that LCC as well as other PET hydrolases were found in public metagenome databases will certainly advance biotechnological plastic degradation and recycling in the near future (Bornscheuer, 2016; Danso et al., 2018; Wei et al., 2020, 2022).

Despite the many achievements in the last two decades, the activity of PET hydrolases is still assessed by simply measuring the weight loss of the residual bulk PET polymer after depolymerization (Wei et al., 2019a, 2019b; Yoshida et al., 2016) or the chromatographic analysis and quantification of degradation intermediates and/or products such as terephthalic acid (TPA) and its monoesters and diesters (Eberl et al., 2009; Herrero Acero et al., 2011; Palm et al., 2019). Recently, an isothermal titration

<sup>1</sup>Institute of Biochemistry, Department of Biotechnology & Enzyme Catalysis, University of Greifswald, Felix-Hausdorff-Straße 4, 17487 Greifswald, Germany

<sup>2</sup>Institute of Molecular Biotechnology, TU Graz, Petersgasse 14, 8010 Graz, Austria

<sup>3</sup>College of Life Science & Technology, Huazhong Agricultural University, Shizishan Street 1, Wuhan 430070, China

<sup>4</sup>Lead contact

\*Correspondence: thomas.bayer@uni-greifswald.de (T.B.), ren.wei@uni-greifswald.de (R.W.)

<https://doi.org/10.1016/j.isci.2022.104326>



calorimetry-based method has been established for directly assessing the enthalpy of ester hydrolysis, thus enabling a real-time monitoring of the enzymatic PET hydrolysis (Vogel et al., 2021). All these strategies suffer from laborious sample preparation and the only low to moderate sample throughput, impeding the characterization of novel biocatalysts – not only limited to polyester hydrolases – and the screening of large protein libraries (Markel et al., 2020; Wei et al., 2020, 2022; Yi et al., 2021). This obstacle was addressed by a Fenton chemistry-mediated fluorometric detection assay for TPA in a 96-well microtiter plate format, suitable for high-throughput (HT) screening applications (Pfaff et al., 2021; Wei et al., 2012). The assay is based on the formation of hydroxyl radicals mediated by an Fe(II)-ethylenediaminetetraacetic acid complex in the presence of molecular oxygen (O<sub>2</sub>) (Saran and Sumner, 1999; Wei et al., 2012; Welch et al., 2002); hydroxyl radicals and TPA then react to the fluorescent 2-hydroxyterephthalate ( $\lambda_{\text{excitation}} = 315 \text{ nm}$ ,  $\lambda_{\text{emission}} = 421 \text{ nm}$ ).

Complementary, genetically encoded biosensor systems have been used for the detection of small molecules and included transcription factors (TFs), riboswitches, or enzyme-coupled sensor devices (Bayer et al., 2021; Dietrich et al., 2010; Lehtinen et al., 2017; Liu et al., 2015, 2017; Yi et al., 2021). To date, only two biosensors have been reported to detect TPA *in vivo*. The first was assembled by Pardo et al. and comprised the TF TphR and its regulatory nucleotide sequences from *Comamonas testosteroni* and the superfolder green fluorescent protein (sfGFP) (Pardo et al., 2020). TphR is a transcriptional activator, which – upon binding of TPA – acts as the inducer of a gene cluster responsible for the conversion of TPA to protocatechuate in *Comamonas* strains (Kasai et al., 2010). Their TF-based biosensor system facilitated the screening of TPA transporter variants, in other words, the improved uptake of TPA from the environment in *Acinetobacter baylyi* ADP1 through fluorescence-activated cell sorting (Pardo et al., 2020). The second example featured sfGFP as the fluorescence reporter and the promiscuous TF XylS from *Pseudomonas putida*, which was engineered by Li and coworkers to bind TPA additionally to reported benzoic acid derivatives (Li et al., 2022). With the efficient detection of TPA in living cells, these sensing devices have yet to be tested for the directed evolution of PET hydrolases by the HT-assisted detection of TPA as PET degradation product.

Most recently, the luciferase LuxAB from *Photobacterium luminescens* (*P. luminescens*) was introduced for the detection of structurally diverse aldehydes in *Escherichia coli* (*E. coli*) (Bayer et al., 2021). In the present work, the carboxylic acid reductase from *Mycobacterium marinum* (CAR<sub>Mm</sub>) was shown to transform TPA into the corresponding aldehydes 4-carboxybenzaldehyde (4-CBAL) and terephthalaldehyde (TAL) *in vivo* (Figure 1). The coupling of the enzymatic reduction to the LuxAB biosensor device yielded bioluminescence that semiquantitatively reflected increasing amounts of TPA in PET hydrolysis samples obtained through various hydrolases. The system not only provides a biosensor-based HT assay for TPA but the first biocatalytic route toward highly reactive TPA-derived aldehydes such as TAL, avoiding hazardous chemical procedures (Barnicki, 2017; Snell and Weissberger, 1940). Following the transformation of TAL in the same reaction vessel, the corresponding diamine was yielded and will allow for potential industrial applications (Brindell et al., 1976; Rohan et al., 2015; Suematsu et al., 1983; Wang et al., 2021).

## RESULTS

### Optimization of whole-cell biotransformations and evaluation of HT assay conditions

In a previous study, the monooxygenase LuxAB from *P. luminescens* was expressed in *E. coli* K-12 MG1655 RARE (Kunjapur et al., 2014), herein referred to as *E. coli* RARE, and provided a reliable detection tool for aldehydes in living cells in a 96-well microplate format (Bayer et al., 2021), importantly, beyond the previously reported long-chain aliphatic aldehydes (Colepiccolo et al., 1989). Furthermore, LuxAB was suitable to sense aldehydes, including aromatic products such as benzaldehyde, cuminaldehyde, and 2-phenylacetaldehyde that were enzymatically produced from carboxylic acid substrates by the co-expression of CAR<sub>Mm</sub> in the same cell (Bayer et al., 2021). Prompted by the structural relatedness of these aromatic aldehydes to TPA-derived aldehydes, the capabilities of (1) CAR<sub>Mm</sub> – to reduce one or both carboxylic acid functionalities of TPA to the aldehyde – and (2) LuxAB – to accept aldehyde products formed *in situ*, thereby yielding bioluminescence – were investigated.

Therefore, chemically competent *E. coli* BL21(DE3) cells were transformed with pACYCDuet-1/*car<sub>Mm</sub>:ppt<sub>Ni</sub>* to co-express CAR<sub>Mm</sub> and a phosphopantetheinyl transferase from *Nocardia iowensis* (PPT<sub>Ni</sub>) (Bayer et al., 2021). The PPT is required to posttranslationally modify apoCARs to yield the functional holo-CAR enzymes (Akhtar et al., 2013; Finnigan et al., 2017; Horvat and Winkler, 2020). Whereas TPA was not converted in resting cells (RCs) of untransformed *E. coli*, the detection of 4-(hydroxymethyl) benzaldehyde (4-HMBAL) and 1,4-benzenedimethanol (1,4-BDM; 32.7 ± 3.5% combined yields) by gas chromatography equipped

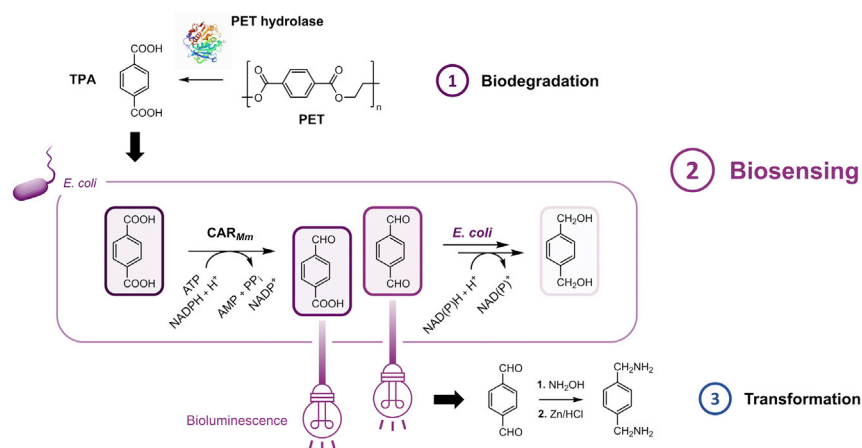


**Figure 1. Enzyme-coupled biosensor for the detection of TPA in *E. coli***

(1) The biocatalytic degradation of PET by hydrolases releases monomeric molecules including TPA and ethylene glycol (not shown). The PET hydrolase structure in the scheme was adapted from PDB: 6THT (Tournier et al., 2020). (2) TPA can be reduced to the corresponding dialdehydes and monoaldehydes by  $CAR_{Mm}$  (accessory  $PPT_{Ni}$  not shown). These aldehydes are sensed by LuxAB, thereby emitting bioluminescence. Endogenous enzymes further reduce aldehydes to the corresponding primary alcohols. (3) The reactive TAL can be captured as aldoxime (not shown) and further converted to the diamine by reductive amination and basic work-up in a one-pot cascade, interconverting polymer precursors as future upcycling option after further optimization.

with a flame ionization detector (GC/FID) indicated both the activity of  $CAR_{Mm}$  toward TPA and the further reduction of aldehydes by endogenous host enzymes (Figure 1 and Table 1) (Bayer et al., 2017; Kunjapur et al., 2014; Kunjapur and Prather, 2015). However, biotransformation mixtures contained up to 75% unreacted TPA besides the over-reduced products after 24 h (Figure S1A). Although a similar conversion of TPA was achieved with RCs of *E. coli* RARE (Figure S1B), the utilization of *E. coli* BL21(DE3)  $\Delta lpp$  enhanced the bioreduction of TPA significantly (Figure 2A). RCs of the engineered strain harboring  $pACYCDuet-1/car_{Mm}:ppt_{Ni}$  were prepared and biotransformations were carried out as outlined below. The resulting suspension contained a mixture of TPA ( $31.1 \pm 5.9\%$ ), 4-CBAL ( $36.8 \pm 9.9\%$ ), 4-HMBAL ( $6.5 \pm 2.2\%$ ), and 1,4-BDM ( $13.7 \pm 5.7\%$ ) according to GC/FID (Figure 2A); the highly reactive TAL could only be detected in traces. The nonessential *lpp* gene encodes one of the most abundant cellular proteins in terms of copy number (Li et al., 2014) and controls the (mechanical) properties of the inner and outer membrane (Asmar et al., 2017; Mathelié-Guinlet et al., 2020). Not only was its deletion suggested to affect the permeability of the cellular envelope for small molecules (Ni et al., 2007); it increased expression levels of  $CAR_{Mm}$  according to sodium dodecyl sulfate-polyacrylamide gel electrophoresis (SDS-PAGE) analysis (Figure S2). This may be explained by the reallocation of cellular resources (Li et al., 2014) and might provide a general approach to improve heterologous protein production.

Subsequently, RCs of *E. coli* BL21(DE3)  $\Delta lpp$  as well as *E. coli* RARE were prepared either expressing only LuxAB or the luciferase together with  $CAR_{Mm}/PPT_{Ni}$ . *E. coli* RARE exhibits reduced aromatic aldehyde-reducing activity (Kunjapur et al., 2014) and has been employed by various groups to increase the persistence of aldehydes for both their production *in vivo* (Bayer et al., 2017; Horvat and Winkler, 2020; Kunjapur et al., 2016) and their efficient detection (Bayer et al., 2021; Ressmann et al., 2019).

Satisfyingly, the previously established HT assay conditions yielded bioluminescence in the presence of TPA-derived aldehydes in both *E. coli* strains expressing LuxAB (Bayer et al., 2021). At 1 mM final concentration, the highest fold-increase in bioluminescence was observed in the presence of 4-CBAL and TAL, both elevating bioluminescence about 8-fold above background in RCs of *E. coli* BL21(DE3)  $\Delta lpp$  after 15 min, followed by 4-HMBAL (4-fold) (Figure 2B). As expected, TPA did not increase bioluminescence in RCs only expressing the biosensor, but signals increased more than 4-fold when co-expressing LuxAB and  $CAR_{Mm}/PPT_{Ni}$  in the same cell (Figure 2C). Similar results were obtained with RCs of *E. coli* RARE upon the addition of TPA (Figure S3; 1 mM final concentration); to extenuate the cytotoxic effects of initially high aldehyde levels and in accordance with previous findings, 4-CBAL, TAL, and 4-HMBAL could be efficiently detected at 0.1 mM final concentration in *E. coli* RARE (Figure S3) (Bayer et al., 2021). The

**Table 1. List of compounds**

Compound (Abbreviation)	Retention time [min]	RRF
Terephthalic acid (TPA)	6.90–7.00	0.243
4-Carboxybenzaldehyde (4-CBAL)	3.70–3.80	0.297
4-(Hydroxymethyl) benzoic acid (4-HMBA)	4.14	0.216
Terephthalaldehyde (TAL)	4.23	0.932
4-(Hydroxymethyl) benzaldehyde (4-HMBAL)	5.22	1.132
1,4-Benzenedimethanol (1,4-BDM)	5.51	1.168
1,4-bis-(Aminomethyl) benzene (1,4-bis-AMB)	5.27	0.830
Benzylamine (BAM)	2.76	0.783
Methyl benzoate (IS)	3.28	–

The retention times for benzoic acid and 2-phenylacetic acid and their corresponding aldehydes and primary alcohols as well as GC/FID-based quantification were reported previously (Bayer et al., 2021). Relative response factors (RRFs) were used as mean values of independently prepared standard solutions ( $n \geq 3$ ) analyzed by GC/FID.

established reduction of 2-phenylacetic acid to 2-phenylacetaldehyde by  $CAR_{Mm}$  was included as positive control for the HT assay because the latter is accepted by LuxAB (Figure 2B–2C). DMSO slightly increased background luminescence over time, which had also been shown for other cosolvents like ethanol and acetonitrile (Bayer et al., 2021). Supporting the results of the HT assay (Figure 2C), the activity of the CAR enzyme toward 4-CBAL and 4-HMBA could be confirmed by GC/FID analysis of extracts from biotransformations employing  $CAR_{Mm}/PPT_{Ni}$  (Figures S1C–S1D).

Motivated by the functional CAR/Luciferase biosensor couple for the detection of TPA, the assay was tested with hydrolysate samples obtained after the enzymatic degradation of PET.

### Assaying TPA in PET hydrolysis samples under HT conditions

For the preparation of PET hydrolysates, the codon-optimized genes of LCC, the engineered variant LCC-ICCG (Tournier et al., 2020), and the polyester hydrolase-1 (PES-H1) (Zimmermann et al., 2019) were expressed from pET26b vectors in *E. coli* BL21(DE3) cultivated in auto-induction medium (AIM) supplemented with kanamycin and finally purified as described in this study.

The enzymatic degradation of amorphous PET film (Gf-PET, purchased from Goodfellow Ltd.) by LCC, LCC-ICCG, and PES-H1 was adapted from Tournier et al. as outlined below (Tournier et al., 2020). Hydrolysates were processed as described in this study and analyzed by the  $CAR_{Mm}/LuxAB$  biosensor system under HT conditions (Figure 3) as well as calibrated high-performance liquid chromatography (HPLC; Table S2).

In the presence of 1 mM TPA, the bioluminescence increased about 4-fold and 5-fold in RCs of *E. coli* BL21(DE3)  $\Delta lpp$  and *E. coli* RARE, respectively, after 1 h. While the fold-increase in bioluminescence plateaued in *E. coli* BL21(DE3)  $\Delta lpp$  for 4 h (Figure S4), it increased more than 17-fold in *E. coli* RARE cells during the same reaction time (Figure 3). This difference can be explained by the distinct metabolic backgrounds of the two strains as highlighted earlier. The knockout of several alcohol dehydrogenases and aldo-keto reductases in *E. coli* RARE increases the persistence of (aromatic) aldehydes *in vivo*, including TPA-derived aldehydes (Kunjapur et al., 2014). In contrast, the activity of these endogenous enzymes in *E. coli* BL21(DE3)  $\Delta lpp$  continuously reduces reactive aldehydes to the corresponding primary alcohols such as 1,4-BDM (Figure S1), which is not a substrate for LuxAB (Figure 2B).

Whereas bioluminescence signals were elevated >3-fold with PET hydrolysates obtained by the wild-type enzymes PES-H1 and LCC, bioluminescence increased >7-fold in LCC-ICCG samples after 4 h (Figure 3). This may be attributed to higher concentrations of potassium terephthalate salts in PET hydrolysates obtained by the LCC-ICCG variant compared to LCC, for example. Based on the fold-increases, TPA concentrations in the supernatants of the three hydrolysates were calculated and suggested  $38.3 \pm 3.8$  mM,  $39.3 \pm 1.3$  mM, and  $95.5 \pm 10.7$  mM for PES-H1, LCC, and LCC-ICCG, respectively. Similar TPA yields in the same concentration range (56 mM, 47 mM, and 111 mM, respectively) were determined by HPLC (Table S2).

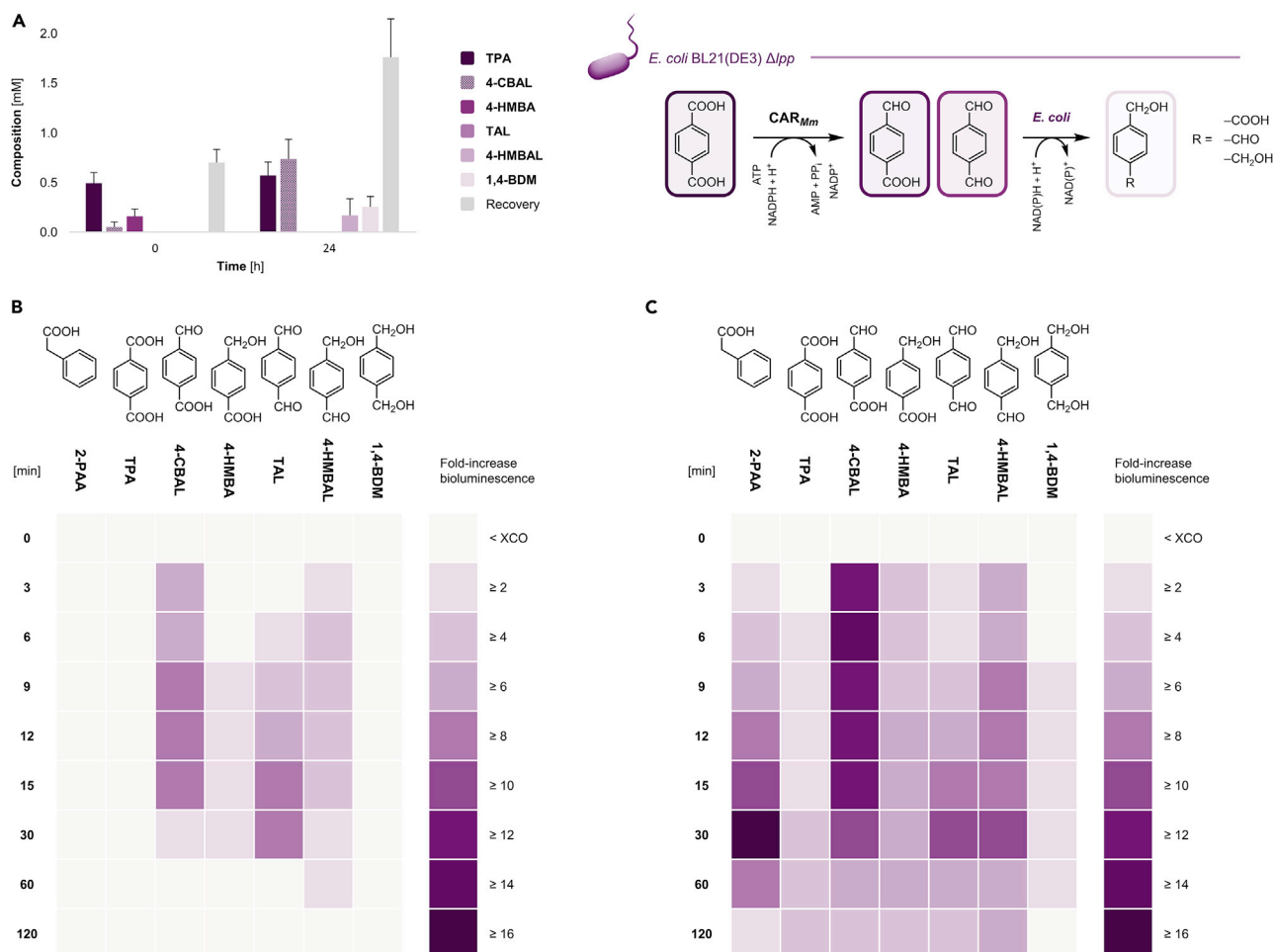


**Figure 2. Enzyme-coupled biosensor assembly in *E. coli* BL21(DE3)  $\Delta lpp$**

(A)  $CAR_{Mm}$  reduces TPA to 4-CBAL and TAL, which are further reduced to 4-HMBA, 4-HMBAL, and 1,4-BDM by endogenous enzymes *in vivo*;  $PPT_{Ni}$  for posttranslational modification of  $CAR_{Mm}$  is omitted for clarity. Experiments were performed in RCs of *E. coli* BL21(DE3)  $\Delta lpp$  ( $OD_{600} \approx 10.0$ ) co-expressing enzymes from pACYCDuet-1/ $car_{Mm};ppt_{Ni}$  (Bayer et al., 2021) in the presence of 2 mM TPA and 5% (*v/v*) DMSO as organic cosolvent. Sampling: 0 h (after the addition of TPA and mixing) and 24 h. Recoveries were reduced because of low solubility of TPA in resting cell medium (RCM) and the volatility of reaction compounds. GC yields are presented as mean values + standard deviation (SD) [mM] of biological replicates ( $n = 3$ ); see also Figure S1.

(B) Direct detection of aldehydes (1 mM) by increasing bioluminescence over time in RCs of *E. coli* BL21(DE3)  $\Delta lpp$  expressing LuxAB from pLuxAB. (C) *In situ* production of aldehydes from carboxylates (1 mM) in RCs of *E. coli* BL21(DE3)  $\Delta lpp$  co-expressing LuxAB and  $CAR_{Mm}/PPT_{Ni}$ ; 2-phenyl acetic acid (2-PAA) was used as control. Experiments were performed in the presence of 1% (*v/v*) DMSO under HT assay conditions as described previously (Bayer et al., 2021); data presented as mean fold-increase bioluminescence obtained from biological replicates ( $n = 3$ ). For results employing *E. coli* RARE, see Figure S3.

Given that the biosensor system is operating in living cells, the cytotoxicity of both carboxylates and the corresponding aldehydes (Bayer et al., 2017, 2021; Kunjapur and Prather, 2015), as well as the transient nature of bioluminescence signals (Fleiss and Sarkisyan, 2019) may interfere with the quantitative determination, allowing for marginal deviations from HPLC data. Nonetheless, the analysis of PET hydrolysates under HT conditions employing RCs of *E. coli* RARE yielded a reproducible fold-increase in bioluminescence based on the enzymatic transformation of TPA into the corresponding aldehydes and their detection by LuxAB, ultimately, reflecting TPA concentrations in PET hydrolysate samples semiquantitatively.

### Transformation of TAL by a chemo-enzymatic cascade in one pot

The chemical synthesis of (aromatic) aldehydes can be troublesome because of the high reactivity of the carbonyl group (Ferguson, 1946; Kunjapur and Prather, 2015). A promising alternative to specifically synthesize aldehydes are the well-established enzymatic reductions of carboxylates by CARs (Bayer



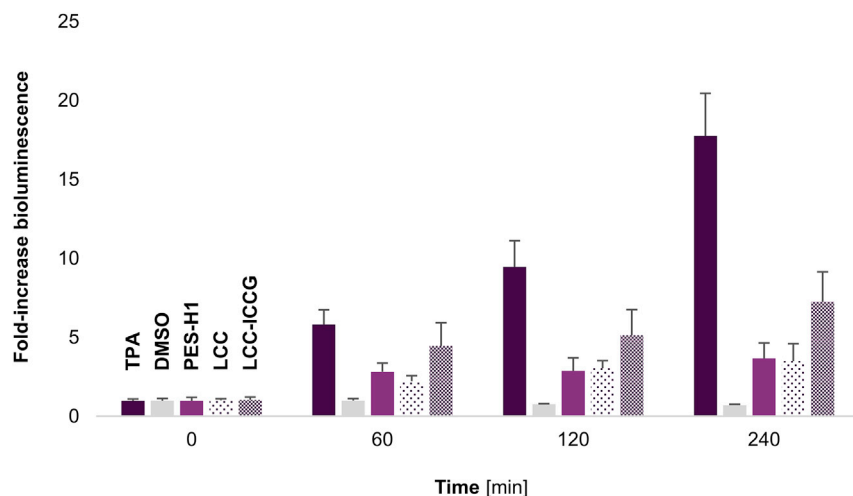


**Figure 3. PET hydrolysis samples analyzed under HT conditions in *E. coli* RARE**

The enzyme-coupled biosensor system yielded bioluminescence in the presence of 1 mM TPA (positive control) and hydrolysates obtained by the enzymatic degradation of Gf-PET films by PES-H1, LCC, and LCC-ICCG; the bioluminescence did not increase in the presence of 1% (*v/v*) DMSO over monitoring time. Experiments were performed in RCs of *E. coli* RARE under HT assay conditions as described previously (Bayer et al., 2021); data presented as mean values of the fold-increase in bioluminescence + SD of biological replicates ( $n \geq 3$ ). For results employing *E. coli* BL21(DE3)  $\Delta$ *lpp* RCs, see Figure S4.

et al., 2017, 2021; Butler and Kunjapur, 2020; Finnigan et al., 2017; Horvat and Winkler, 2020; Qu et al., 2018).  $CAR_{Mm}$  readily accepts TPA as indicated by the bioluminescence signals in the LuxAB-based HT assay (Figures 2C and S2B) and confirmed by the detection of 4-CBAL and TAL as intermediates and the corresponding over-reduced compounds 4-HMBAL and 1,4-BDM according to GC/FID. 4-HMBAL and 1,4-BDM are exclusively formed by the endogenous activities of host enzymes (Bayer et al., 2017; Kunjapur et al., 2014) (Figures 2A and S1). To the best of our knowledge, the CAR-catalyzed reduction of TPA is the first reported biocatalytic route forming TPA-derived aldehydes such as TAL, substituting hazardous chemical procedures (Snell and Weissberger, 1940). Depending on the purity and downstream application of plastic monomers from biocatalytic degradations, not all TPA is suitable for the resynthesis of virgin PET. Therefore, (bio)chemical transformation strategies for the re-use (*i.e.*, upcycling) of plastic precursors is of interest (Tiso et al., 2021). Recently, Sadler and Wallace synthesized vanillin from hydrolyzed waste PET by combining TPA-transforming enzymes from *Comamonas* sp. to yield intermediate catechol that was converted to the product by the activities of a CAR and an engineered catechol *O*-methyltransferase in *E. coli* RARE (Kunjapur and Prather, 2019; Sadler and Wallace, 2021).

In the following proof-of-concept example, benzaldehyde and TAL were produced from benzoic acid and TPA, respectively, by  $CAR_{Mm}/PPT_{Ni}$  in *E. coli* BL21(DE3) or *E. coli* RARE RCs. The aldehydes were quenched in the presence of an excess of hydroxylamine hydrochloride ( $NH_2OH \cdot HCl$ ) to form the corresponding aldoximes. Subsequently, reductive amination was performed in one pot by the addition of zinc powder and acidification (Ayedi et al., 2013). After extraction under basic conditions, the expected primary amines – benzylamine (BAM;  $35.3 \pm 0.7\%$ ) and 1,4-bis-(aminomethyl) benzene (1,4-bis-AMB;  $15.0 \pm 5.0\%$ ) – could be detected by GC/FID (Figure 4); benzyl alcohol and 1,4-BDM, respectively, were the major byproducts. Structurally related diamines find applications in synthesis of polyurethanes and polyamides, for example (Wang et al., 2021). In addition, although not further investigated in this study, the formation of imines might contribute to the low yield and the poor recovery of material in reactions starting from TPA (Godoy-Alcántar et al., 2005; Simion et al., 2001).

## DISCUSSION

The expanding number of new PET hydrolases from natural resources including metagenomes as well as protein engineering endeavors calls for tools for their rapid characterization (Wei et al., 2022; Wiltschi et al., 2020). Furthermore, the functional assessment of these enzymes depends – with very few exceptions (Pfaff

et al., 2021; Vogel et al., 2021) – on chromatographic methods characterized by only modest sample throughputs (Markel et al., 2020; Wei et al., 2020; Yi et al., 2021). To address this issue, this work coupled the activity of CAR<sub>Mm</sub> to reduce TPA in different *E. coli* strains to the corresponding aldehydes (4-CBAL, TAL, and 4-HMBAL) with the genetically encoded biosensor LuxAB from *P. luminescens*. The latter emits detectable bioluminescence in the presence of TPA-derived aldehydes (Figures 1, 2 and S3). As TPA is a building block of PET, the CAR/LuxAB couple was employed to detect terephthalates in hydrolysate samples obtained from PET degradation, catalyzed by the wild-type polyester hydrolases PES-H1 and LCC and the engineered variant LCC-ICCG. Not only was TPA reliably detected by reproducible fold-increase in bioluminescence values in independently carried out assay set-ups under HT conditions (Figures 2C and 3); samples containing terephthalate from PET hydrolysis by PES-H1, LCC, and LCC-ICCG exhibited steady fold-increases over 4 h under HT assay conditions in *E. coli* RARE, which was in agreement with HPLC data. This sufficed to distinguish between wild-type enzymes and a variant with increased PET degradation activity and offers a semiquantitative screening tool for PET hydrolase libraries in the future.

Lastly, with the biocatalytic production of TAL from TPA, we accessed a highly reactive aldehyde intermediate that could be transformed into the corresponding primary diamine, for example, in aqueous reaction media (Figure 4A). The chemo-enzymatic three-step cascade also yielded >30% BAM from benzoic acid via the aldehyde and aldoxime intermediates (Figure 4B).

In conclusion, the presented work featured a complementary biosensor tool for the HT detection of TPA in living cells and suggested new routes for the bio-based interconversion of polymer building blocks, supporting efforts toward a circular plastic economy, the reduction of CO<sub>2</sub> emissions, and the stewardship of resources.

### Limitations of the study

Although the utilization of *E. coli* BL21(DE3)  $\Delta lpp$  significantly increased the CAR-catalyzed conversion of TPA *in vivo*, it was not superior to the established *E. coli* RARE strain for the LuxAB-based detection of aldehydes over longer reaction times because of their different metabolic backgrounds. However, the reproducible detection of TPA by the CAR<sub>Mm</sub>/LuxAB-coupled biosensor under HT assay conditions in *E. coli* RARE enabled the semiquantitative assessment of terephthalate salts in the supernatants obtained from the biocatalytic degradation by various PET hydrolases. Even though calculated yields were in the same concentration range according to calibrated HPLC, discrepancies arise from operating the biosensor system in whole-cells of *E. coli* because of the cytotoxicity of TPA and the corresponding aldehydes, for example. Accordingly, the bioluminescence yielded by the LuxAB-catalyzed reaction is transient and influenced by the metabolic background, the viability and physiological state of cells including aeration; because LuxAB is a monooxygenase, the generation of bioluminescence depends on the aldehyde substrate and O<sub>2</sub>. In addition, expression levels of enzymes, intracellular cofactor availability, and the background luminescence in living cells can add to variations but are easily addressed by appropriate (negative) controls, and the normalization of bioluminescence signals as discussed in detail previously (Bayer et al., 2021).

The interconversion of TPA into 1,4-bis-AMB through a three-step chemo-enzymatic cascade operating in one-pot only yielded only  $15.0 \pm 5.0\%$  of the diamine and could not be improved by employing *E. coli* RARE, for example. The poor recovery of material (<50%) can be explained by the low solubility of TPA in aqueous solutions and the volatility of reaction intermediates. Furthermore, the formation of imines from aldehyde and amine precursors in aqueous solutions has been reported (Godoy-Alcántar et al., 2005; Simion et al., 2001) and will be investigated as a contributing factor in the future. Nonetheless, the reductive amination could be achieved in an aqueous buffer system, which advances the original protocol (Ayedi et al., 2013) and puts it in the context of transforming PET-derived TPA.

### STAR★METHODS

Detailed methods are provided in the online version of this paper and include the following:

- KEY RESOURCES TABLE
- RESOURCE AVAILABILITY
  - Lead contact
  - Materials availability

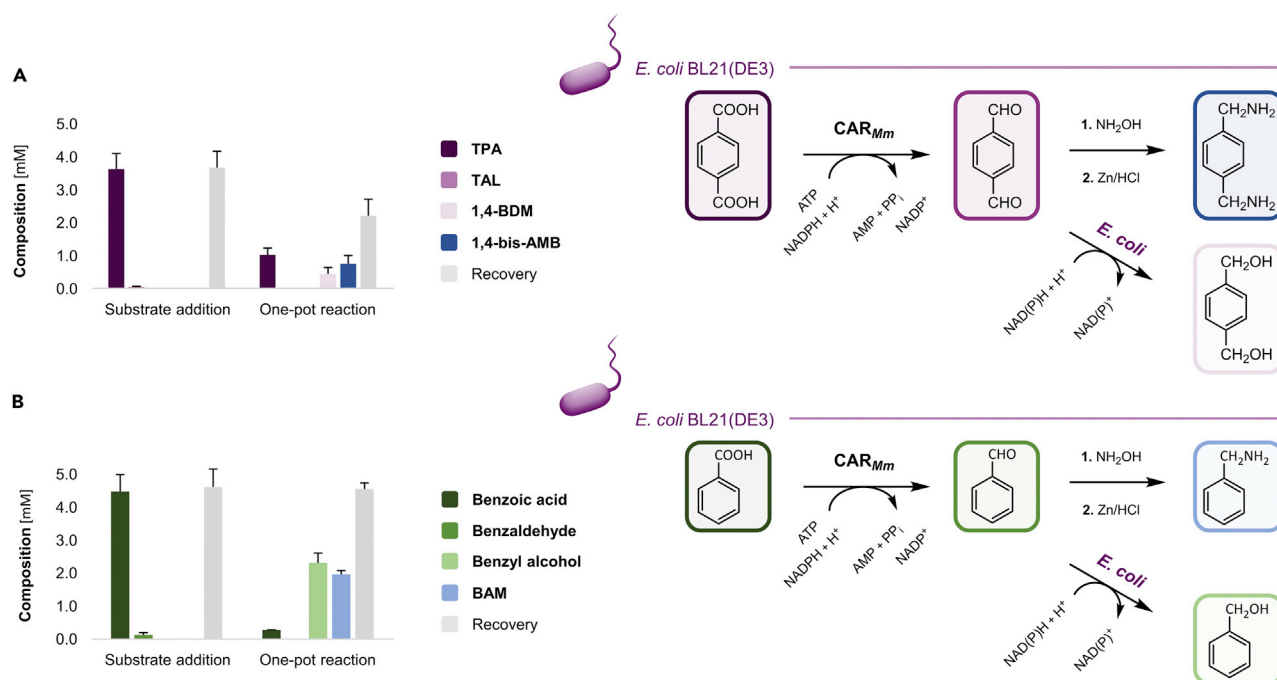


**Figure 4. Chemo-enzymatic one-pot cascades**

Carboxylates are reduced by  $CAR_{Mm}$  in RCs of *E. coli* BL21(DE3) to the corresponding aldehydes;  $PPT_{Ni}$  is omitted for clarity. In the presence of  $NH_2OH \cdot HCl$ , the oximes are formed (not shown), which are reduced to the primary amines (shades of blue) after the addition of  $Zn/HCl$  to the same reaction vessel.

(A) The TAL intermediate yields the desired 1,4-bis-AMB, besides 1,4-BDM as the major byproduct. Recoveries were reduced due to low solubility of TPA in RCM containing 5% (*v/v*) DMSO as organic co-solvent, the volatility of reaction compounds, and the formation of yet to be identified byproducts such as imines (Godoy-Alcántar et al., 2005; Simion et al., 2001).

(B) Benzoic acid in the presence of 5% (*v/v*) ethanol was reduced to benzaldehyde, yielding the desired BAM after reductive amination and benzyl alcohol as the sole byproduct. Experiments were performed in RCs ( $OD_{600} \approx 10.0$ ) co-expressing enzymes from  $pACYCDuet-1/car_{Mm};ppt_{Ni}$  (Bayer et al., 2021).

Sampling: (1) after the addition of  $NH_2OH \cdot HCl$  (2.2 and 1.1 equiv for TPA and benzoic acid, respectively) and carboxylic acid and mixing; (2) after performing the reductive amination in one-pot. GC yields are presented as mean values  $\pm$  SD [mM] of biological replicates ( $n = 3$ ). Performance was similar with RCs of *E. coli* RARE producing  $27.2 \pm 6.6\%$  BAM and  $13.1 \pm 8.0\%$  1,4-bis-AMB ( $n = 2$ ).

- Data and code availability
- EXPERIMENTAL MODEL AND SUBJECT DETAILS
- METHOD DETAILS
  - Strain engineering
  - Enzyme production and resting cell preparation
  - PET hydrolysis
  - LuxAB-based detection of TPA-derived aldehydes *in vivo* (96-well plate format)
  - Whole-cell biotransformations and chemo-enzymatic cascade one-pot reaction
- QUANTIFICATION AND STATISTICAL ANALYSIS
- ADDITIONAL RESOURCES

## SUPPLEMENTAL INFORMATION

Supplemental information can be found online at <https://doi.org/10.1016/j.isci.2022.104326>.

## ACKNOWLEDGMENTS

T.B. was funded through the Erwin Schrödinger Fellowship (project no.: J4231-B21) granted by the Austrian Science Fund (FWF). R.W., L.P., Y.B., and U.T.B. acknowledge funding received from the European Union's Horizon 2020 research and innovation program under grant agreement no. 870294 (MIX-UP project) and no. 953214 (upPE-T project). S.W. was supported by a Humboldt research fellowship. The authors would like to thank Prof. K.L.J. Prather (Massachusetts Institute of Technology, USA) for donating *E. coli* RARE. We thank Dr. C.W. Grathwol (University of Greifswald, Institute of Pharmacy, Germany) for providing

reference compounds and I. Menyes (University of Greifswald, Institute of Biochemistry, Germany) for technical support regarding analytics. The Symrise AG (Holzminden, Germany) kindly provided the genes encoding the enzymes CAR<sub>Mm</sub> and PPT<sub>Ni</sub>. Research was supported by the Federal Ministry of Food and Agriculture (BMEL; FKZ 22001617), Germany.

## AUTHOR CONTRIBUTIONS

Conceptualization, T.B. and R.W.; Methodology, T.B. and R.W.; Investigation, T.B., A.B., Y.B., L.P., and S.W.; Resources, U.T.B. and R.W.; Data Curation, T.B. and L.P.; Writing—Original Draft, T.B.; Writing—Reviewing & Editing, A.B., U.T.B., Y.B., L.P., R.W., and S.W.; Visualization, T.B. and A.B.; Supervision, T.B., U.T.B., and R.W.; Project Administration, T.B., U.T.B., and R.W.; Funding Acquisition, T.B., U.T.B., R.W., and S.W.

## DECLARATION OF INTERESTS

The authors declare no competing interests.

Received: November 28, 2021

Revised: April 4, 2022

Accepted: April 26, 2022

Published: May 20, 2022

## REFERENCES

- Akhtar, M.K., Turner, N.J., and Jones, P.R. (2013). Carboxylic acid reductase is a versatile enzyme for the conversion of fatty acids into fuels and chemical commodities. *Proc. Natl. Acad. Sci. U S A* 110, 87–92. <https://doi.org/10.1073/pnas.1216516110>.
- Asmar, A.T., Ferreira, J.L., Cohen, E.J., Cho, S.-H., Beeby, M., Hughes, K.T., and Collet, J.-F. (2017). Communication across the bacterial cell envelope depends on the size of the periplasm. *PLoS Biol.* 15, e2004303. <https://doi.org/10.1371/journal.pbio.2004303>.
- Ayedi, M.A., Le Bigot, Y., Ammar, H., Abid, S., Gharbi, R.E., and Delmas, M. (2013). Synthesis of primary amines by one-pot reductive amination of aldehydes. *Synth. Commun.* 43, 2127–2133. <https://doi.org/10.1080/00397911.2012.714830>.
- Barnicki, S.D. (2017). Synthetic organic chemicals. In *Handbook of Industrial Chemistry and Biotechnology*, J.A. Kent, T.V. Bommaraju, and S.D. Barnicki, eds. (Springer International Publishing), pp. 423–530. [https://doi.org/10.1007/978-3-319-52287-6\\_7](https://doi.org/10.1007/978-3-319-52287-6_7).
- Bayer, T., Becker, A., Terholsen, H., Kim, I.J., Menyes, I., Buchwald, S., Balke, K., Santala, S., Almo, S.C., and Bornscheuer, U.T. (2021). LuxAB-based microbial cell factories for the sensing, manufacturing and transformation of industrial aldehydes. *Catalysts* 11, 953–1017. <https://doi.org/10.3390/catal11080953>.
- Bayer, T., Milker, S., Wiesinger, T., Winkler, M., Mihovilovic, M.D., and Rudroff, F. (2017). *In vivo* synthesis of polyhydroxylated compounds from a “hidden reservoir” of toxic aldehyde species. *ChemCatChem* 9, 2919–2923. <https://doi.org/10.1002/cctc.201700469>.
- Bornscheuer, U.T. (2016). Feeding on plastic. *Science* 351, 1154–1155. <https://doi.org/10.1126/science.aaf2853>.
- Brindell, G.D., Lillwitz, L.D., Wuskell, J.P., and Dunlop, A.P. (1976). Polymer applications of some terephthalaldehyde derivatives. *Ind. Eng. Chem. Prod. Res. Dev.* 15, 83–88. <https://doi.org/10.1021/i360057a017>.
- Butler, N., and Kunjapur, A.M. (2020). Carboxylic acid reductases in metabolic engineering. *J. Biotechnol.* 307, 1–14. <https://doi.org/10.1016/j.jbiotec.2019.10.002>.
- Colepicolo, P., Cho, K.W., Poinar, G.O., and Hastings, J.W. (1989). Growth and luminescence of the bacterium *Xenorhabdus luminescens* from a human wound. *Appl. Environ. Microbiol.* 55, 2601–2606. <https://doi.org/10.1128/aem.55.10.2601-2606.1989>.
- Danso, D., Schmeisser, C., Chow, J., Zimmermann, W., Wei, R., Leggewie, C., Li, X., Hazen, T., Parales, R.E., and Streit, W.R. (2018). New insights into the function and global distribution of polyethylene terephthalate (PET)-degrading bacteria and enzymes in marine and terrestrial metagenomes. *Appl. Environ. Microbiol.* 84, e02773–17. <https://doi.org/10.1128/AEM.02773-17>.
- Dietrich, J.A., McKee, A.E., and Keasling, J.D. (2010). High-throughput metabolic engineering: advances in small-molecule screening and selection. *Annu. Rev. Biochem.* 79, 563–590. <https://doi.org/10.1146/annurev-biochem-062608-095938>.
- Eberl, A., Heumann, S., Brückner, T., Araujo, R., Cavaco-Paulo, A., Kaufmann, F., Kroutil, W., and Guebitz, G.M. (2009). Enzymatic surface hydrolysis of poly(ethylene terephthalate) and bis(benzoyloxyethyl) terephthalate by lipase and cutinase in the presence of surface active molecules. *J. Biotechnol.* 143, 207–212. <https://doi.org/10.1016/j.jbiotec.2009.07.008>.
- Eriksen, M., Lebreton, L.C.M., Carson, H.S., Thiel, M., Moore, C.J., Borerro, J.C., Galgani, F., Ryan, P.G., and Reisser, J. (2014). Plastic pollution in the world's oceans: more than 5 trillion plastic pieces weighing over 250,000 tons afloat at sea. *PLoS One* 9, e111913. <https://doi.org/10.1371/journal.pone.0111913>.
- Ferguson, L.N. (1946). The synthesis of aromatic aldehydes. *Chem. Rev.* 38, 227–254. <https://doi.org/10.1021/cr60120a002>.
- Finnigan, W., Thomas, A., Cromar, H., Gough, B., Snajdrova, R., Adams, J.P., Littlechild, J.A., and Harmer, N.J. (2017). Characterization of carboxylic acid reductases as enzymes in the toolbox for synthetic chemistry. *ChemCatChem* 9, 1005–1017. <https://doi.org/10.1002/cctc.201601249>.
- Fleiss, A., and Sarkisyan, K.S. (2019). A brief review of bioluminescent systems (2019). *Curr. Genet.* 65, 877–882. <https://doi.org/10.1007/s00294-019-00951-5>.
- Geyer, R., Jambeck, J.R., and Law, K.L. (2017). Production, use, and fate of all plastics ever made. *Sci. Adv.* 3, e1700782. <https://doi.org/10.1126/sciadv.1700782>.
- Godoy-Alcántar, C., Yatsimirsky, A.K., and Lehn, J.-M. (2005). Structure-stability correlations for imine formation in aqueous solution. *J. Phys. Org. Chem.* 18, 979–985. <https://doi.org/10.1002/poc.941>.
- Herrero Acero, E., Ribitsch, D., Steinkellner, G., Gruber, K., Greimel, K., Eiteljoerg, I., Trotscha, E., Wei, R., Zimmermann, W., Zinn, M., et al. (2011). Enzymatic surface hydrolysis of PET: effect of structural diversity on kinetic properties of cutinases from *Thermobifida*. *Macromolecules* 44, 4632–4640. <https://doi.org/10.1021/ma200949p>.
- Hopewell, J., Dvorak, R., and Kosior, E. (2009). Plastics recycling: challenges and opportunities. *Philos. Trans. R. Soc. B Biol. Sci.* 364, 2115–2126. <https://doi.org/10.1098/rstb.2008.0311>.

- Horvat, M., and Winkler, M. (2020). *In vivo* reduction of medium- to long-chain fatty acids by carboxylic acid reductase (CAR) enzymes: limitations and solutions. *ChemCatChem* 12, 5076–5090. <https://doi.org/10.1002/cctc.202000895>.
- Jiang, Y., Chen, B., Duan, C., Sun, B., Yang, J., and Yang, S. (2015). Multigene editing in the *Escherichia coli* genome via the CRISPR-Cas9 system. *Appl. Environ. Microbiol.* 81, 2506–2514. <https://doi.org/10.1128/AEM.04023-14>.
- Kasai, D., Kitajima, M., Fukuda, M., and Masai, E. (2010). Transcriptional regulation of the terephthalate catabolism operon in *Comamonas* sp. strain E6. *Appl. Environ. Microbiol.* 76, 6047–6055. <https://doi.org/10.1128/AEM.00742-10>.
- Kawai, F., Kawabata, T., and Oda, M. (2020). Current state and perspectives related to the polyethylene terephthalate hydrolases available for biorecycling. *ACS Sustain. Chem. Eng.* 8, 8894–8908. <https://doi.org/10.1021/acssuschemeng.0c01638>.
- Kawai, F., Kawabata, T., and Oda, M. (2019). Current knowledge on enzymatic PET degradation and its possible application to waste stream management and other fields. *Appl. Microbiol. Biotechnol.* 103, 4253–4268. <https://doi.org/10.1007/s00253-019-09717-y>.
- Kunjapur, A.M., Hyun, J.C., and Prather, K.L.J. (2016). Deregulation of S-adenosylmethionine biosynthesis and regeneration improves methylation in the *E. coli* *de novo* vanillin biosynthesis pathway. *Microb. Cell Factories* 15, 61. <https://doi.org/10.1186/s12934-016-0459-x>.
- Kunjapur, A.M., and Prather, K.L.J. (2019). Development of a vanillate biosensor for the vanillin biosynthesis pathway in *E. coli*. *ACS Synth. Biol.* 8, 1958–1967. <https://doi.org/10.1021/acssynbio.9b00071>.
- Kunjapur, A.M., and Prather, K.L.J. (2015). Microbial engineering for aldehyde synthesis. *Appl. Environ. Microbiol.* 81, 1892–1901. <https://doi.org/10.1128/AEM.03319-14>.
- Kunjapur, A.M., Tarasova, Y., and Prather, K.L.J. (2014). Synthesis and accumulation of aromatic aldehydes in an engineered strain of *Escherichia coli*. *J. Am. Chem. Soc.* 136, 11644–11654. <https://doi.org/10.1021/ja506664a>.
- Lehtinen, T., Santala, V., and Santala, S. (2017). Twin-layer biosensor for real-time monitoring of alkane metabolism. *FEMS Microbiol. Lett.* 364, 1–7. <https://doi.org/10.1093/femsle/fnx053>.
- Li, G.-W., Burkhardt, D., Gross, C., and Weissman, J.S. (2014). Quantifying absolute protein synthesis rates reveals principles underlying allocation of cellular resources. *Cell* 157, 624–635. <https://doi.org/10.1016/j.cell.2014.02.033>.
- Li, J., Nina, M.R.H., Zhang, X., and Bai, Y. (2022). Engineering transcription factor XylS for sensing phthalic acid and terephthalic acid: an application for enzyme evolution. *ACS Synth. Biol.* 11, 1106–1113. <https://doi.org/10.1021/acssynbio.1c00275>.
- Liu, D., Evans, T., and Zhang, F. (2015). Applications and advances of metabolite biosensors for metabolic engineering. *Metab. Eng.* 31, 35–43. <https://doi.org/10.1016/j.ymben.2015.06.008>.
- Liu, Y., Zhuang, Y., Ding, D., Xu, Y., Sun, J., and Zhang, D. (2017). Biosensor-based evolution and elucidation of a biosynthetic pathway in *Escherichia coli*. *ACS Synth. Biol.* 6, 837–848. <https://doi.org/10.1021/acssynbio.6b00328>.
- Markel, U., Essani, K.D., Besirlioglu, V., Schiffels, J., Streit, W.R., and Schwaneberg, U. (2020). Advances in ultrahigh-throughput screening for directed enzyme evolution. *Chem. Soc. Rev.* 49, 233–262. <https://doi.org/10.1039/C8CS00981C>.
- Mathélié-Guinlet, M., Asmar, A.T., Collet, J.-F., and Dufrene, Y.F. (2020). Lipoprotein Lpp regulates the mechanical properties of the *E. coli* cell envelope. *Nat. Commun.* 11, 1789. <https://doi.org/10.1038/s41467-020-15489-1>.
- Müller, R.-J., Schrader, H., Profe, J., Dresler, K., and Deckwer, W.-D. (2005). Enzymatic Degradation of poly(ethylene terephthalate): rapid hydrolyse using a hydrolase from *T. fusca*. *Macromol. Rapid Commun.* 26, 1400–1405. <https://doi.org/10.1002/marc.200500410>.
- Ni, Y., Reye, J., and Chen, R.R. (2007). Lpp deletion as a permeabilization method. *Biotechnol. Bioeng.* 97, 1347–1356. <https://doi.org/10.1002/bit.21375>.
- Palm, G.J., Reisky, L., Böttcher, D., Müller, H., Michels, E.A.P., Walczak, M.C., Berndt, L., Weiss, M.S., Bornscheuer, U.T., and Weber, G. (2019). Structure of the plastic-degrading *Ideonella sakaiensis* MHETase bound to a substrate. *Nat. Commun.* 10, 1717–1810. <https://doi.org/10.1038/s41467-019-09326-3>.
- Pardo, I., Jha, R.K., Bermel, R.E., Bratti, F., Gaddis, M., McIntyre, E., Michener, W., Neidle, E.L., Dale, T., Beckham, G.T., and Johnson, C.W. (2020). Gene amplification, laboratory evolution, and biosensor screening reveal MucK as a terephthalic acid transporter in *Acinetobacter baylyi* ADP1. *Metab. Eng.* 62, 260–274. <https://doi.org/10.1016/j.ymben.2020.09.009>.
- Pfaff, L., Breite, D., Badenhörst, C.P.S., Bornscheuer, U.T., and Wei, R. (2021). Fluorimetric high-throughput screening method for polyester hydrolase activity using polyethylene terephthalate nanoparticles. In *Methods in Enzymology*, G. Weber, U.T. Bornscheuer, and R. Wei, eds. (Academic Press), pp. 253–270. <https://doi.org/10.1016/bs.mie.2020.11.003>.
- Qu, G., Guo, J., Yang, D., and Sun, Z. (2018). Biocatalysis of carboxylic acid reductases: phylogenesis, catalytic mechanism and potential applications. *Green Chem.* 20, 777–792. <https://doi.org/10.1039/C7GC03046K>.
- Rahimi, A., and García, J.M. (2017). Chemical recycling of waste plastics for new materials production. *Nat. Rev. Chem.* 1, 0046. <https://doi.org/10.1038/s41570-017-0046>.
- Meys, R., Kätelhön, A., Bachmann, M., Winter, B., Zibunas, C., Suh, S., and Bardow, A. (2021). Achieving net-zero greenhouse gas emission plastics by a circular carbon economy. *Science* 374, 71–76. <https://doi.org/10.1126/science.abg9853>.
- Ressmann, A.K., Schwendenwein, D., Leonhartsberger, S., Mihovilovic, M.D., Bornscheuer, U.T., Winkler, M., and Rudroff, F. (2019). Substrate-independent high-throughput assay for the quantification of aldehydes. *Adv. Synth. Catal.* 361, 2538–2543. <https://doi.org/10.1002/adsc.201900154>.
- Rohan, R., Pareek, K., Cai, W., Zhang, Y., Xu, G., Chen, Z., Gao, Z., Dan, Z., and Cheng, H. (2015). Melamine-terephthalaldehyde-lithium complex: a porous organic network based single ion electrolyte for lithium-ion batteries. *J. Mater. Chem. A* 3, 5132–5139. <https://doi.org/10.1039/C4TA06855F>.
- Ronkvist, Å.M., Xie, W., Lu, W., and Gross, R.A. (2009). Cutinase-catalyzed hydrolysis of poly(ethylene terephthalate). *Macromolecules* 42, 5128–5138. <https://doi.org/10.1021/ma9005318>.
- Sadler, J.C., and Wallace, S. (2021). Microbial synthesis of vanillin from waste poly(ethylene terephthalate). *Green Chem.* 23, 4665–4672. <https://doi.org/10.1039/D1GC00931A>.
- Kakadellis, S., and Rosetto, G. (2021). Achieving a circular bioeconomy for plastics. *Science* 373, 49–50. <https://doi.org/10.1126/science.abj3476>.
- Saran, M., and Summer, K.H. (1999). Assaying for hydroxyl radicals: hydroxylated terephthalate is a superior fluorescence marker than hydroxylated benzoate. *Free Radic. Res.* 31, 429–436. <https://doi.org/10.1080/1071576990300991>.
- Simion, A., Simion, C., Kanda, T., Nagashima, S., Mitoma, Y., Yamada, T., Mimura, K., and Tashiro, M. (2001). Synthesis of imines, diimines and macrocyclic diimines as possible ligands in aqueous solution. *J. Chem. Soc. Perkin Trans. 1*, 2071–2078. <https://doi.org/10.1039/B102749M>.
- Simon, N., Raubenheimer, K., Urho, N., Unger, S., Azoulay, D., Farrelly, T., Sousa, J., van Asselt, H., Carlini, G., Sekomo, C., et al. (2021). A binding global agreement to address the life cycle of plastics. *Science* 373, 43–47. <https://doi.org/10.1126/science.abi9010>.
- Snell, J.M., and Weissberger, A. (1940). Synthesis of terephthalaldehyde. *Org. Synth.* 20, 92. <https://doi.org/10.15227/orgsyn.020.0092>.
- Studier, F.W. (2005). Protein production by auto-induction in high-density shaking cultures. *Protein Expr. Purif.* 41, 207–234. <https://doi.org/10.1016/j.pep.2005.01.016>.
- Suematsu, K., Nakamura, K., and Takeda, J. (1983). Synthesis of aromatic polyimines by the condensation of aromatic dialdehyde and diamine. *Colloid Polym. Sci.* 261, 493–501. <https://doi.org/10.1007/BF01419833>.
- Sulaiman, S., Yamato, S., Kanaya, E., Kim, J.-J., Koga, Y., Takano, K., and Kanaya, S. (2012). Isolation of a novel cutinase homolog with polyethylene terephthalate-degrading activity from leaf-branch compost by using a metagenomic approach. *Appl. Environ. Microbiol.* 78, 1556–1562. <https://doi.org/10.1128/AEM.06725-11>.
- Tiso, T., Narancic, T., Wei, R., Pollet, E., Beagan, N., Schröder, K., Honak, A., Jiang, M., Kenny, S.T., Wierckx, N., et al. (2021). Towards bio-upcycling of polyethylene terephthalate. *Metab. Eng.* 66,

167–178. <https://doi.org/10.1016/j.ymben.2021.03.011>.

Tournier, V., Topham, C.M., Gilles, A., David, B., Folgoas, C., Moya-Leclair, E., Kamionka, E., Desrousseaux, M.-L., Texier, H., Gavalda, S., et al. (2020). An engineered PET depolymerase to break down and recycle plastic bottles. *Nature* 580, 216–219. <https://doi.org/10.1038/s41586-020-2149-4>.

Vogel, K., Wei, R., Pfaff, L., Breite, D., Al-Fathi, H., Ortmann, C., Estrela-Lopis, I., Venus, T., Schulze, A., Harms, H., et al. (2021). Enzymatic degradation of polyethylene terephthalate nanoplastics analyzed in real time by isothermal titration calorimetry. *Sci. Total Environ.* 773, 145111. <https://doi.org/10.1016/j.scitotenv.2021.145111>.

Vollmer, I., Jenks, M.J.F., Roelands, M.C.P., White, R.J., van Harmelen, T., de Wild, P., van der Laan, G.P., Meirer, F., Keurentjes, J.T.F., and Weckhuysen, B.M. (2020). Beyond mechanical recycling: giving new life to plastic waste. *Angew. Chem. Int. Ed.* 59, 15402–15423. <https://doi.org/10.1002/anie.201915651>.

Wang, X., Gao, S., Wang, J., Xu, S., Li, H., Chen, K., and Ouyang, P. (2021). The production of biobased diamines from renewable carbon sources: Current advances and perspectives. *Chin. J. Chem. Eng.* 30, 4–13. <https://doi.org/10.1016/j.cjche.2020.12.009>.

Wei, R., Oeser, T., Billig, S., and Zimmermann, W. (2012). A high-throughput assay for enzymatic polyester hydrolysis activity by fluorimetric detection. *Biotechnol. J.* 7, 1517–1521. <https://doi.org/10.1002/biot.201200119>.

Wei, R., Oeser, T., Then, J., Kühn, N., Barth, M., Schmidt, J., and Zimmermann, W. (2014). Functional characterization and structural modeling of synthetic polyester-degrading hydrolases from *Thermomonospora curvata*. *AMB Express* 4, 44. <https://doi.org/10.1186/s13568-014-0044-9>.

Wei, R., Breite, D., Song, C., Gräsing, D., Ploss, T., Hille, P., Schwerdtfeger, R., Matsysik, J., Schulze, A., and Zimmermann, W. (2019a). Biocatalytic degradation efficiency of postconsumer polyethylene terephthalate packaging determined by their polymer microstructures. *Adv. Sci.* 6, 1900491. <https://doi.org/10.1002/adv.201900491>.

Wei, R., Song, C., Gräsing, D., Schneider, T., Bielytskyi, P., Böttcher, D., Matsysik, J., Bornscheuer, U.T., and Zimmermann, W. (2019b). Conformational fitting of a flexible oligomeric substrate does not explain the enzymatic PET degradation. *Nat. Commun.* 10, 5581. <https://doi.org/10.1038/s41467-019-13492-9>.

Wei, R., Tiso, T., Bertling, J., O'Connor, K., Blank, L.M., and Bornscheuer, U.T. (2020). Possibilities and limitations of biotechnological plastic degradation and recycling. *Nat. Catal.* 3, 867–871. <https://doi.org/10.1038/s41929-020-00521-w>.

Wei, R., von Haugwitz, G., Pfaff, L., Mican, J., Badenhorst, C.P.S., Liu, W., Weber, G., Austin, H.P., Bednar, D., Damborsky, J., and Bornscheuer, U.T. (2022). Mechanism-based design of efficient PET hydrolases. *ACS Catal.* 12, 3382–3396. <https://doi.org/10.1021/acscatal.1c05856>.

Welch, K.D., Davis, T.Z., and Aust, S.D. (2002). Iron autoxidation and free radical generation: effects

of buffers, ligands, and chelators. *Arch. Biochem. Biophys.* 397, 360–369. <https://doi.org/10.1006/abbi.2001.2694>.

Wiltschi, B., Cernava, T., Dennig, A., Galindo Casas, M., Geier, M., Gruber, S., Haberbauer, M., Heidinger, P., Herrero Acero, E., Kratzer, R., et al. (2020). Enzymes revolutionize the bioproduction of value-added compounds: from enzyme discovery to special applications. *Biotechnol. Adv.* 40, 107520. <https://doi.org/10.1016/j.biotechadv.2020.107520>.

Wright, S.L., and Kelly, F.J. (2017). Plastic and human health: a micro issue? *Environ. Sci. Technol.* 51, 6634–6647. <https://doi.org/10.1021/acs.est.7b00423>.

Yi, D., Bayer, T., Badenhorst, C.P.S., Wu, S., Doerr, M., Höhne, M., and Bornscheuer, U.T. (2021). Recent trends in biocatalysis. *Chem. Soc. Rev.* 50, 8003–8049. <https://doi.org/10.1039/D0CS01575J>.

Yoshida, S., Hiraga, K., Takehana, T., Taniguchi, I., Yamaji, H., Maeda, Y., Toyohara, K., Miyamoto, K., Kimura, Y., and Oda, K. (2016). A bacterium that degrades and assimilates poly(ethylene terephthalate). *Science* 351, 1196–1199. <https://doi.org/10.1126/science.aad6359>.

Zhang, Y., Werling, U., and Edelman, W. (2012). SLiCE: a novel bacterial cell extract-based DNA cloning method. *Nucleic Acids Res.* 40, e55. <https://doi.org/10.1093/nar/gkr1288>.

Zimmermann, W., Wei, R., Hille, P., Oeser, T., and Schmidt, J. (2019). EP3517608A1: New Polypeptides Having a Polyester Degrading Activity and Uses Thereof. <https://patents.google.com/patent/EP3517608A1/en>.

## STAR★METHODS

### KEY RESOURCES TABLE

REAGENT or RESOURCE	SOURCE	IDENTIFIER
<b>Bacterial and virus strains</b>		
<i>E. coli</i> BL21(DE3)	Thermo Scientific™	Cat#EC0114
<i>E. coli</i> BL21(DE3) $\Delta$ lpp	This paper	N/A
<i>E. coli</i> DH5 $\alpha$	Thermo Scientific™	Cat#18265017
<i>E. coli</i> K-12 MG1655 RARE	Prof. K.L.J. Prather (Kunjapur et al., 2014)	Addgene Bacterial strain #61440
<b>Chemicals, peptides, and recombinant proteins</b>		
PET film	Goodfellow GmbH	Cat#ES301445
Terephthalic acid (TPA; CAS: 100-21-0)	Sigma-Aldrich	Cat#185361
4-Carboxybenzaldehyde (4-CBAL; CAS: 619-66-9)	Acros	Cat#154580050
4-(Hydroxymethyl) benzoic acid (4-HMBA; CAS: 3006-96-0)	Sigma-Aldrich	Cat#382639
Terephthalaldehyde (TAL; CAS: 623-27-8)	Alfa Aesar	Cat#A14930
4-(Hydroxymethyl) benzaldehyde (4-HMBAL; CAS: 52010-97-6)	Carbosynth Ltd	Cat#FH140138
1,4-Benzenedimethanol (1,4-BDM; CAS: 589-29-7)	TCI	Cat#D0605
1,4-bis-(Aminomethyl) benzene (1,4-bis-AMB; CAS: 539-48-0)	Sigma-Aldrich	Cat#8.41656
Benzoic acid (CAS: 65-85-0)	Sigma-Aldrich	Cat#242381
Benzaldehyde (CAS: 100-52-7)	Acros	Cat#378361000
Benzyl alcohol (CAS: 100-51-6)	Fluka	Cat#77013
Benzylamine (BAM; CAS: 100-46-9)	Sigma-Aldrich	Cat#185701
Methyl benzoate (CAS: 93-58-3)	Sigma-Aldrich	Cat#M29908
2-Phenylacetic acid (2-PAA; CAS: 103-82-2)	Fluka	Cat#78490
2-Phenylacetaldehyde (2-PAAL; CAS: 122-78-1)	Acros	Cat#37091
2-Phenylethanol (CAS: 60-12-8)	Fluka	Cat#77861
Lysonase™ Bioprocessing Reagent	Merck-Millipore	Cat#71230
ROTI®Garose-His/Co Beads	Carl Roth	Cat#1235.1
Recombinant protein (C-term. 6xHis, purified): leaf-branch compost cutinase (LCC)	This study	G9BY57
Recombinant protein (C-term. 6xHis, purified): leaf-branch compost cutinase variant (LCC-ICCG)	This study	PDB: 6THT
Recombinant protein (C-term. 6xHis, purified): polyester hydrolase-1 (PES-H1)	This study	PDB: 7CUV
Q5® polymerase	NEB	Cat#M0491S
Q5® mutagenesis kit	NEB	Cat#E0554S
<b>Deposited data</b>		
Raw and analyzed data	This paper	N/A

(Continued on next page)

<b>Continued</b>		
REAGENT or RESOURCE	SOURCE	IDENTIFIER
<b>Experimental models: Organisms/strains</b>		
<i>E. coli</i> strains, see above: Bacterial and virus strains	This paper	N/A
<b>Oligonucleotides</b>		
<i>lpp</i> -up_F, primer for strain engineering, see <a href="#">Table S1</a>	This paper (Thermo Scientific™)	N/A
<i>lpp</i> -up_R, primer for strain engineering, see <a href="#">Table S1</a>	This paper (Thermo Scientific™)	N/A
<i>lpp</i> -down_F, primer for strain engineering, see <a href="#">Table S1</a>	This paper (Thermo Scientific™)	N/A
<i>lpp</i> -down_R, primer for strain engineering, see <a href="#">Table S1</a>	This paper (Thermo Scientific™)	N/A
pTarget_F, primer for strain engineering, see <a href="#">Table S1</a>	This paper (Thermo Scientific™)	N/A
pTarget_R, primer for strain engineering, see <a href="#">Table S1</a>	This paper (Thermo Scientific™)	N/A
$\Delta$ <i>lpp</i> -gRNA_F, primer for strain engineering, see <a href="#">Table S1</a>	This paper (Thermo Scientific™)	N/A
$\Delta$ <i>lpp</i> -gRNA_R, primer for strain engineering, see <a href="#">Table S1</a>	This paper (Thermo Scientific™)	N/A
<b>Recombinant DNA</b>		
Plasmid: pCDFduo/ <i>luxAB</i>	<a href="#">Bayer et al., 2021</a>	NCBI: WP_088373098 ( <i>luxA</i> ); NCBI: P19840 ( <i>luxB</i> )
Plasmid: pACYCDuet-1/ <i>car<sub>Mm</sub></i> ; <i>ppt<sub>Ni</sub></i>	<a href="#">Bayer et al., 2021</a>	NCBI: WP_012393886 ( <i>car<sub>Mm</sub></i> ); NCBI: ABI83656 ( <i>ppt<sub>Ni</sub></i> )
Plasmid: pET26b/ <i>lcc</i>	This paper (BioCat GmbH); ( <a href="#">Tournier et al., 2020</a> )	NCBI: G9BY57
Plasmid: pET26b/ <i>lcc</i> -ICCG	This paper (BioCat GmbH); ( <a href="#">Tournier et al., 2020</a> )	PDB: 6THT
Plasmid: pET26b/ <i>pes-H1</i>	This paper (BioCat GmbH); ( <a href="#">Zimmermann et al., 2019</a> )	PDB: 7CUV
Plasmid: pCas	Addgene ( <a href="#">Jiang et al., 2015</a> )	Addgene Plasmid #62225
Plasmid: pTarget	Addgene ( <a href="#">Jiang et al., 2015</a> )	Addgene Plasmid #62226
Plasmid: pTarget- $\Delta$ <i>lpp</i>	This paper	N/A
<b>Software and algorithms</b>		
Geneious Prime® 2022.0.2	Biomatters Ltd	<a href="http://www.geneious.com">www.geneious.com</a>
OligoEvaluator™	Sigma-Aldrich	<a href="http://www.oligoevaluator.com/LoginServlet">http://www.oligoevaluator.com/LoginServlet</a>
Microsoft Office 16.0	Microsoft Corporation	<a href="http://www.microsoft.com">www.microsoft.com</a>
<b>Other</b>		
96-well plate (flat bottom, black polystyrene)	Greiner Bio-One	Cat#655079

## RESOURCE AVAILABILITY

### Lead contact

Further information and requests for resources and reagents should be directed to and will be fulfilled by the lead contact, Dr. Thomas Bayer ([thomas.bayer@uni-greifswald.de](mailto:thomas.bayer@uni-greifswald.de)).



### Materials availability

- For the assembly of the pTarget- $\Delta lpp$  plasmid in this study, the templates pCas (#62225) and pTarget (#62226) were purchased from Addgene (Watertown, USA). Subsequently, pTarget- $\Delta lpp$  and pCas were used to knock-out the *lpp* gene from the genome of *E. coli* BL21(DE3). The genes encoding the leaf-branch compost cutinase (LCC) and the LCC-ICCG variant (Tournier et al., 2020) and the polyester hydrolase-1 (PES-H1) (Zimmermann et al., 2019) were codon-optimized for the expression in *E. coli*, synthesized, and cloned in frame with the C-terminal 6xHis tag present in pET26b by the BioCat GmbH (Heidelberg, Germany). Accession numbers of proteins are provided in the [Key resources table](#).
- *E. coli* BL21(DE3) (#EC0114) and DH5 $\alpha$  (#18265017) were initially purchased from Thermo Scientific™ (Darmstadt, Germany) and propagated as described below. *E. coli* BL21(DE3)  $\Delta lpp$  is available from the [lead contact](#) upon request. *E. coli* RARE was acquired from the Prather group (Kunjapur et al., 2014) but is also available from Addgene (#61440).
- There are restrictions to the availability of the previously constructed pCDFduo/*luxAB*, herein referred to as pLuxAB, and pACYCDuet-1/*car<sub>Mm</sub>:ppt<sub>Ni</sub>* plasmids (Bayer et al., 2021) due to material transfer agreements (MTAs). Further information is available from the [lead contact](#) upon request.
- Otherwise, this study did not generate new unique reagents.

### Data and code availability

- The genome of *E. coli* BL21(DE3) and associated metadata were retrieved from the National Center for Biotechnology Information (NCBI; GenBank: CP001509.3). The accession numbers of protein sequences are listed in the [Key resources table](#).
- This paper does not report original code.
- Any additional information required to re-analyze the data reported in this paper is available from the [lead contact](#) upon request.

## EXPERIMENTAL MODEL AND SUBJECT DETAILS

*E. coli* BL21(DE3), *E. coli* BL21(DE3)  $\Delta lpp$ , *E. coli* DH5 $\alpha$ , and *E. coli* RARE were propagated in 4–5 mL lysogeny broth (LB) medium (25 g L<sup>-1</sup>; Sigma-Aldrich, Buchs, Switzerland) in Infors HT Multitron incubator shakers (Bottmingen, Switzerland) at 37°C with shaking (150–180 rpm) for 12–16 h. If not stated otherwise, chemically competent *E. coli* cells were produced by using 0.1 M CaCl<sub>2</sub> and transformed with plasmid DNA (25–100 ng) by heat-shock at 42°C for 45 s as previously described (Bayer et al., 2021). For the efficient transformation of *E. coli* RARE, plasmids were passed through *E. coli* DH5 $\alpha$  (Bayer et al., 2021). *E. coli* transformants harboring pLuxAB and pACYCDuet-1/*car<sub>Mm</sub>:ppt<sub>Ni</sub>* were propagated in LB medium supplemented with streptomycin (25  $\mu$ g·mL<sup>-1</sup>) and chloramphenicol (34  $\mu$ g·mL<sup>-1</sup>), respectively. Only half the concentration of antibiotics was used for the selection and subsequent propagation of strains harboring both plasmids. For the selection and propagation on plates, LB containing 1.5% (*w/v*) agar (Carl Roth, Karlsruhe, Germany) and supplemented with antibiotics – if applicable – was used.

## METHOD DETAILS

### Strain engineering

The non-essential *lpp* gene encodes a cellular ‘bulk’ protein (Li et al., 2014), which controls the (mechanical) properties of the inner and outer membrane and the width of the periplasmic space (Asmar et al., 2017; Mathelié-Guinlet et al., 2020). The deletion of the *lpp* gene from the *E. coli* genome has been suggested to affect the permeability of the cellular envelope for small molecules (Ni et al., 2007) that might also influence the uptake of TPA and derivatives. Furthermore, expression levels of CAR<sub>Mm</sub>/PPT<sub>Ni</sub> were increased in *E. coli* BL21(DE3)  $\Delta lpp$  according to SDS-PAGE analysis (Figure S2). This may be due to the re-allocation of cellular resources (Li et al., 2014).

*E. coli* BL21(DE3)  $\Delta lpp$  was constructed by using a previously developed two-plasmid-based CRISPR/Cas9 system (Jiang et al., 2015). The two key plasmids, pCas (#62225) and pTarget (#62226), were purchased from Addgene (Watertown, USA). The pTarget- $\Delta lpp$  plasmid was constructed by first engineering the flanking sequence of the *lpp* gene by the assembly of three DNA fragments using a sequence- and

ligation-independent cloning extract-based protocol (Zhang et al., 2012): (1) the *lpp*-up fragment (amplified from the *E. coli* genome employing the primers *lpp*-up\_F/R), (2) the *lpp*-down fragment (amplified from the genome of *E. coli* using the primers *lpp*-down\_F/R), and (3) the pTarget fragment. The latter was amplified by using the primers pTarget\_F/R. Next, the guide RNA (gRNA) was introduced employing the Q5® mutagenesis kit (New England Biolabs, Frankfurt/Main, Germany) with the primer pair  $\Delta$ *lpp*-gRNA\_F/R. The resulting pTarget- $\Delta$ *lpp* was Sanger sequenced (Eurofins Genomics, Ebersberg, Germany) to confirm the insertion of gRNA and the flanking sequences of the *lpp* gene. Subsequently, *E. coli* BL21(DE3)  $\Delta$ *lpp* strain was constructed by using pCas and pTarget- $\Delta$ *lpp* according to Jiang and co-workers (Jiang et al., 2015). Briefly, competent *E. coli* BL21(DE3) cells were transformed with pCas as described above. In the resulting pCas transformants, the  $\lambda$ -Red system was induced with 0.2% ( $\omega/\nu$ ) arabinose and electrocompetent cells were prepared. Next, the pTarget- $\Delta$ *lpp* plasmid was introduced by electroporation; transformants were selected on LB agar plates supplemented with kanamycin and streptomycin. Colony polymerase chain reaction (PCR) was performed for genotyping the colonies. The plasmids pTarget- $\Delta$ *lpp* and pCas were cured sequentially in the presence of 0.5 mM isopropyl- $\beta$ -D-thiogalactopyranoside (IPTG) and by culturing at 37°C, respectively. Finally, the successful construction of *E. coli* BL21(DE3)  $\Delta$ *lpp* was confirmed by PCR amplification and DNA sequencing of the genome sequence flanking the knocked-out *lpp* gene.

Desalted DNA oligonucleotides were ordered from Invitrogen/Thermo Fisher Scientific and dissolved in nuclease-free water (Invitrogen, Darmstadt, Germany). Primer sequences are given in Table S1. PCRs were performed on a Biometra TAdvanced thermal cycler (Analytik Jena, Jena, Germany) employing Q5® polymerase as suggested by the supplier (New England Biolabs).

### Enzyme production and resting cell preparation

Production of LuxAB and CAR<sub>Mm</sub>/PPT<sub>Ni</sub> was performed in *E. coli* transformants harboring pLuxAB and pACYCDuet-1/*car*<sub>Mm</sub>:*ppt*<sub>Ni</sub>, respectively. For cultivation, auto-induction medium (AIM; 2.5% ( $\omega/\nu$ ) lysogeny broth medium, 1 mM MgSO<sub>4</sub>, 25 mM (NH<sub>4</sub>)<sub>2</sub>SO<sub>4</sub>, 50 mM KH<sub>2</sub>PO<sub>4</sub>, 50 mM Na<sub>2</sub>HPO<sub>4</sub>, 5% ( $\omega/\nu$ ) glycerol, 0.5% ( $\omega/\nu$ ) glucose, 2% ( $\omega/\nu$ )  $\alpha$ -lactose) supplemented with chloramphenicol (34  $\mu$ g·mL<sup>-1</sup>) and streptomycin (25  $\mu$ g·mL<sup>-1</sup>), respectively, was used. Only half the concentration of antibiotics was used for the selection and subsequent cultivation of strains harboring both plasmids. The AIM was adapted from Studier (Studier, 2005).

Briefly, a single colony of the desired strain was grown in LB medium supplemented with the appropriate antibiotic(s) at 37°C (180 rpm) for 12–16 h. AIM containing antibiotic(s) was inoculated with 0.2% ( $\nu/\nu$ ) pre-culture in baffled flasks and incubated in Infors HT Multitron incubator shakers (Bottmingen, Switzerland) at 37°C (180 rpm) for 4–6 h (6 h for co-transformants, 5 h for cells harboring pLuxAB, and 4 h for cells harboring pACYCDuet-1/*car*<sub>Mm</sub>:*ppt*<sub>Ni</sub>). Enzyme production was performed at 20°C (150 rpm) for 16–20 h. The optical density at 600 nm (OD<sub>600</sub>) of cultures was determined with a UV-1280 spectrophotometer (Shimadzu, Kyoto, Japan). Cells were harvested by centrifugation (4,000 × g, 4°C) for 15–20 min using a Heraeus Fresco 17 centrifuge or a Heraeus Labofuge 400R (Thermo Fisher Scientific) (Bayer et al., 2021).

RCs of *E. coli* were prepared after cultivation by re-suspension in RCM (22 mM KH<sub>2</sub>PO<sub>4</sub>, 42 mM Na<sub>2</sub>HPO<sub>4</sub>, 8.56 mM NaCl, 1 mM MgSO<sub>4</sub>, 1 mM CaCl<sub>2</sub> and 1% ( $\omega/\nu$ ) glucose) to a final OD<sub>600</sub>  $\approx$  10.0 as previously described (Bayer et al., 2021).

Similarly, LCC, LCC-ICCG, and PES-H1 were produced in *E. coli* BL21(DE3) transformants by cultivation in AIM supplemented with kanamycin (50  $\mu$ g·mL<sup>-1</sup>) at 21°C (150 rpm) for 23 h (Tournier et al., 2020). To produce PES-H1, the time of cultivation was reduced from 23 h to 20 h. Cells were harvested, re-suspended in lysis buffer (7 mL per g wet cell pellet; 50 mM Na<sub>2</sub>HPO<sub>4</sub>, 300 mM NaCl, pH 8), and processed according to Tournier and co-workers (Tournier et al., 2020). After cell disruption by freezing/thawing, 1  $\mu$ L Lysonase™ Bioprocessing Reagent (#71230; Merck-Millipore, Darmstadt, Germany) per mL cell suspension was added and incubated at 28°C (220 rpm) for 1 h. They lysate was clarified by centrifugation (6,000 × g, 4°C) for 45 min. Subsequently, enzymes were purified from the supernatant through their C-terminal 6xHis tags by cobalt affinity chromatography (ROTI® Garose-His/Co Beads, Carl Roth, Karlsruhe, Germany). The three hydrolases were eluted with elution buffer (50 mM Na<sub>2</sub>HPO<sub>4</sub>, 300 mM NaCl, pH 8.0) supplemented with 250 mM (LCC and LCC-ICCG) or 100 mM imidazole (PES-H1). The target proteins were desalted with

50 mM Na<sub>2</sub>HPO<sub>4</sub> buffer (pH 8.0) and used for the hydrolysis of Gf-PET film (Goodfellow, Hamburg, Germany) as describe below.

Protein expression was confirmed by 12.5% (*w/v*) SDS-PAGE of denatured whole-cell samples normalized to OD<sub>600</sub> = 7.0 (Figure S2) or purified enzymes, using the Mini-PROTEAN electrophoresis system (Bio-Rad, Feldkirchen, Germany) and following standard protocols; gels were stained with InstantBlue™ Protein Stain (Expedeon, Heidelberg, Germany) for at least 30 min (Bayer et al., 2021).

### PET hydrolysis

The enzymatic degradation of amorphous PET film (Goodfellow, Hamburg, Germany) was performed in 1 M potassium phosphate buffer (pH 8.0) at 72°C with shaking (1 000 rpm; ThermoMixer C, Eppendorf, Hamburg, Germany) for 24 h; the enzyme concentration of 1 mg per g PET in a total reaction volume of 1.5 mL was used as published before (Tournier et al., 2020). The clarified supernatants were analyzed according to Palm et al. by reverse-phase HPLC on a VWR Hitachi LaChrom Elite system (VWR International, Radnor, USA), equipped with a Kinetex® column (5 μM EVO C18 100 Å, 150 x 4.6 mm; Phenomenex®, Aschaffenburg, Germany), with a gradient of acetonitrile and 0.1% (*v/v*) formic acid in water at 30°C after injection of 10 μL sample. Within 12 min, acetonitrile was increased from 5 to 44% and then to 70% after 15 min. The ratio remained constant for another 3 min. TPA was detected at 240 nm and quantification was facilitated by standard calibration using commercial reference compounds (Palm et al., 2019). Samples were prepared from independent PET hydrolysis experiments with LCC, LCC-ICCG, and PES-H1 and subsequent HPLC measurements and quantification (n ≥ 2; Table S2).

### LuxAB-based detection of TPA-derived aldehydes *in vivo* (96-well plate format)

RCs of the desired *E. coli* strain expressing either LuxAB or LuxAB together with CAR<sub>Mm</sub>/PPT<sub>Ni</sub> were prepared as before in biological replicates (n ≥ 3). To 198 μL RCs (OD<sub>600</sub> ≈ 10.0) per well, 2 μL of the target compound, dissolved in DMSO, were added to a final concentration of 1 mM concentration, if not stated otherwise, in a total volume of 200 μL containing 1% (*v/v*) DMSO as co-solvent per well (flat bottom, black polystyrene 96-well plate, #655079; Greiner Bio-One, Frickenhausen, Germany). It was mixed gently. The bioluminescence was measured immediately on a Varioskan™ LUX multimode plate reader (Thermo Fisher Scientific). The change in bioluminescence was monitored at 25°C for up to 1 h and the fold-increase in bioluminescence above background in the presence of directly added or enzymatically produced aldehydes calculated as described in detail previously (Bayer et al., 2021). Data were generated from biological replicates and presented as mean values + SD (n ≥ 3). These results are shown in Figures 2B–2C and Figure S3 for RCs of *E. coli* BL21(DE3) Δ*lpp* and *E. coli* RARE, respectively.

For the screening of PET hydrolysates, samples were clarified by centrifugation (13,000 × g, 1 min) using a Heraeus Labofuge 400R (Thermo Fisher Scientific). The supernatant was diluted 1:10 by mixing 100 μL of the hydrolysis sample with 200 μL DMSO and 700 μL RCM. Subsequently, 10 μL of the resulting dilution were added to 190 μL RCs (OD<sub>600</sub> ≈ 10.0) per well. The 96-well plate was processed as before and the bioluminescence was measured up to 4 h. Data were generated from biological replicates and presented as mean values + SD (n ≥ 3). These results are shown in Figures 3 and S4 for RCs of *E. coli* RARE and *E. coli* BL21(DE3) Δ*lpp*, respectively.

### Whole-cell biotransformations and chemo-enzymatic cascade one-pot reaction

RCs (OD<sub>600</sub> ≈ 10.0) expressing CAR<sub>Mm</sub>/PPT<sub>Ni</sub> were prepared as before. Whole-cell biotransformations were performed in glass vials with screwcaps (4 mL) at 2–5 mM TPA concentration and 5% (*v/v*) DMSO as co-solvent (V<sub>total</sub> = 0.5 mL) in Infors HT Multitron incubator shakers (Bottmingen, Switzerland) at 25°C (230–250 rpm) for 0–24 h. For GC analysis, samples (100 μL) of the biotransformation mixtures were taken immediately after the addition of substrate and mixing (t ≈ 0 h) and again after 24 h. Subsequently, samples were acidified with 2 M HCl (10 μL) and extracted two times with ethyl acetate (200 μL) containing 1 mM methyl benzoate as internal standard (IS) by vortexing for 1 min. For phase separation, samples were centrifuged (13,000 × g, 4°C) for 1 min. The combined organic phases were desiccated over Na<sub>2</sub>SO<sub>4</sub> and transferred into a GC vial with insert, capped, and submitted to GC analysis. Compound identification was performed by the comparisons of retention times of commercial standards (Table 1), unless stated otherwise; quantification and calculation of GC yields were performed by employing relative response factors (RRFs) as described in detail previously (Bayer et al., 2021) and below. Data were generated from biological replicates and presented as mean values + SD (n ≥ 3). When employing RCs of *E. coli* BL21(DE3) or

*E. coli* RARE, reaction mixtures contained mainly unreacted TPA after 24 h ( $58.2 \pm 16.0\%$  for *E. coli* BL21(DE3) and  $51.0 \pm 12.1\%$  for *E. coli* RARE as shown in Figures S1A and S1B, respectively). Conversions of TPA could be improved by the utilization of *E. coli* BL21(DE3)  $\Delta/lpp$ . After 24 h reaction time, biotransformation mixtures only contained  $31.1 \pm 5.9\%$  TPA, besides TPA-derived aldehydes including 4-CBAL and the over-reduced 4-HMBAL and 1,4-BDM (Figure 2A). Additionally, 4-CBAL and 4-(hydroxymethyl) benzoic acid (4-HMBA) were identified as substrates for CAR<sub>Mm</sub> as shown in Figures S1C and S1D, respectively. These results are in agreement with the LuxAB-based detection of corresponding aldehydes employing either RCs of *E. coli* BL21(DE3)  $\Delta/lpp$  (Figure 2) or *E. coli* RARE (Figure S4) in the HT assay. Furthermore, whole-cell biotransformations suggest the activity of endogenous enzymes (e.g., aldehyde dehydrogenases) that oxidize aldehydes to the corresponding carboxylic acids (Figures S1C–S1E). This is in accordance with previous findings (Bayer et al., 2017).

For the chemo-enzymatic reaction in one-pot, TPA was reduced by CAR<sub>Mm</sub> in whole-cell biotransformations under the conditions given above ( $V_{\text{total}} = 0.1$  mL) in the presence of 2.2–2.5 eq  $\text{NH}_2\text{OH} \cdot \text{HCl}$  in biological replicates ( $n \geq 2$ ). After 12–16 h of reaction time, 5.5 eq zinc powder were added and the cell suspension acidified with 10 M HCl (20  $\mu\text{L}$ ). After incubation with shaking at room temperature for 4 h, 30% (v/v) ammonia solution (10  $\mu\text{L}$ ) and 5 M NaOH (10  $\mu\text{L}$ ) were added (Ayedi et al., 2013). It was mixed for 15 min before extracting two times with ethyl acetate (200  $\mu\text{L}$ ) containing 1 mM IS as before. Combined organic phases were dried over  $\text{Na}_2\text{SO}_4$  and submitted to GC analysis using a GC-2010 Plus (Shimadzu) equipped with a flame ionization detector (FID; Shimadzu) and a ZB-5MSi column (length: 30 m; inner diameter: 0.25 mm; film thickness: 0.25  $\mu\text{m}$ ) from Phenomenex (Torrance, USA). GC/FID method (hydrogen, 0.96  $\text{mL} \cdot \text{min}^{-1}$  flow rate; injector and detector: 320°C): 100°C, hold 1 min, 20°C per min to 250°C, hold 5 min; total time: 13.5 min.

## QUANTIFICATION AND STATISTICAL ANALYSIS

Quantification was performed for (1) biocatalytic reactions performed in whole cells of *E. coli* (i.e., RCs) in biological replicates ( $n \geq 3$ ) and in combination with reductive amination reactions in one-pot ( $n \geq 2$ ) and (2) the enzymatic degradation of PET for independent hydrolysis reactions ( $n \geq 2$ ). Compound identification was realized by the comparison of the retention times of commercial standards by (1) GC/FID and (2) HPLC analysis. From the corresponding peak areas, yields were calculated (1) by employing RFFs for each compound of interest (Table 1) and (2) by linear standard calibration for TPA (slope = 49,134.00; axis intercept = 58,547.00;  $R^2 > 0.99$ ).

For the semi-quantitative assessment of amounts of TPA in PET hydrolysis samples, dilutions were analyzed by the CAR/LuxAB-based HT assay employing biological replicates of RCs ( $n \geq 3$ ). The fold-increase in bioluminescence was proportional to the concentration of TPA as described in the main text and could be calculated from TPA samples with known concentration (1 mM).

Statistical analysis included the calculations of mean values, SDs, and the determination coefficient ( $R^2$ ) by the integrated functions of the standard spreadsheet software Microsoft Excel (version 16.0).

GC yields are presented as bars representing mean values + SD in Figures 2A, 4, and S1. Both experimental and statistical details can also be found in the corresponding figure legends and in the main text.

HPLC yields are given as mean values  $\pm$  SD in Table S2. Experimental details can be found in the main text and statistical details in the legend of Table S2.

The mean fold-increase in bioluminescence + SD is depicted as bars in Figures 3 and S4. Both experimental and statistical details can also be found in the corresponding figure legends and in the main text.

## ADDITIONAL RESOURCES

The OligoEvaluator™ (Sigma-Aldrich; <http://www.oligoevaluator.com/LoginServlet>) was used to predict secondary structures and dimer formation of DNA oligonucleotides (Table S1).

**iScience, Volume 25**

**Supplemental information**

**Biosensor and chemo-enzymatic one-pot cascade  
applications to detect and transform PET-derived  
terephthalic acid in living cells**

**Thomas Bayer, Lara Pfaff, Yannick Branson, Aileen Becker, Shuke Wu, Uwe T. Bornscheuer, and Ren Wei**

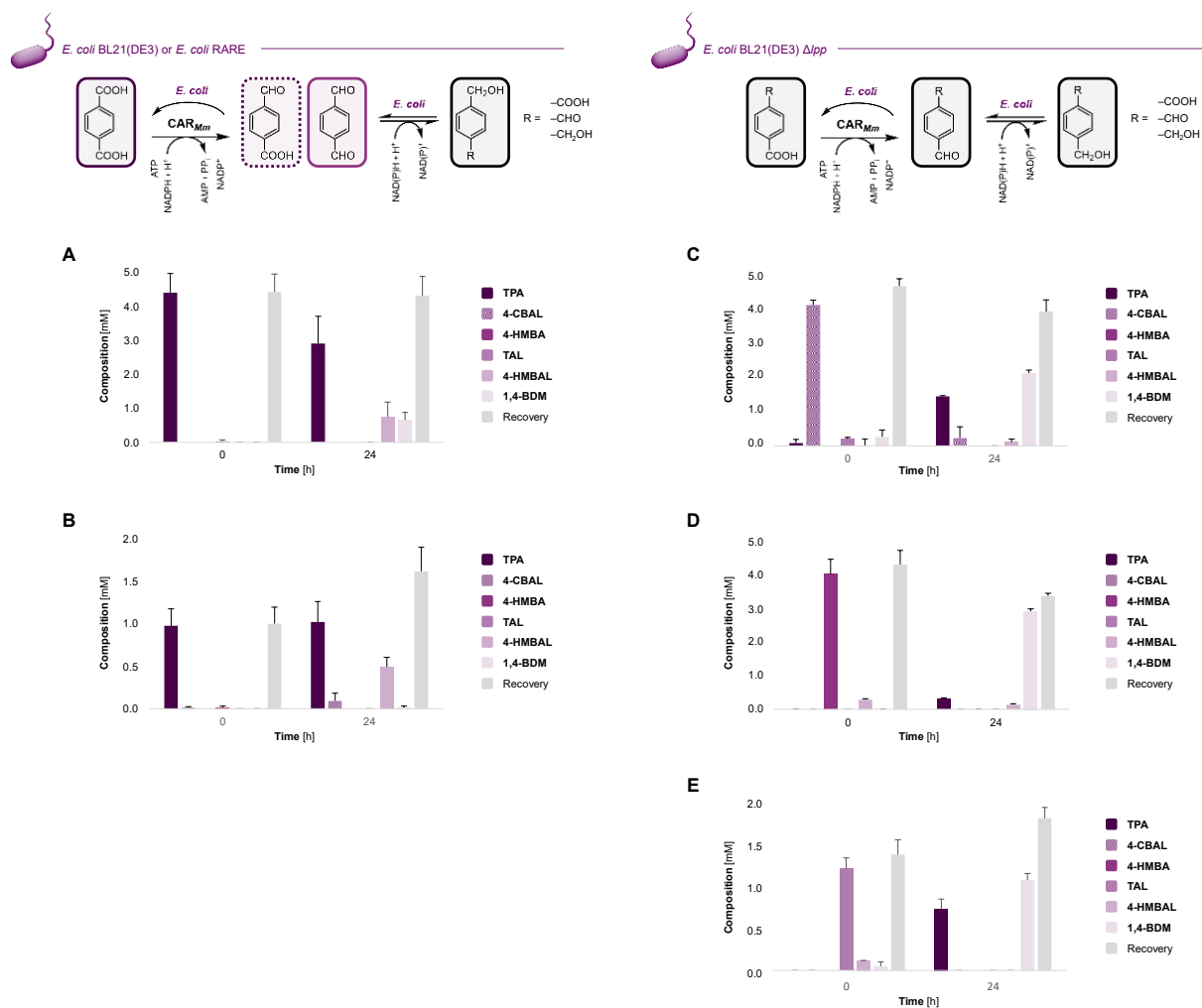


**Figure S1. CAR-catalyzed reductions of TPA and derivatives *in vivo*, related to Figure 2A. (A)** Bioreduction of TPA by  $CAR_{Mm}$  in *E. coli* BL21(DE3) yields a mixture of the over-reduced 4-HMBAL and 1,4-BDM, besides unreacted substrate. **(B)** Bioreduction of TPA by  $CAR_{Mm}$  in *E. coli* RARE mainly yields 4-HMBAL, indicating reduced aromatic aldehyde reducing activity compared to *E. coli* BL21(DE3), 4-CBAL, and unreacted TPA. **(C)**  $CAR_{Mm}$  reduces the carboxylate group in 4-CBAL to the corresponding TAL. Endogenous enzymes not only reduce aldehydes to the corresponding primary alcohols like 1,4-BDM but also oxidize them to the carboxylates as indicated by the detection of TPA after 24 h. This is in accordance with previous findings (Bayer et al., 2017). **(D)**  $CAR_{Mm}$  reduces the carboxylate group in 4-HMBA to the corresponding 4-HMBAL. Endogenous enzymes reduce the aldehydes to the corresponding primary alcohols like 1,4-BDM; TPA could be detected in traces after 24 h. **(E)** The highly reactive TAL is both oxidized and reduced by endogenous enzymes, yielding TPA and 1,4-BDM, respectively. On top, arrows indicate the activities of (host) enzymes;  $PPT_{Ni}$  necessary for posttranslational modification of  $CAR_{Mm}$  is omitted for clarity. Experiments were performed in RCs of *E. coli* ( $OD_{600} \approx 10.0$ ) co-expressing enzymes from  $pACYCDuet-1/car_{Mm}:ppt_{Ni}$  (Bayer et al., 2021) in the presence of 2–5 mM substrates and 5% (v/v) DMSO as organic co-solvent. Sampling: 0 h (after the addition of substrate and mixing) and 24 h. Recoveries were reduced due to low solubilities and/or the volatility of compounds. GC yields are presented as mean values + standard deviation (SD) [mM] of biological replicates ( $n \geq 3$ ).

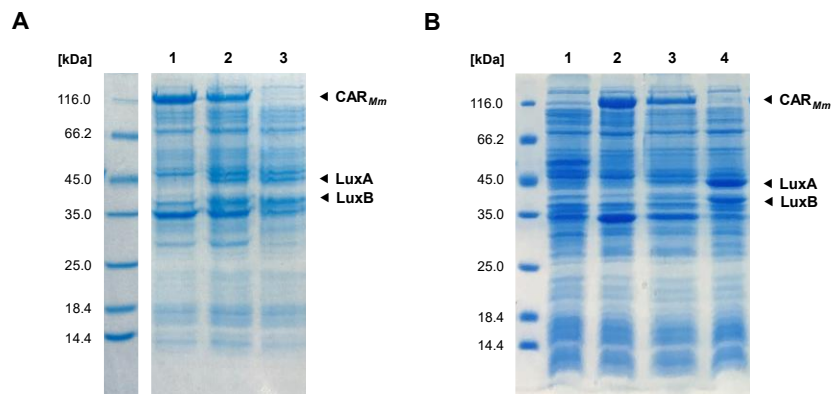


**Figure S2. SDS-PAGE analysis of whole-cell samples, related to Figure 2A, Figure S1, and STAR Methods.** (A) Expression of (1)  $CAR_{Mm}/PPT_{Ni}$  from pACYCDuet-1/ $car_{Mm}:ppt_{Ni}$  [ $CAR_{Mm}$ : 129 kDa], (2)  $CAR_{Mm}/PPT_{Ni}$  and LuxAB from pLuxAB [LuxA: 43 kDa, LuxB: 37 kDa], and (3) LuxAB in *E. coli* BL21(DE3). (B) Whole-cell samples of (1) untransformed *E. coli* BL21(DE3)  $\Delta lpp$  or expressing (2)  $CAR_{Mm}/PPT_{Ni}$ , (3)  $CAR_{Mm}/PPT_{Ni}$  and LuxAB, and (4) LuxAB;  $PPT_{Ni}$  [23 kDa] was not detectable due to low expression levels in corresponding samples. Proteins were produced from pACYCDuet-1/ $car_{Mm}:ppt_{Ni}$  and pLuxAB (Bayer et al., 2021); the detailed protocol is given in the main text. Sample loading normalized to  $OD_{600} = 7.0$ ; SDS-PAGE and gel staining performed as described in the main text. Irrelevant lanes were cropped in (A), the brightness of both pictures was increased by 20%; (  $\blacktriangleleft$  ) indicate protein bands of interest.

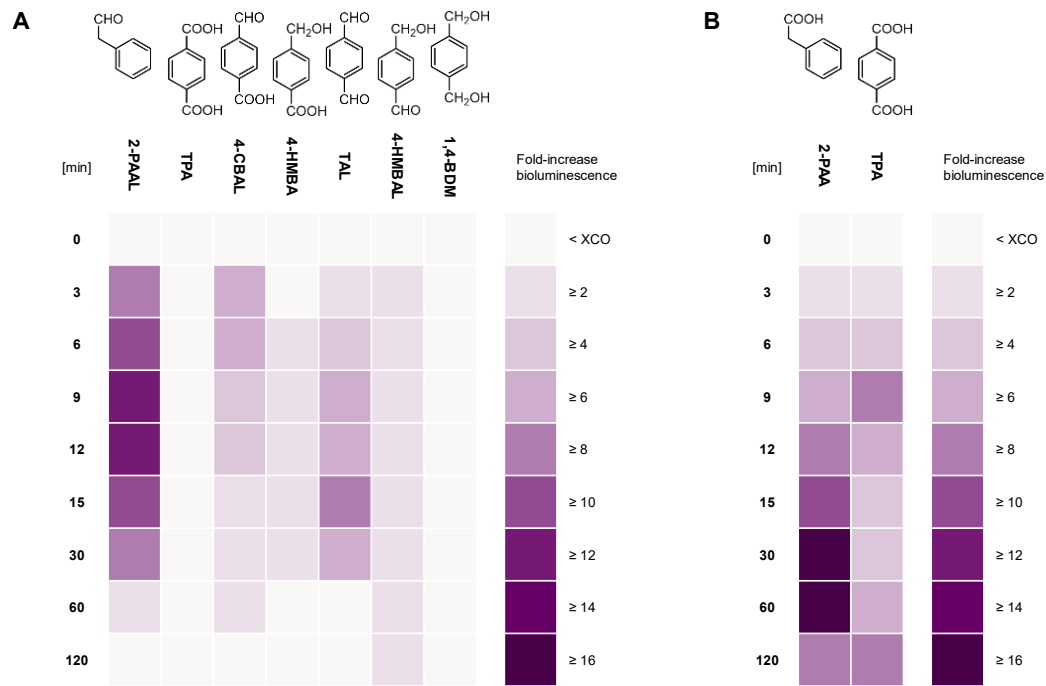


**Figure S3. LuxAB-based HT detection of aldehydes in *E. coli* RARE, related to Figure 2B–C. (A)** Direct detection of TPA-derived aldehydes (0.1 mM) by increasing bioluminescence over time in RCs of *E. coli* RARE expressing LuxAB from pLuxAB; 2-PAAL was used as the positive control. Whereas TPA and 1,4-BDM did not yield bioluminescence, the addition of 4-HMBA yielded background luminescence at 1 mM final concentration. **(B)** *In situ* production of aldehydes from 2-PAA and TPA (1 mM) in RCs of *E. coli* RARE co-expressing LuxAB and CAR<sub>Mm</sub>/PPT<sub>Ni</sub>. Experiments were performed in the presence of 1% (*v/v*) DMSO under HT assay conditions as described previously (Bayer et al., 2021) and in the main text; data presented as mean fold-increase bioluminescence obtained from biological replicates (*n* = 3).



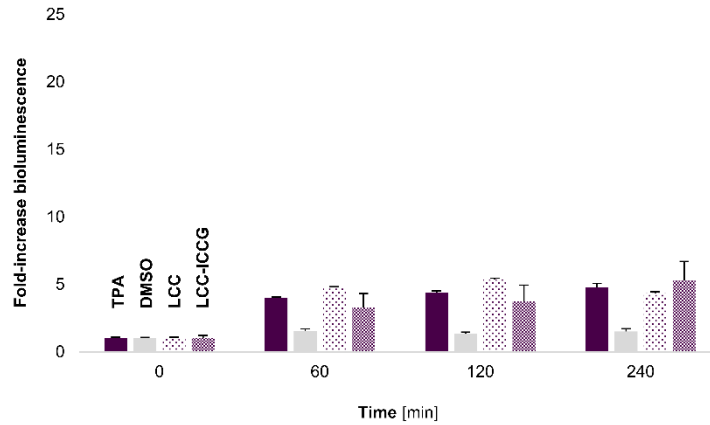


**Figure S4. PET hydrolysis samples analyzed under HT conditions in *E. coli* BL21(DE3)  $\Delta lpp$ , related to Figure 3.** The enzyme-coupled biosensor system yielded bioluminescence in the presence of 1 mM TPA (positive control) and hydrolysates obtained by the enzymatic degradation of Gf-PET films by wildtype LCC and the LCC-ICCG variant. The bioluminescence did not increase in the presence of 1% (v/v) DMSO over monitoring time (negative control). While the bioluminescence plateaued around 4-fold above background in *E. coli* BL21(DE3)  $\Delta lpp$  after 1 h incubation time, it increased in RCs of *E. coli* RARE proportionally to the amounts of TPA present in PET hydrolysis samples (see **Figure 3** in the main text). Experiments were performed in RCs of *E. coli* BL21(DE3)  $\Delta lpp$  under HT assay conditions as described previously (Bayer et al., 2021) and in the main text; data presented as mean values of the fold-increase in bioluminescence + SD of biological replicates (n = 3).

**Table S1.** List of DNA oligonucleotides, related to **STAR Methods**

<b>Primer</b>	<b>Sequence (5' – 3')</b>
<i>lpp</i> -up_F	gagtcgacctgcagaagcttGTAAAGAACTGGCTCTGCAGAG
<i>lpp</i> -up_R	acaggtactaCCCTCTAGATTGAGTTAATCTCC
<i>lpp</i> -down_F	atctagagggTAGTACCTGTGAAGTGAAAAATG
<i>lpp</i> -down_R	gagctgcacatgaactcgagATGAATGCACCGGATATTAAGC
pTarget_F	ctcgagttcatgtgcagctc
pTarget_R	aagcttctgcaggtcgactc
$\Delta$ <i>lpp</i> -gRNA_F	AGTAGAACCCgtttagagctagaaatagcaagtt
$\Delta$ <i>lpp</i> -gRNA_R	CTGCTGGCAGactagtattatacctaggactgagc

**Table S2.** HPLC yields of TPA in PET hydrolysates, related to **Figure 3** and **STAR Methods**

<b>PET hydrolase</b>	<b>TPA yields [mM]</b>
PES-H1	56.0 $\pm$ 0.1
LCC	47.8 $\pm$ 3.1
LCC-ICCG	111.1 $\pm$ 15.3

Yields are given as mean values  $\pm$  SDs of independent PET hydrolysis experiments and subsequent HPLC measurement for LCC (n = 3) and LCC-ICCG (n = 2) and as mean value  $\pm$  SD of a technical replicate (n = 2) for PES-H1.

## **Eigenständigkeitserklärung**

Hiermit erkläre ich, dass diese Arbeit bisher von mir weder an der Mathematisch-Naturwissenschaftlichen Fakultät der Universität Greifswald noch einer anderen wissenschaftlichen Einrichtung zum Zwecke der Promotion eingereicht wurde.

Ferner erkläre ich, dass ich diese Arbeit selbstständig verfasst und keine anderen als die darin angegebenen Hilfsmittel und Hilfen benutzt und keine Textabschnitte eines Dritten ohne Kennzeichnung übernommen habe.

---

Lara Pfaff



## List of Publications

L. Pfaff, J. Gao, Z. Li, A. Jäckering, G. Weber, J. Mican, Y. Chen, W. Dong, X. Hu, C. G. Feiler, Y. Ao, C. P. S. Badenhorst, D. Bednar, G. J. Palm, M. Lammers, J. Damborsky, B. Strodel, W. Liu, U. T. Bornscheuer, R. Wei, Multiple Substrate Binding Mode-Guided Engineering of a Thermophilic PET Hydrolase. *ACS Catal.* **2022**, *12*, 9790–9800.

S. Brott, L. Pfaff, J. Schuricht, J. Schwarz, D. Böttcher, C. P. S. Badenhorst, R. Wei, U. T. Bornscheuer. Engineering and Evaluation of Thermostable IsPETase Variants for PET Degradation. *Eng. Life Sci.* **2021**, *22* (3-4), 192-203.

L. Pfaff, D. Breite, C. P. S. Badenhorst, U. T. Bornscheuer, R. Wei. Fluorimetric High-Throughput Screening Method for Polyester Hydrolase Activity Using Polyethylene Terephthalate Nanoparticles. In *Methods in Enzymology*; Elsevier, **2021**; Vol. 648, pp 253–270.

T. Bayer, L. Pfaff, Y. Branson, A. Becker, S. Wu, U. T. Bornscheuer, R. Wei, Biosensor and chemo-enzymatic one-pot cascade applications to detect and transform PET-derived terephthalic acid in living cells. *iScience* **2022**, *25*, 104326.

### Publications not covered in this thesis

R. Wei, G. von Haugwitz, L. Pfaff, J. Mican, C. P. S. Badenhorst, W. Liu, G. Weber, H. P. Austin, D. Bednar, J. Damborsky, U.T. Bornscheuer. Mechanism-Based Design of Efficient PET Hydrolases. *ACS Catal.* **2022**, *12*, 3382–3396.

I. E. Meyer Cifuentes, P. Wu, Y. Zhao, W. Liu, M. Neumann-Schaal, L. Pfaff, J. Barys, Z. Li, J. Gao, X. Han, U. T. Bornscheuer, R. Wei, B. Öztürk. Molecular and Biochemical Differences of the Tandem and Cold- Adapted PET Hydrolases Ple628 and Ple629, Isolated From a Marine Microbial Consortium. *Front. Bioeng. Biotechnol.* **2022**, *10*:930140.

K. Vogel, R. Wei, L. Pfaff, D. Breite, H. Al-Fathi, C. Ortmann, I. Estrela-Lopis, T. Venus, A. Schulze, H. Harms, U. T. Bornscheuer, T. Maskow. Enzymatic Degradation of Polyethylene Terephthalate Nanoplastics Analyzed in Real Time by Isothermal Titration Calorimetry. *Sci. Total Environ.* **2021**, *773*, 145111.

Y. Branson, C. P. S. Badenhorst, L. Pfaff, C. Buchmann, R. Wei, U. T. Bornscheuer. High-Throughput Screening for Thermostable Polyester Hydrolases. In *Methods in Molecular Biology*, 2022, Vol. 2555, accepted for publication.

G. von Haugwitz, X. Han, L. Pfaff, Q. Li, H. Wei, J. Gao, K. Methling, Y. Ao, Y. Brack, J. Mican, C. G. Feiler, M. S. Weiss, D. Bednar, G. J. Palm, M. Lalk, M. Lammers, J. Damborsky, G. Weber, W. Liu, U. T. Bornscheuer, R. Wei. Structural Insights into (Tere)phthalate-ester Hydrolysis by a Carboxylesterase and its Role in Promoting PET Depolymerization. *ACS Catal.* 2022, under review.

N. A. Tarazona, R. Wei, S. Brott, L. Pfaff, U. Bornscheuer, A. Lendlein, R. Machatschek. Rapid depolymerization of poly(ethylene terephthalate) thin-films by a dual enzyme system and its impact on material properties. *Chem. Catal.*, under review.

P. R. Neubauer, O. Blifernez-Klassen, L. Pfaff, M. Ismail, O. Kruse, N. Sewald. Two Novel, Flavin-Dependent Halogenases from the Bacterial Consortia of *Botryococcus braunii* Catalyze Mono- and Dibromination. *Catalysts* **2021**, *11*, 485.

## Acknowledgments

Zuallererst möchte ich dir, Uwe, meinen tiefsten Dank für deine engagierte und kompetente Betreuung während meiner Doktorarbeit aussprechen. Ich bin dir unglaublich dankbar, dass du mir damals die Möglichkeit eröffnet hast, Teil deiner großartigen Arbeitsgruppe zu werden, in der ich in den letzten Jahren wachsen und viel dazulernen konnte. Ich schätze deine motivierenden Ratschläge, dein stets entgegengebrachtes Vertrauen, und den Rückhalt und die Freiheit, die du mir während dieser Zeit in verschiedenen Projekten gegeben hast, sehr. Außerdem danke ich dir, dass du weiterhin das Vertrauen in mich hast und ich für ein weiteres Jahr Teil deiner Gruppe sein darf. Vielen Dank!

Ren, durch deine jahrelange Expertise auf dem Gebiet des Plastikabbaus, konntest du mir in den letzten 2 ½ Jahren, mit unglaublich viele Tipps und Tricks und selbstverständlich Wissen zur Seite stehen. Ich habe sehr viel gelernt und bin dir dafür sehr dankbar.

Gerlis, Yannick und Caro, ich danke euch für die unglaublich großartige Zeit im C\_FunGene, die zugegebenermaßen projektbezogen nicht immer leicht war, aber dessen Schwierigkeiten ich durch eure Unterstützung und positiven Zuspruch, letztendlich immer überwinden, konnten. Ich werde unseren EU-Meetings in Brüssel und vor allem Straßburg, die Geburtstagslunches, Kaffeepausen und andere unvergessliche Abende immer in Erinnerung behalten. Ihr seid in kürzester Zeit von Arbeitskollegen zu Freunden geworden. Es war ein absolutes Vergnügen mit euch zu arbeiten! Vielen lieben Dank!

Chris, thank you very much for your support during my PhD. It was a pleasure listening to your brilliant ideas and working with you on the book chapter as well as the other papers.

Thomas, ich danke dir, dass du damals extra für mich frühzeitig aus deiner Wohnung ausgezogen bist und einige Monate auf den Sofas deiner Freunde verbracht hast, sodass ich mich direkt in Greifswald zuhause fühlen und ankommen konnte. Danke für die wissenschaftlichen Diskussionen, die beispielweise zur Veröffentlichung von Article IV geführt haben, aber vor allem für die tollen Momente außerhalb des Labors, besonders solche Abende, in die Titanic involviert war.

Theresa und Yannik, wir haben damals ungefähr zur gleichen Zeit unseren PhD begonnen und sowohl gute als auch schlechte Zeiten miteinander durchgestanden. Ich bin dankbar für eure Freundschaft und werde unsere Konzertabende, Geburtstage, Zumba-Sessions und Trips zum Strand, um nur einige zu nennen, nie vergessen.

Selbstverständlich möchte ich mich auch bei allen anderen Mitgliedern der Arbeitsgruppe für die immer sehr angenehme und freundschaftliche Atmosphäre im Labor und in den Kaffeepausen (während Corona sogar in den Online-Kaffeepausen) bedanken. Mein besonderer Dank geht auch an Dominique, Mark, Ina, Angelika, Ivonne und Astrid, die die Gruppe immer am Laufen halten. Dominique, danke, dass du mir besonders im ersten halben Jahr, als Ren der Arbeitsgruppe noch nicht beigetreten war, in der Thematik über plastikabbauende Enzyme unter die Arme gegriffen hast. Es war eine Freude mit dir, und Stefan und Mark, das Proteinpraktikum, auch unter widrigsten Bedingungen während Corona, zu betreuen. Ebenfalls bedanken möchte ich mich bei den ehemaligen Mitgliedern der Arbeitsgruppe Henrik, Aileen, Simon, Eva, Sascha. Ihr habt mir den Start in dieser Arbeitsgruppe leicht gemacht und ich habe unsere gemeinsame Zeit sehr genossen.

Außerdem möchte ich mich bei dem MIXUP- Projekt und upPE-T Projekt für die finanzielle Unterstützung bedanken.

Dominique, Lotte und Franca, ich bin unglaublich dankbar für unsere Freundschaft. Wer hätte gedacht, dass, als wir uns damals, vor nunmehr 9 Jahren, kennengelernt haben, so viele großartige Momente miteinander erleben würden. Ihr habt mich immer unterstützt und mich immer motiviert, egal wie ausweglos die Situation manchmal ausgesehen hat. Vielen Dank!

Zu besonderem Dank bin ich meiner Familie für ihre Unterstützung verpflichtet, ohne die all dies nicht möglich gewesen wäre. Luca, ich danke dir für deine (sarkastischen) Kommentare, die mich in sehr emotionalen Momenten, immer aufgeheitert und motiviert haben. Du hast immer ein Licht am Ende des Tunnels gesehen!